

UNIVERSITY OF THE
WEST of SCOTLAND

UWS

**Prediction of the Gas
Emission and Movement
from Soil Media with
Concern of Energy and
Environment**

by

Ahmed Al Makky



Submitted to the University of the West of Scotland

for the Degree of

Doctor of Philosophy

School of Engineering

February 2016

This page is intentionally left blank



**Prediction of the Gas Emission
and Movement from Soil Media
with Concern of Energy and
Environment**

by

Ahmed Al Makky

Thesis

**Submitted to the University of the West of Scotland
for the Degree of**

**Doctor of Philosophy
School of Engineering**

February 2016

This page is intentionally left blank

@Ahmed Al Makky 2024

All rights reserved. No part of this publication may be reproduced, stored in a retrieval system or transmitted in any form or by any means, electronic, mechanical or photocopying, recording, or otherwise without the prior permission of the publisher.

This page is intentionally left blank

Table of Contents

List of Figures	vi
List of Tables.....	xvii
Acknowledgements	xix
Declaration	xx
Abstract	xxiii
List of Symbols and Abbreviations.....	xxv
- Abbreviations	xxv
- Roman Symbols	xxvii
- Greek Symbols	xlvii
- Superscripts and Subscripts.....	lii
Publications	liv
Chapter 1	1
Introduction	1
1.1. Introduction.....	1
1.2. Respiration Chambers.....	3
1.3. Motivation.....	4
1.4. Thesis Objectives	6
1.5. Thesis Layout.....	7
Chapter 2	9

Literature Review	9
2.1. Introduction.....	9
2.2. Soil Carbon dioxide efflux Model	13
2.3. Soil Parameters that affect CO ₂ efflux	19
2.4. Respiration Chamber Shape, Operation Mode and Design Regulations	26
2.5. Chamber Gas Sensors, Location of Instillation and Calibration	46
2.6. Chamber Temperature Increase/Decrease and its Relation to efflux	53
2.7. Pressure effects on efflux Measurement in Chambers.....	71
2.8. Respiration Chamber Characteristics.....	83
2.9. Chambers Anchoring or Insertion into the Soil.....	86
2.10. The Role of Soil pH/Bacteria on Carbon Dioxide Production and Transport in Soil.....	89
2.11. Summary.....	99
Chapter 3	100
Experimental Design	100
3.1. Introduction.....	100
3.2. Chamber Design Requirements	100
3.3. Proposed Chamber Designs	102
3.4. Experimental Study.....	112
3.5. Location of Study.....	125

3.6. The City of Paisley Site Climate Description	129
3.7. The Soil Analysis efflux Software	133
3.8. Summary	146
Chapter 4	148
Numerical Flow Model	148
4.1. Introduction.....	148
4.2. The Reason for using the CFD Tool	148
4.3. The K-Epsilon Turbulence Model	150
4.4. The None-Linear Eddy Viscosity Model.....	152
4.5. Darcy Model	152
4.6. Permeability Calculation.....	156
4.7. Soil Porosity.....	159
4.8. Summary	163
Chapter 5	165
CFD simulations and Experimental Results and Discussion	165
5.1. Introduction.....	165
5.2. Static Case Experimental Data Analysis	166
5.3. Conclusions from Experimental Data.....	183
5.4. The Static Chamber Case Numerical Simulation	185
5.5. The Dynamic Chamber Case Numerical Simulation.....	205

5.6. The Dynamic Chamber Case with a Rotating Fan Mesh.....	226
5.7. Summary.....	244
Chapter 6.....	245
Conclusion and Future Research.....	245
6.1. Conclusion.....	245
6.2. Future Work.....	246
References.....	249
Appendices.....	276
A-I Chamber dimensions.....	276
A-II Blowing Fan Parameters.....	277
A-III Lead Battery Parameters.....	278
A-IV The Respiration Chamber Perspective View.....	279
A-V The Side View of the Respiration Chamber.....	280
A-VI The Top View of the Respiration Chamber.....	281
A-VII The Respiration Sampling Tube.....	282
A-VIII The Circulation Fan Model.....	283

This page is intentionally left blank

List of Figures

Figure 1: The used designed chamber at UWS, located on the grass land site.....	2
Figure 2: LI-8100A Automated Soil CO ₂ Flux System and soil chambers provided by LICOR [4]	4
Figure 3 : An example case of measured carbon dioxide concentrations in relation to time in, the blue curve represents the ideal case and the red curve represents the disturbed measurement.....	6
Figure 4: IPCC IS92a projections of atmospheric carbon dioxide concentrations and temperature in relation to number of years and the HadCM2 SUL climate model simulations of temperature over land (excluding Antarctica).....	10
Figure 5: Licor`s developed apparatus that measures photosynthesis LI-6400XT [62].	26
Figure 6: Available commercial chambers by Li-COR LI-8100A Automated.....	26
Figure 7: The eight types of greenhouse configurations [64]	27
Figure 8: The occurring flow pattern around a cylindrical chamber [75]. What affects mainly the measurement is the horseshoe vortex, arch vortex.....	33
Figure 9: A summary of the 6 cases of external flows occurring around a cylinder represented in relation to the Reynolds number for flow characterization [81].	35
Figure 10: Probability distribution of annual wind speeds example.....	37
Figure 11: The box shaped chamber with the horseshoe vortex at prism-wall junction, this vortex which mainly disturbs concentration measurements in the chamber [85].	38
Figure 12: A small in height static chamber.	39

Figure 13: LI-8100A Automated Soil CO ₂ Flux System and soil chambers provided by LICOR [4]	40
Figure 14: A chamber with no internal obstacles except the tree branches.....	43
Figure 15: The PP Systems SRC-1 none transparent chamber model used to measure soil efflux.	56
Figure 16: The CPY-4 transparent chamber used to measure efflux from low lying vegetation.....	57
Figure 17: Emissivity of water vapour in a mixture with none radiating gases at 1-atm total pressure [36].....	59
Figure 18: Correction factor for obtaining water vapour emissivities at pressures other than 1 [atm] [114].....	60
Figure 19: Emissivity of carbon dioxide in a mixture with none radiating gases at 1-atm total pressure [114].....	61
Figure 20: Correction factor for obtaining carbon dioxide emissivities at pressures other than 1 [atm] [114].	62
Figure 21: An illustration showing plant activity during the day which is called Photosynthesis (shown on the right hand side) and the night activity which is called Cellular Respiration (shown on the Left hand side).....	69
Figure 22: The aeration process through the top soil surface.	78
Figure 23: Typical growth curve for a bacterial population. Note that the phase of growth depends on the parameter used to monitor growth [192].	92
Figure 24: Determination of total microbial activity (mgCO ₂ – C) in sample of soil mixed with different types of organic matter, incubated at 25[°C] [193]	93

Figure 25: The proposed spherical chamber concept.....	102
Figure 26: The static cylindrical chamber design shown on the left with the incubators and gas cylinders on the right-hand side.	104
Figure 27: The dynamic respiration chamber notably it uses two blowing fans.	105
Figure 28: Using the clamp method to fix the top chamber cover.....	107
Figure 29: Specifying for the studied fan what acting pressure is occurring on the soil surface inside the chamber, the working point shown in red.	107
Figure 30: The chamber design agreed on to build.....	109
Figure 31: The used respiration chamber a prespective view with a numbring notation referring to its different main parts.	112
Figure 32: The wireless sensors box is composed of a wireless carbon dioxide concentration, temperature relative humidity sensor.	114
Figure 33: The respiration chamber gas sampling tube used to take collect gas samples in relation to the chamber's height.....	115
Figure 34: The wireless USB connection that will be connected to the laptop.	116
Figure 35: The electrical blowing fan with its side white cover. The fan is intended to be used for the dynamic chamber operational mode.....	117
Figure 36: The fan battery used on site deploymen (left) moreover the power battery charger (right) used in lab trials	117
Figure 37: The blowing fan connecting rib likewise the 4 connecting metal threaded beams for the fan with the chamber. Furthermore, one of the plastic tubes used to cover the threaded metal beams is shown.....	118

Figure 38: The respiration chamber fixture foundation used to provide a confined closure within the chamber's gas volume.	119
Figure 39: A screen shot showing the automated control panel software GSSVGHP V4.0 interface used with the respiration chamber.....	120
Figure 40: A test case run showing carbon dioxide readings from the sensor readings after analysis, carbon dioxide concentration in relation to time for a dynamic case.	122
Figure 41: The flow chart showing the experimental setup steps for the dynamic chamber experiment.	123
Figure 42: The flow chart showing the experimental setup steps for the static chamber experiment.....	124
Figure 43: Topographic map of the location of study, the site is located on UWS paisley campus, the elevation key is located on the right-hand side, and location is in the light green colour range.....	126
Figure 44: The grass land location of study at UWS paisley campus.....	127
Figure 45: Volume and mass fraction distribution for a grassland site.....	128
Figure 46: The relation of soil moisture with relative microbial activity for soil. Adapted from [197].....	129
Figure 47: The mean, max and min temperatures of the city of Glasgow [214].	130
Figure 48: The average rain fall data for the city of Glasgow in 2015 [214].	131
Figure 49: Paisley location average radiative flux for the year 2015.	132
Figure 50: Soil Analysis efflux software structure.	134

Figure 51: The software interface used to calculate air density within the chamber.	135
Figure 52: The software interface used to calculate blowing fan parameters within the chamber.	137
Figure 53: The software interface showing the soil temperature variation according to soil depth, time of day soil geotechnical and thermo-physical properties.	139
Figure 54: The software interface the studies variation of temperature with depth.	140
Figure 55: The software interface that calculates the volume and mass fractions and other geotechnical parameters according location type.	143
Figure 56: The organic material volume fraction calculation which are split into roots, hums and living organisms.	144
Figure 57: Studying the change of porosity, mass diffusion according to the temperature profile at a specified time of the day.....	145
Figure 58: USDA and UK-ADAS Soil textural triangle.....	157
Figure 59: Porosity is the ratio of the total volume of pores in a soil sample over the total volume of the soil sample.	159
Figure 60: The side length of each sample is 2.25 mm. (a) is taken using X-ray microtomography. (b) is taken using the Object-based modelling [218].....	162
Figure 61: A comperson between none corrected concntration measurments and correct ones.	168
Figure 62: This plot shows a comparision between chamber temperature and species concntration levels, it shows the linnear relation ship through curve fitting MATLAB provides also exponential curve fitting.	169

Figure 63: Absolute values of measured carbon dioxide measurements, filtered measurements of carbon dioxide.	172
Figure 64: Absolute concentration measurements compared with efflux measurements in time for a two our experiment.	174
Figure 65: measured relative carbon dioxide concentrations with relative humidity affects.	175
Figure 66: Dew point temperature and temperature plots in comparison with concentration.	177
Figure 67: The relationship between species concentration and light intensity inside the chamber.	178
Figure 68: Change of internal pressure as a function of temperature.	180
Figure 69: Internal chamber partial air Pressure shown in red and internal partial carbon dioxide pressure shown in blue.	182
Figure 70: Using histogram for concentration and fitting the data to a normal density function to get good measurements for the efflux.	184
Figure 71: The modelled gas and porous domain.	187
Figure 72: The created geometrical domain used to generate the calculation mesh.	188
Figure 73: on the left the image shows the gas and porous soil domain moreover the right handside image shows the generated mesh quality for both the soil and gas volume domain.	189

Figure 74: The highlighted boundary condition represent the interface boundary condition between the gas volume and soil porous domain furthermore represents the boundary of the porous domain with the atmosphere.	194
Figure 75: The side boundary surfaces that have been assigned an opening boundary condition are laminated in light green.	196
Figure 76: Convergence of the solution check in relation to accumulated time step, momentum and mass solution convergence on the left and the mass transfer on the right.	198
Figure 77: validation plot showing a comparison case of concentration measurements between an experimental and numerical case.	199
Figure 78: The distribution of temperature contours in the static operational mode of a chamber at time instance 80 [s].	200
Figure 79: Temperature difference contours for a 10 [s] time difference inside the chamber gas volume and porous soil domain.	201
Figure 80: The contour plot of the courant number at an instance of time 80 [s] from 360 [s].	202
Figure 81: A Courant number contour plot according to time difference of frames of 5 [s] between 75 [s] and 80 [s].	203
Figure 82: The numerical simulation at the first 20 [s] showing how mass gradually diffuses within time.	204
Figure 83: The inflow and out flow boundary surface for the fan location is highlighted in green.	210

Figure 84: Convergence of the solution check in relation to accumulated time step, momentum and mass solution convergence on the left and the K-Epsilon components used in the turbulence model on the right.	211
Figure 85: A convergence check of the solution for temperature in the energy equation moreover the same check for both gases enthalpy convergence.....	212
Figure 86: Validation plot showing a comparison case between experiential results and the numerical model concentration.	213
Figure 87: Vertical velocity values of the velocity field inside the chamber gas volume.	214
Figure 88: Inner pressure distribution inside a dynamic respiration chamber and within the porous domain.	215
Figure 89: The distribution of temperature contours in the static operational mode of a chamber at time instance 30 [s].	216
Figure 90: The contour plot of the courant number at an instance of time 80 sec from 360 [s].	217
Figure 91: A time difference of frames of 5 [s] between 75 [s] and 80 [s].	218
Figure 92: The static case Courant number contour plot in the porous domain.	219
Figure 93: The courant number difference contour plot in the porous media.	220
Figure 94: The captured vector field for the applied streamline function showing the aeration process for the top soil layer.	221
Figure 95: Stream lines show the circulated flow pattern within the chamber gas volume.	222

Figure 96: The numerical simulation at the first 35 [s] capturing how mass gradually diffuses within time.....	223
Figure 97: Concentration difference between two seconds time step at instance 33 and 34.....	224
Figure 98: The modelled gas volume with the fan cylindrical geometry in addition to the porous domain shown at the bottom.	227
Figure 99: a close up image of the rotating fan mesh coupled with the chamber gas volume mesh.	228
Figure 100: The two separate coordinate systems setups for the simulation whereby one is setup as a fixed one for the chamber gas volume furthermore the second is assigned for the rotating fan volume as shown highlighted in green.	230
Figure 101: A close up view of the blowing fan, through using a cross sectional plane that goes through the blowing fan setup. This shows the velocity vector field while the coloured contours represent the pressure gradient.	234
Figure 102: Validation plot showing a 100 [ppm] asymptotic behaviour concentration for a rotating mesh case.....	235
Figure 103: Convergence of the solution check for 360 time step accumulation, this is for mas momentum and volume fractions.....	236
Figure 104: The pressure distribution on the soil surface is shown furthermore the velocity vector field is also illustrated with the provided colour key for it.	238
Figure 105: Air Velocity distribution in both the gas volume domain and the porous domain at instance of time 350 [s], the left-hand key is for the gas volume likewise the right-hand side key is for the porous domain.....	239

Figure 106: The stream line distribution in the chamber. The colour key is for pressure distribution contour on the soil surface.	240
Figure 107: The study of pressure distribution in both the porous and gas volume domains at an instance of time 350 [s].	241
Figure 108: The Courant number contours both in the gas volume and porous domain at an instance of time 350 [s].	242
Figure 109: The concentration distribution in both the gas chamber volume and porous domain at time instance 350 [s].	243

This page is intentionally left blank

List of Tables

Table 1: Categories relating to chamber design and biological and physical parameters	111
Table 2: Categories relating to total chamber cost also apparatus weight moreover chamber gas volume additionally the used gas sensor method as well as electrical power source and finally chamber base fixture method.....	111
Table 3: A summary of the soil properties for the grassland site location at UWS Paisley campus.	147
Table 4: Soil porosities depending on type of texture [34].	161
Table 5 : The diameter of the pores classification [34].	163
Table 6: Mesh information for the static chamber case.	189
Table 7: Mesh information representing the dynamic rotating mesh case.	229

This page is intentionally left blank

Acknowledgements

Thank you Allah for all the blessings you have given me. Thank you for the wonderful parents and brother (Ibrahim), who have supported me all along, funded my studies and helped me grow into a better person. To them I dedicate this thesis especially to my dad who in 1981 dedicated his PhD thesis to me and now in 2016 I am dedicating my work to him. I would like to thank my supervisor Professor Abdul Ghani Olabi. My thanks are also to Professor Desmond Gibson.

Furthermore, I extend my thanks to Dr Abed Alaswad and Dr Shigeng Song for their unlimited support throughout the project.

Many thanks to my Grand Mother Fatima Nehlawi, Aunti Handi Dalbani, Aunti Huda Al Makky, Huda Tabbakh, Nosaba Sabbagh, Fatimah Sabbagh and Aunti Huda Tello for being of great support throughout my difficult times. Many thanks to Dr Harion Al Rashid, Dr Khalid Athgahfy, Dr Vineet Sivadasian and Eng. Hassan Awad for listening to me every day throughout the difficult days during the PhD period. Moreover, my warmest respect to Dr Torsten Howind, Dr Ahmad-Zoubi, Imran Shabbir and Cristina Rodriguez for their recognition of my research qualities and interest in working together. Furthermore I would also like to thank Dr Ahmed Haydar, Dr Fathia Abdoul Jawad, Mrs Iman Fakhani, Mrs Rana Nameah, Moutaz Al Zaeem, Mrs Mais Bakkar, Razan Othman, Shereen Mawed and Lama Walaya for their deep care, payers and sincere interest to my success. The list is long and many others have contributed to my success thank you all.

26 February 2016

This page is intentionally left blank



DECLARATION OF ORIGINALITY

I declare that this is an original study based on my own work and that I have not submitted it for any other course or degree.

A handwritten signature in black ink, which appears to read "A. Mackay", is written over a horizontal line.

Signature _____

This page is intentionally left blank

Abstract

Efficient respiration chambers have become an essential tool for biologists to determine carbon dioxide efflux from specific soil site locations in the last century. Respiration chambers measure the role of specific soil site locations on the global warming issue. Measurement deviations of the carbon dioxide efflux do occur in closed static/dynamic respiration chambers as reported by many researchers. This is attributed on many occasions to occurring external meteorological disturbances while measurements are taken. The ultimate goal of the PhD project is to design a new static/dynamic respiration chamber that uses an available gas sensor to measure carbon dioxide efflux resulting from soil biological activity furthermore to develop software with interface for data analysis. In the past few year's improvements in gas sensor technology and available commercial chambers have created a new approach to the technology of measuring soil efflux. Several respiration chamber designs in this research are proposed. It is followed by experimental rig selection and design optimisation is followed. An innovative portable device is made it uses a novel sampling tube connected to a newly developed non-dispersive infrared gas sensor. Experiments on a grassland location using the chamber where done. Computational fluid dynamics is applied to the study to model mass transfer and fluid flows by using ANSYS commercial software. This is for the purpose to check accurate efflux readings can be modelled in the respiration chamber. A remarkable agreement between experimental and numerical results was achieved meaning that CFD can be used to develop future respiration chamber designs.

This page is intentionally left blank

List of Symbols and Abbreviations

- Abbreviations

BC	<i>Boundary Condition</i>
CAD	<i>Computer Aided Design</i>
CFD	<i>Computational Fluid Dynamics</i>
DNS	<i>Direct Numerical Simulation</i>
EC	<i>Eddy Covariance</i>
GPP	<i>Gross Primary Production</i>
IRGA	<i>Infra-Red Gas Analyser</i>
LES	<i>Large Eddy Simulation</i>
PIV	<i>Particle Image Velocimetry</i>
RANS	<i>Reynolds-Averaged Navier-Stokes</i>
SPAC	<i>Soil-Plant-Atmosphere-Continuum</i>
USDA	<i>United States Department of Agriculture</i>
PDE	<i>Partial Differential Equation</i>
CFL	<i>Courant–Friedrichs–Lewy</i>
rms	<i>Root Mean Square</i>

This page is intentionally left blank

- Roman Symbols

Symbol	Description	Units
A	Sample area cross section	$[m^2]$
A_s	Covered soil surface area by chamber	$[m^2]$
A_f	Flow obstructing chamber area	$[m^2]$
A_{si}	Soil surface interface area	$[m^2]$
A_{Fan}	Fan outlet blowing area	$[m^2]$
A_{inner}	Covered soil surface area by chamber	$[m^2]$
$A_{Soil Area}$	Bacteria location soil surface area	$[m^2]$
A'	Infinitesimal planar control surface	$[m^2]$
A_n	Area of a single pore	$[m^2]$
a_{nm}	The amplitude of the pressure wave with nth	$[Pa]$

	period and mth wave length	
a_1	Macro-pores constant for the permeability equation	[1]
a_2	Meso-pores constant for the permeability equation	[1]
a_3	Micro-pores Constant for the permeability equation	[1]
\mathbf{B}	Body force vector	[N]
C	Carbon dioxide constants in Sutherland equation	[K]
C_D	Drag force coefficient	[1]
C_w	Dissolved gas concentration in water	[mole/m ³]
C_0	Solute concentration at the cell surface	[mol/m ³]
C_b	Solute concentration in bulk soil	[mol/m ³]
$C_{\epsilon 1}$	K-Epsilon model constant	[1]

$C_{\epsilon 2}$	K-Epsilon model constant	[1]
C_{μ}	K-Epsilon model constant	[1]
c	Soil heat capacity	[J/kgK]
c_v	specific heat capacity for air at constant volume	[J/kgK]
C_{pw}	Correction factor for water vapour emissivity	[1]
C_{pc}	Emissivity correction factor for carbon dioxide	[1]
D	chamber diameter	[m]
D_i	Circulation fan diameter	[m]
D_0	Solute diffusivity through bacterial cell	[m ² /s]
D_{CO_2}	Carbon dioxide mass diffusion	[m ² /s]
D_{Fan}	Blowing fan diameter length	[m]

D_{CO_2}	The gas diffusion coefficient for carbon dioxide	$[m^2/s]$
D_e	Effective gas diffusion coefficient	$[m^2/s]$
$D_{(CO_2)_0}$	Diffusion coefficient at reference state	$[m^2/s]$
D_n	Total Integrated area for permeability function	$[m^2]$
D_{sand}	Sand grain diameter	$[m]$
D_{silt}	Silt grain diameter	$[m]$
D_{clay}	Clay grain diameter	$[m]$
D_{total}	Total area of pores	$[m^2]$
d_{av}	The average pore diameter for a segment of pore sizes	$[m]$
d	Arrhenius Pre-exponential constant	Depends on order of reaction

\bar{d}	Average characteristic length scale for pores	Depends on order of reaction
d_{pe}	Arrhenius Pre-exponential constant	Depends on order of reaction
E	Exponential activation energy constant	[kJ/mole]
E_i	Biochemical processes activation energy	[kJ/mole]
$E_{f_{total}}$	None-dimensional form of the efflux	[1]
ef	efflux	[mole/m ² s]
ef_{soil}	Gas efflux for a soil layer	[mole/m ² s]
$ef_{chamber}$	Gas efflux	[mole/m ² s]
ef_{total}	Carbon dioxide total efflux	[mole/m ² s]
ef_{Plants}	Carbon dioxide efflux from plants	[mole/m ² s]
$ef_{Bacteria}$	Carbon dioxide efflux from bacteria	[mole/m ² s]

$ef_{tDynamic}$	Dynamic total efflux measurement	[mole/m ² s]
ef_{tStaic}	Total static efflux	[mole/m ² s]
$ef_{Location}$	Respiration quotients for different soil locations	[mole/m ² s]
ef	Soil efflux	[mole/m ² s]
ef_{BP}	Total efflux for a bacterial community	[mole/m ² s]
ef_{mcell}	Individual efflux from a single soil microbial cell	[mole/m ² s]
$ef_{Total\ Bacteria}$	Total generated efflux from aerobic bacteria at a specified location soil surface area	[mole/m ² s]
F_w	weight force	[N]
F_{wind}	Acting wind force	[N]
f	vortex shedding frequency	[Hz]

g	Earths gravitational acceleration	$[m/s^2]$
H	Chamber height	$[m]$
h	Lever arm for the wind force	$[m]$
h_o	O horizon thickness	$[m]$
\bar{h}	Average heat transfer coefficient for convection	$[W/m^2K]$
K	Shape factor	$[1]$
K_b	Constant	$[1]$
K_{Solu}	Solubility constant	$[L\ atm/mol]$
k	Soil permeability	$[m^2]$
k_c	Layer soil thermal conductivity	$[W/m\ K]$
K^{ij}	Area porosity tensor	$[1]$
K_{perm}	Permeability	$[m^2]$
K_{loss}	Empirical loss coefficient	$[1]$

L	Total thickness of the soil layer	[m]
L_h	Chamber total height	[m]
L_S	Characteristic dimension	[m]
M	Molar mass of dry air	[kg/kmole]
MW_{CO_2}	Carbon dioxide molecular weight	kg/kmol
N	Number of revaluations for the selected fan	[rpm]
N_b	Total number of bacterial cells	[1]
P	Soil surface interface pressure function	[Pa]
P_t	Total atmospheric pressure	[Pa]
P_k	Turbulence production	[m ² /s ³]
P_c	Carbon dioxide partial pressure	[Pa]

P_v	Vapour pressure	[Pa]
P_u	Fan power required in a respiration chamber	[W]
P_o	Standard pressure at sea level pressure	[Pa]
P_{in}	Chamber inside pressure	[Pa]
P_{av}	Average external pressure component	[Pa]
P_{fc}	Instantaneous external fluctuating pressure component	[Pa]
P_{TS}	Total atmospheric pressure at soil surface	[Pa]
P_{TB}	Total atmospheric pressure at soil depth	[Pa]
P_{atm}	Atmospheric pressure	[Pa]
P_{out}	outside the atmospheric pressure	[Pa]

P_{CO_2}	Partial pressure for carbon dioxide	[Pa]
P_{CO_2s}	Partial atmospheric pressure of carbon dioxide at the soil surface	[Pa]
P_{TS}	Total top soil pressure (surface)	[Pa]
P_{TB}	Total bottom soil pressure	[Pa]
$P_{SurfaceCO_2}$	Carbon dioxide partial pressure at soil surface	[Pa]
$P_{BottomCO_2}$	Carbon dioxide partial pressure at soil bottom of soil layer	[Pa]
\dot{p}	modified pressure	[Pa]
P_1	Initial chamber pressure	[Pa]
P_2	Final chamber pressure	[Pa]
Q	Fan volumetric aeration rate	[m ³ /s]

Q_{con}	Heat conduction at the site location	[W]
Q_{abs}	Chamber absorbed heat	[W]
Q_{inc}	Rate at which radiation is incident on the surface	[W]
Q_{Fan}	Volumetric flow rate of a blowing fan	[m ³ /s]
Q_{total}	Total heat transfer at one location	[W]
Q_{Soilw}	Gained heat at the site location	[W]
Q_{emit}	Emitted radiation from the chamber surface	[W]
Q_{conv}	Heat convection at the site location	[W]
Q_{rad}	Heat radiation at the site location	[W]

Q_{Soilw}	Heat is transferred to the soil mass when a chamber is placed on location	[W]
Q_{totaln}	The summation of the total heat without a chamber	[W]
Q_{CO_2}	Carbon dioxide volumetric flow rate	[m ³ /s]
q	Soil layer heat source or sink term	[W]
q_{CO_2}	Darcean velocity	[m/s]
R	Ideal gas constant	[J/K mole]
R^{ij}	Resistance to flow in the porous medium	
Re	Boundary layer Reynolds number	[1]
Re_{cr}	Critical Reynolds number	[1]
Re_x	Boundary layer Reynolds number at distance x	[1]

Re_s	Reynolds number for soil (porous media)	[1]
RQ_n	Respiration quotient for a specific type of bacteria n	[1]
RQ_{GL}	Respiration quotient for grassland	[1]
$RQ_{Location}$	Respiration quotient for a specific location	[1]
$RQ_{Total\ Bacteria}$	Summation term for all bacteria respiration quotients	[1]
S	Diameter of a bacterial cell	[m]
S^H	Heat source or sink	
St	Strouhal Number	[1]
T	Temperature	[K]
T_s	Chamber outer wall shell temperature	[K]
T_a	Average soil temperature	[K]

T_i	Initial chamber temperature after closure	[K]
T_0	Carbon dioxide reference temperature	[K]
T_o	Sea level standard temperature	[K]
T_n	Summation of all torque components	[K]
T_c	Chamber gas volume temperature	[K]
T_{zt}	Soil temperature cyclic function of time and depth	[K]
T_{bl}	Soil temperature at bottom of the top layer	[K]
T_{ss}	Soil temperature at the surface interface with the atmosphere	[K]
T_{wind}	Wind torque	[Nm]

T_{weight}	Weight torque	[Nm]
T_{ins}	Soil temperature within layer	[K]
T_{Soil}	Soil temperature	[K]
$T_{\text{heatedair}}$	Average air temperature inside the chamber	[K]
$T_{\text{ChmaberWall}}$	Respiration chamber wall temperature	[K]
T_1	Inner chamber temperature at start of the measurement process	[K]
T_2	Inner chamber temperature at the end of the measurement process	[K]
t	Instance of time	[s]
\mathbf{U}	Vecloity vector field	[m/s]
\bar{U}	Average flow velocity at the studied location	[m/s]

u_{cr}	Critical blowing wind velocity	[m/s]
u_{∞}	free stream velocity	[m/s]
u_*	Friction velocity	[m/s]
V	Studied volume of soil	[m ³]
V_c	Chamber volume	[m ³]
V_e	Effective chamber volume	[m ³]
V_V	Soil void volume	[m ³]
V_g	Soil gas volume	[m ³]
V_l	Soil liquid volume	[m ³]
V_T	Soil sample Total volume	[m ³]
V_B	Soil bulk volume	[m ³]
V'	The volume available to flow in an infinitesimal control cell surrounding the point	[m ³]

v_{CO_2}	Average pore velocity for carbon dioxide	[m/s]
v_{rms}	Mean root square velocity	[m/s]
w	Frequency of the cyclic behaviour	[Hz]
w_i	Biochemical processes respiration	[mole/s]
x	The distance downwind is represented by x	[m]
X_m	Pressure wave length of m th wave in the X - direction	[m]
Y_m	Pressure wave length of m th wave in the Y- direction	[m]
Y_{CO_2}	Gas species concentration	[mole/m ³]
y	The crosswind distance is represented by Y	[m]
z	Soil depth elevation	[m]

z_{gs}	Distance from the soil surface to the tip of the gas sensor	[m]
z_0	Soil valid depth to apply the partial pressure equation	[m]
$\frac{q_{w-c}}{L}$	Chamber total rate of heat transfer per unit of length	[W/m]
$\frac{q_{c-c}}{L}$	Radiative heat transfer per linear (m) from the carbon dioxide to the chamber wall	[W/m]
$\frac{q_{total}}{L}$	Total radiant flux per unit length from the contained carbon dioxide and water vapour in the chamber to the heated air inside the chamber	[W/m]
$[CO_2]$	Concentration of carbon dioxide	[mole/m ³]

$[O_2]$	Concentration of oxygen	$[\text{mole}/\text{m}^3]$
$[CO_2]_S$	Molar concentration of carbon dioxide on the soil surface	$[\text{mole}/\text{m}^3]$
$[CO_2]_B$	Molar concentration of carbon dioxide at the bottom of the soil surface	$[\text{mole}/\text{m}^3]$

This page is intentionally left blank

- Greek Symbols

Symbol	Description	Units
α	Absorptivity of the chamber transparent shell	[1]
α_s	Carbon dioxide source term starting from the soil surface	mol/m ³ s
α_{gs}	Carbon dioxide source term starting from the soil depth	mol/m ³ s
α_{CO_2}	Source term for carbon dioxide	W/m ³
Γ_e	Effective thermal diffusivity	m ² /s
γ	volume porosity	[1]
δ	Soil constructivity	[1]
δ_t	Boundary layer thickness	m
∇p_{CO_2}	Carbon dioxide pressure gradient	Pa
$\Delta P_{in\ n}$	Chamber internal pressure term	Pa
$\Delta P_{in\ 1}$	Rise of internal chamber pressure due to rise of temperature	Pa

$\Delta P_{in 2}$	Rise of internal pressure due to blowing fans	Pa
$\Delta P_{out 1}$	External pressure perturbations	Pa
$\Delta P_{out n}$	Chamber outer pressure term	Pa
ΔQ	Heat gain or loss	W
ΔT	Chamber temperature	K
ϵ	Soil porosity	[1]
ε	Chamber surface emissivity	[1]
ε_r	Average rate of dissipation per unit mass	m^2/s^3
$(\epsilon_w)_1$	Emissivity of water vapour	[1]
$(\epsilon_c)_1$	Emissivity for carbon dioxide	[1]
$(\epsilon_w)_{actual}$	Actual gas emissivity from water vapour	[1]
$(\epsilon_c)_{actual}$	Actual emissivity for carbon dioxide in chamber gas volume	[1]
η	Kolmogorov length scale	m

η_w	Thermal efficiency for the process of heat transfer to a soil location without chamber cover	[1]
η_{wt}	Thermal efficiency for the process of heat transfer to a soil location with chamber cover	[1]
θ	Volumetric water content	m^3
μ	Air dynamic viscosity	Pa s
μ_e	Effective viscosity	Pa s
μ_{CO_2}	Carbon dioxide dynamic viscosity	Pa s
$\mu_{(CO_2)_0}$	Carbon dioxide reference dynamic viscosity	Pa s
ρ	Air density	kg/m^3
ρ_s	Density of the soil	kg/m^3
ρ_{CO_2}	Carbon dioxide gas density near the soil surface	kg/m^3
σ	Stephan Boltzmann constant	W. m. K^{-4}
σ_t	Time period	s

σ_k	K-Epsilon model constant	[1]
σ_ε	K-Epsilon model constant	[1]
τ	Soil tortisity	[1]
τ_p	Period of cycle	s
τ_w	Soil surface wall shear stress	Pa
ν	kinematic viscosity	m ² /s
ϕ_{xm}	The phase angle of mth wave in the x-direction	[1]
ϕ_{ym}	The phase angle of mth wave in the y-direction	[1]

This page is intentionally left blank

- Superscripts and Subscripts

Symbol	Description
\tilde{a}	Filtering operation
\bar{a}	Average operation
\grave{a}	Fluctuating operation

This page is intentionally left blank

Publications

Conference Paper

- A NUMERICAL AND EXPERIMENTAL STUDY OF A NEW DESIGN OF CLOSED DYNAMIC RESPIRATION CHAMBERS

A. Al Makky, A.G.Olabi, A.Alaswad, D.Gibson, and S. Song.

Journal Paper

- Prediction of the Gas Emission from Porous Media with the concern of Energy and Environment. Authors: A. Al Makky, A.Alaswad, D. Gibson, A. G. Olabi Article Type: Renewable & Sustainable Energy Reviews. (In print)

- Renewable Energy Scenario and Environmental Aspects of Soil Emission Measurements. Authors: A.Al Makky, A.Alaswad, D.Gibson, A. G. Olabi Article Type: Renewable & Sustainable Energy Reviews. (In print)

- A NUMERICAL AND EXPERIMENTAL STUDY OF A NEW DESIGN OF CLOSED DYNAMIC RESPIRATION CHAMBER

Authors: A.Al Makky, A.Alaswad, Des Gibson; A. G. Olabi

Article Type: Research Paper Environmental Pollution. (Accepted)

This page is intentionally left blank

Chapter 1

Introduction

1.1. Introduction

Carbon dioxide soil flux modelling in closed dynamic respiration chambers is a challenging task. This is attributed on many occasions to the very small concentrations of carbon dioxide being transported between soil and the atmosphere. This thesis describes the innovative portable device which was made exclusively to accurately measure carbon dioxide flux. The blowing fan creates a forced convective flow to occur in the chamber making the RANS turbulence model [1] a necessity to model the occurring flow in the gas domain, the Darcy model was used for the porous domain. A clear understanding of the measurement process was achieved through measuring all the important parameters in relation to time. A MATLAB code using soil physical models was written to help in linking the interaction of the many factors for such a complex process. The gathered simulation and experimental data are obtained through the use of ANSYS, MATLAB. A remarkable agreement between experimental and numerical results was achieved meaning that CFD can be used to develop future respiration chamber designs showing an absolute concentration rise of 100 [ppm] for carbon dioxide for a duration of 6 [min] measurement. The rational for this study is to interpret and quantify for a specific soil location how biologically produced carbon dioxide contributes to the green house affect. It is known by scientists that one of the physical properties of carbon dioxide contained in the atmosphere is that it reflects heat back to the earth's surface. Consequently, gradually the earth's atmosphere traps

more heat. Respiration chambers can be used to quantify the soil efflux they come in different shapes and sizes this depends on their application of use. They are composed of two main parts; namely the chamber shell and the gas sensor. To quantify the amount of produced carbon dioxide at one location, an enclosed cavity or space like a chamber is used. The main activity of the project is to study a respiration chamber, that is through proposing a Chamber design at the UWS, collecting experimental data from it, in addition to conducting CFD numerical simulations using ANSYS (to model the fluid flow) and applying physical models to the soil using a written MATLAB code at UWS this contributes in the ease of studying each case of concern. The chamber covers a circular area of the soil. Figure 1 shows the experimental apparatus the black box at the top represents the wireless gas sensor box.



Figure 1: The used designed chamber at UWS, located on the grass land site.

1.2. Respiration Chambers

An efflux is something that flows out or forth from a porous medium (Soil) which for our case of concern is carbon dioxide. Carbon dioxide produced in soil is due to occurring biological activity in it, measuring accurately the production of gas species from the soil is a complex problem using chambers.

Scientists know that no ideal experimental chamber exists [2], therefore the aim is always to reduce measured errors. That is due to the great spatial variability in soil emissions, and to the fact that the quantification of these emissions is complicated by the high spatial variability exhibited by many microbial processes [3]. Respiration chambers are produced both privately for research groups and by commercial companies.

Different types of chambers are available depending on the intended quantity to be measured as shown in Figure 2, the figure presents three examples of chambers produced by the LICOR Company with different design configurations. The transparent chamber is intended to be used to measure total flux from a specific location. It is automated to ventilate the chamber, while the none transparent one is the total flux excluding the flux resulting from photosynthesis process. The top hat type chamber is used for a quick site deployment where ventilation is conducted manually, mostly intended for soil flux measurements. The yellowish case is used for data collection and storage on the site of interest.



Figure 2: LI-8100A Automated Soil CO₂ Flux System and soil chambers provided by LICOR [4] .

1.3. Motivation

The rationale for this study is to improve our understanding of global warming through understanding the factors that control carbon dioxide production whereby that is achieved through the use of respiration chambers as shown in Figure 2. In the general context studying respiration chambers can give scientist some insight to how fertile the studied site is. That is by measuring the rate of carbon dioxide produced for a certain site of concern and predict its impact on global warming issue. Scientists using

these chambers can quantify the soil site carbon budget. The developed method can be used to validate other classical methods used in carbon dioxide measurements. The main activity of the project is to study a respiration chamber that is through proposing a design collecting experimental data from it. In addition to conducting CFD numerical simulations using ANSYS (to model the fluid flow) and applying physical models to the soil using a written MATLAB code for the project this contributes in the ease of studying each case of concern. The merits are reduction in research costs further more finding to what extents we can improve experimental result from obtained numerical results. Quantifying mass transfer occurring from in and out of the chamber in relation to occurring surrounding disturbance. The Potential challenges of the project are: Is its multi-disciplinary nature where: Soil Chemistry, Soil Biochemistry, Soil Geomechanics, Soil Physics, Atmospheric Meteorology, Soil Carbon Dynamics, Heat Transfer in Porous Media, Atmospheric Computational Fluid Dynamics, Computational Fluid Dynamics in Porous Media, Design of Chemical Process, etc. While the Potential outcomes of the project include a: comprehensive understanding of external disturbances (The external disturbances are blowing winds, pressure, rain, etc) impact on the measurement of the carbon efflux in addition to this study providing the methodology to study other greenhouse gases of interest in future. Unfortunately, external disturbances cause deviations of concentration measurements. These deviations in measurements case over or under prediction of the measured efflux depending on the type of used chamber. This challenge applies to all measured species not one species specifically [5] . As shown in Figure 3 external disturbances (shown in red) can cause deviations from the predicted carbon dioxide concentration profile

(shown in blue). Hence the numerical data proves that CFD is a reliable too to produce good results as we will later see in chapter 5.

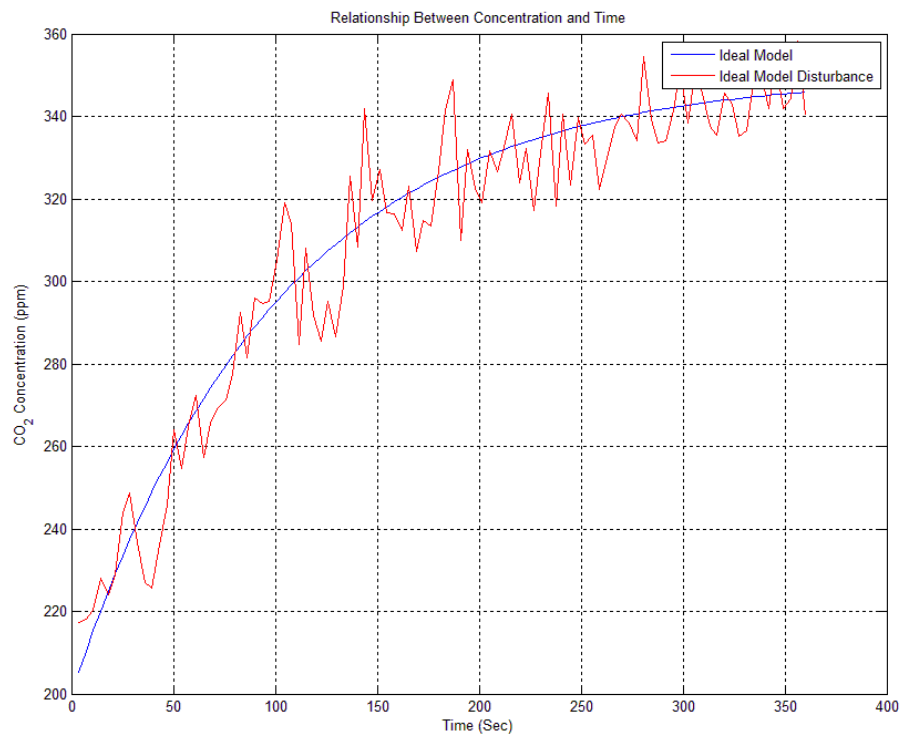


Figure 3 : An example case of measured carbon dioxide concentrations in relation to time in, the blue curve represents the ideal case and the red curve represents the disturbed measurement.

1.4. Thesis Objectives

The literature review part of this thesis surveys the relationship of soil respiration efflux with many other disciplines. These are mainly soil physics, soil chemistry, soil biology, heat transfer, geotechnics, meteorology and gas sensors technology. The thesis objectives are illustrated in the following bullet points:

- 1- To derive several forms of efflux equations to link soil physical mechanisms, parameters and soil biological and types of soil textures that affect soil biological efflux respiration.

-
- 2- Developments of chamber design that measure biologically generated carbon dioxide effluxes from soils.
 - 3- Producing an innovative portable device to measure carbon dioxide efflux
 - 4- Developing software code within MATLAB environment.
 - 5- Modelling the mass transport using CFD (ANSYS).
 - 6- Validation of the software code with experiments.

1.5. Thesis Layout

This thesis draws on the results reviewed in the previous section and is organised as follows.

Chapter 1: This chapter provides an introductory description of the drive of this study in addition to project objectives. Likewise, a brief description of available respiration chambers in addition to the made respiration chamber used to measure carbon dioxide efflux is presented. Finally, a thesis outline is given.

Chapter 2: This chapter covers the latest available literature relating to static and dynamic chambers. This is done through firstly covering the soil efflux model. Secondly comes surveying the surrounding parameters that disturb the efflux. This is followed by respiration chamber shape considerations operational mode and design regulation. For the reason that gas sensors serve to be the back bone of the measurement process they are discussed focusing specifically on location of installation and calibration. From the surveyed parameters that affect efflux measurement and production chamber internal temperature and pressure effects are

discussed thoroughly. To reduce gas leakage from within the respiration chamber methods of chamber anchoring or insertion into the soil are. Finally, the role of soil pH/Bacteria on carbon dioxide production and transport in soil is presented.

Chapter 3: This chapter covers the design requirements for respiration chamber design, five respiration chamber designs are proposed. The selection criteria for the agreed upon design is considered. A detailed description of all the main parts of the chamber is covered. The site climate location description is studied by surveying the meteorological parameters.

Chapter 4: This chapter covers both the numerical model used to model the flow inside the gas volume represented by the K-Epsilon model. Likewise, the chapter covers the Darcy model used to model the flow inside the porous domain. The selection of the porous domain simulation input parameters is shown. This is illustrated by the developed approach used to calculate soil permeability. Also specified later how soil porosity values are selected for the studied grass land location.

Chapter 5: This chapter covers all the obtained experimental results from the respiration chamber. The data is analysed in detail for all the measured parameters furthermore three main CFD simulations are studied. The study is done for a static chamber case, dynamic chamber case and finally for a dynamic chamber case with a rotating fan mesh.

Chapter 6: This chapter covers the work conclusion with research future work.

Chapter 2

Literature Review

2.1. Introduction

Soil can be defined as a complex system, consisting of a mixture of organic and mineral particles, soil solution and air, resulting from the interaction between biotic and abiotic factors; it is the medium in which plants acquire water and nutrients through their roots system. An efflux is something that flows out or forth from a porous medium (Soil) which for our case of concern is carbon dioxide. Carbon dioxide gas in the soil is produced due to the occurring biological activity in the soil domain. Measuring accurately the production of gas species from the soil is a complex problem. This is due to the great spatial variability in soil emissions and to the fact that the quantification of these emissions is complicated by the high spatial variability exhibited by many microbial processes [6]. What also enforces the spatial variability is that soil chemical composition varies from one location to another [7]. To quantify the amount of the produced carbon dioxide at one location it is captured in an enclosed cavity or space which can be a chamber. This method was first proposed by Henrik Lundegardh [8] in the form of the respiration bell. In the general context using respiration chambers can give scientists some insight to how fertile the site of concern is. That is by measuring the rate of carbon dioxide produced for a certain site of concern and predict its impact on global warming issues [9]. Consequently with the increase of carbon dioxide concentrations in the atmosphere, planet earth responds to

it in the form of the green house affect [10]. This has lead scientists to use numerical nonlinear models to predict future concentrations of carbon dioxide in the atmosphere [11], on the other hand others used more sophisticated models such as the dynamic global vegetation model [12] as shown in Figure 4.

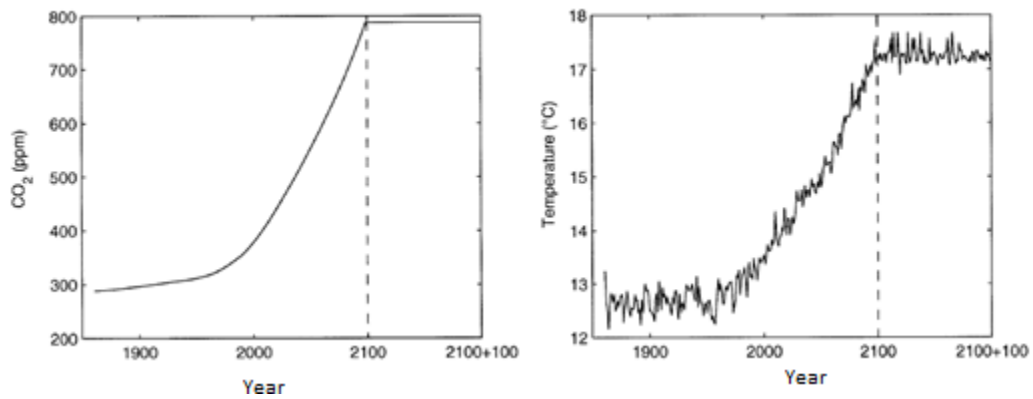


Figure 4: IPCC IS92a projections of atmospheric carbon dioxide concentrations and temperature in relation to number of years and the HadCM2 SUL climate model simulations of temperature over land (excluding Antarctica).

The used chamber methods have been surveyed and new methods proposed since the early 80s [13] with growing interest in the global warming issue, Kyoto protocol. Scientists using these chambers can quantify the soil site carbon budget [14]. With the increase of carbon dioxide concentrations in the atmosphere, planet earth responds to it in the form of the green house affect [10]. For instance global warming is attributed to burning excessive amounts of fossil fuels [15] it is also linked to the rise of human population around the world. Therefore using sustainable sources of energy to support the growing in population nations comes of priority for future, as the study showed for the country of Sudan [16]. A matter of immediate concern in the hazardous energy situation in most African countries is that forest resources are gradually declining. The

supply of fuel wood is becoming more difficult to sustain and demand especially that it is already exceeding the potential supply [17]. Therefore one of the main requirements of green energies is to be characterised as efficient systems furthermore for governments to apply policies that make citizens gradually use less fossil fuels [18]. As a result, new fuels are being introduced to the global market as for example in Malaysia palm oil is considered a sustainable source of fuel particularly that palm oil is one of the most productive bio-diesel crop. Moreover, its waste streams can be used to produce vast amounts of bio-gas and other values added products [19]. Likewise another sustainable type of fuel is ethanol what was evident that more research needs to be applied to get convincing proofs of its environmental friendliness as shown in the comparison between E10 and E0 [20].

On the other hand, another approach to reduce carbon dioxide emissions is to lessen the industrial source of the gas. This is by using renewable sources of energy whereby wind power seems to be an attractive option as stated by [21]. Another source of sustainable source of energy is microalgae as a biodiesel fuel. It is still in the phase of development [22] one of the main outstanding challenges is the reduction of its production cost. With the gradual growth of available computational resources many optimization algorithms are being proposed by scientists. This is to manage renewable energy sources according to its availability characteristics [23]. A way to assess renewable sources of energy is to apply exergetic analysis on them as suggested by Hepbasli [24]. Likewise life cycle assessment is also necessary for renewable source of energy [25] as an example for electrical generation systems. It is noted by Alanne

et al. [26] that the energy system of the future is going to be a mixture of centralized and distributed sub-systems, operating parallel to each other.

Scientists have an option to choose from several methods for measuring soil carbon dioxide efflux. They can be summarised into four methods, starting with the chamber soda lime [27] or alkali solution method which absorbs the respired carbon dioxide from the soil, it is an easy and cheap method to apply. The second method is by using the soil carbon dioxide gradient system method [28], generally this method is much complicated and not easy to setup. It requires the insertion of the gas sensors inside the soil layers of the studied location. This action disturbs the location integrity in addition to that gas sensors are expensive. The third method is the Eddy covariance method sometimes referred to as micrometeorological method [29], the positive point about it that it doesn't disturb the location of study, because all the necessary sensors are attached to a tower overhead the location of study. This method can be regarded as an expensive method and represents a more attractive option to measure carbon dioxide emissions from spacious locations such as farmlands or from plant community canopy emissions can also be studied taking advantage of the tower setup. Finally, the fourth method is by using respiration chambers that use gas sensors such as infra-red gas sensors. These chambers are easy to use and setup, they do introduce disturbance to the soil surface upper crust when using the chamber fixture method such as the clamp method. The developed methods can be used to validate and calibrate other classical methods used in carbon dioxide measurements. After surveying hundreds of publications in this area, the researcher would realize the problem of under or over prediction of measured efflux, as an example [30] due to external turbulence.

2.2. Soil Carbon dioxide efflux Model

Through the discussion of simple analytical models to calculate carbon dioxide flux in reference [31] stated that 75% of the efflux comes from the top 20 cm of the soil. This means that the atmospheric soil interface is the place to start building the numerical model. Any site location has a set of standard soil layers that have been characterized by geotechnical engineers.

2.2.1. Chamber Gas Volume efflux

By considering the most biologically activate layer near the top soil surface can help in modelling the produced efflux. Assuming no external disturbances occur and by applying Fick`s first law in in the z direction. The considered ideal efflux is the static efflux, which represents a steady case where the species concentration profile does not change with time. Applying Fick`s first law [32]on the gas part of the chamber results in equation (2.1). Where ef_{chamber} is the gas flux [$\mu\text{mol m}^{-2}\text{s}^{-1}$]. The term D_{CO_2} is the gas diffusion coefficient for carbon dioxide in the contained air in the chamber [m^2s^{-1}]. Gas diffusion is a function of temperature, once the chamber average temperature is obtained gas diffusion can be found Cussler [32].

$$ef_{\text{chamber}} = -D_{\text{CO}_2} \frac{\partial Y_{\text{CO}_2}}{\partial z} \quad (2.1)$$

Trace gas species concentration Y_{CO_2} [$\mu\text{mol m}^{-3}$] is a function of elevation z [m] inside the chamber and can be represented by equation (2.2), the distance z_{gs} [m] is from the soil surface to the tip of the gas sensor. The carbon dioxide source term starting from the soil surface is α_s [$\mu\text{mol m}^{-3}\text{s}^{-1}$], this term incorporates soil bacterial, plant root, and plant leaf activity.

$$Y_{\text{CO}_2} = \frac{\alpha_s}{2D_{\text{CO}_2}} (z_{\text{gs}}^2 - z^2) \quad (2.2)$$

2.2.2. Soil Volume efflux

Fick's first law can also be applied to the soil part entrained under the chamber [33] as shown in equation (2.3) for simplicity it can be applied for one standard soil layer. The gas efflux for a soil layer is ef_{soil} [$\mu\text{mol m}^{-2}\text{s}^{-1}$]. The effective gas diffusion coefficient D_e [m^2s^{-1}] as proposed by Koorevarr et al. [34] for carbon dioxide in the air in the soil pores. The trace gas concentration Y_{CO_2} [$\mu\text{mol m}^{-3}$] is a function of the vertical position z (m) in the soil:

$$ef_{\text{soil}} = -D_e \frac{\partial Y_{\text{CO}_2}}{\partial z} \quad (1.3)$$

The controlling parameters of D_e are presented in equation (2.4) where ϕ is the air porosity in the soil location. The term δ is soil constructivity which usually takes a value of 0.9 to 1, it depends on how compact are the fine soil particles are at the location. Soil tortisity is represented by τ and takes values from 0.5 to 6 as Cussler [32] it all depends on the effective pore diameters created by rocks in the soil layer:

$$D_e = \frac{\tau D_{\text{CO}_2} \phi}{\delta} \quad (1.4)$$

Equation (2.3) can be extended to consider several layers of soil. During the sampling duration of an experiment heat affects the diffusion process in both the chamber gas entrainment and the covered soil by the chamber. The diffusion coefficient for two states can be found relying on Cussler [32], looking at equation (2.5) the diffusion

coefficient for carbon dioxide at the studied state is $D_{\text{CO}_2}[\text{m}^2/\text{s}]$ while for the reference state is $D_{(\text{CO}_2)_0}[\text{m}^2/\text{s}]$. The reference temperature is T_0 [K] while the reference pressure P_0 [Pa]. The studied case temperature is T [K] while the studied state pressure is P [Pa].

As evident the diffusion coefficient for carbon dioxide is proportionally related to the temperature term $T^{3/2}$ while it is disproportionally connected with the pressure term P [Pa]. Soil either gains heat or losses it depends on the daily cyclic heat pattern, diffusion in soil cavities is enhanced by temperature rise as shown in the following equation:

$$D_{\text{CO}_2} = D_{(\text{CO}_2)_0} \left(\frac{T}{T_0} \right)^{3/2} \frac{P_0}{P} \quad (2.5)$$

Equation (2.5) proves that the diffusion coefficient in soil cavities is proportionally related to small pressure changes, hence low-pressure atmospheric disturbances contribute to measured efflux deviations. It also proves the temperature sensors need to be used at locations inside the soil layer.

By substituting equations (2.3) and (2.4) into the Reynolds transport equation the relation of concentration and soil depth can be found in equation (2.6). The trace gas concentration in the soil is $Y_{\text{CO}_2} [\mu\text{mol m}^{-3}]$ and z_d [m] is the vertical position from the soil depth to the soil surface.

The carbon dioxide source term starting from the soil depth is $\alpha_{\text{gs}} [\mu\text{mol m}^{-3}\text{s}^{-1}]$, this term can incorporate soil bacterial and plant root activity.

$$Y_{\text{CO}_2} = \frac{\alpha_{\text{gs}}\delta}{2\tau D_{\text{CO}_2}\phi} (z_d^2 - z^2) \quad (2.6)$$

In conclusion static chambers rely mainly on diffusion for mass transport which is a kinematic property as seen in equations (2.1) and (2.3). Both equations are used for a steady state case where the efflux does not change with time, which is by taking two concentration measurements at the start and end of the soil layer. Equation (2.3) is used in the soil gradient method.

Equations (2.2) and (2.5) main advantage is they can easily model the concentration profile inside the chamber and in a soil layer as a function of elevation. Consequently, by curve fitting the experimental data the volumetric source term α_{gs} in equation (2.6) can be found. Experimentally this link between the soil and chamber entrainment efflux has been verified by [35] showing a relationship between efflux and soil parameters covered in equation (2.6). That was by capturing the carbon dioxide concentration plots in relation to soil depth inside the chamber and soil.

Some researchers [36] proposed in order to get accurate efflux measurements is to decompose the carbon dioxide total efflux ef_{total} into different flux components relating to the different sources of it in the soil as shown in equation (2.7), relating to sources ranging between plant, root and microbial fluxes.

$$ef_{\text{total}} = \sum_1^N ef_n = ef_{\text{Bacteria}} + ef_{\text{Plants}} + \dots + ef_N \quad (2.7)$$

For a conducted experiment when data analysis comes in place the none-dimensional form of the efflux Ef_{total} can be applied when using dynamic chambers, this is shown

in equation (2.8). The dynamic total efflux measurement $ef_{tDynamic}$ is normalized by the total static efflux ef_{tStaic} .

$$Ef_{total} = \frac{ef_{tDynamic}}{ef_{tStaic}} \quad (2.8)$$

Rochette et al [37] use equation (2.9), it can be derived from the Reynolds transport equation. It represents the case of rise of carbon dioxide concentration in relation to time in a respiration chamber from ambient concentration to the state of species saturation. The state of species saturation in the chamber is identified when any discrete increase in concentration doesn't change the efflux slope.

The power of this model is that it can be applied to an unsteady case for both a closed static or dynamic chamber. Concentration is measured in relation to time this is represented by the derivative $\partial Y_{CO_2} / \partial t$ [mole/m³s] with time. While V_c [m³] is chamber volume and A_s [m²] covered soil surface area by chamber:

$$ef = \frac{V_c}{A_s} \frac{\partial Y_{CO_2}}{\partial t} \quad (2.9)$$

A linear regression model is applied to curve fit the experimental data where equation (2.9) can also be extrapolated. Its simplicity comes from that it constitutes to several process (biological, mass convective and diffusive) occurring inside the chamber and location soil. Things become more complex for an unsteady case inside the chamber when species diffusion and convection are considered in the model as shown in equation (1.10):

$$\begin{aligned} \frac{\partial \rho Y_{CO_2}}{\partial t} + \rho \left(u \frac{\partial Y_{CO_2}}{\partial x} + v \frac{\partial Y_{CO_2}}{\partial y} + w \frac{\partial Y_{CO_2}}{\partial z} \right) & \quad (2.10) \\ = D \left(\frac{\partial^2 Y_{CO_2}}{\partial x^2} + \frac{\partial^2 Y_{CO_2}}{\partial y^2} + \frac{\partial^2 Y_{CO_2}}{\partial z^2} \right) + \alpha_s & \end{aligned}$$

Equation (2.10) is not feasible to be solved by hand. It is solved using numerical methods, solving it by hand is very tedious and time consuming. Hence this requires the use of computational fluid dynamics software.

2.2.3. Soil efflux Relating to RQ

One way for developing efflux models is to consider grass land physical and geo-mechanic properties to build the model. A grass land is regarded by the scientific community as an ideal case for optimum biological activity [38], besides the idea that vast areas of planet earth are covered by grass [39]. By measuring the carbon dioxide production, atmospheric oxygen consumption can be measured for a certain location. The consumption of oxygen all depends on the studied site soil structure, meaning that aeration is important for the production of carbon dioxide. The respiration quotient [40] in equation (2.11) is defined as the ratio of $[CO_2]$ Produced $[mol/m^3s]$ over $[O_2]$ Consumed $[mol/m^3s]$ for a pre-defined volume of soil:

$$RQ_{Location} = \frac{[CO_2]}{[O_2]} \quad (2.11)$$

The Respiration quotient for a specific location such as a grassland land [41] is $RQ_{GL} = 1.3 [mol CO_2 mol^{-1} O_2]$. Researchers have already found the respiration quotients for different soil locations (grassland, peatland, forest site, rangeland, etc.). Hence site location oxygen consumption can directly be found instantaneously when

the carbon dioxide efflux is measured. Proving that each location has its characteristic efflux is based on substituting equation (2.11) into (2.9) which gives equation (2.12)

$$ef_{\text{Location}} = \frac{V_c}{A_s} [O_2] RQ_{\text{Location}} \quad (2.12)$$

2.3. Soil Parameters that affect CO2 efflux

The soil carbon dioxide efflux challenge can be summarized into four research lines mentioned by Kutsch et al. [8]: soil chemistry, physical mechanism, physiological research line and the ecological research line. The soil chemistry research line will be covered in section 2.10. The ecological research line will focus on resilience ecology. The physiological research line that focuses on the environmental interactions with soil as mentioned by Smith et al. [42, 43] which have connected soil efflux to soil biology and physics. Bulk density is an indicator of soil compaction and soil health as found by Pengthamkeerati et al. [44]. Carbon dioxide is produced by the living organisms in the soil at different scales [45], organisms activity is governed mainly by temperature, minerals, air and water content. Any of these factors if not provided in a substantial quantity has an impact on the metabolism process. Mainly the focus here in this section is the physical mechanism whereby the recommended approach to study the physical mechanism is very much like the one adopted by Sanci et al. [46] for a dynamic chamber case. An artificial experiment is built that has all the soil parameters that affect the efflux, then exploring the direct and indirect effects of them by changing their values to see what soil efflux changes occurs. The conclusion from the paper in simple context is that carbon dioxide fluxes are governed mainly by the constraints of

soil structure (excluding external disturbances such as atmospheric temperature and pressure). Another approach taken Butnor et al. [47] is to apply a sensitivity analysis case to the soil parameters of interest, where by fixing several parameters and changing one in reasonable ranges can give good results for efflux predictions.

In conclusion it seems to be evident that what controls the carbon dioxide mass transport process is the existing cavities within the soil as mentioned by [48, 49]. These are indicated to explicitly by soil air porosity while in a more general concept soil permeability.

2.3.1. Soil efflux relation to Reynolds Number

The change in quantities of water, air, soil temperature, soil chemical constituents with time controls the efflux intensity. That is evident from the Darcy equation [50], it is usually used to model the occurring mass transport process in soil. Mainly researchers apply it for calculating incompressible liquids such as for water, but it can also be applied to compressible fluids such as air, carbon dioxide, etc. By applying the Darcy equation specifically for carbon dioxide results in equation (2.13). This is for a specified volume of soil with one of its inlets located at the bottom of the soil layer (O Horizon) and outlet is located at the soil interface with the atmosphere. The parameters that govern the transport properties are gas viscosity: μ_{CO_2} [Pa. s]. The soil layer depth thickness is taken as L [m], The soil sample permeability k [m^2]. The sample area cross section is referred to as A [m^2]. The carbon dioxide partial pressure difference is taken at two points of the O Horizon, the first at the soil surface $p_{\text{SurfaceCO}_2}$ [Pa] and the second at the bottom of the soil layer p_{BottomCO_2} [Pa]. All this leads to calculate the

carbon dioxide volumetric flow rate Q_{CO_2} [m^3/s], considering the flow direction from inside the soil to the atmospheric interface:

$$Q_{CO_2} = -\frac{kA}{\mu_{CO_2}} \frac{(p_{SurfaceCO_2} - p_{BottomCO_2})}{L} \quad (2.13)$$

Carbon dioxide partial pressure difference can be calculated by measuring the total pressure at two points. The top soil pressure (surface) is P_{TS} [Pa], and the bottom soil pressure is P_{TB} [Pa]. Likewise molar ratios are used to represent carbon dioxide concentration at both the soil surface and at the bottom of the soil layer:

$$p_{SurfaceCO_2} - p_{BottomCO_2} = \frac{n_{SurfaceCO_2}}{n_t} P_{TS} - \frac{n_{BottomCO_2}}{n_t} P_{TB} \quad (2.14)$$

By applying equation (2.14) into (2.13) gives equation (2.15) where molar concentration on the soil surface is $[CO_2]_S$ and at the soil bottom layer is $[CO_2]_B$:

$$Q_{CO_2} = -\frac{kA}{\mu_{CO_2}} \frac{([CO_2]_S \cdot P_{TS} - [CO_2]_B \cdot P_{TB})}{L} \quad (2.15)$$

By multiplying both sides of the equation by carbon dioxide density and dividing by (cross sectional area and carbon dioxide molecular weight) the efflux equation becomes (2.16):

$$ef = -\frac{k \cdot \rho_{CO_2}}{MW_{CO_2} \cdot \mu_{CO_2}} \frac{([CO_2]_S \cdot P_{TS} - [CO_2]_B \cdot P_{TB})}{L} \quad (2.16)$$

The Darcean velocity q_{CO_2} [m/s] can be calculated from equation (2.17):

$$q_{\text{CO}_2} = -\frac{k}{\mu_{\text{CO}_2}} \nabla p_{\text{CO}_2} \quad (2.17)$$

Hence by applying the pressure derivative to equation (2.17) leads to (2.18):

$$q_{\text{CO}_2} = -\frac{k}{\mu_{\text{CO}_2}} \frac{([\text{CO}_2] \cdot P_{\text{TS}} - [\text{CO}_2]_0 \cdot P_{\text{TB}})}{L} \quad (2.18)$$

The average pore velocity for carbon dioxide can be calculated using equation (2.19).

This is by knowing the soil air porosity value ϕ and the Darcian velocity v_{CO_2} [m/s]

in the soil:

$$v_{\text{CO}_2} = \frac{q_{\text{CO}_2}}{\phi} \quad (2.19)$$

Substituting equation (2.18) into equation (2.19) results in equation (2.20) which shows the relationship between average flow velocity for carbon dioxide with porosity and permeability:

$$v_{\text{CO}_2} = -\frac{k}{\mu_{\text{CO}_2} \phi} \frac{([\text{CO}_2] \cdot P_{\text{TS}} - [\text{CO}_2]_0 \cdot P_{\text{TB}})}{L} \quad (2.20)$$

With occurring pressure gradients on the soil surface produced by blowing winds, suction occurs at one location and blowing occurs at another what connects both points are the soil gas cavities, this pressure difference between two points in response creates a flow in the various soil layers, for simplicity it can be very much described as underground mine ventilation principle. This is for the reason that soil structural cavities are connected in a random manner.

For the case of microscopic fluid dynamics [51] energy transfer in the fluid is accomplished by molecular interaction (diffusion). This is where the average pore velocity q_{CO_2} and the average characteristic length scale for pores \bar{d} . The Reynolds number for soil (porous media) is given by equation (2.21):

$$Re = \frac{\rho_{CO_2} q_{CO_2} \bar{d}}{\mu_{CO_2}} \quad (2.21)$$

The viscous forces dominate over the inertia forces and only the local geometry influences the flow. Knowing that the average pore velocity is in equation (2.19) then substituting it into the Reynolds number (2.21) gives:

$$Re = \frac{\rho_{CO_2} \tau v_{CO_2} \bar{d}}{\mu_{CO_2} \emptyset} \quad (2.22)$$

By substituting equation (2.20) into (2.22)

$$Re = \left| \frac{k \rho_{CO_2} \tau \bar{d}}{(\mu_{CO_2} \emptyset)^2} \frac{([CO_2] \cdot P_{TS} - [CO_2]_0 \cdot P_{TB})}{L} \right| \quad (2.23)$$

Or by substituting equation (2.23) into (1.16) the researcher can find the relationship between the Reynolds number and the carbon dioxide efflux as shown in equation (2.24):

$$ef = Re \frac{1}{\tau \bar{d}} \frac{\mu_{CO_2} \emptyset^2}{MW_{CO_2}} \quad (2.24)$$

In porous media the flow can be characterized according to 4 regimes stated by Kaviani [52]. The process is achieved by using the Reynolds number shown in

equation (2.22). The power of the derived equation (2.24) can give hints to what type of flow type is occurring in the soil according to the measured efflux values. So for the first case of a Darcy or creeping flow regime it occurs when $Re < 1$. Subsequently for the second case is the inertial flow regime which occurs in ranges of $1 - 10 < Re < 150$. Meanwhile for the third case of an unsteady laminar flow regime it falls in the range of $150 < Re < 300$. Finally, the fourth case is the unsteady or chaotic flow regime condition when $Re < 300$.

Considering the geometrical parameter's to be fixed, external disturbances represented by the pressure term P_{TS} in equation (2.18) contributes to the transport process through the soil.

Occurring blowing winds over the soil inflict changing wall shear stress over the soil creating regions of positive and negative pressure gradients, this was proved by Ling et al. [53] for a case of mercury vapour. An interpretation of this efflux underestimation was mentioned by Butnor and Johnsen [54], who stated that the effective chamber volume $V_e[m^3]$ being measured is the volume of the chamber $V_c[m^3]$ including the volume of the air-filled spaces near the soil surface $V_s[m^3]$ where \emptyset is air porosity, this crystalizes equation in the following form (2.25):

$$ef = \frac{V_s \emptyset + V_c}{A_s} \frac{\partial Y_{CO_2}}{\partial t} \quad (2.25)$$

To overcome this problem of emission underestimation Venterea [55] have derived mathematical models to study the variables. Top surface soil litter dynamics dose affect soil respiration as reported by Valentini et al. [56], forest sites have less

vegetation cover and more of plant dead litter [57] likewise they are characterized with high water drainage rates [58] meaning that forest sites have a lower efflux in comparison with grassland locations as proven by Smith and Johnson [59]. Xu and Baldocchi [60] have opted to measure grasslands efflux at different locations between Mediterranean and Californian grassland locations.

This helps to see what deviations by using the proposed model would occur between the two locations that unite in the same category of classification. This leads to the conclusion that each site has its own characteristic efflux. This pattern becomes recognizable with experiments conducted on different site locations; as a result, effluxes can be fitted into site categories (grassland, peatland, forest Site, rangeland, etc.).

It was also stated by Subke et al. [61] that when using a dynamic chamber, if the amount of organic carbon available for microbial decomposition remains unchanged, the total amount of carbon dioxide efflux will remain constant. It is known that a segment of the total flux is produced by plant photosynthesis, the photosynthesis efflux depends on the density of the vegetation cover in the studied location.

This has led commercial companies to make different types of chambers according to the required intended flux to measure as an example: SRC-1, LI-6400, SRC-MV5, CFX-2, etc. The apparatus LI-6400XT is shown on Figure 5.



Figure 5: Licor`s developed apparatus that measures photosynthesis LI-6400XT [62].

2.4. Respiration Chamber Shape, Operation Mode and Design Regulations

Many commercial companies have introduced different chamber designs, (e.g. LI-COR) as shown in Figure 6 to measure carbon dioxide fluxes and other gases of interest such as (CH₄, NO_x, etc.), these have been developed and regular functionality bugs have been resolved for the end user.



Figure 6: Available commercial chambers by Li-COR LI-8100A Automated Soil Gas Flux System [63].

An agreement in the research community is noticed on the four shape configurations of cube, cuboid, cylinder and hemisphere for small and medium sized chambers; for large applications other configurations have been surveyed by [64] such as the 8 greenhouse types shown in Figure 7. Unfortunately the majority of commercial chambers are still expensive [65]. There are four common chamber operating regimes for the ones that use gas sensors in the market today; all revolve around the following four working modes [8]: closed dynamic, closed static [66], open dynamic and open static.

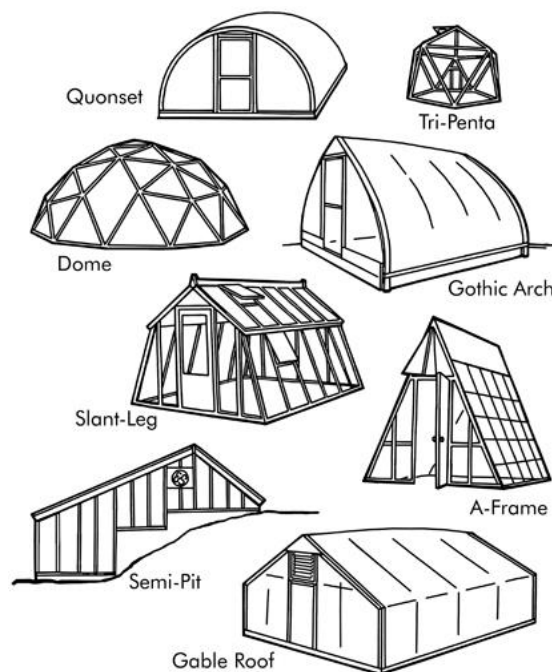


Figure 7: The eight types of greenhouse configurations [64].

The closed chamber approach is where the chamber is placed over the soil without the existence of any opening to the atmosphere from the chamber's outer shell. The open chamber method is where holes exist in the chamber's shell to achieve pressure equilibrium between inside and the outside atmosphere likewise the same applies to

temperature and species concentration. The term static refers to a chamber that either has a switched off fan or no fan at all, while dynamic refers to the existence of a gas mixture circulation method that can be an internal blowing fan or an external environmental system.

The four working modes have been studied and site suitability operation mode according to site properties has been found [67]. Operational mode is based on steady or unsteady mode flow conditions meaning that when no induced flow is occurring in the chamber and diffusion is dominant then it can be regarded as a steady state case, while for a case of induced convection with blowing fans in the chamber a turbulent flow pattern would occur in the chamber characterizing it as an unsteady state. The proposal to use automated closed chambers has been investigated by [68] making it an attractive option in the presence of geographical restrictions, reduced equipment costs, accuracies at high and low efflux rates, fully automated measurements and good suitability for long term continuous measurement projects.

Gao et al. has specified chamber design approaches this is seen for the dynamic chamber case in [69] in addition to a study applied to a dynamic chamber design located on a rangeland [70]. Conversely Butnor et al. [47] looks more in detail to the relationship between soil parameters and different chamber designs and how that affects efflux measurements.

One way proposed to evaluate chamber design and its system was proposed by [47], that is done through comparing the efflux measurement for the developed one against the efflux for the three considered chambers models. Chambers have to satisfy

minimum design requirements to perform their role to the optimum level of acceptable measurement accuracy. Commercial chamber design companies take into consideration of design regulations [71] a set to achieve reliable efflux measurements, these are as follows:

- Minimize the changes in the natural microclimate within the respiration chamber [72].
- Minimize disturbances of the soil, which contains the various sources of carbon dioxide from plant roots to bacteria, etc.
- Cause no change to the pressure inside the respiration chamber [73].
- Cause no build up or depletion of carbon dioxide that might cause substantial changes in the gradient of carbon dioxide concentration or cause leakage of carbon dioxide into or out of the respiration chamber.
- Measure water vapour pressure with a correction factor.

2.4.1. Chamber Dimensional Factors and Outer Shell Shape considerations

Chamber dimensional factors as mentioned by Pihlatie, M.K., et al [5] proved to be a contributing factor to concentration measurement deviations. It is stated that underestimation of efflux was related to the chamber height, volume and the soil covered area together with the increase of design parameter values. These factors have been studied extensively using numerical models Gao and Yates [74].

From an aerodynamic perspective done by Palau-Salvador, G., et al [75] the reason for that is due to the creation of the circulation region behind the chamber as shown in Figure 8, the intensity of the aft region depends on the blowing wind velocity.

Some chamber designers have opted to use either the cylindrical, box or hemisphere shape; the shape selection criteria is mainly based on the ease of manufacture, and on the manufacturing funds allocated for the research project. Height of chamber as emphasized by Matthias, A.D., et al [76] is of importance as the study investigated the effect of chamber heights ranging from 5 [cm] to 30 [cm].

The majority of chambers are about half a meter or less in height. Consequently, this means that usually chambers interact with the flow boundary layer. The respiration chamber according to its height H [m] can be determined if it is submerged in the boundary layer [77] thickness δ [m] using equation (1.27). Chamber designers would encounter two cases during the aerodynamic design process the first is that he either knows the distance where the boundary layer starts from. The second one is whereby he knows the thickness of the boundary layer based on assuming that it is bigger or equal to the chamber height.

2.4.2. The Cylindrical Shape Respiration Chamber

Speaking of the first case considering an external laminar flow regime occurs. The distance downstream from the start of the boundary layer is x [m] and the Reynolds number relating to the boundary layer distance is shown in equation (2.26). Where air density is ρ [kg/m³] while u_{∞} [m/s] is the free stream velocity and the air dynamic viscosity is μ [Pa. s] all equations in this section are taken from Schlichting [78].

$$\text{Re}_x = \frac{\rho u_\infty x}{\mu} \quad (2.26)$$

The boundary layer thickness δ_t [m] is calculated from equation (2.27):

$$\delta_t \approx 4.91 \frac{x}{\sqrt{\text{Re}_x}} \quad (2.27)$$

The chamber can only be submerged if it satisfies the following condition (2.28) for the laminar flow case, where H [m] is the chamber height:

$$\delta_t > H \quad (2.28)$$

To calculate the boundary layer thickness for an external turbulent flow is by using equation (2.29). Note it has the same defined variables as equation (2.27):

$$\delta_t \approx 0.328 \frac{x}{\text{Re}_x^{1/5}} \quad (2.29)$$

Again, the chamber can only be submerged if it satisfies the following condition (2.30) for a turbulent flow case:

$$\delta_t > H \quad (2.30)$$

The second case is where boundary layer thickness is assumed to known. Whereby it is equal to chamber height or over $\delta_t \geq H$ this is for a laminar case. Then by substituting equation (2.26) into (2.27) and dealing with the parameter of distance x as an unknown equation (2.31) is derived:

$$x = 24.1 \frac{\rho u_{\infty} H^2}{\mu} \quad (2.31)$$

To avoid repetition the same approach can be applied for the turbulent boundary layer case which results in equation (2.32):

$$x = 263.4 \left(\frac{\rho u_{\infty}}{\mu} \right)^{1/4} H^{5/4} \quad (2.32)$$

In conclusion open spaces of chamber deployment where no obstacles of different heights are distributed around the chamber boundary layers would occur at some distance x around the chamber.

What lessens the impact of generated boundary layers on chambers is by deploying it to locations that either have reasonably low wind speeds or the height of plantation or obstacles is similar to the chamber's height. This is sometimes referred to as surface roughness.

The boundary layer occurs as the flow runs parallel to the soil surface [79] it helps in dampening the occurring flow disturbance at the head of the chamber till some point. Consequently, it all depends on the continuity of kinetic energy provided by the blowing winds to the external flow around the chamber to preserve the created boundary layer. It is stated Pihlatie [5] that tall chambers over estimate efflux measurements this can be attributed to the generated horse shoe and arch vortex as shown in Figure 8.

The trailing vortex has a minor affect, because its intensity increases as it moves away from the chamber. To tackle the problem of the arch and horseshoe vortex designers

are advised to see how they are generated, the generation process is described in detail by [80].

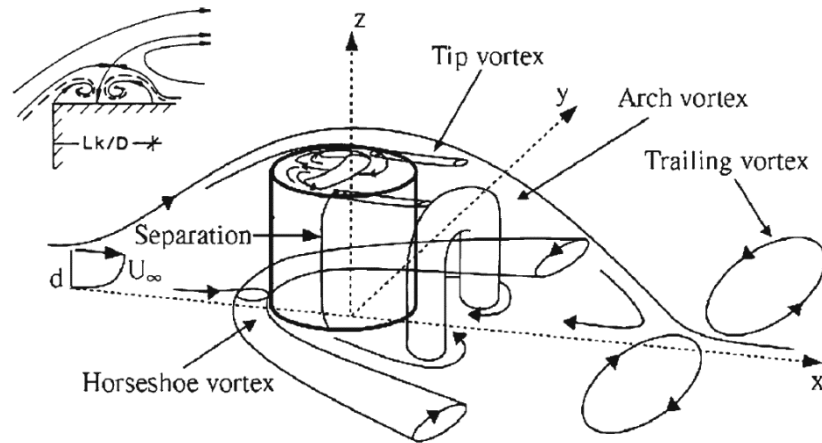


Figure 8: The occurring flow pattern around a cylindrical chamber [75]. What affects mainly the measurement is the horseshoe vortex, arch vortex.

External flows refer to blowing winds occurring externally around the chamber shell. During the design process of a chamber, two important dimensionless numbers are used in the phase of occurring flow pattern characterization.

These are the Reynolds (2.33) and the Strouhal numbers (1.34). The Reynolds number is calculated in relation to the dimensional characteristic length L [m] of the chamber. The average flow velocity at the studied location is \bar{U} [m/s] and ϑ [Pas] is the kinematic viscosity [m²/s] for air. Hence L [m] can be the chamber diameter for a cylinder shape case and. The Reynolds number:

$$Re = \frac{\bar{U}L}{\vartheta} \quad (2.33)$$

The Strouhal Number (2.34) has the same two terms of dimensional characteristic length and average flow velocity used in (2.33). The vortex shedding frequency is f [s^{-1}] :

$$St = \frac{f L}{\bar{U}} \quad (2.34)$$

Lots of aerodynamic material is available for cylinders in relation to St and Re numbers, which allows the chamber designer to find the critical flow frequency that causes external flow disturbance.

To discuss the argument, it requires the assumption of using a 1 [m] diameter cylindrical chamber with constant physical flow properties and applying it to equation (2.25). This helps in finding the external wind blowing velocity relation to the Reynolds regime characterization.

Looking at Figure 9 the first flow regime is for the case of unseparated flow represented by the condition (2.35). This is for a calm day with no obvious blowing winds $u < 7.1 \times 10^{-5}$ [m/s], consequently no expected under or over flux measurements.

$$5 < Re \quad (2.35)$$

Cylindrical chambers usually are usually deployed on sites that are characterized to have blowing velocities in the range of 7.1×10^{-5} [m/s] $< u < 6 \times 10^{-4}$ [m/s] meaning the flow regime exists in the range of (2.36) and is described to have a fixed pair of foppl vortices in wake. Hence less accurate efflux measurements will result due to the generated weak arch vortex.

$$5 < Re < 40$$

(2.36)

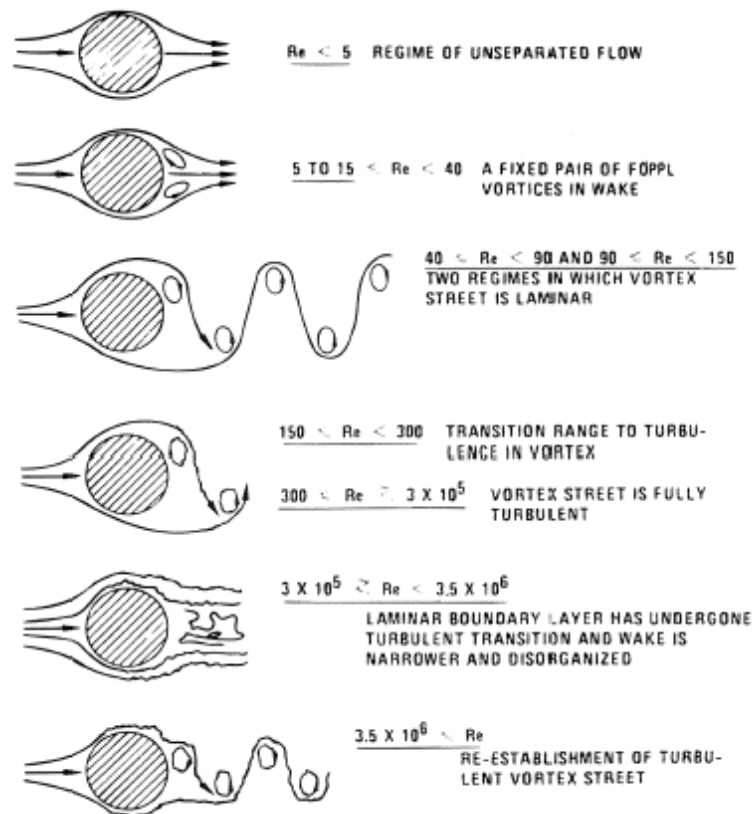


Figure 9: A summary of the 6 cases of external flows occurring around a cylinder represented in relation to the Reynolds number for flow characterization [81].

Small wind flow velocities in the range of 6×10^{-4} [m/s] $< u < 0.02$ [m/s] are characterised for the case of (2.37). This is where two regimes are considered, the flow starts off at $Re=40$ in which the vortex street is laminar and moves on to the transitional stage at $Re=150$.

The vortex transition stage from laminar to turbulent is located between $Re = 150$ and $Re = 300$. The first discussed phase the vortex street is laminar meaning that the arch vortex is still weak to create a substantial negative pressure region after the chamber. The second phase is when the vortex street start developing in a full turbulent vortex

this is when the frequency and strength of the suction affect becomes evident on the measurements by the arch vortex.

$$40 < Re < 300 \quad (2.37)$$

The majority of site locations have average wind flow velocities in the range of 0.02 [m/s] $< u < 5$ [m/s] meaning they are characterized by (2.38). This is the case where Vortex Street is fully turbulent.

$$300 < Re < 3.5 \times 10^5 \quad (2.38)$$

Wind blowing velocities are in the range of 5 [m/s] $< u < 50$ [m/s] as characterized in (2.39). Once wind velocities exceed 10 [m/s] then the disturbances of the efflux measurements should be visible.

The laminar boundary layer has undergone turbulent transition and the wake is narrower and disorganized.

$$3.5 \times 10^5 < Re < 3.5 \times 10^6 \quad (2.39)$$

Reported cyclone wind velocities [82] are 35 [m/s] this is the maximum anticipated velocity. Therefore, the case (2.40) represents the case of reestablishment of turbulent vortex street, hence fitting to the last stated category towards the bottom of Figure 9. This case rarely happens and can be regarded as the maximum value case for specific chamber designs to be deployed in the regions of cyclones.

$$3.5 \times 10^6 < Re_{\text{Cyclone}} \quad (2.40)$$

This leads to the conclusion for cylindrical chambers that by predicting the Strouhal number for a certain external flow regime the intensity and frequency of the occurring vortex shedding can be found using equation (2.34).

Hence over or under prediction of efflux measurements can be corrected. The relationship between the Strouhal and Reynolds number for a cylinder case in the range $40 < Re < 1200$ is shown in equation (2.41) it is proposed by [83]:

$$St = 0.2731 - \frac{1.1129}{\sqrt{Re}} + \frac{0.4821}{Re} \quad (2.41)$$

Therefore, it is recommended to have prior data of probability distribution of annual wind blowing velocities on the site of interest. This is done either through the use of histograms, Rayleigh or Weibull methods as shown by [84].

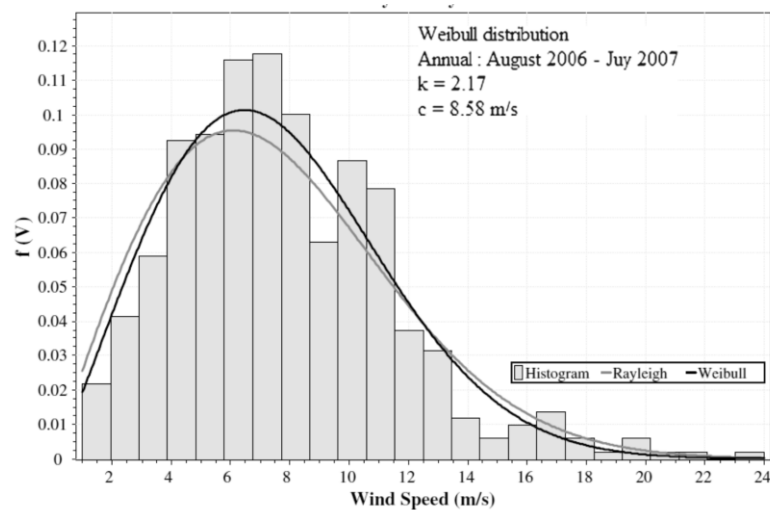


Figure 10: Probability distribution of annual wind speeds example.

Consequently, this helps to determine the compatibility of the chamber shape with its planned location of installation.

2.4.3. The Box Shape Respiration Chamber

Box chambers cause earlier flow separation [85] if they are positioned exactly in the face of the flow, as shown in Figure 11. What mainly causes the disturbance is the horseshoe vortex at the prism wall junction and on a much minor scale the base vortex structure. In conclusion it is best to record the occurring wind blowing directions before setting up the chamber on location. Then, the chamber can be placed in a wedge type flow configuration to lessen the aft flow disturbance over the soil surface which in result affects the efflux measurements.

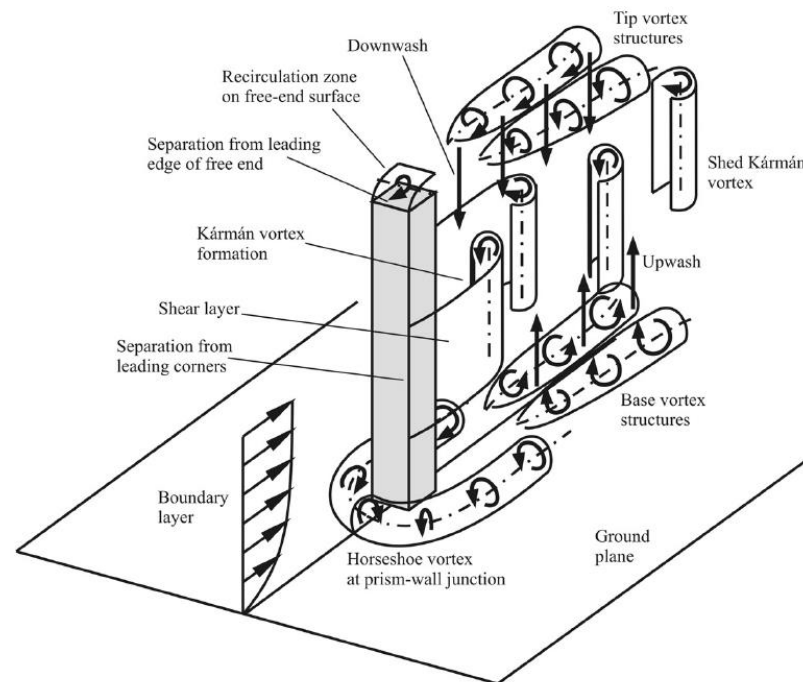


Figure 11: The box shaped chamber with the horseshoe vortex at prism-wall junction, this vortex which mainly disturbs concentration measurements in the chamber [85].

For static chambers Kolari et al. [86] have used small in height chambers as shown in Figure 12. This kind of approach is recommended based on the principle that gas species take time to diffuse therefore small in height chambers reduces data

measurement time. Using small sized chambers as shown by Blevins [81] can decrease the amount of disturbance (flow induced vibration) but on the other hand, it can affect the accuracy of the measured location emissions. That can be evident for the case use (SRC-1, height: 150 [mm]) or (CPY-4, height: 145 [mm]) both produced by PP Systmes [87]. Chamber designers have also opted to use flexible designs, for the case of tall plants where two chambers are fitted in parallel.



Figure 12: A small in height static chamber.

2.4.4. The Hemispherical Shape Respiration Chamber

Some researchers have proposed the use of hemispherical shaped type chambers as found in [79] and in [85]. Hemispherical chambers (dome shaped) [88] are found to be preferable because they don't cause the top head vortex disturbance as seen in the cylindrical Figure 9 and box chamber case Figure 11. They do generate tip hairpins as illustrated by Acarlar and smith [89] but usually they are drawn away by the occurring boundary layer.

The setback in using cylindrical shape chambers is that they produce vortex shedding behind them at site locations characterized with high blowing winds. Avoiding sharp edges on the chambers outer shell is also required to avoid sources of flow turbulence to the external flow. It has been pointed out by Sparks and Huang [82] that external shape irregularities introduce disturbance to the occurring flow around the chamber. It is noticeable in Figure 13 that chamber designers of LI-8100A have filleted the occurring edges of the apparatus in addition to use the collar method to lessen the side effects of apparatus shape irregularities.

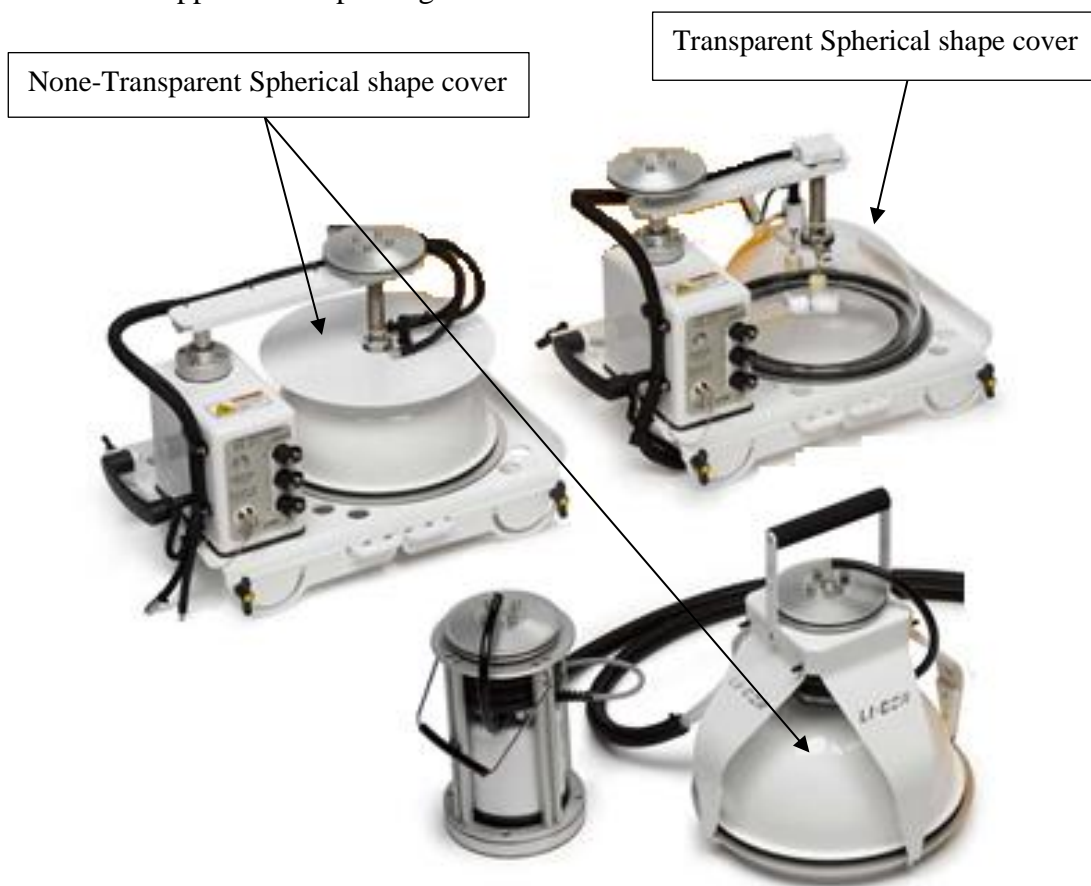


Figure 13: LI-8100A Automated Soil CO₂ Flux System and soil chambers provided by LICOR [4] .

This sets the emphasises for designers that a streamlined chamber outer and inner shell is recommended so that negative pressure regions don't occur on the surface of neighbouring soil outside or inside of the chamber. The negative and positive pressure regions distributed randomly inside and around the chamber cause leakage in and out of the chamber (mass transport fluxes), pressure effects are covered extensively in section 2.7. This is based on the pressure difference through soil porous media according to Darcy law equation (1.13). On the other hand, classical shapes are much easier to manufacture than streamlined chamber shells. Consequently, relatively small respiration chambers should be tested in wind tunnels. However large in size chambers or greenhouses can be tested using commercial CFD packages before the stage of building it begins. Therefore, for the purpose of chamber design evaluation CFD can prove to be less costly before conducting full-size practical tests.

2.4.5. Chamber Static Stability over the Site of Installation

Designers are advised to use equation (2.45) to approximate the chamber static stability over the site of installation while blowing wind occurs. This is by applying the equilibrium of torque at the corner edge of the chamber as shown in (2.42). For this case we apply (2.42) for a cylindrical shape chamber, the same principle can be applied for other shapes. The wind torque is T_{wind} [Nm] and the weight torque is T_{weight} [Nm] :

$$\sum_i T_n = T_{wind} - T_{weight} = 0 \quad (2.42)$$

Substituting into equation (2.42) both the acting wind force F_{wind} [N] and the chamber weight force F_w [N] results in equation (2.43). Additionally, h [m] is the lever

arm for the wind force, while radius R [m] is the lever arm for the chamber weight force.

$$F_{\text{wind}}h = F_w R \quad (2.43)$$

Applying into equation (2.43) the drag force equation parameters on the left-hand side and Newton's second law on the right-hand side will result in equation (2.44). This is where ρ [kg/m^3] is the air density, C_D is the drag force coefficient it can be obtained from [90]. The flow obstructing chamber area is A_f [m^2]. Likewise on the right-hand side m [kg] is the mass of the chamber furthermore the gravitational acceleration is g [m/s^2]:

$$0.5C_D\rho u_{\text{cr}}^2 A_f h = mgR \quad (2.44)$$

Hence the critical blowing wind velocity to achieve chamber turn over can be calculated using equation (1.45):

$$u_{\text{cr}} = \sqrt{\frac{mgR}{0.5C_D\rho A_f h}} \quad (2.45)$$

Leading to that wind velocities at the location should always be lower than the critical velocity as shown in (1.46):

$$u < u_{\text{cr}} \quad (2.46)$$

If the location has high blowing winds furthermore the condition of equation (2.46) cannot be satisfied then the designer can resort to chamber fixing approaches like collars, anchoring etc.

2.4.6. Chambers Internal Geometric Considerations.

It is noticeable in [91] that geometrical constraints inside the chamber cause disturbance to the measurements. This means the lesser the obstacles are there the better the design is, this kind of approach is evident in the available research chamber [86] such as the one shown in Figure 14.



Figure 14: A chamber with no internal obstacles except the tree branches.

Therefore, it is recommended to lessen the usage of the connecting beams inside the chamber that designers usually opt to strengthen the chambers rigidity the same applies to used wiring or sensors inside the chamber. Cylindrical beams create vortex shedding at certain flow speeds [92], sharp edges are a source of turbulence to the flow as shown for backward facing step flow [80]. This leads us to the conclusion that the existence of solid obstacles such as sharp edges, cylindrical beams, cabling or flapping paper (generates flutter) inside the chamber have a strong impact on creating flow disturbance for the case of a dynamic chamber. For a static respiration chamber case solid obstacles play a significant part in delaying the uniform diffusion of carbon

dioxide in the chamber gas volume. On the other hand for the case of a static open chamber the external pressure contributes to the problem of wrong measurements [93] because external disturbance is generated by occurring blowing winds. Furthermore, for the case of open dynamic chambers strong blowing winds might have disastrous effects due to the generation of pressure disturbance between the inside and outside of the chamber. Therefore, the probability of the occurrence of high internal or external pressure is high. This disturbance disrupts the required pressure equilibrium condition to occur inside and outside the chamber.

This length scale for a dynamic chamber can be considered as the blowing fan diameter length D_{Fan} [m], this is for a case where a chamber has obstacles or sharp edges which have a characteristic dimension L_S [m] smaller than the fan diameter (2.47).

$$D_{\text{Fan}} \geq L_S \quad (2.47)$$

Likewise, the length scale of the turbulent flow structure depends on the characteristic length of the secondary source of turbulence, this case occurs when the fan jet hits an obstacle bigger in length than its diameter (2.48). This can be a connecting beam or some instrument inside the chamber.

$$D_{\text{Fan}} \leq L_S \quad (2.48)$$

Meanwhile for the case of static chambers the Kolmogorov length scale η [m] as shown in (2.49) is the smallest scale of disturbance and is the most dominant length scale. Additionally, the average rate of dissipation per unit mass is ϵ_r [m^2/s^3] and the

kinematic viscosity ν [m²/s]. In a dynamic chamber case Kolmogorov length scale do occur in the chamber but at less dominant magnitude.

$$\eta = \left(\frac{U^3}{\epsilon_r} \right)^{1/4} \quad (2.49)$$

The Reynolds number for inner flows mainly relies on the main length scale dimension inside the chamber. The limits for Reynolds in chambers can be found equation (2.50), to ensure that least disturbance to the inner chamber environment can be obtained at the same time for chamber inner mixture circulation to occur.

$$Re \leq Re_{cr} \quad (2.50)$$

Finding the critical Reynolds number is done by assigning several blowing speeds to the circulation fan and then measuring the inner chamber pressure in addition to plotting the concentration curve in relation to time. Plotting the concentration curves in relation to time for the different fan velocities cases comes next. This helps in comparing and optimizing the process for the mentioned cases. Consequently, the most reliable concentration curve is obtained while preserving the built up inner pressure to the minimum. This approach is recommended to be applied experimentally. Another but not easy approach for optimization comes in the form of calculating the flow energy spectrum inside the chamber for different inner chamber pressures. This can be conducted easily through the use of CFD codes, experimentally it is tedious and time consuming to capture the flow fields in the chamber 3D domain. Hence more info is covered by Pope [1]. In conclusion the Strouhal number as it was used for external flows it can also be applied for internal flows as in a form of

disturbance frequency characterization and intensity. Hence for inner flows it can be applied mainly to the cylindrical connecting inner beams or to the sharp edges in the chamber. Inner beams having a circular cross section are favoured in comparison with the ones that have a box cross section, for the purpose of reducing the number of sharp edges used down to two. Sharp edges and inner beams are unwanted for designers in a chamber hence one way around such a geometrical constraint is to use them if needed at a small scale in heights and diameters. Consequently designers can rely on the viscous forces occurring in the flow as well as the Kolmogorov length scales concentrated near the flow stagnation regions to dampen the flow disturbance according to the energy cascade theory mentioned in Davidson [94].

2.5. Chamber Gas Sensors, Location of Instillation and Calibration

One of the most essential parts of the respiration chamber is the gas sensor. Selecting the appropriate gas sensor for a certain type of respiration chamber always posed a challenge to scientists and designers. Unfortunately, there is no simple approach to make this selection hence designers and researchers are advised to seek assistance from sensor specialists. Each sensor has certain capabilities and limitations; thus, the suitability of a gas sensor depends largely on the application in which it is to be used. Different techniques for measuring carbon dioxide efflux have been investigated by many researchers such as [95]. Operational mode of the chamber has an impact on the sensor selection criteria.

2.5.1 Gas Sensors and Static Chambers

For instance static respiration chambers rely on a static pressure environment inside the chamber that provides species diffusion conditions; hence it is a reliable mode to

measure soil biological activity as shown Dilly [41]. On the other hand it is arguable that the unreliability of the static mode at some instances is due to an external disturbance in the measurement. One of the setbacks in the use of static chambers is that relying on the uniform diffusive distribution of species in the gas volume will take a long period of time to achieve. Likewise, it is not guaranteed always for steady conditions to prevail during measurement. Consequently, that will delay the instantaneous understanding of the soil biological activity which changes at every discrete instance of time. The rate of sensor gas sampling per second all depends on the type of sensor and what biological activity is of importance for the study. Therefore this causes a time lag in measurement time till the gas species reaches the sensor head at a predefined location in the chamber. This setback depends mainly on the design constraints of the chamber. Furthermore what sometimes affects the gas sensor as reported by Christiansen et al. [96] is the location of gas sampling intake and outtake from the chamber. The mentioned case is for a gas species analyser that is located externally. It has been stated by Pape et al. [91] that species concentration varies within the chamber height as well as in the radial location. Deviations in efflux measurements are governed by the flow field in the chamber likewise they depend on the diffusion properties of carbon dioxide.

2.5.2 Gas Sensors and Dynamic Chambers

Covering the case of dynamic chambers some researchers like Heinemeyer and McNamara [65] recommended to take gas samples from the head section of the chamber. This was achieved by increasing the chambers volume where by a small cover-box is added at the headspace. Consequently, this resulted in a measurements

accuracy for carbon dioxide of 100 ppm, ideally even lower. Likewise to prove the reliability and accuracy of the mini chamber method Christiansen et al. [97] applied it to measure methane concentrations. Dynamic chambers use blowing fans, the purpose of using mixing fans in chambers is to create a homogenous gas mixture to instantaneously perform carbon dioxide measurements as shown by Martin et al. [98]. The setback of using mixing fans is that they generate turbulence during the mixing process. Consequently that cases an over measurement of the carbon dioxide efflux by an amount of 2-4% as stated by Pumpanen et al. [99]. To resolve the challenge of efflux over prediction gas sample bypass methods to draw out the sample for analysis. Therefore, by using the bypass approach they found that turbulence effects can be omitted from the measurements. Hence the intense mixing that took place in the head space of the chamber was the source of error to the measurement.

2.5.3 Gas Species Sensors

Realistically the objectives researchers and chamber designers are trying to accomplish is to define an instrument specification that meets their minimum requirements. Generally in the scientific community infrared gas sensors have gained the confidence of researchers [100]. The main reason for that is their ability to take measurements at time durations less than a second. Additionally, the following factors/observations should be considered when selecting the gas sensor:

- 1- The specifications should define the gases ranges of the sensors
- 2- Carbon dioxide is what is mainly required to be measured. Additionally, what are also required to be determined are the back ground gases in the monitoring

area. Usually for interest are methane and NO_x which require gas chromatography.

- 3- The temperature ranges (−10 °C to 60 °C) inside the chamber in which the sensor is to be installed should be within the sensor specifications and should be suitable for the gases to be monitored.
- 4- A typical specification for humidity is 95% non-condensing.

Is a continuous mode of measurement important? This kind of mode to run a respiration chamber on comes very handy when deployed on not easy to access locations. Whereby it can be left unattended and data gathering can be conducted and recorded with timed aeration periods. This was clearly shown by the results of [101] notably the point of reliability of repeated measurements is a must. Significantly what is clear from the duration of the measurements those 25 seconds that were required to reach equilibrium concentration state. The jump in concentration was about 300 ppm then it was followed by aeration, while at other instances concentration took 15 minutes to stabilize.

In conclusion, for respiration chambers using a carbon dioxide sensor by its self is not sufficient to understand fully what is happening. Therefore, in parallel to taking concentration measurements, date, time of day has to be recorded to verify the diurnal affects, temperature, inner chamber pressure and outer chamber pressure. A light intensity sensor is required in addition to a day timing recorder when measurements are taken. This means the distribution of carbon dioxide particles in the chambers should increase with temperature according to time of day. Furthermore, light intensity

should be recorded to verify if its cloud or sunny, while rain affects can be predicted by measuring atmospheric humidity. The optimum duration for a measurement, depends on the location of study in general, in specific it depends on the type of location characterization hence grass land, forest land, peat land, swamp, desert, etc. There is a difference in the duration time from site to site, this is attributed to several points, as an example a difference in occurring biological activity on different locations, change of response according to change of temperature. Any chamber has optimum working conditions these either depend on chamber design or in the used type of sensors. Some researchers have used an external apparatus that air conditions the chamber to keep the internal and external environmental conditions the same as seen in some of LI-COR designs.

2.5.4 Temperature effects on Gas Sensors

Diurnal affects as discussed by Wohlfahrt et al. [102] have more of an evident impact on soil efflux measurements in static chambers than dynamic ones. Gas diffusion is a function of temperature according to the kinetic gas theory [103] as shown in equation (2.51), further more temperature varies from day time too night time. Hence carbon dioxide diffusion changes with temperature this is illustrated in equation (2.51) by the relationship of v_{rms} velocity with temperature:

$$v_{rms} = 23.8(T)^{0.5} \quad (2.51)$$

Liang et al. [101] have adopted a continuous approach for data sampling on the site of deployment. In particular it helps in capturing the change of measured parameters in relation to time of day and month of the year. Similarly external uncontrollable

environmental disturbances occur while measurements are taken; these are attributed to seasonal affects. These affects are notably evident in the form of excess blowing winds, rain, heat wave, etc. Diurnal affects become more evident in forest site locations as found by Derwitt et al. [104] in particular the occurrence of dynamic litter, variations in wind pressure relating to tree dynamics, etc.

2.5.5 Sensor Measurement Calibration

Rayment and Jarvis [105] see that no standard calibration method or means has yet been adopted by researchers to test the accuracy of soil respiration measurements. The drive to find the most reliable method of calibration that wins the trust of the researcher is based on finding a method that helps the researcher get repeatable measurements on the same site. During the early stages of research in the field of efflux measurements the soda lime method was the common practice used to capture the carbon dioxide efflux. Then, with the introduction of the gas analyser method the soda lime method became less popular. A comparison between the soda lime and the infra-red gas analyser methods is covered by Pongracic et al. [106] for the reason of calibration what was reported that the soda lime method properly functioned when a 98% moisture content is provided. It was concluded that there was no strong correlation between both used methods on the same forest location. The soda lime method is suitable to be used to calibrate static chambers. A calibration system for soil carbon dioxide-efflux measurement chambers has been put forward by [2] for the case of open and closed dynamic chambers. This is done by firstly calibrating measurements with a previously known efflux. Another common practice used for calibrating chamber efflux measurements for chambers is the Eddy covariance (EC) method [107]

more detailed info about the (EC) method is found in [29]. The Eddy covariance method can also be used to link the relationship between blowing wind velocity, moisture content, temperature, and Carbon dioxide concentrations [108]. The drawbacks of the Eddy covariance method is that it firstly measures the efflux coming from the ecosystem while the interest of the researchers is the amount of carbon dioxide produced by a specific soil site [109]. Secondly It only gives good results for windy conditions, therefore it will be mainly suitable to calibrate dynamic chambers [110].

A way to tackle the calibration challenge is to use soil media with predetermined water content thus soil porosity is known before the experiment. Furthermore, to prepare a soil texture with known ratios of sand silt and clay this helps in knowing the soil permeability for the setup experiment. This is followed by decomposing the sources of the efflux whereby independent effluxes are used to mimic the ones generated by bacteria, plants etc. That is all according to decide on the ratios of efflux contributions when the experiment is setup. This is for the purpose to create a similar example to the studied case for the measured efflux. This method was applied for a dynamic chamber case by Butnor and Johnsen [54] hence what affects the efflux calibration can be identified. Another secondary approach to improve the calibration method for a closed dynamic chamber is by improving the mixing rate within the chamber hence the mixing time previous to the measurement. Consequently both proved to be critical to obtain an adequate correction factor to approximate the true value of carbon dioxide soil efflux in field test sites [46]. One of the challenges facing calibration for both static and dynamic chambers is whether the gas source provides a steady or an

unsteady efflux in time. This was stated in the study by Conen and smith [111] on the linear measurements of nitrogen oxide obtained by accumulating it in a closed chamber. Useful hints for chamber calibration steps are available for a closed chamber type that uses commercial gas analysers type EGM-4 and LI-7000.

2.6. Chamber Temperature Increase/Decrease and its Relation to efflux

In this section the author discusses a general case for a soil site location from a thermodynamic perspective. On a daily basis there is heat transfer represented by total heat $Q_{total}[W]$ into and out of the soil mass at one location. Thus, the gained heat at the site location without the cover of a chamber is $Q_{Soilw} [W]$ as shown in equation (2.52):

$$Q_{Soilw} = Q_{total} \quad (2.52)$$

There are basically three different processes whereby heat can be transported into the soil mass these are: heat conduction $Q_{con}[W]$, heat convection $Q_{conv}[W]$ (with or without latent heat transport) and heat radiation $Q_{rad} [W]$. Furthermore, the summation of these terms leads to the total heat transferred to the soil mass as shown in equation (2.53):

$$Q_{total} = Q_{con} + Q_{rad} + Q_{conv} \quad (2.53)$$

Hence the thermal efficiency for the process of heat transfer to a soil location without chamber cover can be represented in η_w whereby it's the ratio of heat gained for a soil location without an installed chamber over the total heat the location (this is the considered as the ideal case):

$$\eta_w = \frac{Q_{\text{Soilw}}}{Q_{\text{total}}} \quad (2.54)$$

Moreover, considering the comparison case where heat is transferred to the soil mass when a chamber is placed on location $Q_{\text{Soilwt}}[\text{W}]$ this would result in a new load heat term $Q_{\text{totaln}} [\text{W}]$ as shown in:

$$Q_{\text{Soilwt}} = Q_{\text{totaln}} \quad (2.55)$$

The new heat term Q_{totaln} is the summation of the total heat without a chamber with heat gain or loss $\Delta Q [\text{W}]$ as shown in:

$$Q_{\text{totaln}} = Q_{\text{total}} \pm \Delta Q \quad (2.56)$$

This means that with the installation of the chamber on site location the heat load is changed. Hence a new thermal efficiency is defined η_{wt} where it is defined as the ratio of

$$\eta_{\text{wt}} = \frac{Q_{\text{Soilwt}}}{Q_{\text{total}}} \quad (2.57)$$

In conclusion to preserve the locations thermal integrity as much as possible chamber designers must aim to achieve the following assumption:

$$\eta_w \geq \eta_{\text{wt}} \quad (2.58)$$

Consequently this proves the reason why many commercial companies that produce respiration chambers aim to use external environmental systems [112]. That is in order to sustain the same heat balance between inside and outside the chamber. For simplicity equation (2.59) can be used, by measuring the temperature difference ΔT

[Kelvin] experimentally, the amount of gained heat can be calculated by difference in internal energy where c_v is the specific heat capacity for air at constant volume:

$$Q_{\text{totaln}} = c_v \Delta T \quad (2.59)$$

To pursue a more detailed analysis of the temperature effects on soil efflux several temperature models are presented in the following sections.

2.6.1. The Cyclic State efflux Model Related to Soil Layer Depth

Carbon dioxide efflux is produced from the soil and is a function of soil temperature. On a sunny day when the chamber is set up on location after several minutes of deployment heat builds up in the chamber till a certain limit. This heat in turn is then transferred to the mass of soil beneath the chamber gas volume. This process can be modelled based on the lumped analysis approach for time varying convection as shown in equation (2.60). Soil temperature T_{soil} [K] at a specified instance of time t [sec]. The soil heat capacity is c [J/kg K] likewise the density of the soil is ρ_s [kg/m³] this is for a studied volume of soil V [m³] located in the O horizon. The initial chamber temperature after closure is considered as T_i [K]. Furthermore, the average heat transfer coefficient for convection is \bar{h} [W/m²K] this is considered for the soil surface interface A_{si} [m²] within the inner chamber gas volume. Additionally, the asymptotic temperature of the gas volume in the chamber is T_∞ [K].

$$T_{\text{soil}} = (T_i - T_\infty) \exp\left(-\frac{\bar{h}A_{si}}{\rho_s c V} t\right) + T_\infty \quad (2.60)$$

Equation (2.60) proves the point why regular ventilation is required during measurements; this is kind of approach is used in the LI-8100A chamber model as

shown in Figure 6. By substituting equation (2.60) into the Arrhenius equation results in equation (2.61) this resembles a simple form of the efflux equation. Hence the relationship between soil efflux ef [mole/m²s] and soil temperature T_{Soil} can be found where the constant d [mole/m²s] is the pre-exponential constant E [kJ/gmole] the activation energy and R the ideal gas constant.

$$ef = d. \exp\left(\frac{-E}{RT_{Soil}}\right) \quad (2.61)$$

2.6.2. The efflux Model Related to Heat Radiation

Depending on the chambers role of what intended efflux is to be measured, there are transparent chambers and none transparent ones (sometimes called soil flux chambers) like the SRC-1 chamber model [87] as shown in Figure 15. The outer chamber shell for most of the commercial chambers (used to measure soil efflux) is taken to have a white colour.



Figure 15: The PP Systems SRC-1 none transparent chamber model used to measure soil efflux.

The reason for that is with adsorption of heat a rise of internal temperature occurs. Hence an unwanted disturbance to the internal micro climate is eminent. This emitted radiation heat can be calculated using equation (2.62) where Q_{emit} [w] is the emitted radiation from the chamber. Emissivity is referred to as ϵ for a white surface it takes the value of $\epsilon = 0.9$. The Stephan Boltzmann constant is $\sigma = 5.67 \times 10^{-8} W/m^2k^4$. The outer surface shell wall surface of the chamber is A_w [m²]. Likewise, the chamber outer wall shell temperature is T_s [k].

$$Q_{emit} = \sigma\epsilon A_w T_s^4 \quad (2.62)$$

Transparent chambers are used to see the diurnal effects on carbon dioxide efflux measurements this is evident in commercial chamber model CPY-4 made by PP Systems. For instance chamber CPY-4 [113] is used specifically for low laying vegetation this is clearly shown in Figure 16.



Figure 16: The CPY-4 transparent chamber used to measure efflux from low lying vegetation.

In the case of transparent chambers, researchers have noticed on a sunny day that after several minutes of chamber site deployment water condensation starts occurring on chamber walls referring to rise of internal temperature. This is called the absorbed heat $Q_{abs}[w]$ as shown in equation (2.63). The absorptivity of the chamber transparent shell is α and $Q_{inc}[w]$ is the rate at which radiation is incident on the surface:

$$Q_{abs} = \alpha Q_{inc} \quad (2.63)$$

On the contrary the reverse conditions do occur during winter where heat loss dose occur which might cause plant freeze at some instances.

The radiant flux in the chamber is due to carbon dioxide and water vapour contained in the air. Other gases such as N_2 and O_2 have nonpolar, symmetrical molecular structures, thus they do not emit or absorb significant amounts of energy.

In this section a model is proposed for a transparent cylindrical chamber to show the effects of solar radiation on contained water vapour and carbon dioxide in the chambers gas volume and how it contributes in heating the chambers air gas volume. Considering that for a location after duration of time an average temperature inside the chamber becomes of $T_{heatedair} = 310 [K]$ whereby the emissivity doesn't change. Meanwhile for the case of a chamber located at a fixed site the total atmospheric pressure is considered to be $P_t = 1 [atm]$.

Then the water vapour partial pressure is $P_w = 0.02 [atm]$ this is based on making the assumption that the atmospheric water average volume fraction is 2%. Moreover to find the emissivity values for water vapour inside the chamber that has a diameter of

$D = 0.5$ [m] is based on knowing the value of $T_{\text{heatedair}}$ and by calculating $P_w D$ which turns out to be 0.01 m. atm .Hence by using Figure 17 this leads to a value of emissivity of $(\epsilon_w)_1 = 0.14$.

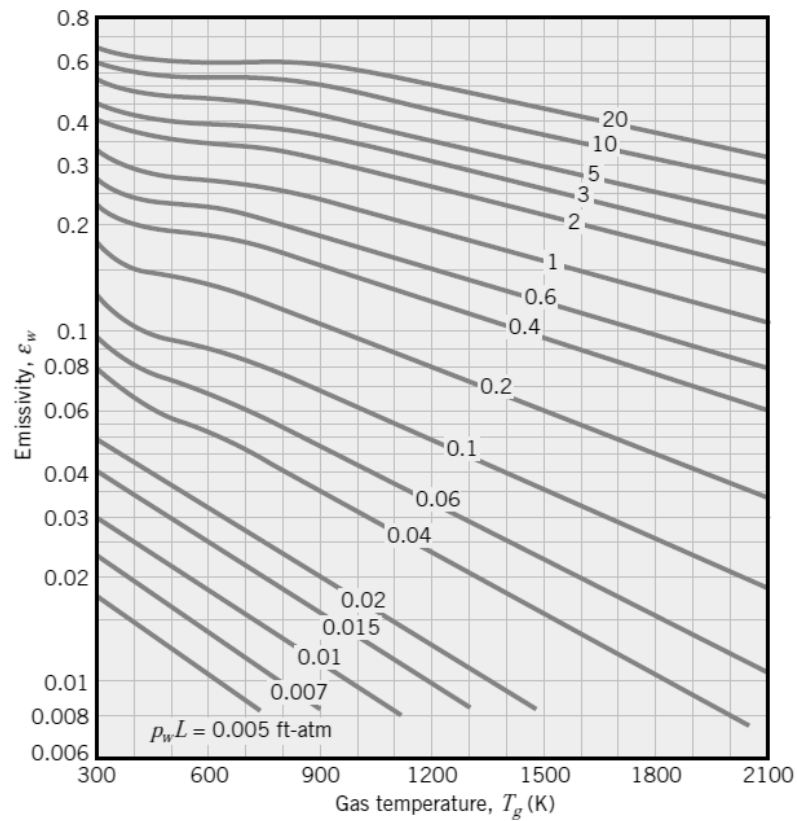


Figure 17: Emissivity of water vapour in a mixture with none radiating gases at 1-atm total pressure [36].

Like wise to find the correction factor of water vapour is by using Figure 18 where the average pressure is $0.5(P_w + P_t) = 0.505$ [atm] moreover we know that $P_w D = 0.01$ [m. atm].

Consequently the correction factor is taken to be $c_{pw} = 1$ hence the actual gas emissivity from water vapour is $(\epsilon_w)_{\text{actual}} = 0.14$. As with the Stephane Boltzmann constant it is $\sigma = 5.67 \times 10^{-8}$ [W/m²k⁴].

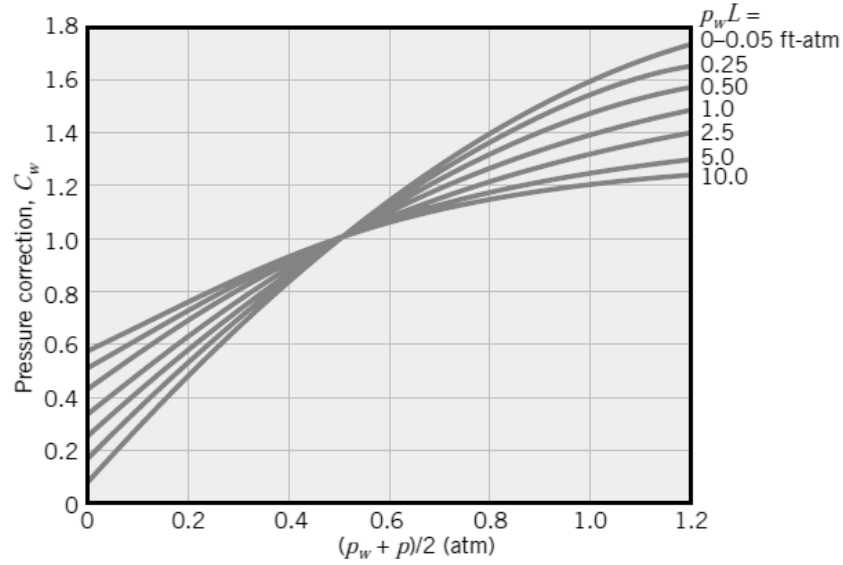


Figure 18: Correction factor for obtaining water vapour emissivities at pressures other than 1 [atm] [114].

The total rate of heat transfer per unit of length L_h [m] for the chamber heated air $T_{\text{heatedair}}$ to the chamber wall if the wall emissivity is unity and its temperature is $T_{\text{ChmaberWall}}$:

$$\frac{q_{w-c}}{L_h} = \pi D (\epsilon_w)_{\text{actual}} \sigma (T_{\text{heatedair}}^4 - T_{\text{ChamberWall}}^4) \quad (2.64)$$

On the other hand, studying gas emissivity for carbon dioxide is based also on considering that the total atmospheric pressure is $P_t = 1$ [atm]. Carbon dioxide partial pressure is taken to be $P_c = 4 \times 10^{-4}$ [atm] based on that the location has an atmospheric concentration of carbon dioxide of 400 ppm. Medium sized respiration chambers have a diameter of $D = 0.5$ m meaning that $P_c D = 2 \times 10^{-4}$ [m.atm]. Hence by knowing $P_c D$ and $T_{\text{heatedair}}$ and using Figure 19 the emissivity for carbon dioxide has an emissivity value of $(\epsilon_c)_1 = 0.006$. However, by using Figure 20 and knowing that total pressure is 1 [atm] and $P_c D$ leads to the emissivity correction factor

for carbon dioxide to be $c_{pc} = 1$. Consequently, the actual emissivity for carbon dioxide is $(\epsilon_c)_{\text{actual}} = 0.006$ whereby it is applied to equation (2.65). Thus, this gives the radiative heat transfer per linear L_h [m] from the carbon dioxide to the chamber wall if the wall emissivity is unity and its temperature is $T_{\text{ChamberWall}}$:

$$\frac{q_{c-c}}{L_h} = \pi D (\epsilon_c)_{\text{actual}} \sigma (T_{\text{heatedair}}^4 - T_{\text{ChamberWall}}^4) \quad (2.65)$$

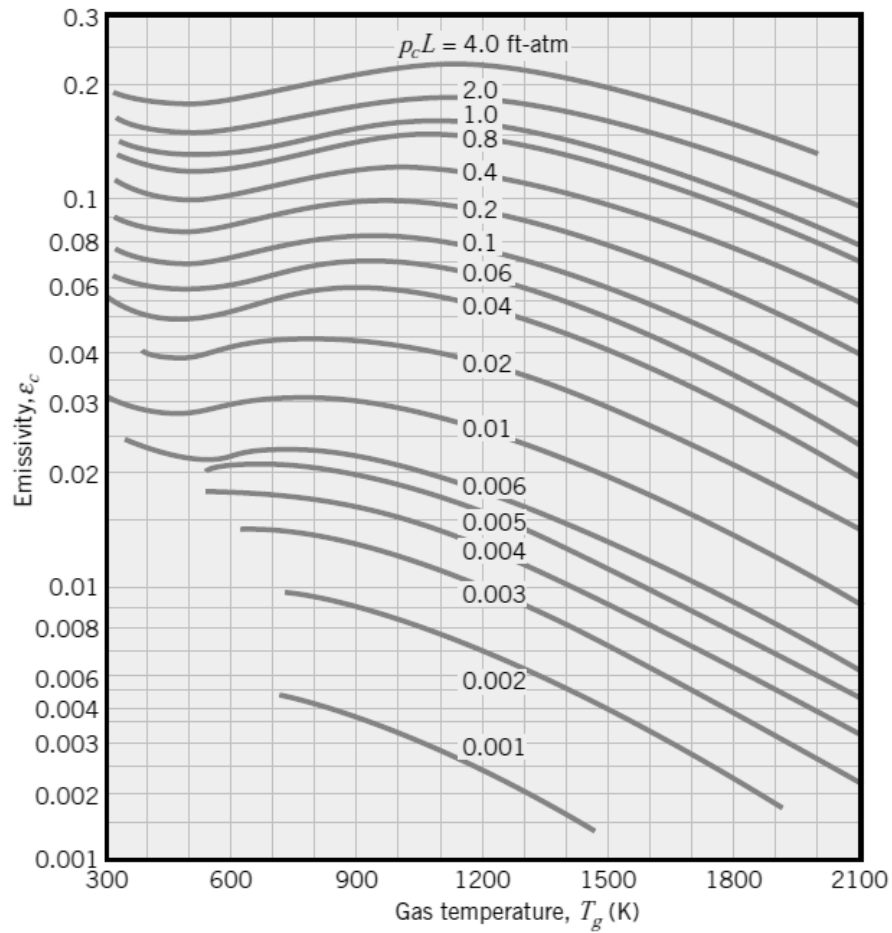


Figure 19: Emissivity of carbon dioxide in a mixture with none radiating gases at 1-atm total pressure [114].

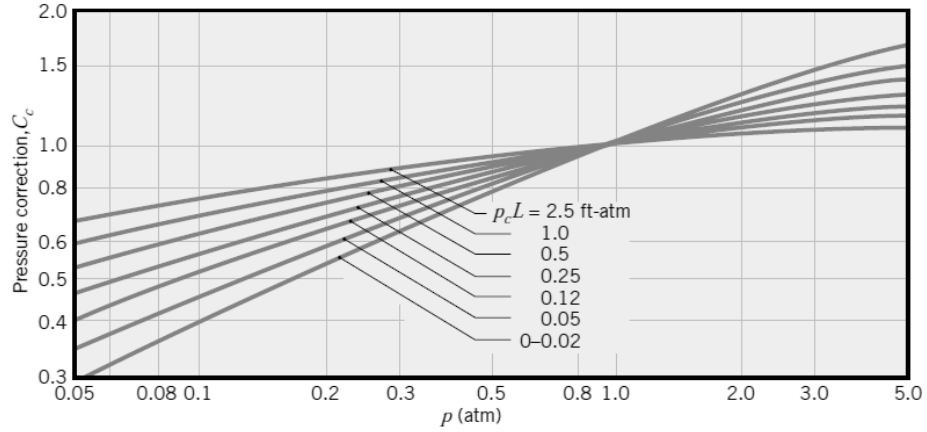


Figure 20: Correction factor for obtaining carbon dioxide emissivities at pressures other than 1 [atm] [114].

Lastly the total radiant flux from the contained carbon dioxide and water vapour in the chamber to the heated air inside the chamber is:

$$\frac{q_{\text{total}}}{L_h} = \pi D(\epsilon_c + \epsilon_w)\sigma(T_{\text{heatedair}}^4 - T_{\text{ChmaberWall}}^4) \quad (2.66)$$

A numerical model based on heat balances was developed by [115] for a soil mulch atmosphere case using the finite difference scheme, where latent heat content and radiative among others were considered. Such a model can give hints to the potential of applying such models in available CFD packages. Rise of chamber inner temperature is attributed to carbon dioxide concentration rise in the chamber due to the high heat capacity of carbon dioxide. For measurements lasting in the range of several minutes to an hour it is assumed that the soil temperature has the same temperature as the ambient air. Hence, the studied case is steady state one.

2.6.3. The Daily Cyclic State efflux Model Related to Soil Layer Depth

The thermal properties of the soil are strongly dependent on soil porosity [34]. The soil temperature which is achieved through the solar radiation projected during the day on the studied soil area reflects on the temperature of the water moisture content, raising the temperature of the soil will increase the evaporation pressure. Soil temperature cyclic behaviour can be modelled using equation (2.63) as shown in detail by Marshall et al. [116], where T_{zt} is a function of time and depth, T_a is the average soil temperature, t is time. Heat conduction is governed by the thermal properties of the soil composition; volumetric heat capacity and heat conductivity are represented in the k_c constant. The frequency of the cyclic behaviour is represented by $w = 2\pi/\tau_p$ where τ_p is the period of cycle which can be day or year. Likewise, the term σ_t represents $w/2k [m^{-2}]$ as seen in the following:

$$T_{zt} = T_a + A_0 e^{-(\sigma_t)^{0.5}z} \sin (wt - (\sigma_t)^{0.5}z) \quad (2.63)$$

Cyclic temperature change during the day and night cases a change of the mass diffusion coefficient, affecting the carbon dioxide efflux produced mainly at the top surface soil layer near the surface. The temperature cycle simple model is covered in many soil physics books, as an example by Marshall et al. [116]. The temperature damping model that considers thermos physical properties of the soil is covered by Koorevaar et al. [34], other interesting approaches are also available in the book by Najafpour [40]. The power of equation (2.64) it can be applied for the top surface layer of soil on both the bacteria and plant roots for a certain depth and time of the day.

$$ef = d. \exp\left(\frac{-E}{RT_{zt}}\right) \quad (2.64)$$

The research paper by Ozgener et al. [117] has also proposed a similar approach to predict temperature variations in relation to time and soil depth for geothermal heat exchanger applications. . Lin et al. [88] noted by using mercury as the measured gas species that the gas efflux is also affected by soil moisture and temperature especially with cyclic patterns of soil wetting.

2.6.4. The Steady state efflux Model Related to Soil Layer Depth

Graf et al. in [118] have pointed to temperature variations in the soil as a cause of this underestimation of flux, where the biological response factor differs from one location to another. That is because they assume a uniform temperature distribution in the studied soil layer while in real life it is not the case. Usually, a uniform temperature is modelled using equation (2.65). The soil temperature at the surface interface with the atmosphere is T_{ss} [k]. The soil temperature at the bottom of the top layer is T_{bl} [k]. The layer soil thermal conductivity is k_c [w/m²k]. The heat source or sink term q [w] can either represent heat gained during the day can be regarded or heat loss term during the night. L [m] is the total thickness of the soil layer.

$$T_{ins} = \left(\frac{T_{bl} - T_{ss}}{L} + \frac{q}{2k_c}(L - z) \right) z + T_{ss} \quad (2.65)$$

Hence by substituting equation (1.18) into the Arrhenius equation [103] leads to equation (2.66) which is a steady state equation relating to the thermal qualities and thickness of the soil slayer.

$$ef = d. \exp\left(\frac{-E}{RT_{ins}}\right) \quad (2.66)$$

Parkin and Kasper have proposed [119] in order to improve efflux measurements is through considering the atmospheric ambient air temperature on the site of study as the contributing factor that affects biological activity. Consequently, this adopted assumption by the research community is wrong because soil air temperature is a function of the lumped heat capacitance of the soil layer as shown in equation (2.60); hence the growth dynamics of bacteria will also be affected hence the efflux will be affected.

$$T_{ins} \neq T_a \quad (2.67)$$

Furthermore researchers like Ozgener et al. [120] have noted that soil wetness affects the total thermal resistance of the soil at the location of study through the use of air-earth heat exchangers

2.6.5. The Steady state efflux Model Related to Soil Layer Depth

Soil efflux is governed by soil temperature as shown by Fang and Moncrieff [121] they also found there is no optimum soil temperature for biological activity and that after a certain temperature rise biological activity is halted. The paper summarises several experimental extrapolated models relating to temperature and soil efflux. Likewise Monson et al. [122] have shown that soils that have high porosity values responded with less sensitivity to temperature changes. Furthermore, what also affects carbon dioxide efflux is the soil microbial community behaviour where they adapt to cold conditions. Therefore, they exhibit a stronger temperature response when

compared to the ones that exist in warmer climates. Some have argued that soil porosity is the contributor for wrong efflux measurements, where low porosity caused underestimation while high porosity caused over estimation [123]. Others like Reth et al. [124] have stated that temperature and porosity are the two major factors affecting efflux. The discussed point can be proved by using the Sutherland equation [125]. The Sutherland equation for carbon dioxide is (2.68), it represents the dynamic viscosity of the gas at two instances, one is the reference state and the second is at the temperature of concern. The carbon dioxide constants are taken as follows $C = 240$ [K] while the reference dynamic viscosity for carbon dioxide is $\mu_{(\text{CO}_2)_0} = 14.8$ [$\mu\text{Pa}\cdot\text{s}$] in relation to the reference temperature $T_0 = 293.15$ [K]:

$$\mu_{\text{CO}_2} = \mu_{(\text{CO}_2)_0} \frac{T_0 + C}{T + C} \left(\frac{T}{T_0} \right)^{1.5} \quad (2.68)$$

By applying the Sutherland equation (2.68) into the Darcy equation (2.13) this leads to the efflux form of the equation as a function of temperature:

$$ef = - \frac{-k \cdot \rho_{\text{CO}_2}}{MW_{\text{CO}_2} \cdot \mu_{(\text{CO}_2)_0}} \frac{T + C}{T_0 + C} \left(\frac{T_0}{T} \right)^{1.5} \frac{([\text{CO}_2]_S \cdot P_{\text{TS}} - [\text{CO}_2]_B \cdot P_{\text{TB}})}{L} \quad (2.69)$$

It is demonstrated by Powers et al.[126] that during a drought an occurrence of a strong dependency of carbon dioxide efflux and isotopic compensation that effects soil water content. Conversely Subke et al.[61] see that a better understanding of the efflux in a forest site location is based on predicting its carbon pool. Tagesson [127] argued that GPP (gross primary production) does not have an effect on efflux production in the forest ecosystems. Forest soil efflux measurements (that contained considerable

sand levels in its texture) taken at different seasons of the year were studied by Yuste et al. [128] they used both the EC and respiration chamber method. Their extrapolated data showed the relationship of soil respiration with temperature. They also found a relationship between carbon dioxide and friction velocity. They also claimed to have derived an efflux model with the required constants to be used for grassland respiration and other sites.

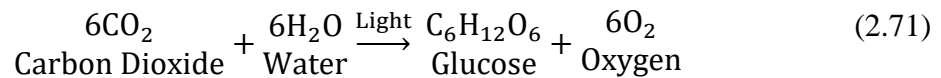
There is a location efflux relationship with seasonal variance shown by Flage et al. [129] done through using the EC method. This was further studied by Pilegaard et al. [130] more specifically for a forest site whereby they focused on time of the year and temperature effects on soil respiration efflux. Attention has been drawn in [130] to diurnal measurements taken over a two year period have shown that climate changes relating to temperature increase the carbon efflux. One of the setbacks stated by Nay et al. [131] in relation to closed systems is that they underestimate the soil efflux by about 15%, which was observed through the collected experimental data.

2.6.5. Chamber Temperature effects on Plant Photosynthesis and Cellular Respiration

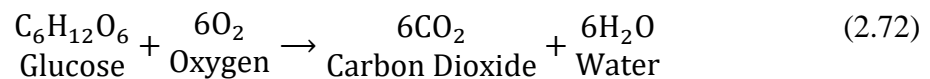
The temperature affects almost all aspects of the respiration processes. These include biological processes, such as germination of seeds, plant growth, root development and activity, microbial activity, etc. The relationship between the temperature and the biochemical processes of the respiration is usually described by an exponential equation called the Arrhenius equation, as in the following:

$$w_i = d_{pe} e^{\frac{-E_i}{RT}} \quad (2.70)$$

Where d_{pe} is a pre-exponential constant, E_i is the activation energy, R is the universal gas constant, and T is the temperature. Photosynthesis is a process used by plants and other organisms to capture the energy of the sun in order to split off the water's hydrogen from oxygen. It is estimated that about 40% of the soil respiration is from plant roots [132]. While hydrogen is combined with carbon dioxide (absorbed from air or water) to form glucose and to release oxygen, photosynthesis is just the opposite of cellular respiration. The chemical equation (2.71) of photosynthesis is 6CO_2 (carbon dioxide) and $6\text{H}_2\text{O}$ (water) and that makes 6O_2 (oxygen) and $\text{C}_6\text{H}_{12}\text{O}_6$ (glucose), or



What is missing in the chemical equation (2.71) is the capture of energy from sunlight. However, the two processes take place through a different sequence of chemical reactions and in different cellular compartments. Cellular respiration in living cells, in turn, use the fuels derived from glucose and oxidize the hydrogen and carbon to release the energy of the sun and to re-form water and carbon dioxide, as expressed in the following formula (2.72)



Plant respiration is limited by the process of diffusion. Plants take in carbon dioxide through holes on the undersides of their leaves known as stoma or pores.

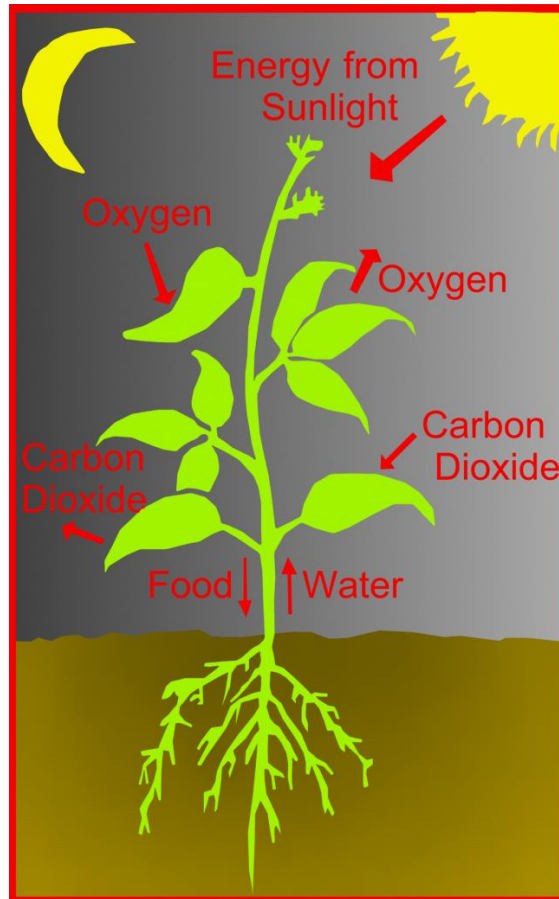


Figure 21: An illustration showing plant activity during the day which is called Photosynthesis (shown on the right-hand side) and the night activity which is called Cellular Respiration (shown on the Left-hand side).

However, most plants require little air. They have relatively few living cells outside their surface because the air (which is required for metabolic content) can penetrate only skin deep. Nevertheless, most plants are not involved in highly aerobic activities, and thus have no need for these living cells. This explains why there are several sources of carbon dioxide. Having plants in the chamber is one of these sources, while the other source is the bacteria of the soil. This occurs during the day activity, while during the night plants perform the role of a carbon dioxide source sink. For more details on the process of photosynthesis, see [133]. When the soil is covered by vegetation, water can then be transported from anywhere in the root zone, via the roots,

stems and leaves into the atmosphere; the so-called soil-plant-atmosphere-continuum (SPAC). The loss of water from soil via plants is called transpiration. Transpiration is mostly a passive process. While the leaf stomata are open for the exchange of carbon dioxide and oxygen for the process of photosynthesis, water vapour is lost to the atmosphere. The deficit is replenished by water uptake by the roots. The driving force for the transpiration stream is the large potential difference between the water in the soil and the water in the atmosphere. Again, the deficit is replenished by the water uptake by the roots. When the winds blow, a thin boundary layer occurs in different regions of the plant and the transport of water vapour from the leaves into the atmosphere is turbulent. In this case, the stomata will close when the roots cannot take up enough water to satisfy the evaporative demand. Then, with the transpiration, photosynthesis is also interrupted, which will result in yield reductions. Under a full vegetation cover, evaporation from the soil can, generally, be neglected. When there is no breeze, the air surrounding a leaf becomes increasingly humid thus reducing the rate of transpiration. When a breeze is present, the humid air is carried away and replaced by the drier air. When the soil is partially covered with vegetation, water is lost by both evaporation and transpiration, which are usually lumped together as evapotranspiration.

The wind speed affects the porosity of the soil due to the increased soil liquid uptake by the plant roots through the wind action on the plant causing more water to be ejected by the plant stems into the chamber entrainment. The type of vegetation that controls the soil processes involving the carbon dioxide fluxes, accumulation, and transport in a chaparral ecosystem is discussed by Feng et al. [134].

2.7. Pressure effects on efflux Measurement in Chambers

Effects of external/internal pressure fluctuations on chamber measurements have been observed. Such fluctuations were found to this led to over and underestimation of efflux measurements. Takle et al. [135] have corroborated past work by demonstrating the importance of heterogeneous pressure fields in promoting gas movement in porous soils. They further suggested that fluctuations in the static pressure fields introduced by wind interactions with terrain and vegetation may lead to pressure pumping effects at the soil surface, hence a large spatial inhomogeneity in soil fluxes of trace gases occurs. Weather patterns play an important role as stated by Flechard et al. [136] in carbon dioxide efflux production for a grassland location. When there is no wind for instance, storage of carbon dioxide in the soil occurs. This carbon dioxide studied for the site is flushed out when the soil surface is subjected to high winds during the day time, while during the night time carbon dioxide accumulates in the soil.

2.7.1. Chamber Ambient Pressure

Once the researcher can identify at what elevation the site is at, he can calculate the atmospheric pressure according to this relation (2.73). The atmospheric pressure P_{atm} [Pa] is related to location elevation z [m] in relation to sea-level. The standard pressure at sea level is $P_0 = 101325$ [Pa]. Earths gravitational acceleration is $g = 9.8$ [m/s²]. The molar mass of dry air is $M = 29$ [g/mole]. The sea level standard temperature is $T_0 = 288.15$ [K] . The universal gas constant $R = 8.314$ [J/mole.Kelvin]:

$$P_{\text{atm}} = P_o \exp\left(-\frac{M}{RT_o}gz\right) \quad (2.73)$$

The number one rule in using chambers is to ensure pressure equilibrium between the inside chamber pressure P_{in} [Pa] and the outside the atmospheric pressure P_{out} [Pa] as shown in equation (2.74):

$$P_{\text{in}} = P_{\text{out}} \quad (2.74)$$

In the case of closed dynamic chambers, some researchers [71, 73] have identified that chamber over pressurization or under pressurization causes efflux under estimation or over estimation respectively. Unfortunately, the case of pressure equilibrium equation (2.74) rarely occurs. The real scenario is represented in equation (2.75) which is an upgrade for equation (2.74). It represents the relative pressure values (that's why the atmosphere pressure term is evident on both sides of the equation) with addition or subtraction of internal $\Delta P_{\text{in } n}$ [Pa] and external pressure $\Delta P_{\text{out } n}$ [Pa] represented in a summation form:

$$P_{\text{atm}} \pm \sum_1^n \Delta P_{\text{in } n} = P_{\text{atm}} \pm \sum_1^n \Delta P_{\text{out } n} \quad (2.75)$$

2.7.2. Chamber Internal Pressure

The author derives an equation for the case of rise of internal chamber pressure. It can be calculated by equation (2.76) for the case of temperature rise, this is by applying the Gay Lussac law to calculate the increase in pressure relating to inner chamber temperature at start of the measurement process T_1 [Kelvin] and at the end of the

measurement process T_2 [Kelvin], where the initial chamber pressure P_1 [Pa] and the final chamber pressure is P_2 [Pa]:

$$\Delta P_{in\ 1} = P_2 - P_1 = P_1 \frac{T_2}{T_1} - P_1 \quad (2.76)$$

For the case of internal blowing fans, the author derived an equation that calculates the rise of internal pressure (2.77). Fan blowing effects can be derived using the conservation of linear momentum law for control volumes. It can be derived for the nearest wall that the fan jet hits or it regarded the flow velocity ends to zero in a control volume. Then based on regarding the pressure is acting homogenously on all chamber surfaces, where fan blowing area is $A_{Fan}[m^2]$. The inner chamber surface area in contact with air including the covered soil surface is $A_{inner}[m^2]$. Air density is ρ [kg/m³] and volumetric flow rate of a blowing fan is Q_{Fan} [m³/s]:

$$\Delta P_{in\ 2} = \frac{A_{inner}}{A_{Fan}} \rho Q_{Fan}^2 \quad (2.77)$$

2.7.3. Chamber External Pressure

Experiments conducted on the soil surface and inside the soil volume [135] have shown that pressure fluctuations over the soil surface cause an inflow or an outflow flux of species from the porous media. Some researchers [107] and [137] have found by using the EC method and chamber methods that pressure fluctuations and turbulence effects cause under-estimation or over-estimation of carbon dioxide efflux. External pressure perturbations occurring near the soil surface $\Delta P_{out\ 1}$ can be taken by

the Reynolds decomposition as shown in equation (2.78), where P_{av} [Pa] is average pressure component and P_{fc} [Pa] is the instantaneous fluctuating pressure component:

$$\Delta P_{out_1} = P_{av} + P_{fc} \quad (2.78)$$

Other more advanced statistical models can be used instead of equation (2.76). Experiments in [138] have shown that external pressure disturbances in the range of [mbars] cases changes in the carbon dioxide flux in [$\mu\text{g}/\text{cm}^2\text{s}$]. This proves from the units the sensitivity of the system response to small changes. The other affect is with increase of internal pressure in the chamber that would lead to an increase in carbon dioxide partial pressure, enhancing the diffusion rate of carbon dioxide through the leaf stomata [139].

2.7.4. Chamber Internal Condensation Pressure

It has been noted that water vapour absorbers carbon dioxide hence lowers the carbon dioxide concentration in respiration chambers [140]. By using the Antoine equation (2.79) where vapour pressure P_v [Pa] and chamber temperature T_c [K]. The researcher can find/predict condensation pressure in the used chamber. Water when condenses affects the gas sensors probe therefore a correction factor is used.

$$P_v = 133.3 \exp\left(20 - \frac{5132}{T_c}\right) \quad (2.79)$$

Hence the condensation pressure condition is when the chamber wall temperature is T_c :

$$\sum_1^n \Delta P_{in\ n} \geq P_v \quad (2.80)$$

In conclusion temperature drop or rise should not occur abruptly inside the chamber. Hence temperature equilibrium between inside and outside the chamber when change dose occur should be slow to overcome the problem of water condensation to occur on the gas tip sensor.

2.7.5. Soil Surface Interface Pressure and Pressure Profile

Researchers using closed dynamic chamber on a forest site location [141] found that efflux measurements are governed by static pressure fluctuations, soil temperature and forest litter. What was also evident by [142] that an increase in pressure above the ambient pressure in closed dynamic chambers resulted in a decrease of carbon dioxide efflux measurements. It is noted in reference [143] that pressure fluctuation frequencies over the soil surface range from 10^{-4} [HZ] to 10^2 [HZ]. Pressure fluctuations with frequencies $< 2\text{Hz}$ have greater penetrable effect on the top soil surface [144] to depths of several centimetres with little attenuation. The theory of soil air movement was introduced by [145] it covers all the necessary aspects to model the mass transport according at the soil interface with the atmosphere. The soil surface pressure field can be described mathematically by equation (2.81) whereby time is t [s] furthermore the scaled period is taken as T_n [s]. The wave length of m th wave in the X-direction is X_m [cm] similarly Y_m [m] is the wave length of m th wave in the Y-direction. The distance downwind is represented by x [cm] while y [cm] is the crosswind distance. The phase angle of m th wave in the x-direction is ϕ_{xm} [radians] likewise the phase angle of m th wave in the y-direction is ϕ_{ym} [radians]. The amplitude of the pressure wave with n th period and m th wave length is a_{mn} [μba]:

$$P = \sum_{n=1}^N \sum_{m=1}^M \left[\frac{a_{nm}}{2} \cos \left(\frac{2\pi t}{T_n} - \frac{2\pi x}{X_m} - \phi_{xm} - \frac{2\pi y}{Y_m} - \phi_{ym} \right) + \frac{a_{nm}}{2} \cos \left(\frac{2\pi t}{T_n} - \frac{2\pi x}{X_m} - \phi_{xm} + \frac{2\pi y}{Y_m} + \phi_{ym} \right) \right] \quad (2.81)$$

In conclusion the rate of aeration can be predicted based on the power of the penetration frequency of the pressure fluctuations. What could further enhance diffusional fluxes significantly more than ground level turbulent pressure fluctuations is the Quasi-stationary pressure fields induced by wind blowing over rough topography [146]. Research by [2] has put forward that turbulence occurring in the chamber gas volume affects the boundary layer occurring over the soil surface. Consequently, this causes an increase in the efflux of carbon dioxide from the soil top layer. Above all the turbulence intensity should not cause substantial flow fluxes to occur from inside to the outside of the chamber.

The soil pressure profile is covered in [147] in particular the authors shows the cyclic pressure behaviour in relation to soil depth starting from the soil surface as shown for the case of several depths. Furthermore the author of [148] studying the thermal properties of several soil samples found a relationship between soil moisture and the cyclic pressure behaviour taking into account a depth of 0.8 [m]. By knowing the concentrations of species and by measuring the total pressure between two points, species partial pressure profile can be found using equation (2.82). The root development activity is limited at the topsoil because the carbon dioxide concentration in the gas phase of a soil generally increases with depth. Scientists have linked the carbon dioxide efflux to soil physical pressure parameters such as [149]. Using the

equations of Fick's law, ideal gas and continuity for carbon dioxide at a steady state, the partial pressure distribution for carbon dioxide P_{CO_2} [kPa] in the soil (valid to a depth of $z_0 = 0.7$ [m]) can be found using the derived equation (2.82):

$$P_{CO_2} = -\alpha_{CO_2} \frac{RT\tau}{2D_{CO_2}\epsilon\delta M_{CO_2}} (z^2 - z_0^2) + P_{CO_2s} \quad (2.82)$$

Soil porosity is represented by ϵ while soil tortisity is represented by τ which can have a value from 1.8 to 6 its value depends mainly on the size of the macro pores. Soil constructivity δ is mainly related to micro and nano-pores it does not vary that much in value and can be taken to have a value in the range of 0.9 to 1. The partial atmospheric pressure of carbon dioxide at the soil surface can be taken as $P_{CO_2s} = 0.0401$ [kPa]. Carbon dioxide molecular weight is $M_{CO_2} = 44$ [kg/kmole]. Furthermore carbon dioxide Mass diffusion D_{CO_2} [m²/s] can be found in [32] as a function of temperature.

The source term for carbon dioxide is referred to as α_{CO_2} [kg/m³s]. Its value for simplicity can considered for a grassland site to be $\alpha_{CO_2} = 10^{-3}$ [kg/m³s] while for a forest site can be taken as $\alpha_{CO_2} = 10^{-4}$ [kg/m³s]. For more accurate values for the carbon dioxide source term for specified categories of soil site locations the researcher is directed to available literature. Furthermore this term changes according to land use changes as mentioned by [150].

In conclusion for the design of an open dynamic chamber which generally encounters carbon dioxide efflux overestimation proposals were presented to tackle such a problem for both calm and windy conditions by using a vented nozzle design that

regulates pressure fluctuations [151-153]. Another vertical vent design proposed by [154] was used on a closed dynamic chamber to regulate internal pressure on windy sites. The use of a multichannel system of interconnected chambers was another alternative to resolve the pressure disturbances issues [155]. Moreover, they opted to use automated pressure compensation counter measures in order to take care of the situation when pressure fluctuations occur. However over and under estimation problems were attributed to the chamber design and gas mixture mixing methods.

2.7.6 Soil Surface Aeration and Pressure Gradient

The aeration process in general is providing regular charges of air to the small finite soil cavities near the soil surface as shown on Figure 22.

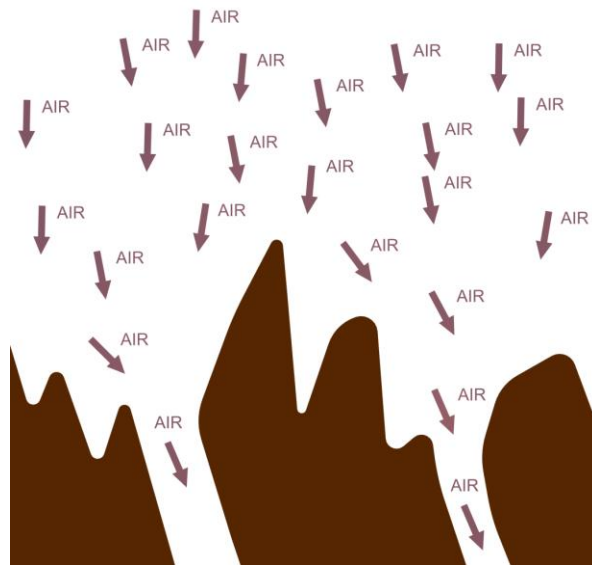


Figure 22: The aeration process through the top soil surface.

The Aeration process supplies oxygen (which makes up 21% of the supplied air) and removes carbon dioxide and other gases from the soil, this exchange process happens

between the soil and the atmosphere interface. The bulk flow of gas in the soil is a result of the pressure gradient for dynamic chambers, while for static chambers it is related on concentration gradients.

Different gases have different friction velocities this is proved mainly using the Eddy covariance method when applied for both carbon dioxide and methane gas as investigated by [156]. The relationship between the friction velocity and efflux has always been an important case to be considered especially for dynamic chambers. Friction velocity u_* for carbon dioxide can be calculated using equation (2.83) whereby the carbon dioxide gas density near the soil surface is ρ_{CO_2} [Kg/m³] moreover the surface wall shear stress is τ_w [Pa] its value can be found in [157] it all depends on the surface roughness of the location:

$$u_* = \sqrt{\frac{\tau_w}{\rho_{CO_2}}} \quad (2.83)$$

Equation (2.83) can be applied on the soil surface inside the gas volume of the chamber and on the outside soil surface located near to the respiration chambers outer shell. There is a relationship between friction velocity and soil interface pressure this can be found by relating it to a macro-flow case. This can be applied for the first soil layer O horizon which has a thickness of $h_o = 5.08$ [cm] . Furthermore by using equation (2.84) adapted from [52] whereby it is applied for a distance range of $0 < z < h_o$. The partial pressure derivative for a discreet distance x on the soil surface can be calculated from the following equation:

$$\frac{dp}{dx} = \frac{u - u_*(1 + 7927h_o)}{(9.7 \times 10^{-9}z^2 + 15853.6 h_o z)} \quad (2.84)$$

Consequently equation (2.84) can be applied for instance to study the generated suction pressure due to the use of circulation fans inside the gas volume of the chamber. Friction velocity is affected by time of day hence temperature this was shown by [158] a dependence of the Eddy covariance measurement reliability on net radiation was found. During high effective net radiation nights, the Eddy covariance method usually underestimates the carbon dioxide efflux produced by the ecosystem. Moreover, efflux measurements using the Eddy covariance method were not reliable for nights with extremely low friction velocity. It was found that during low effective radiation nights with friction velocity lower than 0.07 [m/s] underestimation occurred, while for a case of friction velocity higher than the stated value showed similar measurements between chamber and Eddy covariance method.

For the purpose of aeration equation (2.85) can be used [159] to estimate the required power for an installed circulation fan inside the respiration chamber. K is based on chamber geometry, N is the number of revaluations for the selected fan, P_u [w] is the fan power required in a respiration chamber, D_i [m] is fan diameter, and Q [m³/s] is the aeration rate (Volume of air supplied per minute divided by the soil volume under the chamber)

$$P_g = K \left(\frac{P_u^2 N D_i^3}{Q^{0.56}} \right)^{0.45} \quad (2.85)$$

In conclusion by conducting wind tunnel tests on certain chamber designs or by using ready experimental data the occurring pressure flow frequencies can be calculated. Moreover, by linking soil surface pressure frequencies with turbulence frequencies near the soil surface flow infiltration can be calculated. Hence the occurring mass transport can be predicted additionally efflux measurements can be corrected. The Eddy covariance method is not recommended to be used for calm days with low wind speeds. A proposed approach in the research community is the chamber anchoring method it can be used to reduce gas species leakage due to wall shear affects both ways see page 86.

2.7.7. Solubility of Carbon Dioxide and Oxygen in Soil Water

The gas phase of the soil is characterized by the amount or volume and composition of the studied soil sample. The volume fraction of gas generally decreases with depth in a soil profile due to decreasing porosity that takes place as a result of compaction, biological activity and due to the absorbed water content. In the grassland studied case, a volume fraction of gas between 5-15% is generally considered adequate. The composition of the soil air also varies with depth and time. Due to the free diffusion of the atmospheric components through the soil surface, the composition of the soil air near the surface is almost the same as that in the atmosphere. With depth, the concentration of carbon dioxide increases and that of oxygen decreases because of the biological activity in the soil (respiration of plant roots, micro-organisms and soil fauna).

The Reason for mentioning the two gases Carbon dioxide and Oxygen is their direct relationship to the respiration quotient. Some scientists have found that re-wetting of

peatland in south-east Asia will lead to substantial reductions of net greenhouse gas emissions [160]. Carbon dioxide solubility in the soil water content is governed by Henry's law [161], where P_{CO_2} [Pa] is the partial gas pressure of the gas of interest, K_{Solu} [mole/m³Pa] is the solubility constant and C_w [mole/m³] is the dissolved gas concentration in Water.

$$P_{CO_2} = K_{Solu}C_w \quad (2.86)$$

The dissolving of the different gasses, which is to some extent affected by the relation between the soil pH [162] and the soil stored carbon, this in turn would be to soil total porosity, but it can be small enough to be neglected on the short term measurements. Oxidation–reduction reactions occur under various conditions. Increased carbon dioxide affects the soil pH. Carbon dioxide dissolves in water producing both bicarbonates and carbonates as covered by Sposito [163] and Conklin [164]. According to the total pressure, species concentration and temperature profile in the soil layers prediction of the gas species solubility can be predicted in the soil pores. This is shown in equation (2.87) whereby the solubility constant of Carbon dioxide decreases with temperature, meaning that during the period of mid-day the carbon dioxide dissolves less. While during the night and early morning Carbon dioxide dissolves more.

$$K_{Solu}C_w \leq P_{CO_2s} - \alpha_{CO_2} \frac{RT\tau}{2D_{CO_2}\epsilon\delta M_{CO_2}} (z^2 - z_0^2) \quad (2.87)$$

Soil temperature changes during hourly bases in a more evident way therefore measurements conducted using chambers for 6 minutes or even for 24 minutes are reliable to know what the biological activity of a studied location. Therefore, dynamic

chambers are recommended for such a study, static chambers are recommended for more of hourly or long duration measurements. This in turn in affect will give some reasons why in Bogs the error of measurement deviations would most probably occur especially on hot days. Due to water evaporation rates are high, in addition to occurring water circulation currents due to the occurrence of buoyancy affects based on temperature gradients in the soil layers.

The conclusion is that static chambers as long as the process of aeration is applied regularly all the stored heat gained from solar radiation is released, the same for stored cold air during the night. Dynamic chambers also require aeration, this insures a homogenous gas mixture and temperature mixture. Temperature and concentration profiles are necessary to understand the efflux measurements. It is recommended not to have too many circulation fans in the chambers, so that they won't raise the occurring pressure inside the chamber at the soil surface which would resulting from the increase of carbon dioxide solubility. Chamber ventilation is necessary during measurements because entrained gas in the chamber will store heat which in turn would disturb and increase the soil biological activity. A limiting factor for solubility of carbon dioxide is that metabolism is related to temperature occurring in the soil.

2.8. Respiration Chamber Characteristics

Each type of experimental apparatus has its own pros and cons. It is the responsibility of the researcher to choose the suitable apparatus that meets the required needs. This depends on the drive of the conducted research. The advantages and disadvantages of using chambers are summarized in the following sections:

2.8.1. The Advantages of Using Respiration Chambers

The main advantages of the chambers can be summarized as follows:

1. They are relatively easy to use with no need for highly trained researchers to operate them. For ventilation purposes, the chambers early models open and close manually while the latest models are automated and open and close on the site of deployment [165].
2. They have spatial coverage unlike the EC method where there is no spatial coverage. Thus, air samples are directly measured from a tower located near the studied area.
3. The cost of putting together a research purpose chamber is relatively low in relation to a commercial one. The cylindrical shell (made from transparent plastics) can be custom built, and the chamber can be put together at the research institute workshop for instance. As long as the chambers has a classical volume shape.
4. Fast measurements and short waiting times can be reached because of the advanced features that uses forced convection for soil efflux measurements [166].
5. By using custom built sensor boxes connected to the chamber entrainment, they can be used for measuring photosynthesis, evapotranspiration, respiration, temperature, dew point temperature, pressure, and light intensity simultaneously. Gas species concentration can also be measured. That can be done through the many available types of gas sensors in the market [167].

-
6. The chambers can be used in underwater environments to measure carbon dioxide fluxes from seagrass [168] or on peatland locations [30].
 7. Cylindrical chambers can be used to measure the efflux resulting from plants and tree branches.

2.8.2. The Drawbacks of the Chambers

The main disadvantage of the chambers can be summarized as follows. They were presented in this form to give a clear description to the ideas which varied substantially in topic:

1. The chambers affect the efflux being measured causing collar and pressure problems. The collar problem occurs when the studied soil surface is not flat. The soil that has rocks and gravel would also make it difficult to fix the chamber on the soil surface. The pressure problem occurs when a pressure difference takes place between the inside and outside of the chamber causing leakage in and out of the chamber [93].
 2. If left at the same site for several months, chambers may change the conditions in the soil, such as grass over growing between inside and outside the chamber. The same applies for increase of plantation cover in a forest site location between two seasons of winter and spring.
 3. They are difficult to use in winter especially in critical weather conditions. The accumulation of the snow over the shell leads to the blockage of the solar rays into the chamber affecting the photosynthesis. The chamber might break or deform if surrounding water freezes, crushing its outer shell. In desert
-

locations, extreme heat might cause them to melt down because heat buildup in the chamber would gradually cause the inner chamber to deform and gradually collapse inwards.

4. The differences between the chamber types require calibration. To overcome this problem, there have been many proposals to use cross-calibration functions for the soil carbon dioxide efflux measurement systems [169].
5. It is often cited that a closed chamber underestimates the actual flux due to the mass accumulation or the concentration buildup within the chamber headspace, while a dynamic chamber over estimates the actual flux due to the pressure difference present inside the chamber and caused by drawing an airstream through the chamber. The underestimate bias of closed chambers has been demonstrated in some experiments where concentrations within the chambers headspace showed a nonlinear increase with time, or where the fluxes measured by closed chambers were compared with those measured by dynamic chambers [71].
6. Chambers need to be fixed well to the ground because on windy locations they can be blown off.

2.9. Chambers Anchoring or Insertion into the Soil

Chamber insertion method is by pushing the chamber on or into the ground. The chamber anchoring method is by fixing the chamber onto a fixed base that is inserted into the soil to a predetermined depth, the purpose of such action is to reduce the occurring mass transfer from in and out of the chamber based on external occurring

events, to stop leakage. One method of mechanical fixture is through the use of collars presented by Heinemeyer et al. [170], or through using the insertion method. An extensive study to quantify chamber pressure effects on soil location was investigated by Sah et al. [171]. Numerical models have also been used to evaluate the anchoring method as done by Healy et al. [172]. Heinemeyer et al. [170] have found that collar-insertion depth has a potentially long-lasting effect on measured flux rates and needs to be considered when interpreting past data and planning future studies. They demonstrated the need either to avoid insertion or to measure the amount of cut roots when inserting collars, and for the deployment of less intrusive techniques such as stable isotopes or membrane techniques. The chamber clamp method has been applied for a dynamic chamber case for a grassland site, while mixing fans that blow air in a perpendicular direction to the soil surface were used [91]. The test results strongly suggest that, to get accurate measurements of soil respiration, collar insertion is strongly recommended. After a while, scientist started to investigate the insertion depth applicability, as done by Nobuhiro et al. [173] where the collar was pushed inside the soil to a distance ranged between 5 and 8 cm. Aneja et al. [174] used the anchoring method to a depth of 6 to 8 cm the selected depth purpose is to ensure complete entrainment. Rochette et al. [37] tested the anchoring depth of 10 cm. Jassal et al. [31] stated that 75% of the carbon dioxide efflux comes from the top 20 cm of the soil.

Reliability of the chamber systems was not related to the measurement principle as stated by Pumpanen et al. [99], good results can be achieved with both steady-state and unsteady-state chambers. However, even the same chambers with different collar

designs showed highly variable results. The general trend seemed to be that non-steady-state non-through-flow chambers systematically underestimated measurements by 4–14%. Likewise, no significant differences between through-flow chambers were observed.

In a grassland study [175] anchors have been left for over 10 years. One advantage of leaving anchors in place for long periods of time is that soil disturbance and root damage are minimized. The problem with anchored chambers is that during a rain fall they create ponds of water around the chamber. Chamber-soil contact mode has a significant impact on the efflux measurement as mentioned by [169] this was observed when using collar or insertion mode. The resulting general high efflux values obtained by using the “insertion” mode can be explained through the following three hypotheses:

1. Diffusion conditions would change in the litter and near surface mineral layers while inserting the chamber. When insertion is conducted the soil surface litter is disturbed [176] , therefore the vertical diffusion coefficient is increased resulting in an initial jump of efflux measurements.
2. On a long-term study, carbon dioxide efflux measurements are affected after a collar placement has been installed, due to fine plant roots getting cut during the process
3. When using collar or drilled ring method a distance is created between the structural outer shell and the soil surface. When a blowing fan is used the boundary layer created on the soil surface is thinner for a collar method than

that of a drilled ring, this resulted in an increase in carbon dioxide efflux measurements by the used insertion method [177].

In conclusion static chambers are practical for use for a long period deployment. A way around this problem is to see what correction factor that can be obtained, and when using the anchoring method. So, for example to derive such a factor experimentally the researcher can measure the flux without having an anchoring method at steady conditions and then check the difference in flux resulted from the anchoring.

2.10. The Role of Soil pH/Bacteria on Carbon Dioxide Production and Transport in Soil

Soil pH is a measure of its acidity or alkalinity and it is expressed in a numerical scale. The scale goes from 0.0 to 14.0 with 0.0 being the most acid and 14.0 being the most alkaline. Researchers have explored the relationship between soil efflux and pH and have found that soil pH and relative root mass are found as important factors to describe spatial variation of soil carbon dioxide emission due to vegetation productivity and microbial activity spans [178]. Speaking from a abiotic perspective, by knowing the soil site pH, the mineral constituents of the soil sample can be estimated in a qualitative manner [179]. On the other hand, from a biotic (biological) perspective looking closely at a bacteria cell, we find that it contains several hundred enzymes, most of which are pH dependent and are associated with cell components, such as membranes. Moisture porosity is of importance in relation to pH because it reflects the contained water content of the studied soil on location, studies have showed that moisture porosity till a value of 21% increases CO₂ efflux, then any

increase after that value results in a decline in fluxes[180]. Soil pH plays a major role because it influences several soil factors affecting plant growth [181] which can affect the carbon dioxide measurement , such as:

1. Nutrient leaching occurs if there are big concentration gradients in the soil layers, leaching intensity decreases with depth as a result of water plant uptake and evaporation [182]. Plant nutrients leach out of soils with a pH below 5.0 in a more rapid manner than from soils with values between 5.0 and 7.5. Leaching effects have been studied for grassland and forest sites [162], only on long duration time scales leaching effects can be seen on the carbon dioxide production by the plants and the bacteria, because it directly affects the location carbon pool. Moreover, excess rain fall [183] does affect the soil leaching only if rainfall exceeds a rate of 6.35mm/h.
2. Nutrients availability affects carbon dioxide production in the autotropic and heterotropic process [184]. Plant nutrients are generally most available to plants in the pH range from 5.5 to 6.5. For most plants, the optimum pH range is from 5.5 to 7.0, but some plants will grow in a more acid soil or may require a more alkaline level. That is why the researcher has to make a survey of the existing plants on the studied soil surface. Most of the known bacteria species grow within a pH range from 4 to 9 while in the case of fungi they are acidophilic, with a pH range from 4 to 6 [71].
3. Toxic elements, if found, cause a decrease in the carbon dioxide production [185] because they act as inhibitors for growth and metabolism for bacteria,

for plants they also have unwanted affects [186]. Therefore aluminium and manganese should be in the safe limit depending on type of plant, this has been proved for Rye grass [187].

4. The acidity or alkalinity of the soil plays a role in changing the permeability (soil structure) on the long-term basis, where new pores are created due to the consumption of the chemical constituents and other pores are closed due to new chemical constituents being created. The rate of this change ranges from the micropore to the macropore scale depending on the intensity of the process.

In conclusion chambers should preserve as much as possible the carbon pool of the location. That is by the chamber not contributing directly or indirectly to the soil leaching effect. Unfortunately, extreme weather conditions do occur and cannot be controlled according to the site of study. High blowing winds or sudden temperature rise would increase the water evaporation rate causing soil leaching. Nutrient leaching for soil also occurs if plant root growth is disrupted inside or outside the chamber. Avoiding the creation of water pools around the chamber is recommended because it disturbs the original site ph.

Bacteria play an important role in the decomposition of the organic materials, especially in the early stages of the decomposition when the moisture levels are high. In the later stages of decomposition, fungi tend to dominate. Soil bacteria metabolism is related either to aerobic or anaerobic conditions which links up to soil parameters of porosity and permeability, this proves why there is an important factor of aeration or regular watering.

Microorganisms abound in the soil and are critical to the decomposing of the organic residues and to the recycling of the soil nutrients. The Bacteria are the smallest and most hardy microbe in the soil and can survive under harsh or changing soil conditions. The bacteria are important in producing polysaccharides that cement sand, silt, and clay particles together to form microaggregates and improve the soil structure. Their activity can increase carbon dioxide flux [188]. The decomposition rates in the soil under elevated carbon dioxide would be slower, resulting in an increased carbon storage in the soil [189]. Bacteria growth phases have been characterized and modelled by [190]. A new Growth of bacterial cultures' 50 years on: towards an uncertainty principle instead of constants in bacterial growth kinetics [191]. Bacteria population goes through 5 phases in relation to time these are as follows: lag, exponential, deceleration, stationary and death phase this is shown in Figure 23 :

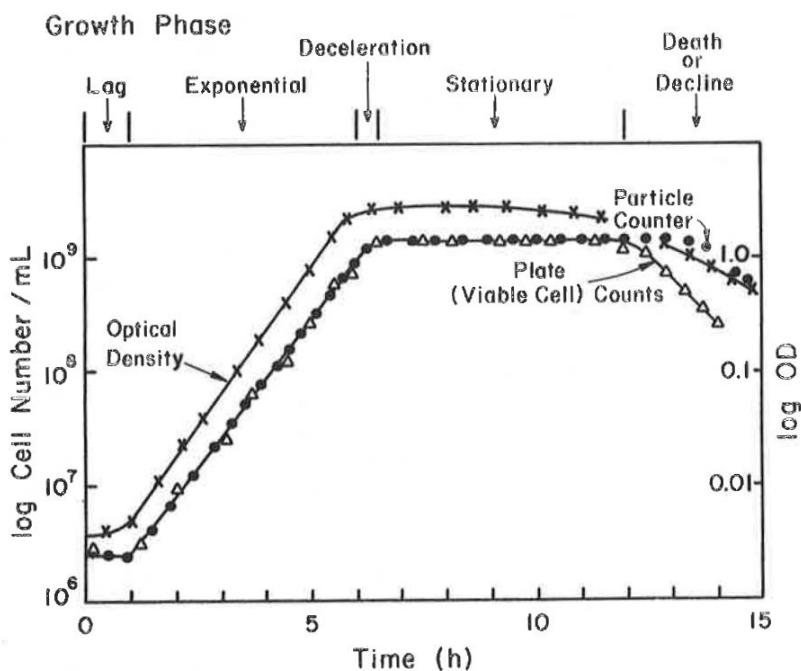


Figure 23: Typical growth curve for a bacterial population. Note that the phase of growth depends on the parameter used to monitor growth [192].

This drives us to the conclusion that one of the main challenges of site location of study is that bacteria cultures are distributed in a random manner and identifying at which stage the soil bacteria is going through is difficult in addition to population distribution. Hence one of the recommended methods of modelling growth and population is by linking these parameters to soil layers through the use of statistical and probability distribution functions.

The carbon dioxide efflux is related to the average value of the log number of bacteria, for each stage of growth cycle. Experimental tests have been conducted through integrated evaluation of soil quality after the incorporation of organic matter and microorganisms [193] this is illustrated in Figure 24. Furthermore, the change of carbon dioxide efflux is related to date of incubation.

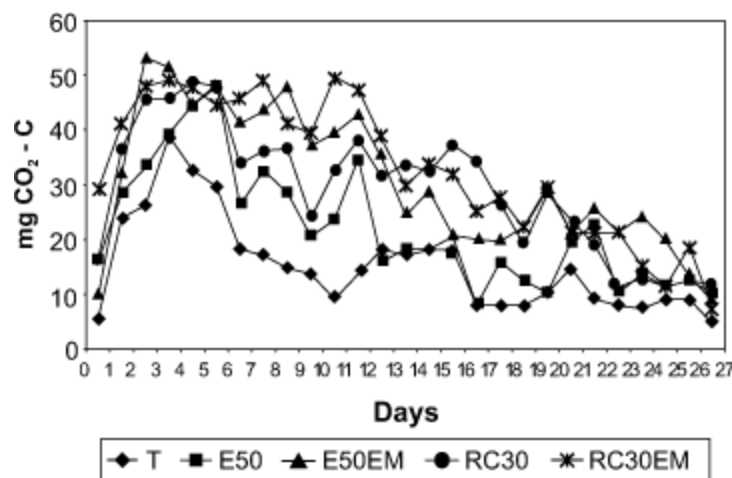


Figure 24: Determination of total microbial activity ($\text{mgCO}_2 - \text{C}$) in sample of soil mixed with different types of organic matter, incubated at 25°C [193] .

There is also an important relationship between bacteria cultures and temperature stated in [194], This has been modelled by for the biokinetic temperature range [195].

At some instances it is been reported that by disturbing the soil at a site of interest a

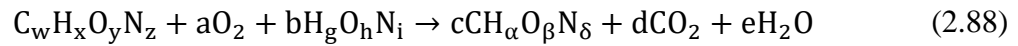
jump in soil flux dose occur [176]. That's resulted in the adoption of the soil tilling method on agricultural locations of farm lands, because with the aeration of the soil biological activity is stimulated. The air of the soil is made up of the same basic constituents as the atmospheric air; however, the ratios of various gases are different and more variable due to that diffusion is the dominant factor for mass transport in soil cavities. Bacteria also gets transported within water flows, when rain storms hit the soil site location [183], this has been proved for an agricultural site, where crop fertilizers where used that contained bacteria. It is very important to point out that almost all the void volume of the soil can be occupied by either air or water. The amount of air in the soil is thus inversely related to the amount of water present. When the air content is around 50% or more of the void volume, the soil is considered to be aerobic and oxidation reactions predominate. When the void volume is occupied by water, the soil becomes anaerobic and reducing reactions predominate. The ratios of volume fraction distribution for masses, Soil atmosphere composition under aerobic and anaerobic conditions. The Aerobic bacteria are those that need oxygen. This means that they are related to the volume of the gas pores, so aerobes tend to dominate when the soil is well drained as an example for a desert soil location. Anaerobes, on the other hand, are the bacteria that do not need oxygen and may find it toxic, these kinds of bacteria can be found in ponds, wetlands, peatland respiration, respiration chambers have also been used in ponds [196]. This means that they are related to the volume of liquid pores. The oxidation reactions in the soil, particularly those carried out by the microorganisms and plant roots increase the amount of carbon dioxide in the soil air to 10 times or more the concentration in the atmospheric air. As a result of

that the oxygen content will be proportionally decreased. When the soil void volume is almost or completely filled with water, the remaining trapped and dissolved oxygen is quickly utilized by the organisms and the oxygen content of any remaining gas will become zero. The soil will then become anaerobic and the reducing conditions will prevail. The Aerobic bacteria are those that need oxygen. This means that they are related to the volume of the gas pores, so aerobes tend to dominate when the soil is well drained. Anaerobes, on the other hand, are the bacteria that do not need oxygen and may find it toxic. This means that they are related to the volume of liquid pores. In this studied attention is paid to both the aerobes and the anaerobes because of their relationship with porosity and permeability.

Microbial activity is the flux of carbon through a biotic system. Microbial activity is normalized with growth microbial activity to give the relative microbial activity. The relative microbial activity in any site is related to the soil porosity. This reflects the rate of production of carbon dioxide for both anaerobic and aerobic conditions. There is a common conceptual relationship [197] that shows where the soil carbon dioxide efflux becomes slow under dry conditions. It reaches a maximal rate at the intermediate soil moisture level, and decreases at high soil moisture content when anaerobic conditions prevail to depress aerobic microbial activity. The optimum relative microbial activity is usually somewhere near field capacity.

In conclusion, lab-based analysis of the soil sample is required to identify the soil bacteria, and then the respiration quotient can be found. The focus here will only be on aerobic bacteria due to its strong relationship with aeration process. The aeration process [192] in the respiration chamber does not consume all the available oxygen in

the chamber. Respiration quotient differs for one type of bacteria to another meaning that each type of bacteria has different stoichiometric coefficients. In general, the process is represented in equation (2.88):



The carbon balance C shown in equation (2.89) is found from equation (2.88):

$$w = c + d \quad (2.89)$$

The hydrogen H balance shown in equation (2.90) is found from equation (2.88):

$$x + bg = c\alpha + 2e \quad (2.90)$$

The oxygen O balance shown in equation (2.91) is found from equation (2.88):

$$y + 2a + bh = c\beta + 2d + e \quad (2.91)$$

The nitrogen N balance shown in equation (2.92) is found from equation (2.88):

$$z + bi = c\delta \quad (2.92)$$

By solving simultaneously, the system of equations (2.89 to 2.92) for a specified type of bacteria: $C_w H_x O_y N_z$. The Respiration quotient for a specific type of bacteria n can be found using equation (2.93). Where the ratio is in d [mole/s] of produced carbon dioxide over a [mole/s] of consumed oxygen:

$$RQ_n = \frac{CO_2 \text{ Produced}}{O_2 \text{ Consumed}} = \frac{d}{a} \quad (2.93)$$

The individual efflux from a single soil microbial cell ef_{mcell} [mole/m²s] can be calculated from equation (2.94). This equation was proposed by [198] where C_0 [mole/m³] is the solute concentration at the cell surface, C_b [mole/m³] is the solute concentration in bulk soil is, D_0 [m²/s] is diffusivity, K_b is constant, θ is the volumetric water content, and S [m] is the diameter of a bacterial cell:

$$ef_{mcell} = \frac{(C_0 - C_b)D_0K_b\theta^3}{S} \quad (2.94)$$

In particular the model can be extended to calculate the total efflux ef_{BP} [mole/m²s] for a bacterial community. Where by the total number of bacterial cells N_b is for a specified area or volume of a soil sample. Then for simplicity this can be applied to the whole soil volume located beneath the respiration chamber:

$$ef_{BP} = N_b ef_{mcell} \quad (2.95)$$

The respiration quotient of the whole bacterial activity at one location is in equation (2.96) this represented by the summation $RQ_{Total\ Bacteria}$ of all respiration quotients.

$$RQ_{Total\ Bacteria} = \sum_1^n RQ_n = RQ_1 + RQ_2 + \dots RQ_n \quad (2.96)$$

To calculate the total generated efflux $ef_{Total\ Bacteria}$ [mole/m²s] from aerobic bacteria at a specified location soil surface area $A_{Soil\ Area}$ [m²]:

$$ef_{Total\ Bacteria} = \frac{[Total\ Consumed\ O_2]. RQ_{Total\ Bacteria}}{A_{Soil\ Area}} \quad (2.97)$$

Soil bacteria types classification can be found in Hoorman [181], Abbott and Murphy [199] this helps in finding the $C_wH_xO_yN_z$ for the bacteria of interest . The main focus on aerobic bacteria is because the respiration chambers measure the biological activity of the top layers of the soil. Respiration chambers have an impact on bacterial activity because they do disturb the bacteria cultures distributed on the location. Chemical reactions are governed by temperature therefore the efflux in equation (2.97) is a function to soil temperature. It has been noted by Fullner [200] that soil temperature affects root growth in parallel soil nutrients also contribute, therefore there should be some heat balance achieved in the respiration chamber gas and the soil volume beneath the chamber. Chambers at some points have negative effects on stem growth especially in rain forests [201] but also this can allow us to identify the complex interactions between canopy foliar and reproductive dynamics, stem growth, soil processes, and nutrient fluxes as exclusion provokes progressively larger soil moisture deficits. Using closed dynamic chambers, Gaumont et al. [202] have pointed out that there is a relationship between soil porosity, carbon dioxide flux and root rhizospheres. That was proved through data measurements collected from the sites of several forests during dry seasons, these showed less activity of the root rhizospheres. Root respiration was found to depend mainly on the soil fertility, which has been discussed extensively in the classical references of [203] and [204]. One concern according the respiration chambers use is that they should minimize their effect on the transport of nutrients, and nutrient exchange with plant roots. In conclusion temperature affects the activity therefore there has to be some balance between the inner temperature of the chamber and atmospheric outer temperature.

2.11. Summary

This chapter surveys the different soil physical, biological and geotechnical parameters and links them to meteorological ones. Consequently, it explores their direct and indirect effects to the produced soil efflux. Furthermore, this chapter proposes several soil temperatures models according to the studied case constraints to see what affects soil efflux production. Regarding the issue of pressure, a clear understanding of what affects the measurement process was achieved through surveying all the internal and external pressure parameters and how they influence the chamber in relation to time when disturbance does occur. The conclusion is that respiration chamber designers need to preserve chamber internal temperature and pressure to be equal to the outer atmosphere for the case of stable external conditions. For the case of unstable external conditions design counter measures are incorporated. Furthermore, the appropriate gas sensor needs to be selected professionally with emphasis on the importance of installation location inside the chamber. Likewise soil bacterial type and soil temperature also has an influence on efflux production.

Chapter 3

Experimental Design

3.1. Introduction

The chapter starts by presenting the chamber design requirements. Furthermore, it covers the proposed five chamber designs and presents the selection criteria of the most feasible design. It reports on the respiration chamber experimental setup with all of its different parts furthermore including the sensors. This is followed by the carbon dioxide measurement methodology. The description of the geological site for the University of the West of Scotland grass land. This will be followed by a description of the climate of the City of Glasgow, Paisley.

3.2. Chamber Design Requirements

The experimental system was designed to study a condition where an emission occurs from a constant gas source at the top layer of the soil. Measuring gas emissions from the soil and the water surfaces to the atmosphere is done through the use of the enclosure-based methods which have either static or dynamic flux chambers. The main objective of this experimental set up is to replicate the environmental interaction between the soil and the air. When the chamber was designed these requirements were made:

- 1- The chamber can operate in steady (switched off fan) and unsteady mode (switched on fan), at the unsteady state the airflow should sweep over the entire covered soil surface.

-
- 2- The gas efflux should be of uniform magnitude over the covered surface by the chamber. The pattern of the airflow in the chamber should be relatively uniform in speed across the swept soil surface. This is to create the necessary suction pressure to draw out the carbon dioxide gas species from the top soil layer.
 - 3- The fan inflow and outflow should ensure that a well-mixed air/CO₂ mixture is circulated inside the chamber.
 - 4- The diffusive flux is dominant in the steady state of operation likewise the advective flow is negligible, on the contrary for the unsteady state the case is vice versa.
 - 5- The pressure difference between the inside and outside of the chamber should be kept to the minimum, that is through using the chamber installation base with the soil.
 - 6- The material for chamber fabrication should be strong to avoid possible structural deformation under field conditions. A deformed chamber body may cause leakage in the system and produce errors.
 - 7- The outside surface of the chamber should be able to reflect solar radiation.

Based on these requirements a simple model has been used for calculating the steady-state flux.

3.3. Proposed Chamber Designs

The two main respiration chamber prototype designs are covered in this section. Hence after the proposal of the designs is to show how the project matured to its final state. Consequently, a computer model of the chamber was made, the dimensional data of the chamber is provided in the appendices.

3.3.1. Proposed Chamber Design 1

Initially at the beginning a hemispherical shaped chamber design was proposed as shown in Figure 25. The shape design is convenient for a static chamber case. It is made to be used in a laboratory with half a sphere as a metal and the other as transparent plastic in material. Care was taken to make the chamber mobile in the lab through equipping it with 4 caster wheels. A soil sample can be brought from location and poured in the metal hemispherical cup. Alternatively, the half spherical container can be filled with sand silt and clay which in return can control permeability values.

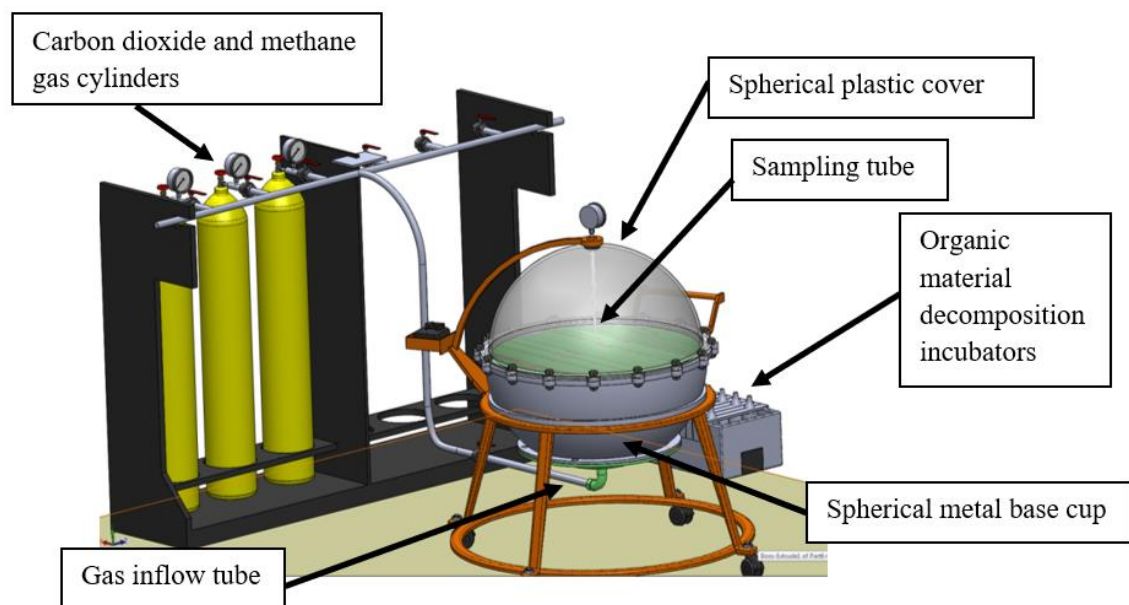


Figure 25: The proposed spherical chamber concept.

Carbon dioxide biological activity can be mimicked by assigning a flux of carbon dioxide pumped at the bottom location of the chamber from a gas cylinder source. The efflux would diffuse through the pre-prepared soil sample consequently the chamber in this case can be used to study soil texture effects on gas species mass transfer. On the other hand, biological activity can be used and controlled to produce carbon dioxide gas by using incubators situated beside the cylinders as shown in Figure 25 .

Hence organic material decomposition rates can be controlled by temperature. Mineral composition in soil water and soil pH can be also be pre-specified which relates to soil porosity. Carbon dioxide concentration measurements can be taken at the top part of plastic hemisphere. Unfortunately, Perspex or metal spherical shell shapes are difficult to manufacture and expensive to be made on an individual basis. Another restriction is the difficulty in taking a hemispherical soil sample from the location. That have all the soil layers intact after the extraction.

3.3.2. Proposed Chamber Design 2

For the reason of some of the manufacturing restrictions furthermore soil sample collection difficulty another design was proposed Figure 26. A static cylindrical lab chamber design was proposed to resolve the manufacturing setback. In particular no blowing wind occurs over the soil surface hence omitting out naturally generated disturbance in nature. Apparently using a cylindrical base allows more soil layers to be added for the setup study. This allows the researcher to have more options to control the different factors of the carbon dioxide efflux.

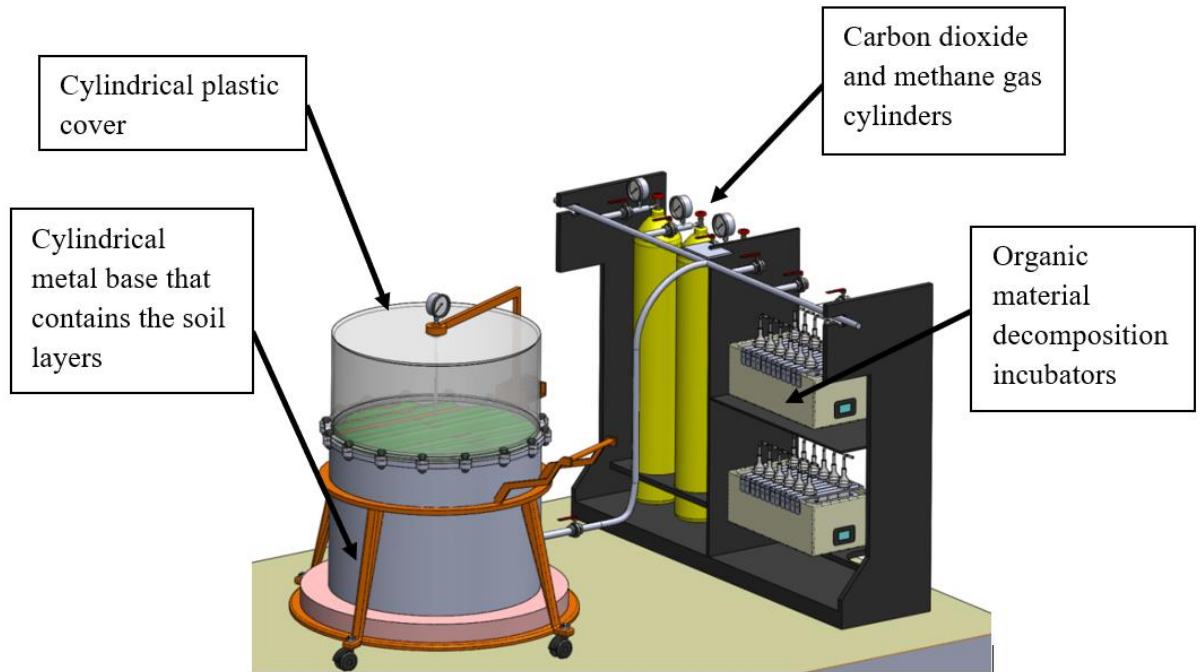


Figure 26: The static cylindrical chamber design shown on the left with the incubators and gas cylinders on the right-hand side.

3.3.3. Proposed Chamber Design 3

The new chamber can be deployed to the site of interest Figure 27. It can be used in two types of regimes static/dynamic. The use of two blowing fans added the dynamic operational mode. During the design process another approach was adopted in this case whereby having in mind reducing the weight of the used chamber and soil site sample disturbance encountered. A new simplified prototype design was put forward by cutting down on the number of used parts. This was achieved by omitting the metal base cup from the design and relying mainly on a smaller in size cylindrical chamber. It would require a portable energy source to power the blowing fans. The blowing fans would increase the rate of mixing inside the chamber, decreasing time of sampling.

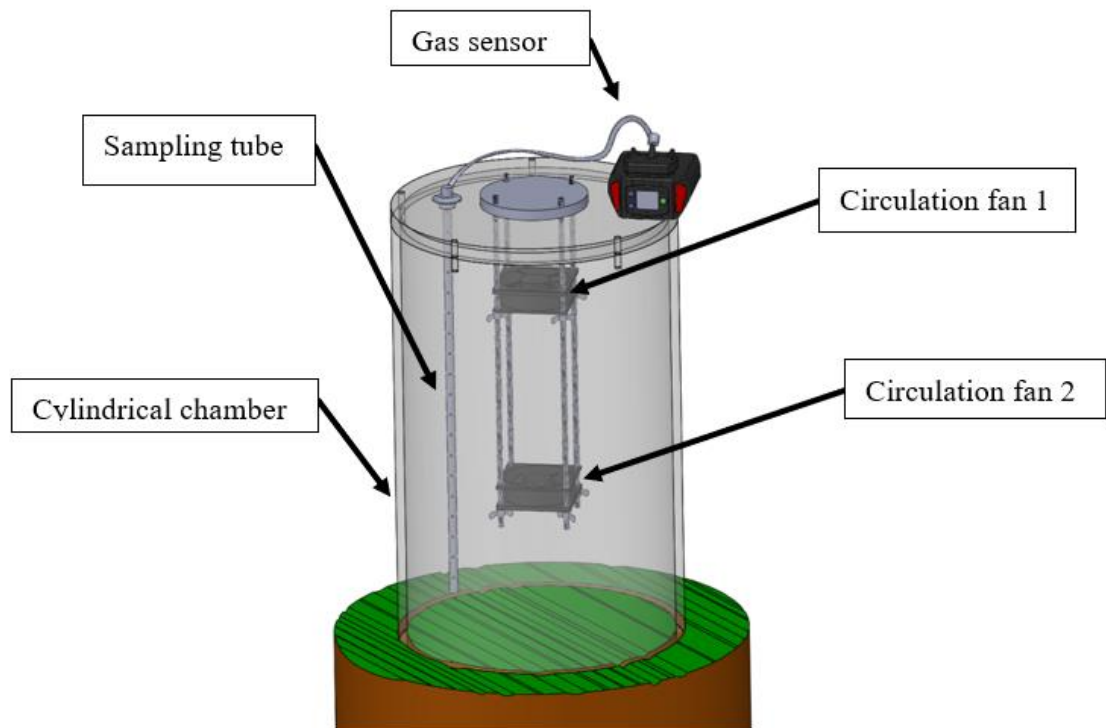


Figure 27: The dynamic respiration chamber notably it uses two blowing fans.

CFD simulations ran inside the chamber gas domain showed that using two blowing fans increases the internal chamber pressure. Therefore, this leads to gas leakage to occur to the outside of the chamber. Likewise using two fans cause excessive inner circulation in parallel they require more battery power. The gas sensor to be used with the chamber is Drager X-am 7000 [205]. What was later observed during on site trials that a chamber base was proposed to be used to protect the chamber base from wear. After testing the gas sensor on site, it was evident that the proposed gas sensor to be used doesn't give instantaneous carbon dioxide measurements to the required time frequency. For instance, it requires a sample to be drawn into the sensor and then it needs about 10 to 15 [s] to analyse the sample and then it produces readings. Consequently, this affects the efflux readings in relation to time whereby the required

efflux jump occurs in the first 150 [s] of data collection. Hence the concentration curve is plotted with fewer points consequently making it difficult to capture the required initial flux jump as shown in Figure 3. The chamber cover is fitted to the chamber shells with 5 screws what was a source of concern is the issue of outer shell screw thread hole wear. This was anticipated as a problem because planned chamber aeration after each experimental measurements period was done through removing the chamber cover. All encountered inner sharp edges inside the chamber were avoided and kept to the minimum. The only left edges where the blowing fans outer casing side edges. This is intended to reduce the sources of flow turbulence inside the chamber while the mixing fans are switched on.

3.3.4. Proposed Chamber Design 4

To resolve the mentioned setbacks in the previous design shown in Figure 27 new design modifications are applied to the chamber which matured into the design shown in Figure 28. To preserve the inner gas environment inside the chamber whereby no leakage would occur during the measurement the chamber was provided with a plastic base shown to have a brown colour. To reduce the acting pressure on the soil surface to about 0.7 [Pa] one fan was considered to be used at a distance of 22 [cm] from the soil surface (as shown in equation (2.77)). The reason for considering that value for pressure is it mimics a case for wind velocity of 1 [m/s] at the location. The acting blowing pressure on the soil can be controlled based on the distance of the blowing fan from the soil surface. The 4 connecting beams are threaded and the fans elevation can be changed manually. The relationship between blowing fan velocity and occurring pressure at the soil surface is shown in Figure 29.

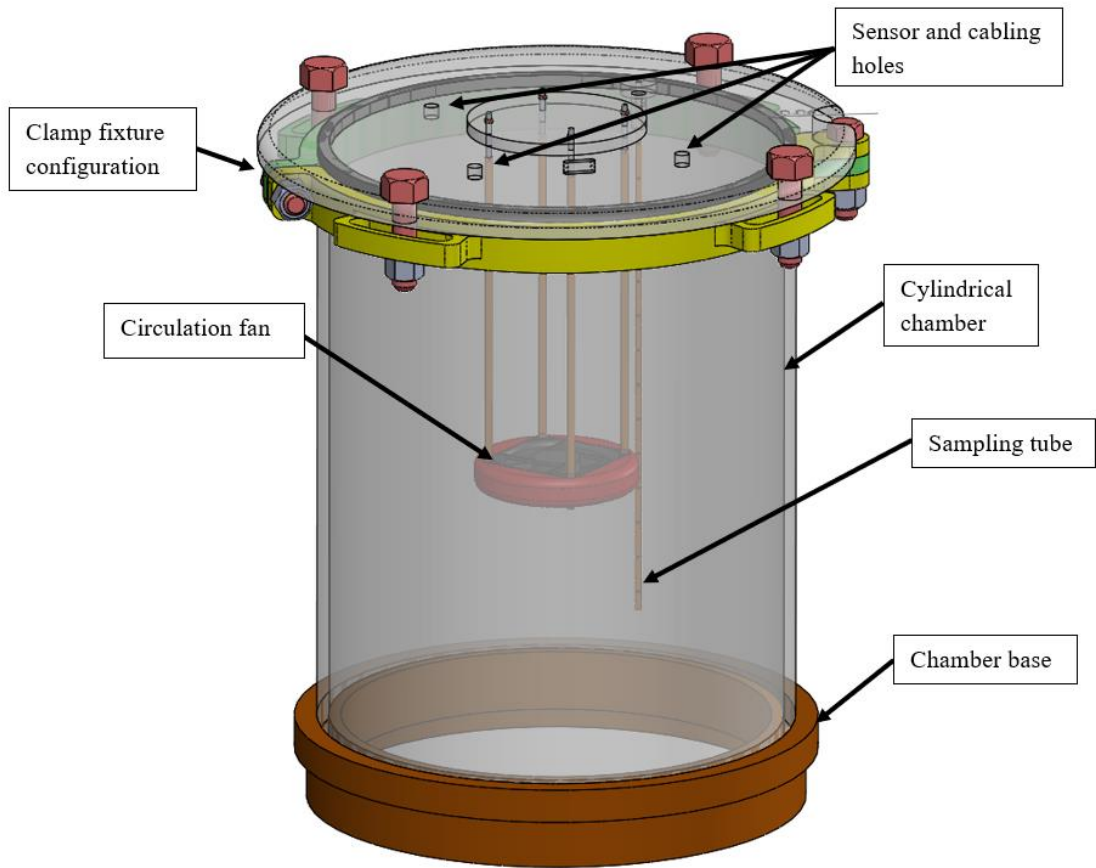


Figure 28: Using the clamp method to fix the top chamber cover.

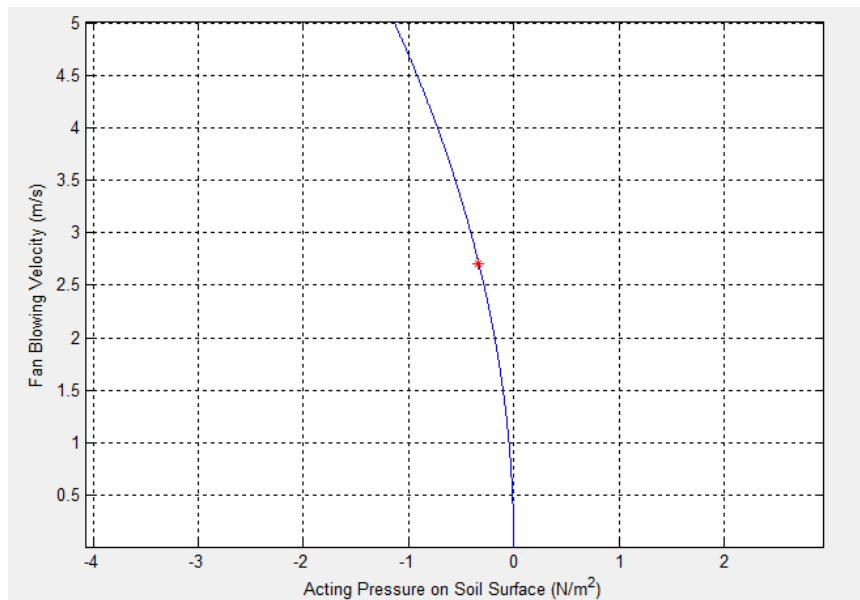


Figure 29: Specifying for the studied fan what acting pressure is occurring on the soil surface inside the chamber, the working point shown in red.

To omit out all the sharp edges inside the chamber a streamlined fan case (shown in red) was fitted to the blowing fan case. A plastic tube cover was applied to the four threaded beams connecting the fan with the chamber cover. Likewise, a clamp cover fixture was added to the chamber. A rubber seal is used to prevent any gas leakage to occur from the chamber cover section. The clamp fixture doesn't require any machining to the expensive chamber shell. By unscrewing the four screws fixing the cover to the clamp chamber ventilation can be achieved during measurements. Later on, the designed clamps proved to be difficult to manufacture and a solution had to be looked for this led to the final form of the chamber.

3.3.5. Proposed Chamber Design 5

The final optimized agreed upon design is shown in Figure 30. A substitute for the clamp cover method was found. The chamber shell is drilled with 6 holes then 6 half threaded studs are glued to the chamber holes. The chamber cover is placed on the 6 studs after placing a rubber seal between both. Six washers are used on the threaded half of the studs to tighten the closure. What is agreed upon is that the chamber ventilation procedure to be used is by raising the chamber out of its base foundation furthermore laying the chamber on its side after each taken measurement. The chamber base preserves the locations integrity to some extent because it is only setup once on the location. Furthermore, the fan is turned on for 2 – 3 [min] to blow out all the accumulated carbon dioxide inside the chamber.

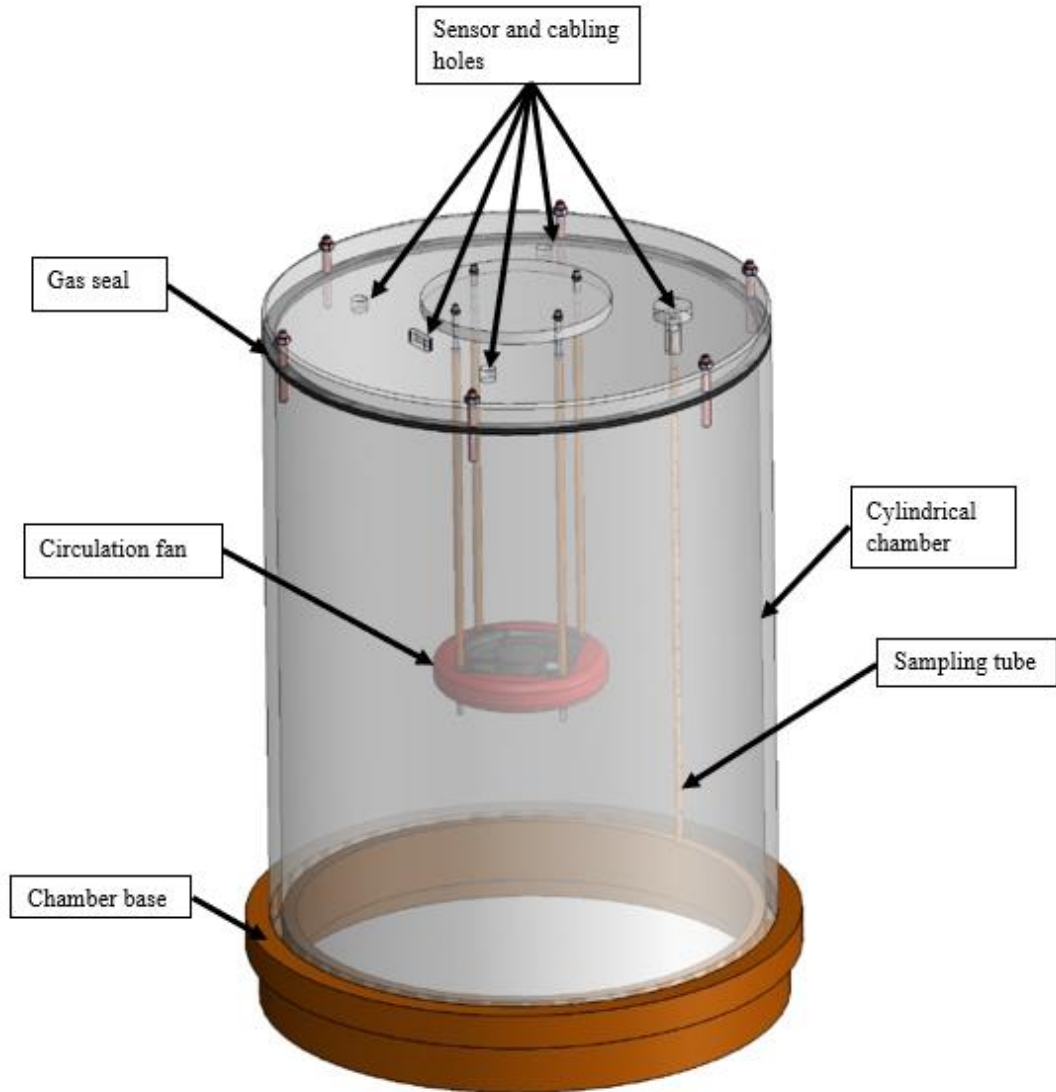


Figure 30: The chamber design agreed on to build.

During the experiment, the system is placed over the soil surface at ambient temperature. The main challenge of concentration measurements is acquiring instantaneous samples hence this was done using a non-dispersive infrared gas sensor. The chamber works on two operating modes these are static and dynamic. The static case means longer measurement time as revealed by the long diffusion time required by the carbon dioxide species to spread in a homogenous manner inside the chamber gas volume. The dynamic chamber mode is used for the reason to rely on diffusion

inside soil layers and on forced convection inside the chamber using the circulation fan. Consequently, that would decrease the time required for onsite deployment and sampling.

Table 1 presents six column categories relating to chamber design and biological and physical parameters. The reason for choosing design 5 is that it can be used for both static and dynamic operational mode. Likewise, it is open from the bottom allowing it to be used on natural locations consequently measuring natural produced efflux from occurring biological activity in both soil and due to photosynthesis from natural sun light rays.

On the other hand,

Table 2 presents six column categories relating to total chamber cost also apparatus weight moreover chamber gas volume additionally the used gas sensor method as well as electrical power source and finally chamber base fixture method. The reason for choosing design 5 is that it is reasonable in price in relation to other designs. Additionally, it is light in weight likewise it uses a non-dispersive gas sensor giving it an advantage to take concentration measurements every 5 seconds. It uses a solid base fixture to preserve the 0.06 [m³] of gas volume enclosed to be analysed without any external gas contamination.

Table 1: Categories relating to chamber design and biological and physical parameters

	Mode of Operation	Chamber Mobility	Chamber Gas Volume Closure	Carbon Dioxide efflux source	Type of Light Source	Type of Soil Sample
Design 1	Static	Lab use only	Complete Closure	Biological / Gas Cylinder	Artificial Lab Light	Natural or Artificial
Design 2	Static	Lab use only	Complete Closure	Biological / Gas Cylinder	Artificial Lab Light	Natural or Artificial
Design 3	Static/ Dynamic	Off-site/Lab use	Open from the bottom	Biological	Artificial Lab Light/ Natural Sun Light	Natural
Design 4	Static/ Dynamic	Off-site/Lab use	Open from the bottom	Biological	Artificial Lab Light/ Natural Sun Light	Natural
Design 5	Static/ Dynamic	Off-site/Lab use	Open from the bottom	Biological	Artificial Lab Light/ Natural Sun Light	Natural

Table 2: Categories relating to total chamber cost also apparatus weight moreover chamber gas volume additionally the used gas sensor method as well as electrical power source and finally chamber base fixture method

	Apparatus Cost £	Apparatus Weight [kg]	Chamber Gas Volume [m ³]	Used Gas Sensor	Power Source	Chamber Base Fixture
Design 1	5000-10000	100	0.1	Drager X-am 7000	Power from Mains	Not required
Design 2	5000-3000	120	0.12	Drager X-am 7000	Power from Mains	Not required
Design 3	800-1000	35	0.06	non-dispersive infrared gas analyzer	Battery/ Power from Mains	Not available
Design 4	5000	30	0.06	non-dispersive infrared gas analyzer	Battery/ Power from Mains	available
Design 5	2000	30	0.06	non-dispersive infrared gas analyzer	Battery/ Power from Mains	available

3.4. Experimental Study

Under the section of experimental study, the description of the chamber main parts is covered.

3.4.1. Chamber Description

The designed and made static/dynamic respiration chamber at UWS is shown in Figure 31. The used annotations on the figure are to name all the necessary parts required to describe the apparatus.

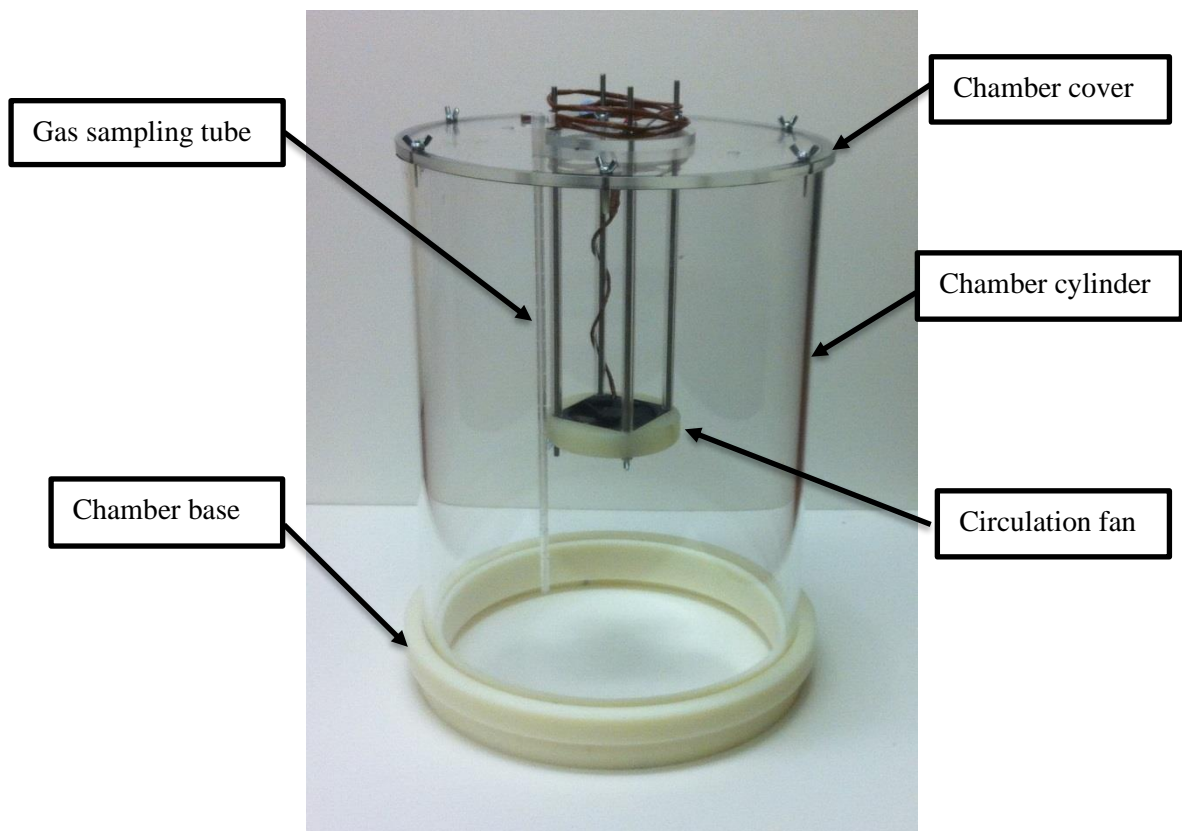


Figure 31: The used respiration chamber a prespective view with a numbring notation referring to its different main parts.

The used experimental apparatus follows the closed dynamic chamber method, where a cylindrical shaped chamber is placed over the surface of the soil. Currently, the

closed dynamic chamber mode of operation is the most common method used by researchers to measure soil respiration. All trace gas flux measurements on the grassland site were performed by placing a novel dynamic flux chamber equipped with one internal blowing fan. This combination allows carbon dioxide to be mixed in a homogenous manner with air in the chamber. The experimental system is a cylindrical transparent plastic (Perspex) chamber that has a height of 0.5125 [m] and a diameter of 0.38 [m]. Likewise, these dimensions create a chamber footprint of 0.113 [m²] in addition to an internal chamber gas volume of 0.06 [m³]. Additional geometric data about the chamber is found in the appendices on page 276.

3.4.2. Sensing Box

The sensing box as shown in Figure 32 is composed of a number of sensors these are all connected to a microcontroller. The sensors can record carbon dioxide concentrations, temperature, relative humidity, Dew point and light intensity sensor. The gas species sensor uses the non-dispersive infrared gas analyzer method which measures carbon dioxide gas concentrations in air shown in number 2 notation on Figure 32. To provide accessibility to the sensors cabling and to the circulation fan several holes are made on the chamber top cap cover. The sensor box is fitted with the wireless antenna to transfer data to the wireless rotor connected to the laptop. The sensing box is fitted to a sampling tube which collects the data from within the chamber. A precise calibration was made before the experiments as recommended by the manufacturer this be measuring atmospheric carbon dioxide concentrations which

should show 400 ppm. Hence when other values occur a reset button is available to calibrate it.

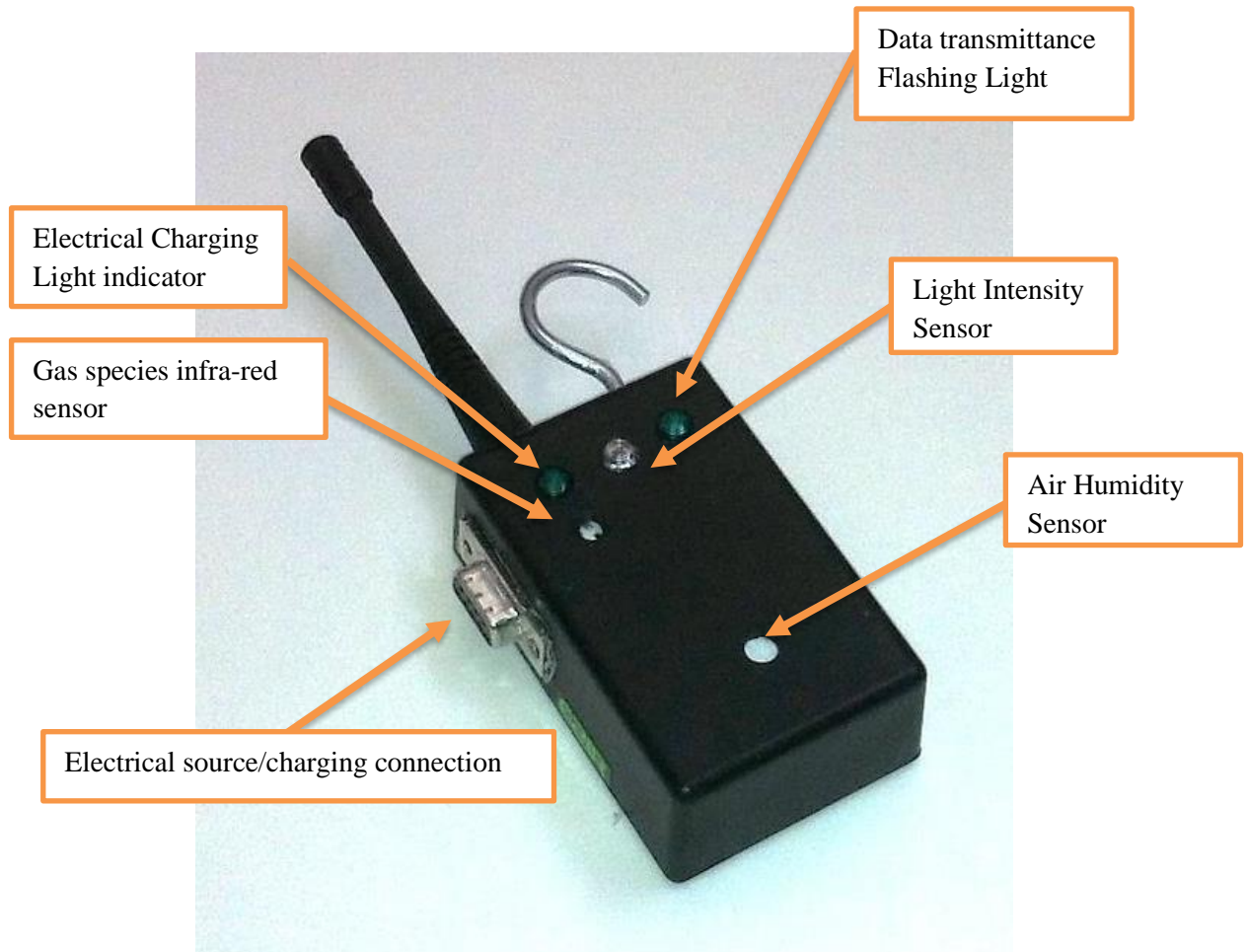


Figure 32: The wireless sensors box is composed of a wireless carbon dioxide concentration, temperature relative humidity sensor.

The gas sensor found within the sensor box is connected to the sampling tube shown in Figure 33 the sampling tube is inserted through a hole located at the chamber top cover. The sampling tube is provided with side holes so that it collects samples from the different elevations from within the chamber gas volume to ensure that a homogenous air/carbon dioxide mixture is sampled. It is made out of transparent plastic to reduce the disturbance to site location and to allow as much natural light to be transferred into the chamber.

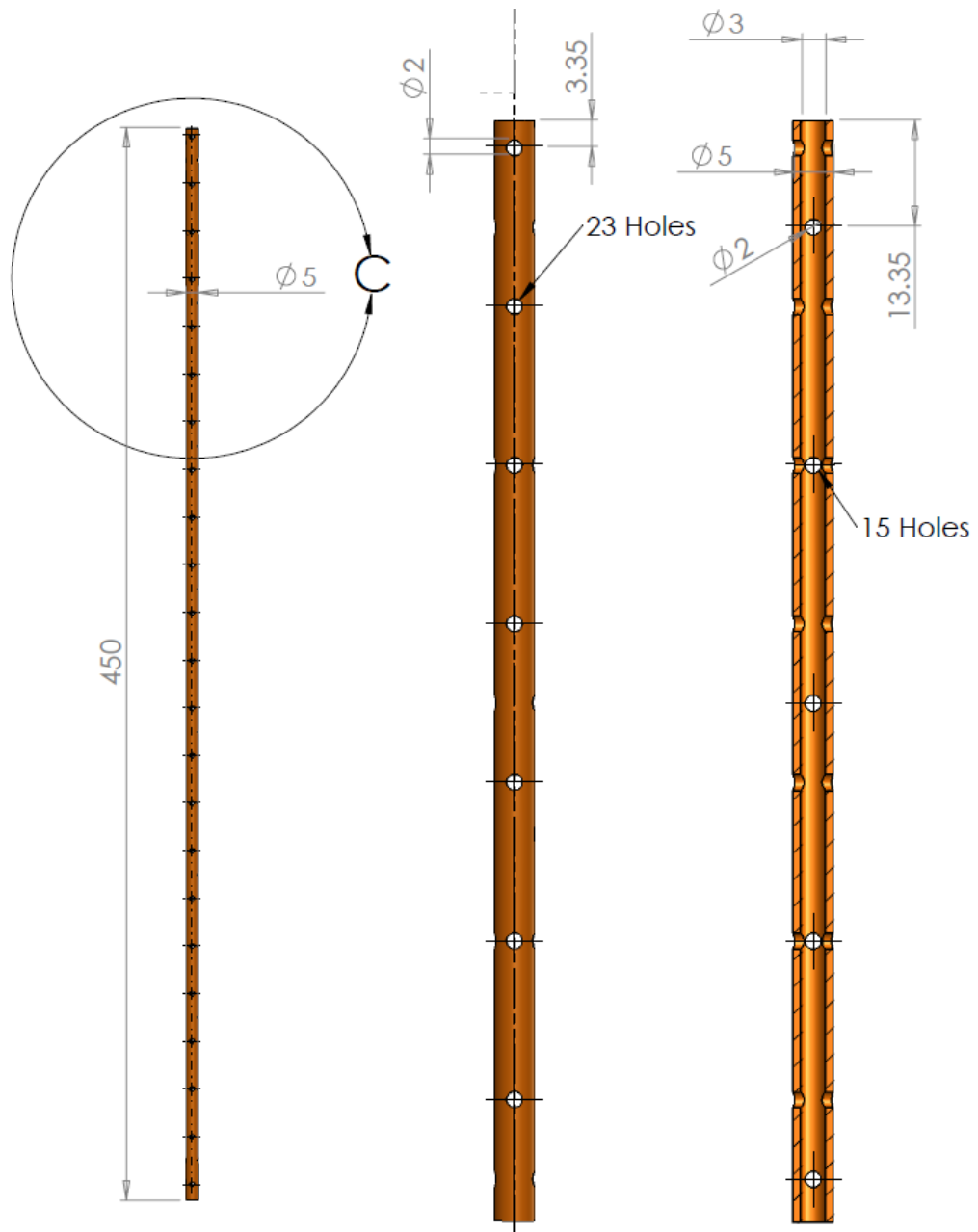


Figure 33: The respiration chamber gas sampling tube used to take collect gas samples in relation to the chamber's height.

3.4.3. Wireless Adaptor

A Wireless USB Adapter WiFi Lan Network Card Antenna is connected to the laptop to receive the data from the wireless sensor. Hence the collected data is instantaneously stored on the computer.



Figure 34: The wireless USB connection that will be connected to the laptop.

Consequently, what follows later is the data analysis stage. The advantage of using a wireless WiFi adapter is that it reduces the required cabling whilst onsite of deployment. This is notable on difficult sites with difficult geography.

3.4.4. Circulation Fan, Battery and Power Transformer

The cap cover installed at the top of the chamber is to allow the proper fitting of the blowing fan configuration at the required distance from the soil surface. The main purpose of using a blowing fan is to decrease the sampling time to ensure a homogenous mixture is obtained to be ready for sampling. The soil surface projected by the fan jet is in a perpendicular manner covered. Thus, this helps to draw out the carbon dioxide species from the top soil layers. The used electrical blowing fan has a blowing velocity of 2.7 [m/s] shown on Figure 35. The blowing fan outer diameter 70 mm the inner fan diameter is 40 [mm]. The fan volumetric flow rate is 0.0095 [m³/sec]. More info about the used fan can be found in the appendices on page 277.



Figure 35: The electrical blowing fan with its side white cover. The fan is intended to be used for the dynamic chamber operational mode.

The Fan is powered by a rechargeable battery that can work up to 12 [hour] deployment or it can alternatively be connected to an electrical transformer. The sensor and fan can work on battery mode while on location or can be plugged to the electrical mains for lab tests or for battery charging using Figure 36. More data can be found about the selected battery properties in the appendices on page 278.



Figure 36: The fan battery used on site deployment (left) moreover the power battery charger (right) used in lab trials .

Emphasis will be drawn on the different parts of the chamber this is due to their direct impact on the flow pattern inside the chamber. They have a direct or indirect effect on the accuracy of species measurement this is something that will be seen in the CFD simulations in chapter 6. Sharp edges are avoided by fitting a rib around the fan main body. This insures the least generated turbulence before and after the fan as shown in Figure 37. The connecting beams are covered by plastic tubing to omit out the threading affects for the four metal beams. The plastic tubes also ensure that the fan when fitted to the chamber shell it is parallel to the soil. The connecting beams are intentionally fitted in parallel to the flow to avoid the occurrence of vortex shedding.

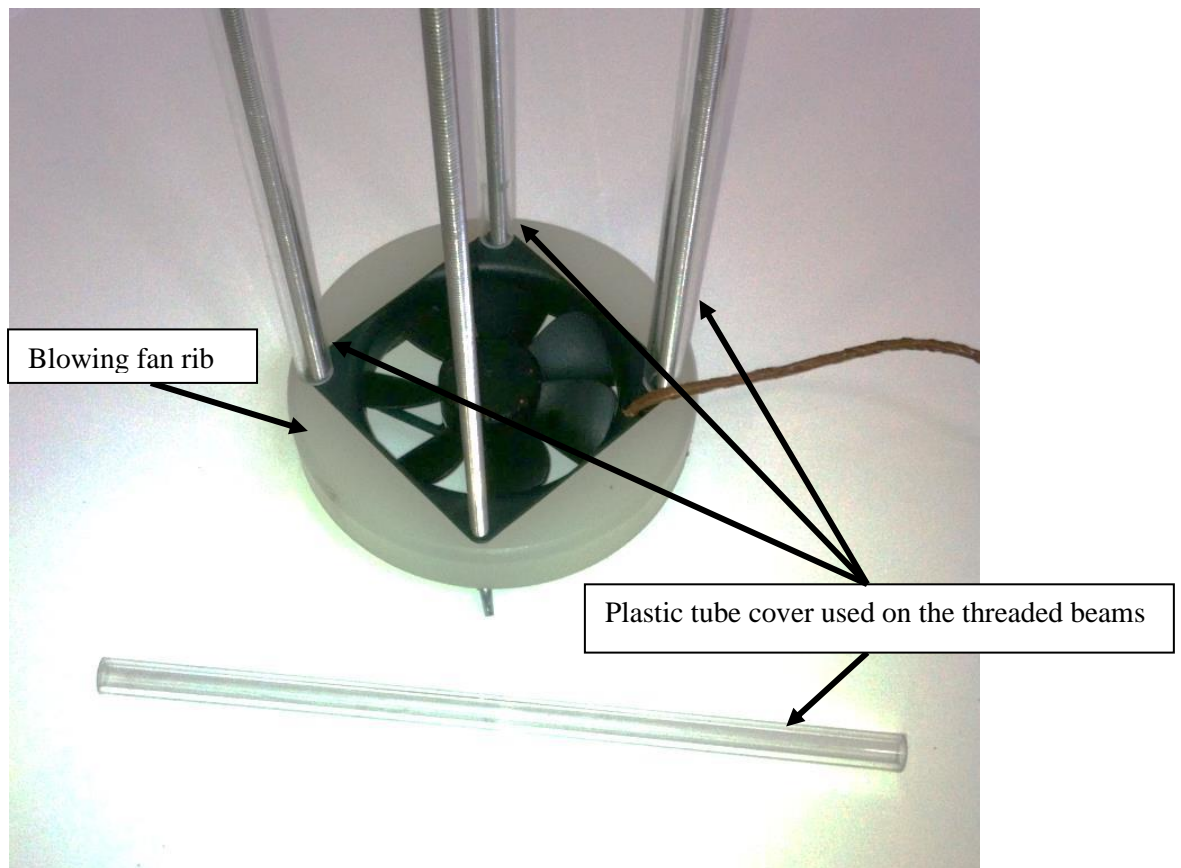


Figure 37: The blowing fan connecting rib likewise the 4 connecting metal threaded beams for the fan with the chamber. Furthermore, one of the plastic tubes used to cover the threaded metal beams is shown.

3.4.5. Chamber Base

The chamber installation at the site was carried out 48 hours before samples collection is started. During gas flux sampling each vent found on the chamber cover is pressure sealed using blue tag. The chamber is setup on the location using the plastic base shown in Figure 38. The role of the base is to protect the chambers side from the soil wear when pushed into the soil. Likewise, the side grooves are made so that the chamber is fitted onto it and ensures no leakage of gas occurs while taking samples. The base contributes in preserving the site location from any disturbance when the chamber is turned on its side for ventilation after a sampling session is done. Consequently, the base also serves as a method to tight seal the inner gas volume inside the chamber. This is achieved by relying on the plastic shells small buckle in shape making the shell when pushed into the base grove to fit tightly.

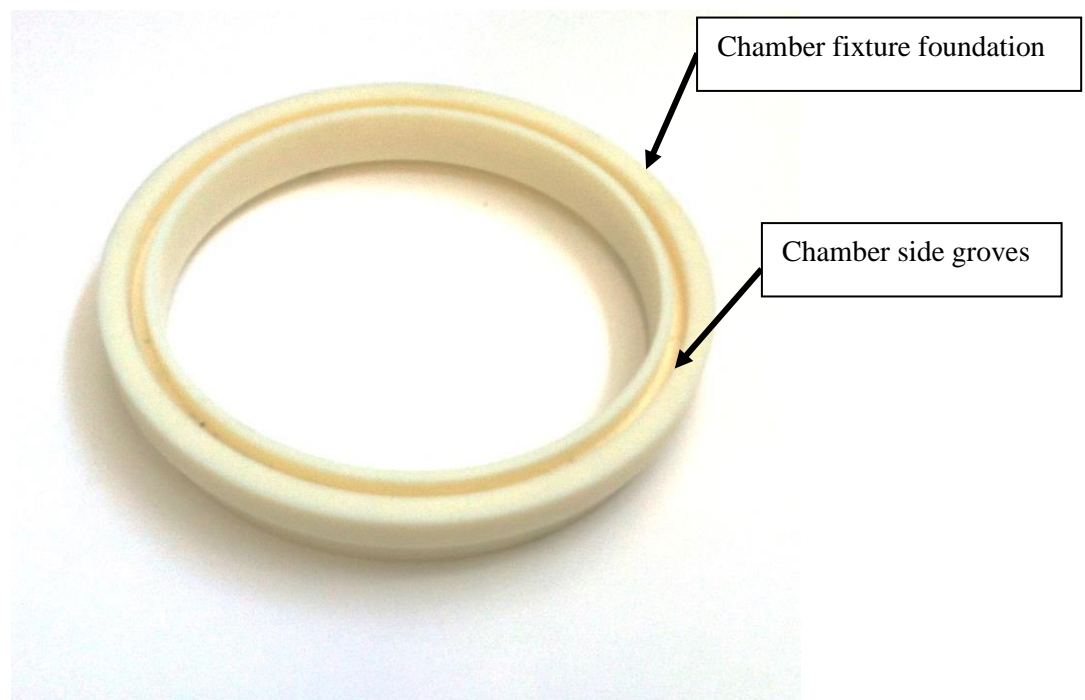


Figure 38: The respiration chamber fixture foundation used to provide a confined closure within the chamber's gas volume.

3.4.6. Automated Data Gathering

Alternatively, instead of using a long cabling network to connect the different sensors together while on site of deployment for the sake of data gathering. A wireless sensor box is used whereby the measured data by the sensors is transmitted back to the wireless rotor (connected to the computer). The software on the computer screen instantaneously presents light intensity, carbon dioxide concentrations, temperature and relative humidity in a continuous plot. At the bottom of the plot window Figure 39 presents instantaneous taken sample values occurring to the pre-set timing for the sensor. Shown on the left-hand side of the program window in Figure 39 is the node list. This list reflects the power of this software/hardware configuration to handle several sensors at one instance of time in collecting data.

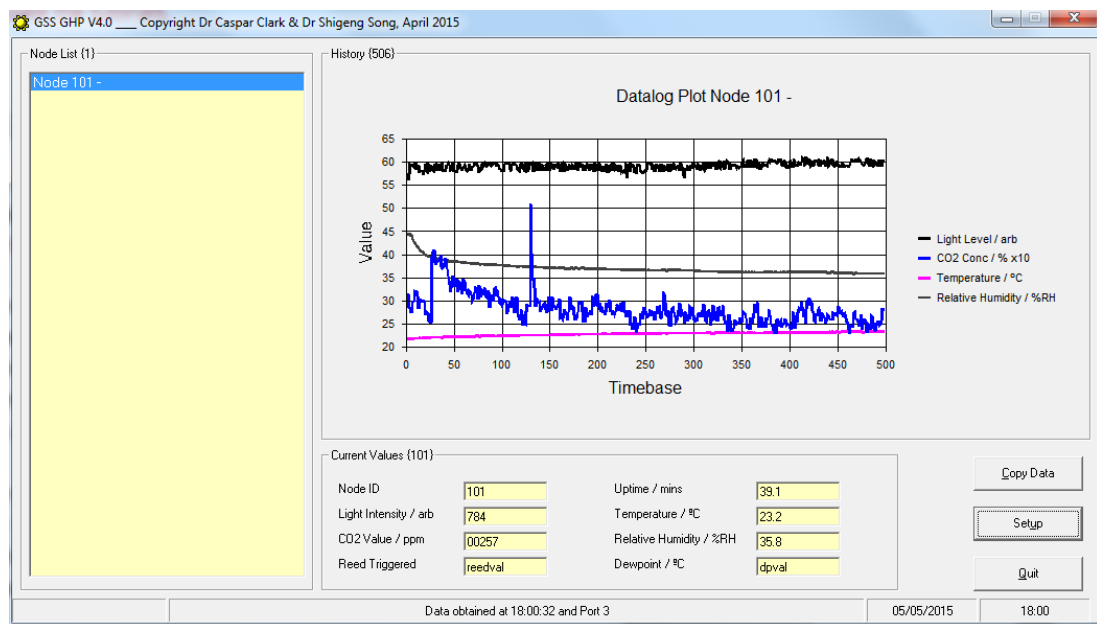


Figure 39: A screen shot showing the automated control panel software GSSVGH V4.0 interface used with the respiration chamber.

Figure 41 shows the dynamic chamber experiment flow chart. The basic sampling procedure is initiated after the chamber concentrations return to near baseline (400-403.7 [ppm] for CO₂) taken from [206].

At this point of time the chamber fan is engaged. The internal air temperature probe was placed on the sampling tube chamber and sealed with blue tag. The following parameters are measured during the experiment these are carbon dioxide concentration in ppm, chamber temperatures, internal chamber pressure, dew point temperature, ambient air temperatures.

The chamber remained sealed for about 6 [min] after which the fan is switched off, the chamber was put on its side again the blowing fan was switched on to flush out all the contained gas in the chamber volume. Then the system was set to re-equilibrate to ambient conditions this process usually takes 2-3 [min].

Care was taken at all sites to minimize the amount of pressure placed upon nearby soils. This is real importance when pushing the chamber into a location, this causes the soil pore sizes to differ affecting the carbon dioxide flux mass transport [207]. Wind speeds remained consistent during each placement although they differed significantly between sites and from the calculated optimum wind speeds. Average wind speeds for the location were about 6 [m/s] from the university onsite weather station [208].

To quantify species concentration changes that occur the experiment input is gathered through the use of a number of sensors located in the sensor box. This is followed by the data interpretation by the researcher and the validation process. One method of validation is using the eddy covariance method quantifying the species diffusion process [209]. Once the experiment is finished the data can be saved and exported to Excel or MATLAB for analysis as shown on Figure 40.

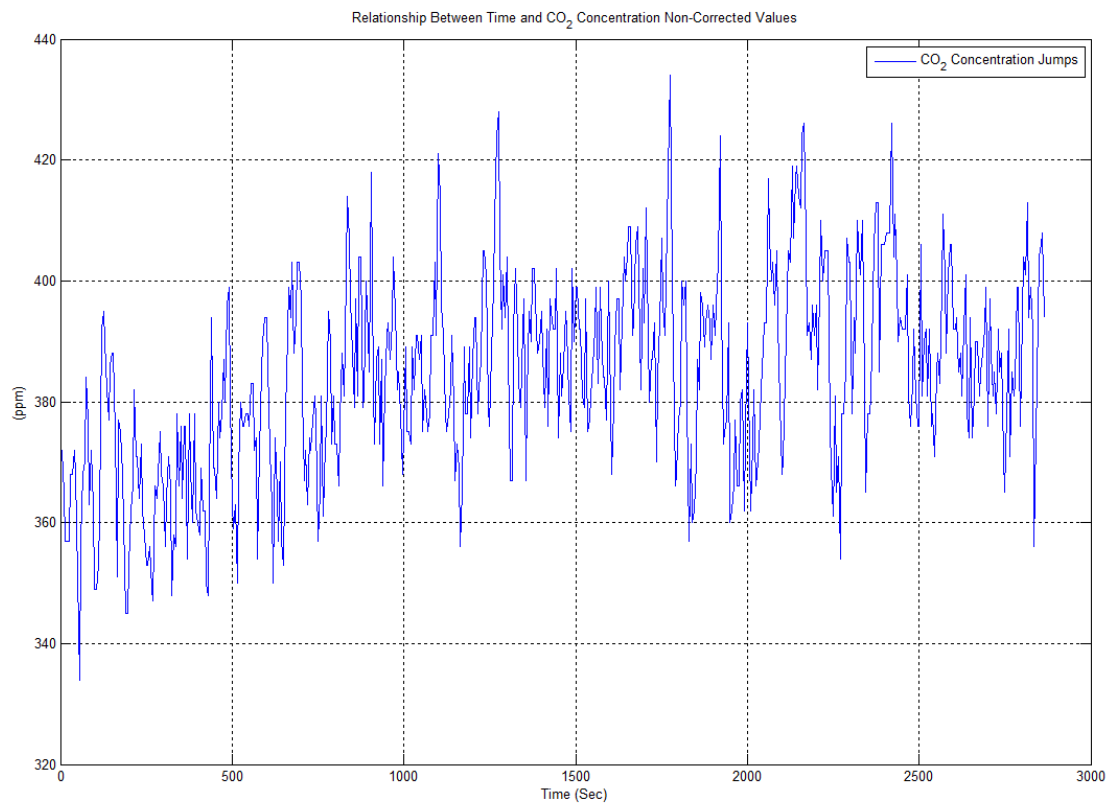


Figure 40: A test case run showing carbon dioxide readings from the sensor readings after analysis, carbon dioxide concentration in relation to time for a dynamic case.

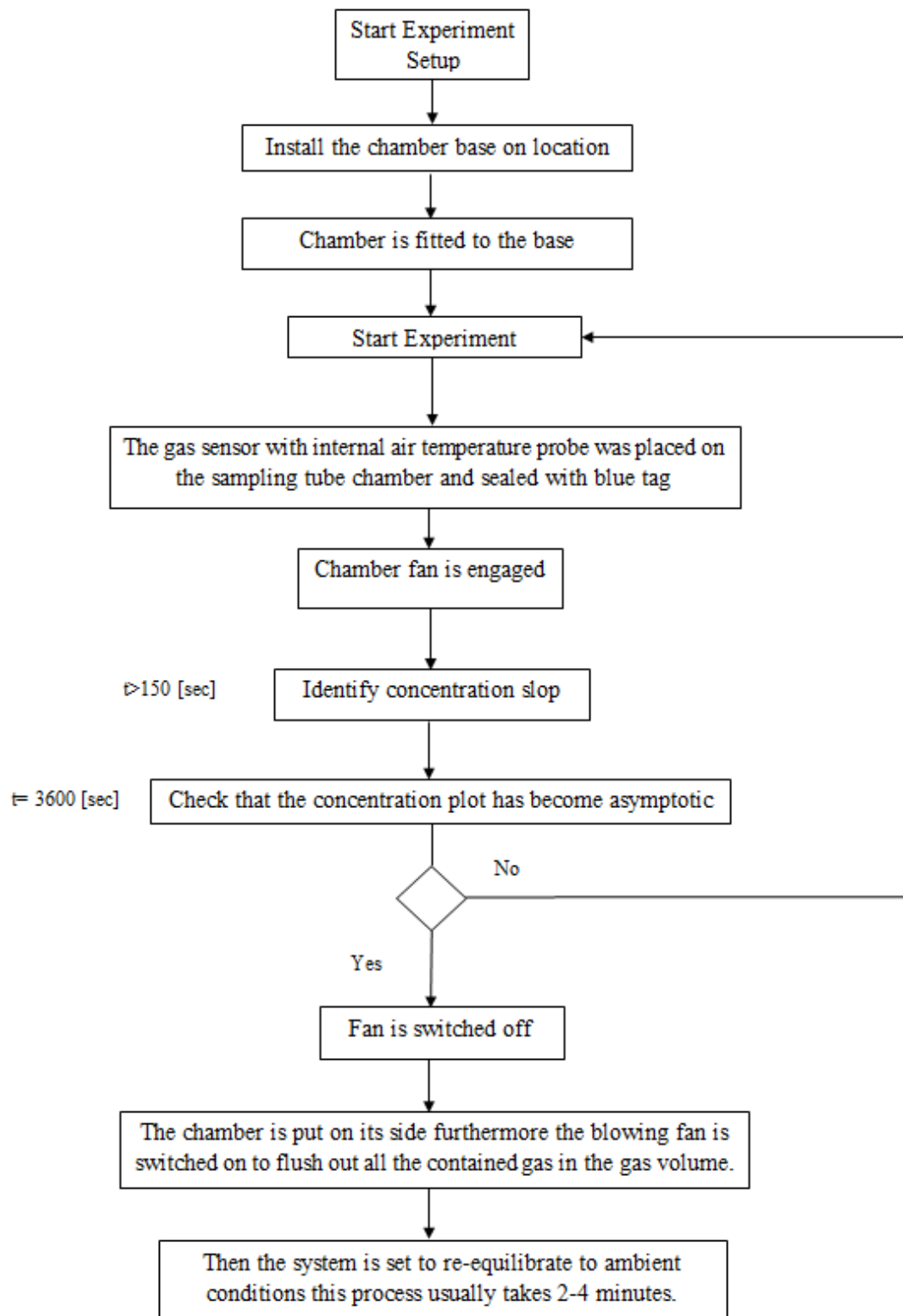


Figure 41: The flow chart showing the experimental setup steps for the dynamic chamber experiment.

Figure 42 shows the flowchart representing the experimental setup steps for static chamber operational mode whereby no fan is switched on.

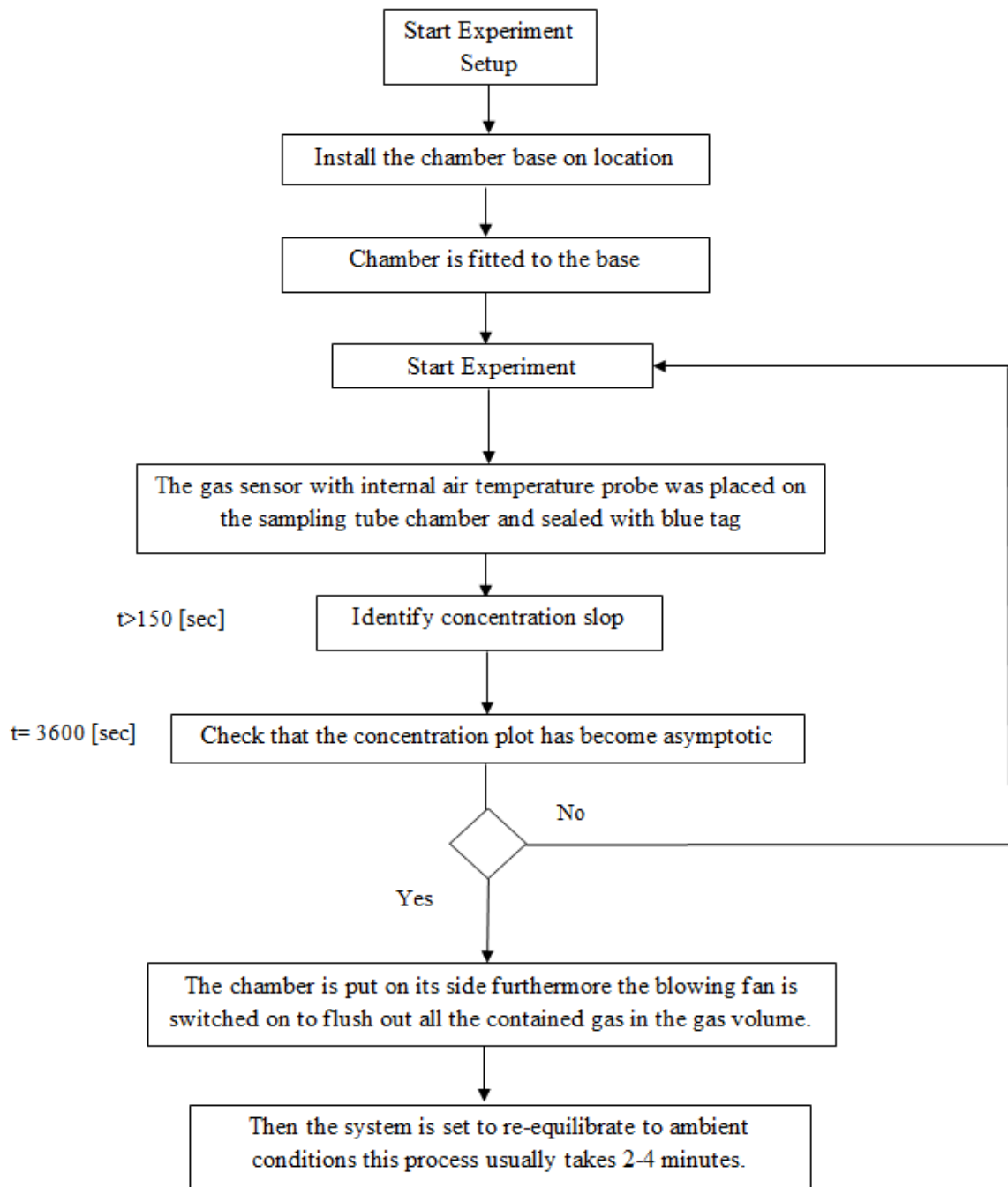


Figure 42: The flow chart showing the experimental setup steps for the static chamber experiment.

By curve fitting the data shown in Figure 40 a linear model is obtained this is used to calculate the average flux density as shown in equation 3.1:

$$\bar{J}_g(t) = \frac{V \Delta C}{A \Delta t} \quad (3.1)$$

The extrapolated curve fit function is later shown in Figure 64 for both species concentration and efflux. Whereby the flux $\bar{J}_g(t)$ is the average flux density furthermore ΔC is the concentration change measured in the chamber headspace in a short time span Δt . Moreover, the ratio V/A is of the chamber gas volume V [m^3] over the entrained soil surface area A [m^2]. To conduct the carbon dioxide analysis data from each 6 minute sampling period the earliest 2 – 3 [min] linear time period is used to calculate the flux of each trace gas, based on the equation 3.1 taken from Gao et al. [209]. Equation 3.1 can be applied to a static or dynamic respiration chamber operational mode which achieves comparable results as mentioned Heinemeyer and McNamara [210]. By substituting the values of chamber volume and soil area into equation 3.2 results in the following equation form 3.2:

$$\bar{J}_g(t) = 0.545 \frac{\Delta C}{\Delta t} \quad (3.2)$$

The volume capacity of the chamber and covered soil area values can be found in the appendices A-I.

3.5. Location of Study

Measurements were taken in Paisley which is located in the western part of Glasgow city. The terrain is moderately hilly near to the location as seen in Figure 43 where the location has an average elevation of 15 m. The dynamic chamber was set up on

managed grassland. The study area is located on the prospect location tract ($55^{\circ}.50' N$, $4^{\circ}.26' W$) [211] as shown in Figure 43. The selected site is a managed grassland located at the UWS Paisley campus on a tended lawn surface, Sampling occurred during (7th- 9th May 2015). The main characteristic of the grassland site is that it has high fertility. The meteorological data was gathered from the university weather station [208], the average measured wind speeds were 5 m/s on location. The chamber sensor box measured in relation to time the following parameters: ambient temperature inside the chamber was 16 C° with a dew point of 10 C° while relative humidity was 40%. The importance of site description comes from the need to link climatic factors with onsite measurements, because soil biological metabolism is strongly influenced by temperature. Atmospheric concentrations of carbon dioxide as provided by [212] on the month of May 2015 were 401ppm.



Figure 43: Topographic map of the location of study, the site is located on UWS paisley campus, the elevation key is located on the right-hand side, and location is in the light green colour range.



Figure 44: The grass land location of study at UWS paisley campus.

Firstly, to find the mass fractions pie chart is done though taking a 1 kg soil sample from the grassland site and using the grass jar method. Consequently, this leads to finding the mass distribution of the constituents as shown in the mass pie chart in Figure 45.

The soil site location is analysed in a mass and volume fraction approach found in [213]. This is done through the use of a MATALB code where all the physical parameters of mass constituents are considered.

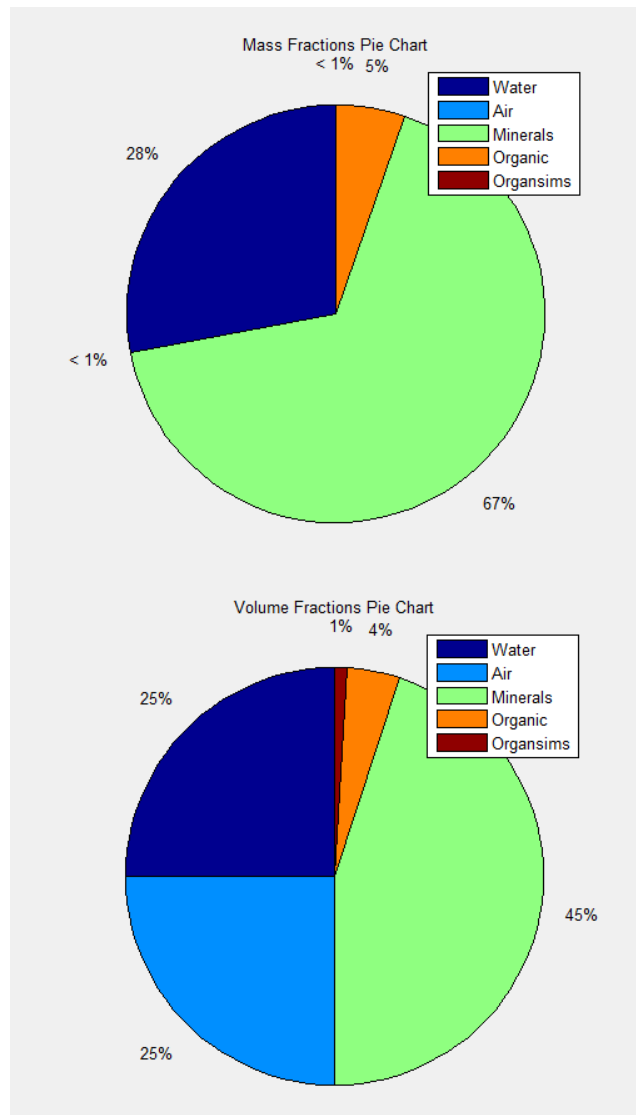


Figure 45: Volume and mass fraction distribution for a grassland site.

It is evident from the figure that 67% of the mass fraction is composed of minerals whereby these are represented by a composition of sand silt and clay. Water represents 28% of the mass fraction while the organic material is 5% finally soil organisms and soil contained air mass fraction is 1%. Figure 46 shows the relative microbial activity for the grassland site related to porosity. This reflects the rate of production of carbon dioxide. In addition, it shows the common conceptual relationship where the soil

carbon dioxide efflux becomes slow under dry conditions. It reaches a maximal rate at the intermediate soil moisture level, and decreases at high soil moisture content when anaerobic conditions prevail to depress aerobic microbial activity. The optimum relative microbial activity is usually somewhere near field capacity. Consequently, the relative microbial activity is about 0.65 for a grass land location whereby its common they have a porosity value of 0.45 as shown in Figure 46.

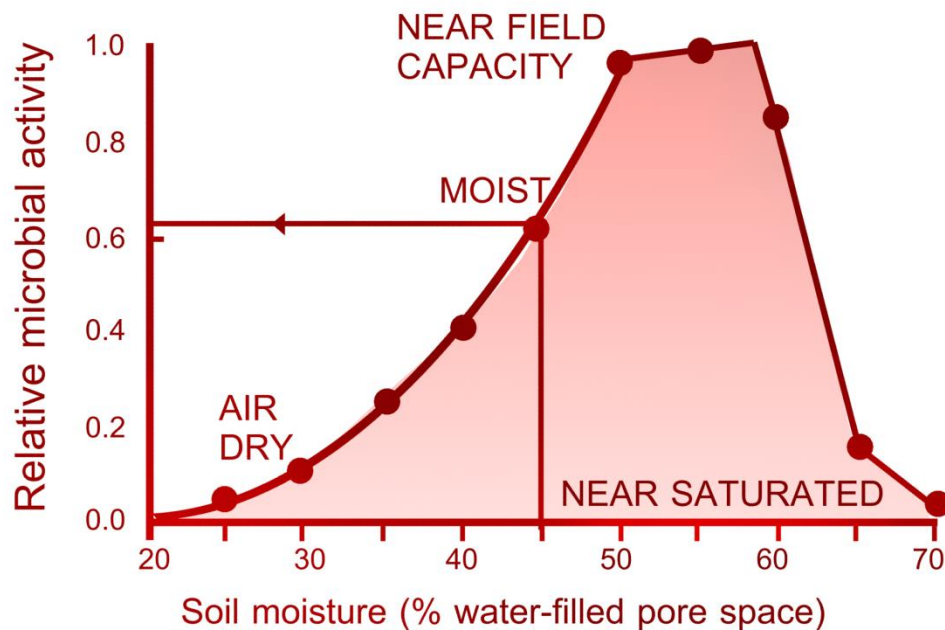


Figure 46: The relation of soil moisture with relative microbial activity for soil. Adapted from [197].

3.6. The City of Paisley Site Climate Description

The importance of the climate description of the site is that soil respiration rates display strong temporal variation over time. In general, the temporal variability can be characterized using four-time scales: diurnal/weekly, seasonal, interannual, and decadal/centennial. In the case under study the time scale fits in the diurnal category.

The City of Glasgow has a temperature climate of four distinct seasons. A general

description of the climate of the city is given with special emphasis on the year 2015. On the basis that it is located on a high land location, Paisley will most probably be exposed to cold winds, fog, and frosts during winter, spring and very early summer.

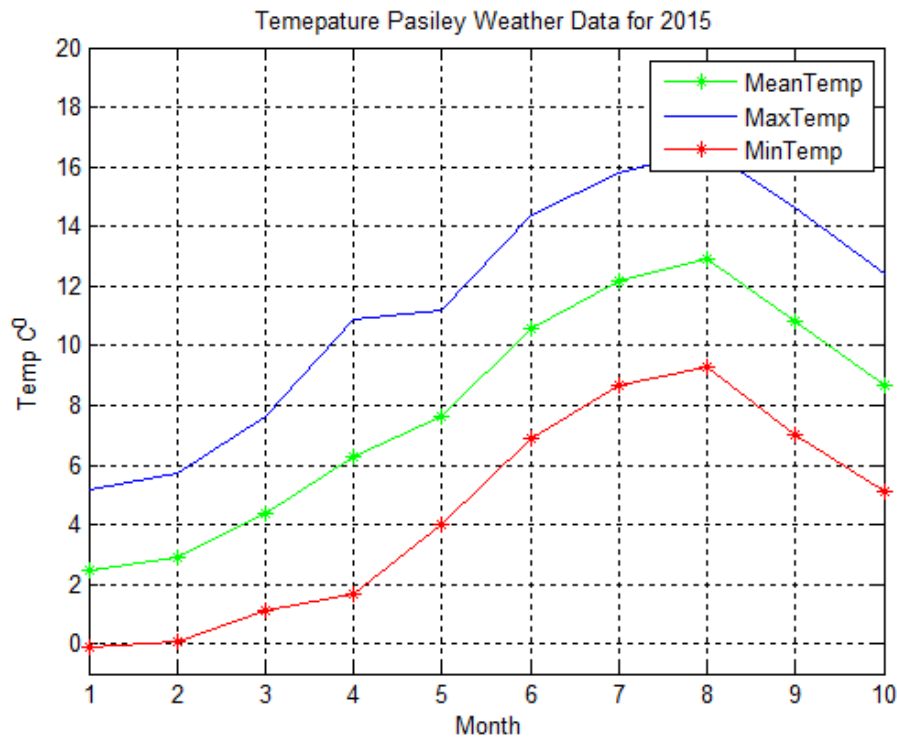


Figure 47: The mean, max and min temperatures of the city of Glasgow [214].

Figure 47 shows that in May the average maximum temperature is 11 [°C] although some days can see high temperatures of up to 11 [°C] and rarely exceeding 30 [°C]. Nights are significantly colder averaging a minimum of 11 [°C], although these can consistently dip below 10 [°C]. The average daytime temperature in winter is 3 [°C] and 0 [°C] at night. Snow may fall in winter from December onwards to as late as April, but quickly melts. The importance of this is that the soil seasonal variation of the soil carbon dioxide efflux has been observed in almost all ecosystems as characterised by Luo and Zhou [138]. The soil respiration rates are

usually the highest in summer and the lowest in winter. For the City of Paisley one main studied case was taken on the 8th of May 2015 during the summer which represents an average respiration time of the year. The importance of temperature comes from its relationship with carbon dioxide efflux due to that bacteria function better at warm conditions as shown previously in Figure 46. Figure 48 shows that the wettest months of the year are November, December and January having an average of 17 days per month with a rainfall exceeding 300 [mm]. It has been stated by Lee et al. [215] that rainfall events make a significant influence on the annual soil carbon efflux even in a cool temperature forest with abundant precipitation. During the month of September, the least rain fall occurs. Changes in the precipitation frequency and intensity have the greatest impact on soil respiration.

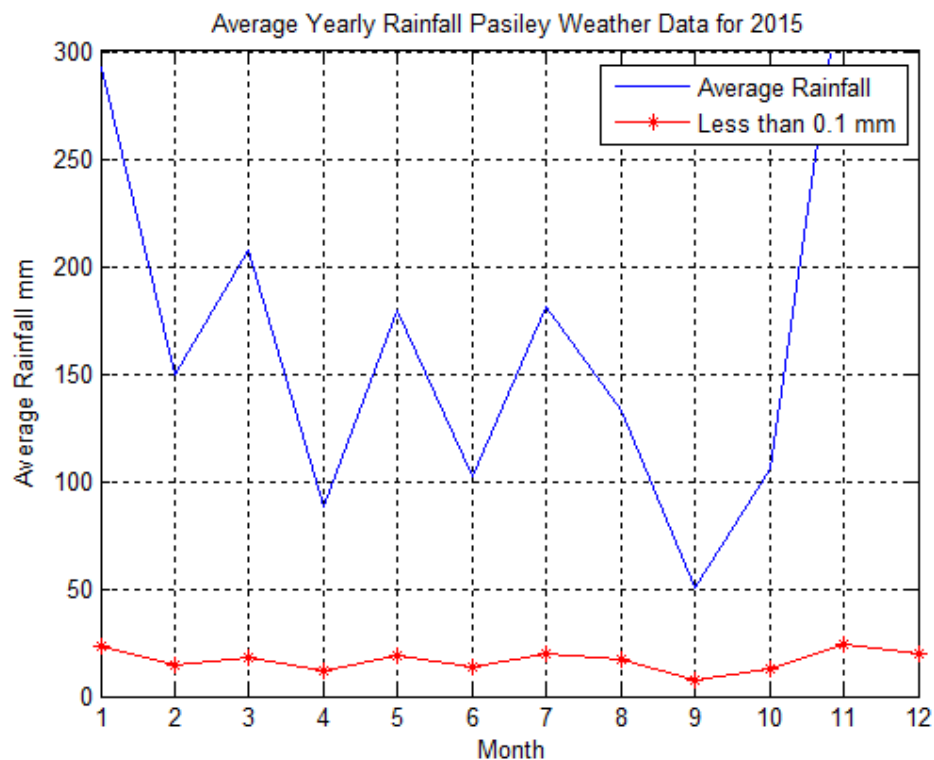


Figure 48: The average rain fall data for the city of Glasgow in 2015 [214].

Two ecosystem systems are being considered here: xeric ecosystem (habitat lacking humidity and water) and mesic ecosystem (habitat with a balanced supply of moisture). For apparent reasons the attention will be focused on the second one. It has been observed that soil respiration in arid or semiarid areas shows dynamic changes within a raining cycle as shown in (section 2.6.2). The rate of respiration in dry soil usually bursts to a very high level after rainfall and then declines as the soil gets drier. Figure 49 shows that from April to July in the year 2015 Glasgow experienced the most sunshine with an average of six hours per day. This indicates that the highest expected carbon dioxide efflux will be encountered during the April, May, June and July period. It is noted that although radiation is one main driving variable for seasonal changes in photosynthesis.

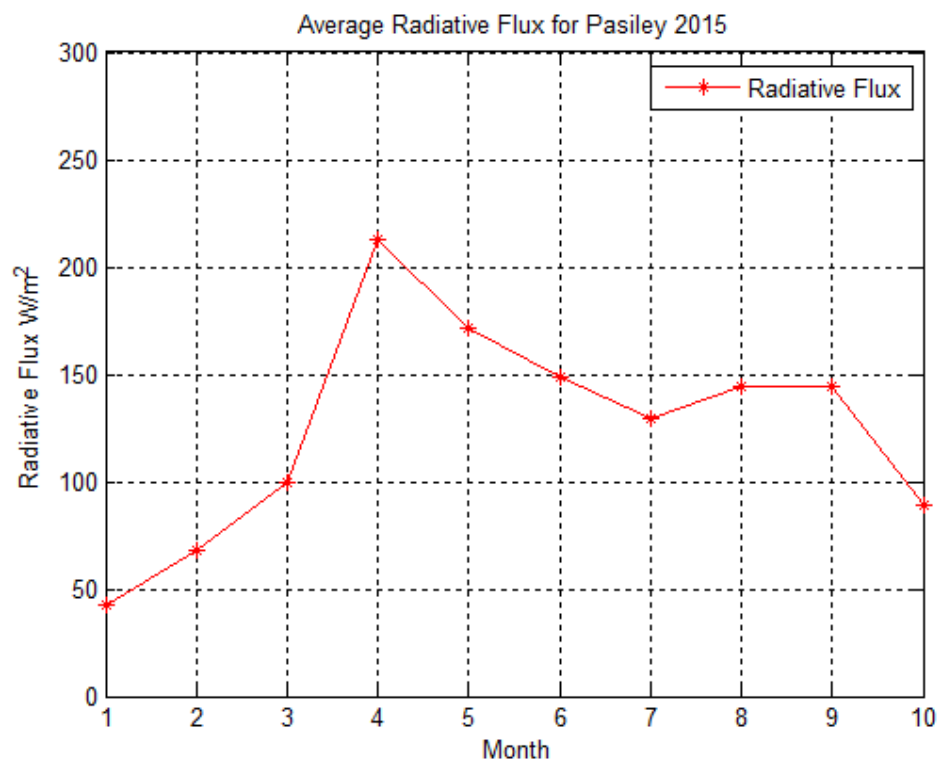


Figure 49: Paisley location average radiative flux for the year 2015.

Temperature also plays a distinctive role in the seasonality of the substrate supply by its effects on phenology of shoot and root growth. This is by taking into account that the efflux from plants should increase in relation to the daily light hours. It can also be beneficial if seasonal wind direction and magnitude data are collected. This can help in predicting the rate of evaporation and soil aeration.

3.7. The Soil Analysis efflux Software

Initially a MATLAB code was written as data collection progressed with time interface was introduced transferring the calculation code into software phase as shown in Figure 50. The code uses a joint database between the different interface windows this helps in linking the chamber design parameters with the location geotechnical, meteorological, physical parameters. The code was written based on some of the derived and presented models in Chapter 2.

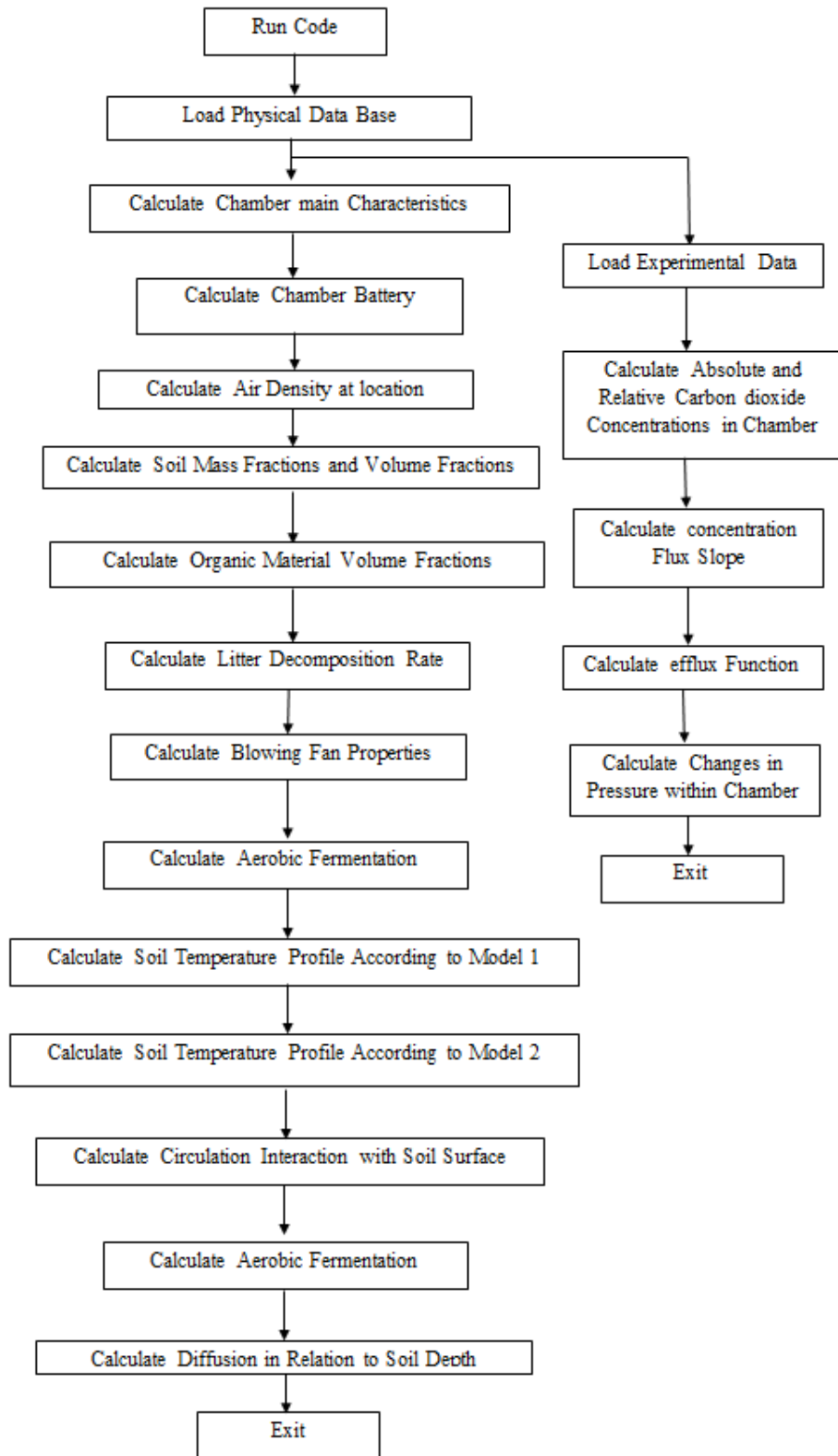


Figure 50: Soil Analysis efflux software structure.

The chamber air density within the gas volume is calculated according to the location's elevation in relation to sea level and site measured air temperature. This is done by typing into the software interface the input parameters as shown in Figure 51. The used model equations are taken from (section 2.7.1). The studied location of concern is presented as a red point on the output plot.

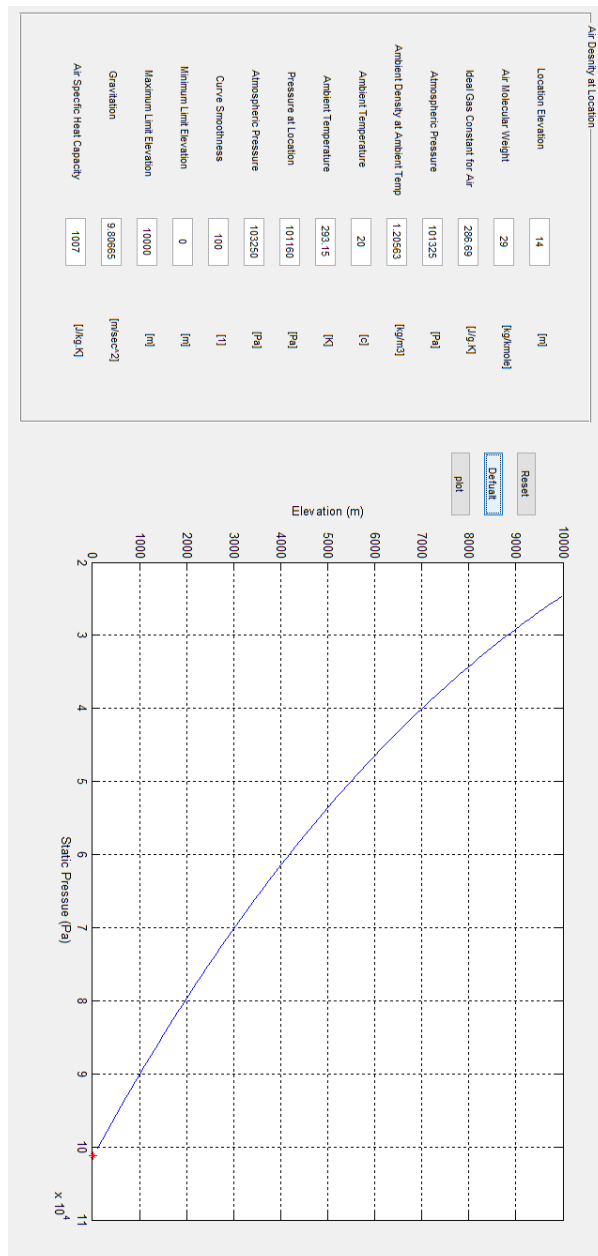


Figure 51: The software interface used to calculate air density within the chamber.

The blowing fan distance from the soil surface in relation to the soil surface is calculated by using the software interface shown in Figure 52. The used equations for the study are shown in (section 2.7.2) the working point is represented in a red colour. Furthermore, the window interface helps in calculating the fans volumetric flow rates, blowing acting force and acting pressure on the soil surface produced within the chamber volume. Calculating the acting force that has resulted from hitting the soil surface this is done by knowing the blowing fan velocity using equation

$$F = \rho Q(v_{\text{fan}} - v_{\text{surface}}) \quad (3.3)$$

Finding fan outlet velocity can be calculated by looking up the volumetric flow rate Q found in the fans technical manual. Likewise, the fans outlet area A can be found from the technical diagrams. Once the values are obtained, they are substituted into equation (3.4):

$$v_{\text{fan}} = Q/A \quad (3.4)$$

Considering that the surface velocity will be taken as $v_{\text{surface}} = 0$. the acting force value can be calculated using equation numbered (3.5):

$$F = \rho Q(v_{\text{fan}}) \quad (3.5)$$

The number of times N the circulation of the total chamber volume V_{Chamber} in accordance to the fan volumetric flow rate is according to equation (3.6):

$$N = V_{\text{total}}/V_{\text{Chamber}} \quad (3.6)$$

Keeping in mind that total circulated volume for total duration time of experiment is as follows $V_{\text{total}} = Q \Delta t$.

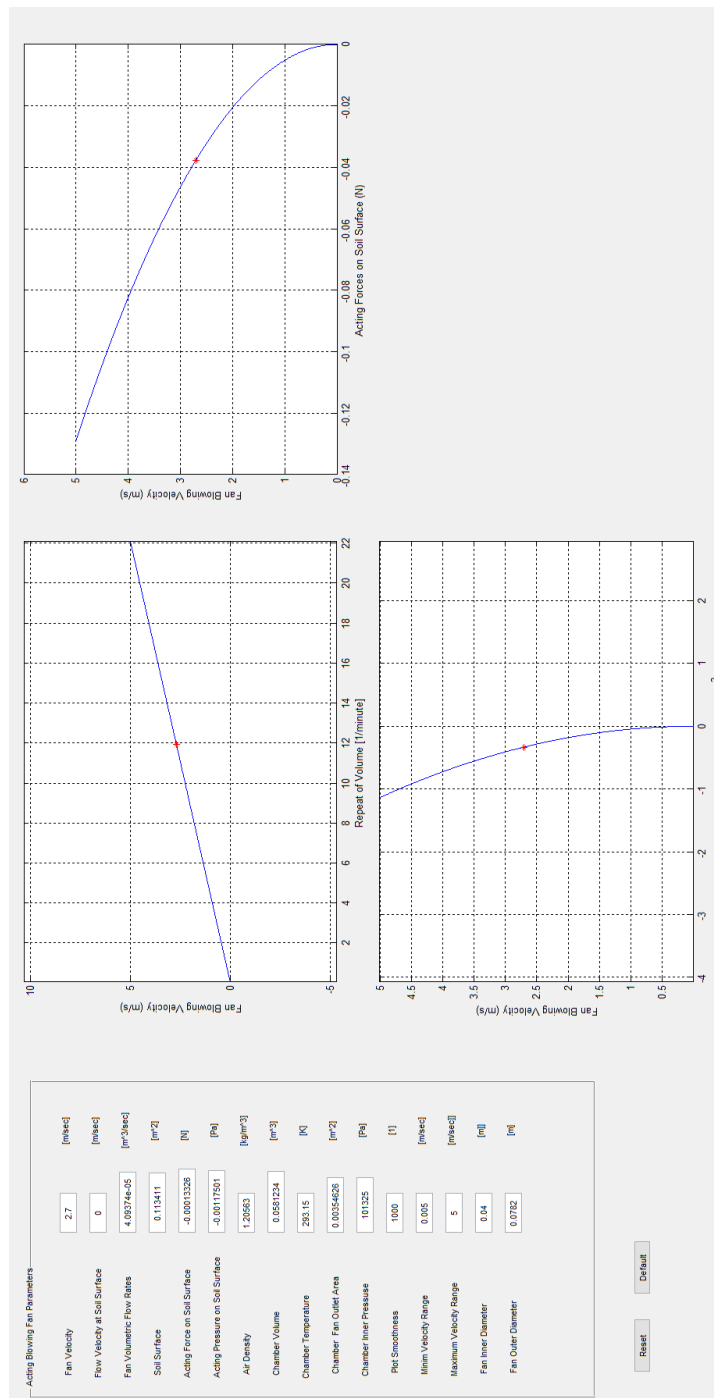


Figure 52: The software interface used to calculate blowing fan parameters within the chamber.

Figure 51 shows that the calculation data output plot is based on the locations soil thermos-physical properties, volume fractions of the soil constituents from sand, silt, clay organic material dead and alive. Consequently, the temperature profile is a function of soil depth, time of day and day of year. The applied model is only applicable for a soil depth study of maximum 0.7 m. This is achieved by applying the model discussed on (section 2.6.3).

Similarly, to the interface used on Figure 53 the interface shown in Figure 54 is used for a similar purpose but mainly focusing on comparing the temperature profiles at certain times of the day.

Hence the power of the plot is that it can incorporate several temperature profiles in relation to soil depth at different times of the day. Furthermore, the user is not restricted to the maximum depth of 0.7 m. The total thermal conductivity λ_{total} for the soil sample is calculated using equation (3.7):

$$\lambda_{total} = \sum_{i=1}^{i=N} r_i \lambda_i = r_{sand} \lambda_{sand} + r_{silt} \lambda_{silt} + r_{clay} \lambda_{clay} + r_{water} \lambda_{water} + r_{air} \lambda_{air} + r_{organic} \lambda_{organic} \quad (3.7)$$

Likewise, the total specific heat capacity C_{total} can be calculated using equation (3.8):

$$C_{total} = \sum_{i=1}^{i=N} r_i C_i = r_{sand} C_{sand} + r_{silt} C_{silt} + r_{clay} C_{clay} + r_{water} C_{water} + r_{air} C_{air} + r_{organic} C_{organic} \quad (3.8)$$

The thermal conductivity and heat capacity physical values are available in the software's database. The user can input also input the values into the model manually.

Hence what is required from the user is to specify the soil samples volumetric fractions.

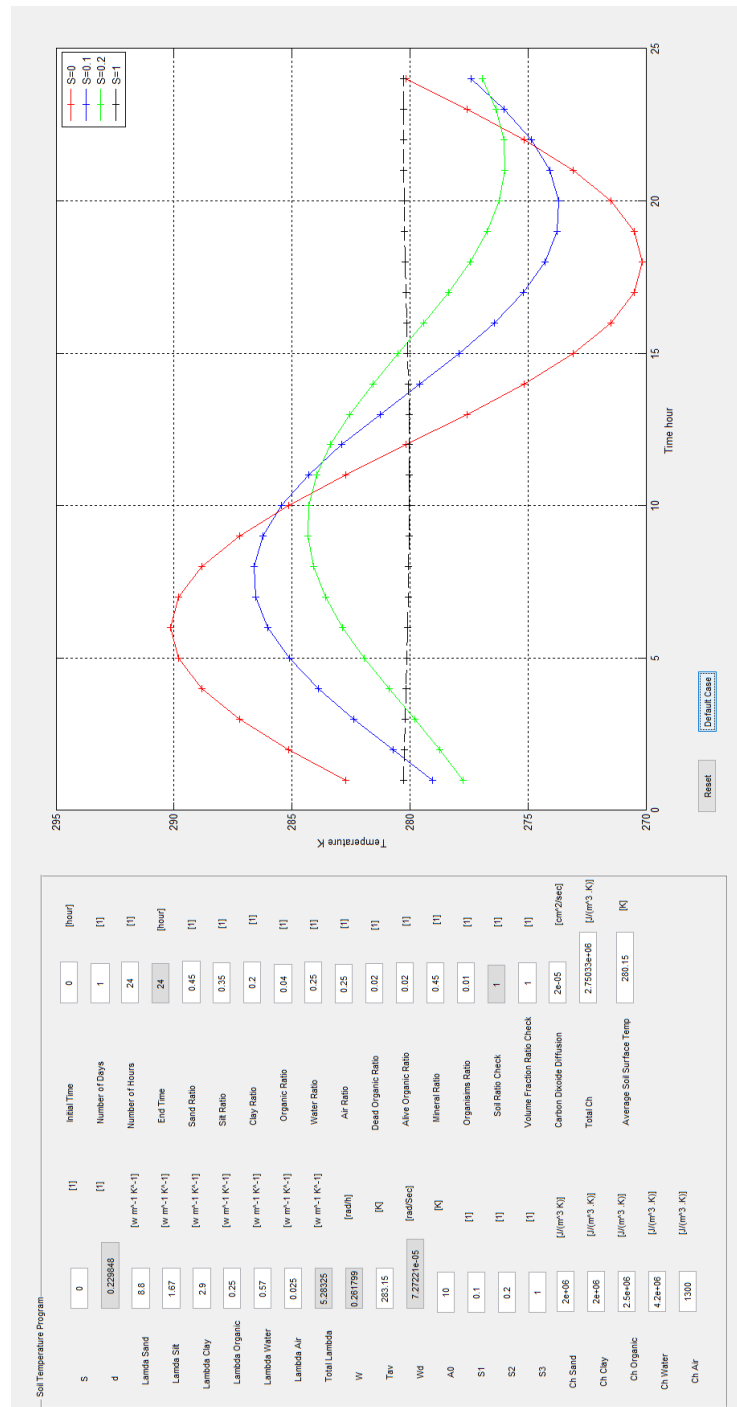


Figure 53: The software interface showing the soil temperature variation according to soil depth, time of day soil geotechnical and thermo-physical properties.

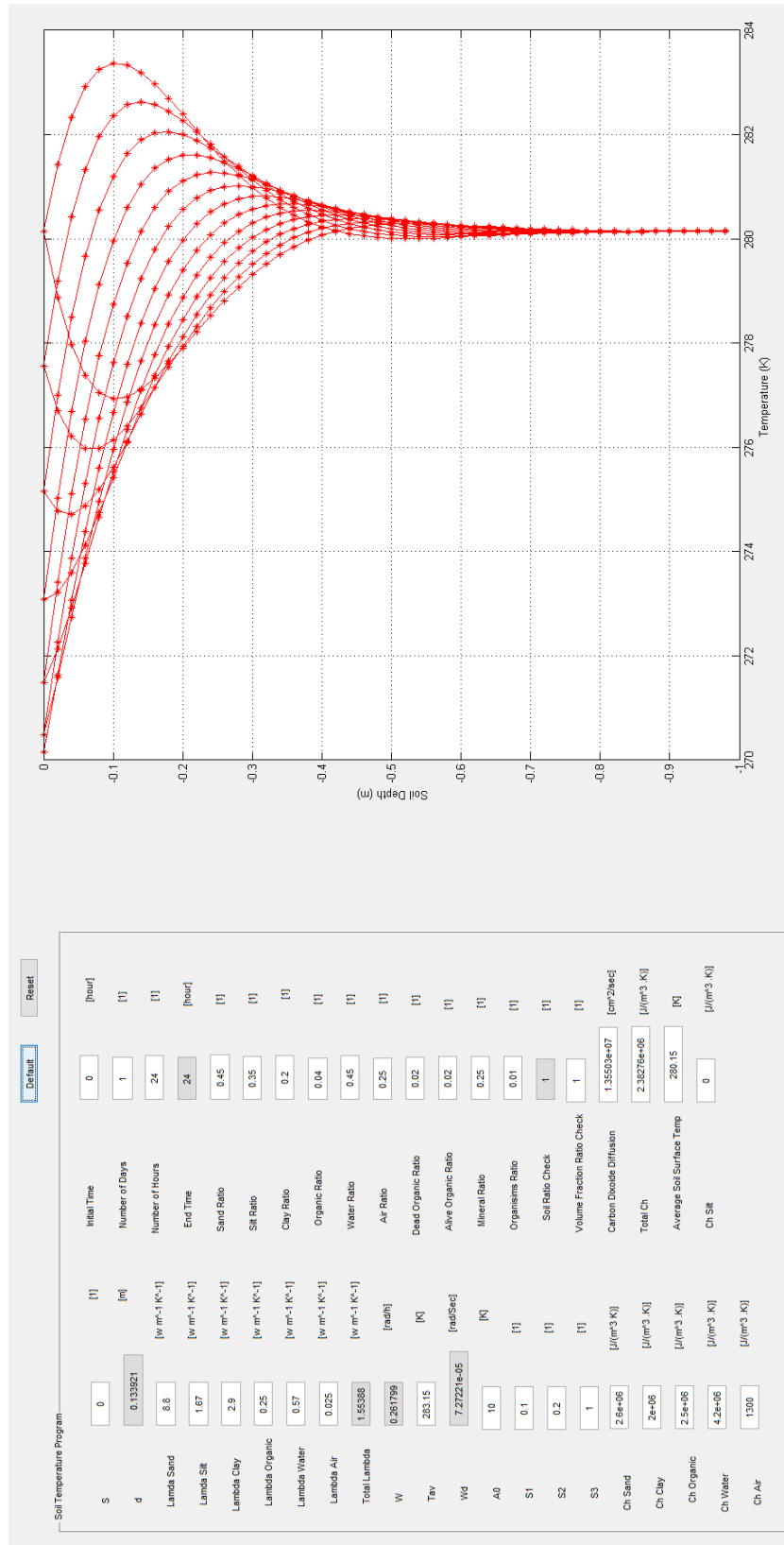


Figure 54: The software interface the studies variation of temperature with depth.

After the researcher has taken a soil sample from the site location and conducted the soil settling method and identified the samples total volume, total mass and mass fraction is inputting the gathered data into the software interface shown in Figure 52. In conclusion of the calculation a mass and volume chart is generated for the specific site moreover a detailed calculation to all specific masses to the organic and none organic material. A good quality soil (which is very similar to the soil of the grassland on the UWS site) is one that is composed of 45% minerals, 25% water, 25% air and 5% organic. This can also be expressed in the equation (3.9):

$$V_{\text{soil}} = V_{\text{minerals}} + V_{\text{organic}} + V_{\text{water}} + V_{\text{air}} \quad (3.9)$$

Figure 56 shows the mineral and organic components are considered to have constant values. The volume of the organic material can be split into two components: alive and dead, which can be expressed in the equation (3.10):

$$V_{\text{organic}} = V_{\text{dead organic}} + V_{\text{alive organic}} \quad (3.10)$$

The interface presented in Figure 53 is used to extract from the calculated volume fractions the detailed volume distribution for organic roots, living organisms and hums ratio are shown in equation (3.11)

$$V_{\text{alive organic}} = V_{\text{Roots}} + V_{\text{Hums}} + V_{\text{Organisms}} \quad (3.11)$$

Just noting that the considered soil density $\rho_{\text{Soil}} = 1100 \text{ kg/m}^3$ [34] for loamy soils,

The water density $\rho_{\text{Water}} = 1000 \text{ kg/m}^3$,

The air density $\rho_{\text{Air}} = 1.29 \text{ kg/m}^3$, and

The organic material density $\rho_{\text{Organic}} = 1200 \text{ kg/m}^3$ [216].

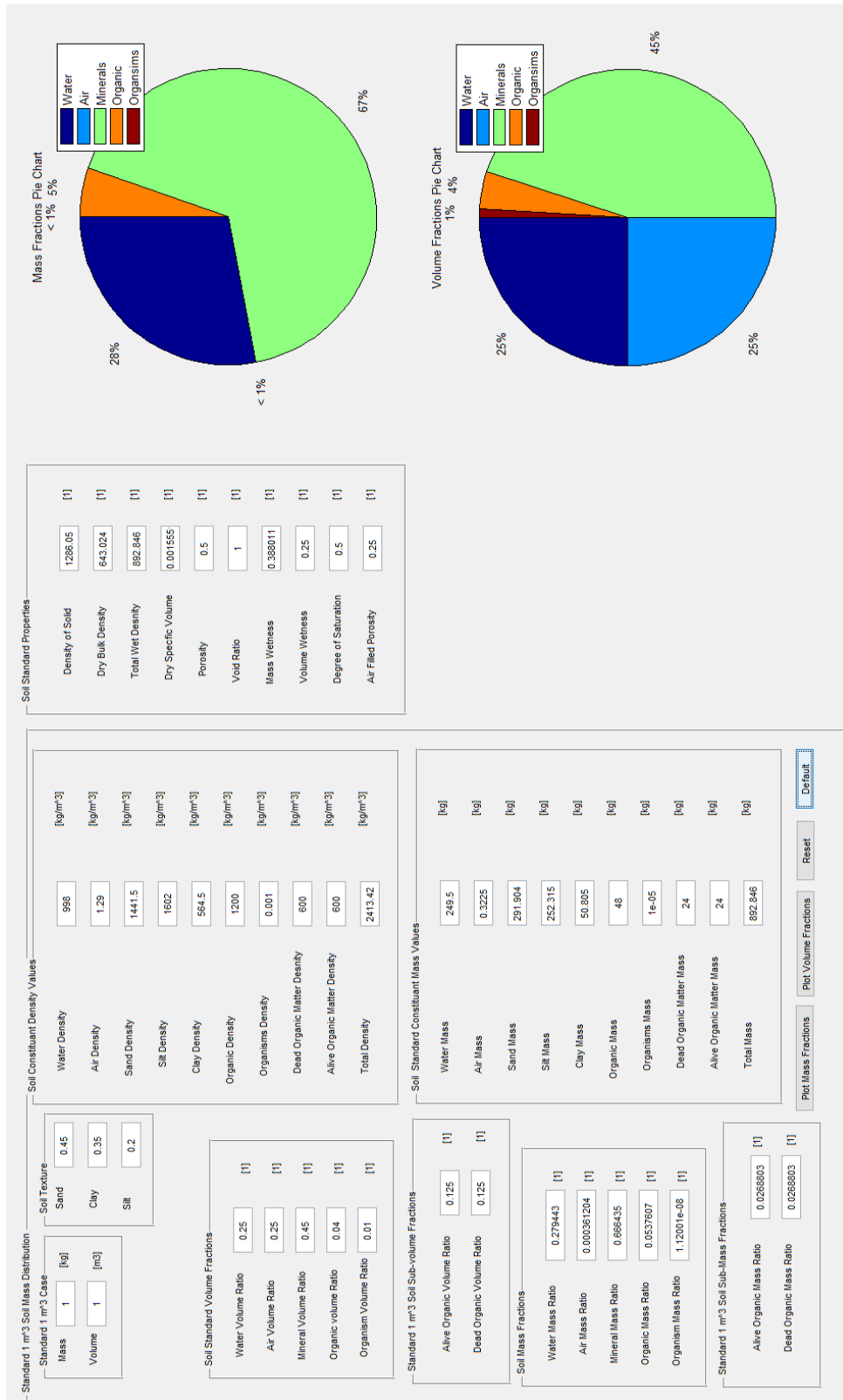


Figure 55: The software interface that calculates the volume and mass fractions and other geotechnical parameters according location type.

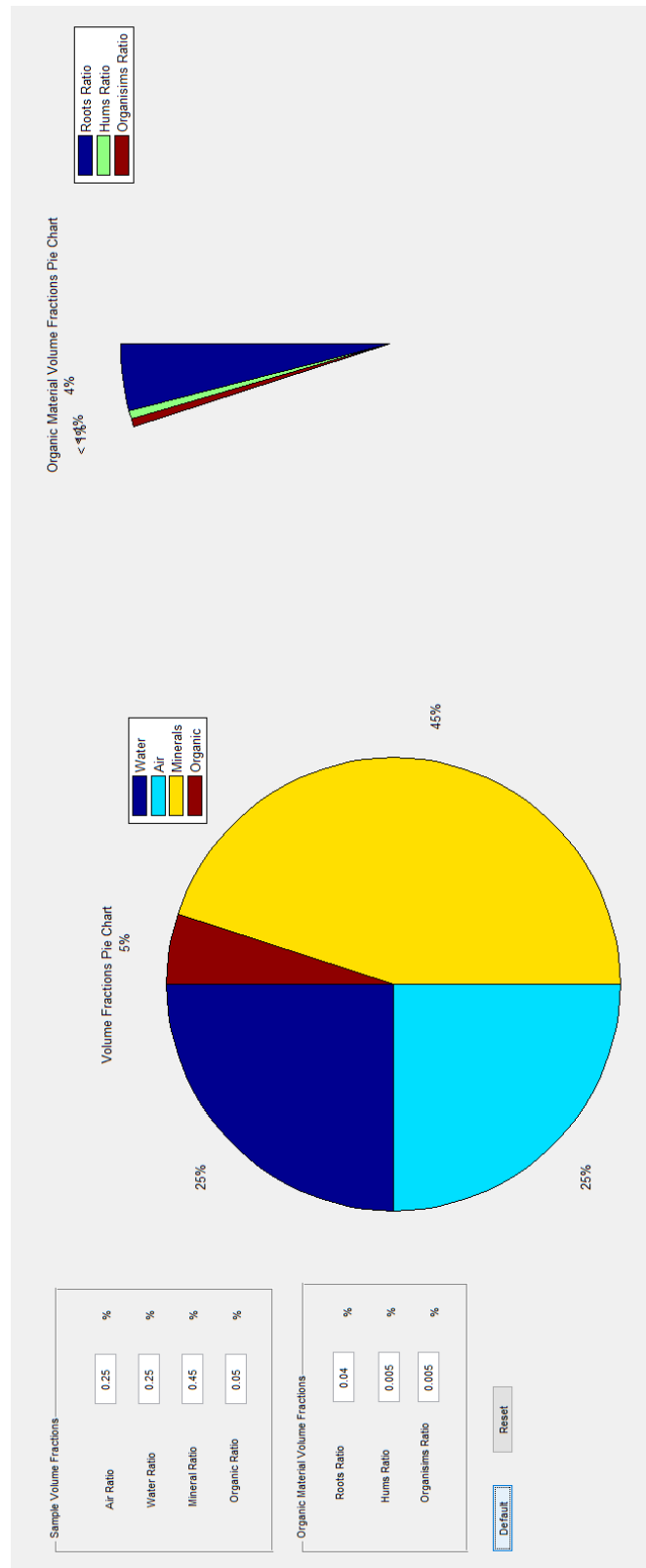


Figure 56: The organic material volume fraction calculation which are split into roots, hums and living organisms.

Lastly comes the software interface shown in Figure 57 whereby it presents three comparative plots. The first on the left-hand side shows the calculated parameters for porosity, tortuosity, constructivity. These plots are done by applying the models discussed in (section 2.2). To apply a random disturbance to the model the equations (3.12-3.14) are used by decomposing the parameters to an average and fluctuating component which are functions to space and time. Equation 3.3 starts in decomposing porosity. The mean value for porosity $\bar{\phi} = 0.45$ the user then can apply the fluctuating ϕ component according to suitability:

$$\phi = \bar{\phi} \pm \hat{\phi} \quad (3.12)$$

Tortuosity is decomposed into two components; the mean value for tortuosity is 1.8:

$$\tau = \bar{\tau} \pm \hat{\tau} \quad (3.13)$$

Likewise, constructivity is decomposed also into two components; the mean value for constructivity is taken 0.998:

$$\delta = \bar{\delta} \pm \hat{\delta} \quad (3.14)$$

The middle plot shows the temperature soil profile in relation to depth at a specified time of the day. The right-hand side plot shows ideal diffusion D_{CO_2} whereby its only a function of the plotted temperature profile within the soil. The effective carbon dioxide mass diffusion D_e in relation to soil depth is calculated by applying the data from the left-hand side and middle plot using equation (3.15)

$$D_e = \frac{\tau D_{CO_2} \phi}{\delta} \quad (3.15)$$

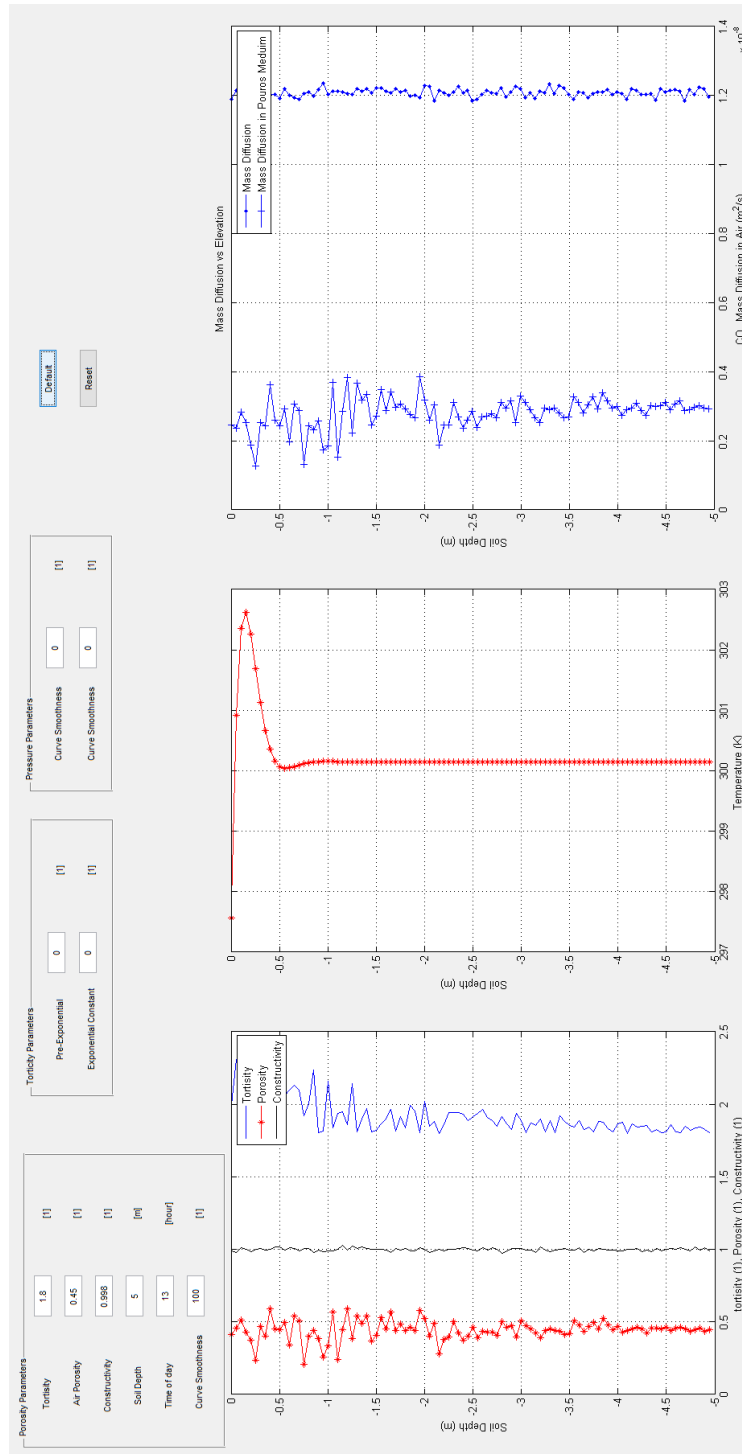


Figure 57: Studying the change of porosity, mass diffusion according to the temperature profile at a specified time of the day.

3.8. Summary

In this chapter the respiration chamber design assumptions are made they are followed by the proposal of five preliminary new designs these will provide the essential guidelines for the proposed chamber designs. What followed in presentation is the design process for the five chambers with all the design restrictions. All of the five designs pros and cons are organized in two tables to assist in the selection process. The selection table part is concluded by selecting chamber design 5.

This is by considering convenient parameters that suite the requirements of use. Chamber design number 5 is described in detail this is achieved by describing all of the apparatus parts in detail. This is to later on to help interrupt the produced numerical and experimental data.

Likewise, the experimental procedure insteps is outlined for the static and dynamic case. The city of paisley climate description is covered by surveying the annual location temperature, rain fall and radiation flux. Soil analysis for the grass land was conducted by finding the volumetric and mass fraction distribution of its material constituents. A MATLAB soil analysis efflux software with interface was developed to assist the research with the soil site analysis. In the next chapter numerical methods using advanced flow modelling codes available in the commercial software ANSYS will be covered. Those of which will be used to flow model mass transport in the gas and porous domains in chapter 5. Table 3 summarizes all the necessary biological parameters for the grass land location.

Table 3: A summary of the soil properties for the grassland site location at UWS Paisley campus.

Properties	Grass Site Sample
PH	6 to 6.8
Relative Microbiological Activity in Relation to Porosity	0.62
Relative Microbiological Activity in Relation to Temp	0.18-0.31
Fertility	High Fertility
Soil Texture	Sandy Loamy

Chapter 4

Numerical Flow Model

4.1. Introduction

Flow field scalars are resolved using the Navier-Stokes equations. The numerical model used to calculate the flow fields inside the inner chamber gas volume and soil domain are covered in this section. Soil porosity basics are covered this helps in finding soil site permeability. Likewise, a new method is developed to find soil permeability as an input value for the simulations.

4.2. The Reason for using the CFD Tool

Developing and using ready numerical models that can produce better predictions for carbon dioxide measurements is the challenge. Publications covering the numerical aspect of the problem have already been covered by several researchers but only for simple geometries such a cylindrical or box shape. That is due to the challenging topic of complex geometries. Solving computational PDEs is one problem at hand, applying the PDEs to complex geometries is another challenge. This forces the researcher to work in another field of science named grid generation consequently it diverges the researcher's attention from the main objective. As an alternative solution to this challenge the researcher would opt to use commercial software which already has a geometrical modelling package with it which is later followed by a meshing package. Complex geometries incorporate curvature and cavities that require very dynamic meshing algorithms to generate the discreet volume elements and surfaces. Consequently, these codes save the researcher time in focusing on the application side

of the problem instead of writing a code from scratch which would consume all his allocated research time and funding. Through numerical modelling more awareness can be gained regarding the dominant parameters involved in processes occurring within closed dynamic and static respiration chambers. This can lead to design optimization at an early stage of the development process. Therefore, on the long run such a method of investigation may take less time and can be less expensive when compared with what is typically encountered in experimental methods. In conclusion the researcher can predict what an experimental apparatus can produce in data output before building it. CFD provides the tools to model the species transport inside and outside the soil domain, allowing the researcher to determine the right points in space to fix the sensors in order to get accurate measurements. Furthermore, CFD can also help in locating leakage regions in and out of the chamber through finding high- and low-pressure regions over the soil surface. It can also help in locating circulation and stagnation regions in the chamber domain which will assist the researcher in finding where the chemical reactions will most probably occur. Quantifying the fluxes and the mass flow rates is also applicable through the use of the tools provided with the ANSYS software. Visualizing flows in a porous media is something tedious and hard to conduct numerically and experimentally. Numerically that is due to the statistical tools required for the process, from curve fitting algorithms and interpolation methods to highly efficient codes that handle large sets of data. To write complex data analysis codes for flow visualization can be a big challenge. While commercial software provides the data analysis tools with the software package. By running simulations, the researcher can visualize the flow patterns in different types of porous media which

in our case is the soil this is something very helpful where in real life it is something invisible for the researcher. Saving the simulation data helps you access the data whenever needed hence saves lots of time. Practical lab experiments cannot be saved once data obtained from the experiment to check the data the whole experiment has to be done from scratch. The provided visualization tools enable the researcher to see the experiment from any angle zooming in to the critical regions and taking as many snapshots as required. The major role of the CFD researcher is to survey the correct input values needed for the simulation. It is followed by the step to build and setup the simulation using the readymade software tools. These are the software modelling package, meshing package and solver setup package. This is followed by selecting the correct solvers to run the simulation and allocating the required hardware resources for the process. Consequently, this helps in making the virtual experimental setup mimic a real-life lab experiment setup. New computer hardware capabilities are continuously developing. Hence an increase in multi-disciplinary cooperation becomes evident; therefore, improved theoretical modelling approaches and modelling software are continuously developed. Within this area of research, the current thesis intends to make a contribution.

4.3. The K-Epsilon Turbulence Model

To conduct the flow simulations ANSYS-CFX commercial software was used. The used turbulence model is the RANS model which is sometimes called K-Epsilon model [217]. The model is applied to the gas domain in the chamber, to resolve the occurring scalar field inside the chamber in relation to time. The turbulent kinetic energy K is defined as the variance of the fluctuations in velocity. This is followed by

ε which is the turbulence Eddy dissipation, which has a dimension of K per unit time; for example. The K-Epsilon model introduces two new variables into the system of equations. The continuity equation is equation (4.1) where ρ is the air density and \mathbf{U} is the velocity vector field:

$$\frac{\partial \rho}{\partial t} + \nabla \cdot (\rho \mathbf{U}) = 0 \quad (4.1)$$

The general momentum equations are:

$$\frac{\partial \rho \mathbf{U}}{\partial t} + \nabla \cdot (\rho \mathbf{U} \otimes \mathbf{U}) - \nabla \cdot (\mu_{\text{eff}} \nabla \mathbf{U}) = -\nabla \dot{p} + \nabla \cdot (\mu_{\text{eff}} \nabla \mathbf{U})^T + \mathbf{B} \quad (4.2)$$

Where \mathbf{B} is the sum of body forces, μ_{eff} is the effective viscosity accounting for turbulence, and \dot{p} is the modified pressure as defined in the following equation:

$$\dot{p} = p + \frac{2}{3} \rho k + \frac{2}{3} \mu_t \bar{\nabla} \mathbf{U} \quad (4.3)$$

The model is based on the Eddy viscosity concept, so that:

$$\mu_{\text{eff}} = \mu + \mu_t \quad (4.5)$$

where μ_t is the turbulence viscosity. The K-Epsilon model assumes that the turbulence viscosity is linked to the turbulence kinetic energy and dissipation via the relation:

$$\mu_t = C_{\mu} \rho \frac{k^2}{\varepsilon} \quad (4.6)$$

Where C_{μ} is k – ε turbulence model constant 0.09. The values of k and ε come directly from the differential transport equations for the turbulence kinetic energy and dissipation rate:

$$\frac{\partial \rho k}{\partial t} + \nabla \cdot (\rho \mathbf{U} k) = \nabla \cdot \left(\left(\mu + \frac{\mu_t}{\sigma_k} \right) \nabla k \right) + P_k - \rho \varepsilon \quad (4.7)$$

In addition

$$\frac{\partial \rho \varepsilon}{\partial t} + \nabla \cdot (\rho \mathbf{U} \varepsilon) = \nabla \cdot \left(\left(\mu + \frac{\mu_t}{\sigma_\varepsilon} \right) \nabla \varepsilon \right) + \frac{\varepsilon}{k} (C_{\varepsilon 1} P_k - C_{\varepsilon 2} \rho \varepsilon) \quad (4.8)$$

Model used constants for (4.7) and (4.8) are taken as $C_{\varepsilon 1} = 1.44$ is, $C_{\varepsilon 2} = 1.92$, $\sigma_k = 1$ and $\sigma_\varepsilon = 1.3$. Turbulence production P_k is the due to viscous and buoyancy forces, which are modelled using equation (1.14):

$$P_k = \mu_t \nabla \mathbf{U} \cdot (\nabla \mathbf{U} + \nabla \mathbf{U}) - \frac{2}{3} \nabla \cdot \mathbf{U} (3 \mu_t \nabla \cdot \mathbf{U} + \rho k) + P_{kb} \quad (4.9)$$

The average flow velocity encountered in the chamber is 2.7 m/s subsequently the flow simulation case is an incompressible flow one. Hence $\nabla \cdot \mathbf{U}$ is small and the second term on the right side of equation (4.9) does not contribute significantly to the production term.

4.4. The None-Linear Eddy Viscosity Model

This is the model applied to the static respiration chamber case simulation it uses the same equations in the K-Epsilon model the only difference is that it does not apply any velocity fluctuations to the previous equations.

4.5. Darcy Model

This Darcy model is derived from Reynolds transport theorem when applied to porous media. This is achieved mainly by considering pressure as scalar quantity in the Reynolds transport theorem. Gas exchange occurs in the studied simulation between

the soil and gas medium, meaning that we can rely on the theory of air movement due to pressure fluctuations [145]. Available in the ANSYS-CFX solver is the porous model which is at once both a generalization of the Navier-Stokes equations and of Darcy's law. The main advantage of using commercial software is that they come with efficient mesh generation algorithms and tools giving the user the advantage of using the CFD code on complex geometries.

The Darcy model [217] retains both advection and diffusion terms and can therefore be used for flows in the soil domain where such effects are important. In deriving the continuum equations, it is assumed that 'infinitesimal' control volumes and surfaces are large relative to the interstitial spacing of the porous medium, but small relative to the scales that wish to resolve.

Thus, from the generated mesh the given control cells and control surfaces are assumed to contain both solid and fluid regions.

The volume porosity γ at a point is the ratio of the volume V^* available to flow in an infinitesimal control cell surrounding the point, and the physical volume of the cell. Hence:

$$V^* = \gamma V \quad (4.10)$$

It is assumed that the vector area A available to flow through an infinitesimal planar control surface A^* is given by equation (4.11) where $K = (K^{ij})$ is called the area porosity tensor:

$$\mathbf{A} = \mathbf{K} \cdot \mathbf{A} \quad (4.11)$$

The dot product of a symmetric rank two tensor with a vector is:

$$\mathbf{K} \cdot \mathbf{A}^i = K^{ij} A_j \quad (4.12)$$

ANSYS CFX presently only allows \mathbf{K} to be isotropic. The general scalar advection-diffusion equation in a porous medium becomes:

$$\frac{\partial \gamma \rho \Phi}{\partial t} + \nabla \cdot (\rho \mathbf{K} \cdot \mathbf{U} \Phi) - \nabla \cdot (\Gamma \mathbf{K} \cdot \nabla \Phi) = \gamma S \quad (4.13)$$

In addition to the usual production and dissipation terms S will contain transfer terms from the fluid to the solid parts of the porous medium. In particular, the equation for conservation of mass:

$$\frac{\partial \gamma \rho}{\partial t} + \nabla \cdot (\rho \mathbf{K} \cdot \mathbf{U}) = 0 \quad (4.14)$$

And momentum is:

$$\frac{\partial \gamma \rho \mathbf{U}}{\partial t} + \nabla \cdot (\rho \mathbf{K} \cdot \mathbf{U} \otimes \mathbf{U}) - \nabla \cdot (\mu_e \mathbf{K} \cdot (\nabla \mathbf{U} + (\nabla \mathbf{U})^T)) = -\gamma \mathbf{R} \cdot \mathbf{U} + \gamma \nabla p \quad (4.15)$$

where \mathbf{U} is the true velocity, μ_e is the effective viscosity-either the laminar viscosity or a turbulent quantity, and $\mathbf{R} = (R^{ij})$ represents a resistance to flow in the porous medium.

This is in general a symmetric positive definite second rank tensor, in order to account for possible anisotropies in the resistance. Speaking in the limit of large resistance, a large adverse pressure gradient must be set up to balance the resistance.

Consequently in that limit, the two terms on the right hand side of equation (4.15) are both large and of opposite sign, and the convective and diffusive terms on the left hand side are negligible. Hence equation (4.15) reduces to:

$$\mathbf{U} = -\mathbf{R}^{-1} \cdot \nabla p \quad (4.16)$$

Subsequently in the limit of large resistance, we obtain an anisotropic version of Darcy's law, with the permeability kept proportional to the inverse of the resistance tensor.

However, unlike Darcy's law, we are working with the actual fluid velocity components \mathbf{U} , which are discontinuous at discontinuity in porosity, rather than the continuous averaged superficial velocity:

$$\mathbf{Q} = \mathbf{K} \cdot \mathbf{U} \quad (4.17)$$

Heat transfer is modeled with an equation of similar form whereby the enthalpy H is substituted into the transport equation to give the following equation :

$$\frac{\partial \gamma \rho H}{\partial t} + \nabla \cdot (\rho \mathbf{K} \cdot \mathbf{U} H) - \nabla \cdot (\Gamma_e \mathbf{K} \cdot (\nabla H)) = \gamma S^H \quad (4.18)$$

Where Γ_e is an effective thermal diffusivity and S^H contains a heat source or sink to or from the porous medium. A generalized form of Darcy's law is given by

$$-\frac{\partial p}{\partial x_i} = \frac{\mu}{K_{\text{perm}}} U_i + K_{\text{loss}} \frac{\rho}{2} |\mathbf{U}| U_i \quad (4.19)$$

Therefore μ is the dynamic viscosity, K_{perm} is the permeability and K_{loss} is the empirical loss coefficient.

4.6. Permeability Calculation

There are many ways to obtain soil permeability values; its importance comes as it is an essential input parameter that is needed for the numerical modelling. What will be derived here in this section is a reliable method to find permeability values for a soil layer as will be shown in equation (1.5).

From the soil texture side experimentally, the location is characterized as having a loamy sand texture which can be located on Figure 58.

with poor drainage with 80% sand, 15% silt and 5% clay. Finding the location intrinsic permeability is based on the model of porous material made up of parallel tubes of uniform sizes stated in [116] as shown in equation (4.20):

$$K = \frac{\theta}{2\pi} D_{\text{total}} \quad (4.20)$$

Where θ is the soil porosity, D_{total} is the total area of pores. To give the model the option of parallel tubes of different sizes pore size distribution is characterized using a histogram, this is later applied to equation (4.20).

The area of a single pore area considered to have a circular area can be found using equation (4.21), where d_{av} is the average pore diameter for a segment of pore sizes:

$$A_n = 0.25\pi d_{\text{av}}^2 \quad (4.21)$$

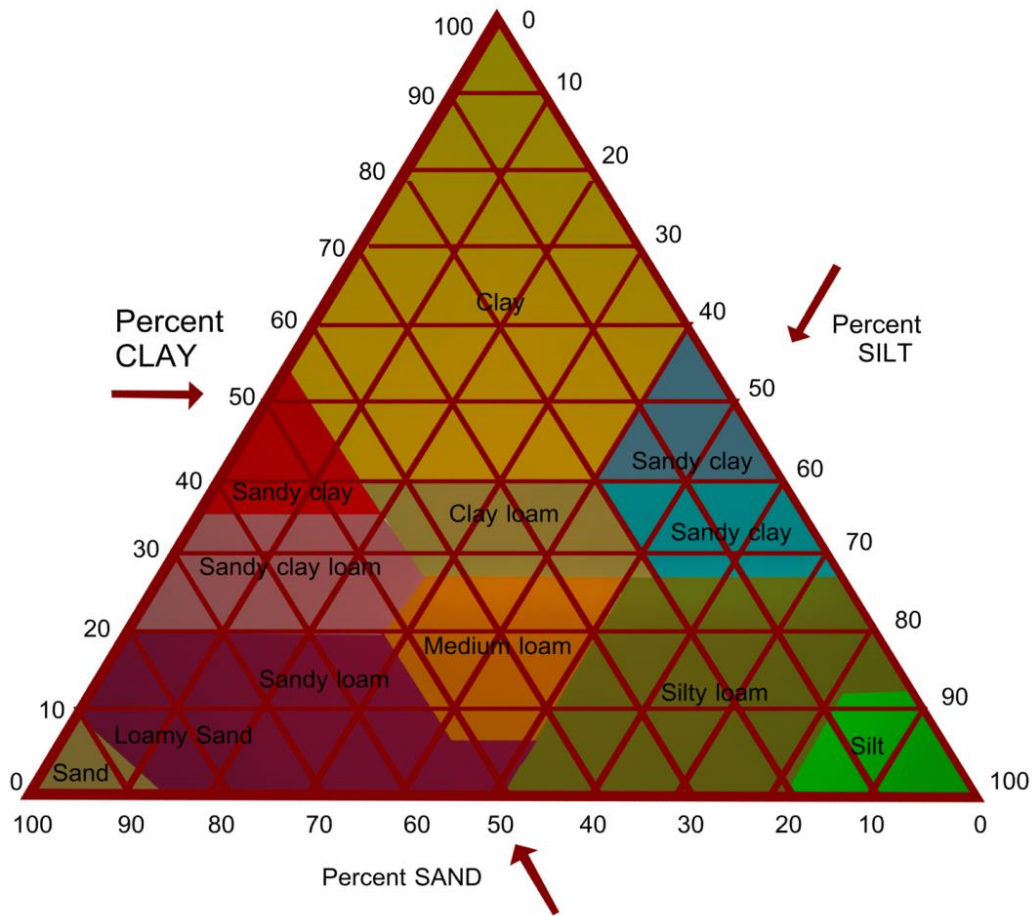


Figure 58: USDA and UK-ADAS Soil textural triangle.

Applying Newton's forward Integration law formula for two points on a single segment of the histogram, where the two points represent the minimum and maximum value of pore diameters at that segment:

$$D_n = \int_{A_n}^{A_{n+1}} r(A)dA = (A_{n+1} - A_n) \frac{r_n}{2} \quad (4.22)$$

By substituting equation (4.11) into (4.22) the area for a segment of pore size can be calculated using equation (4.23):

$$D_n = \pi(d_{n+1}^2 - d_n^2) \frac{r_n}{8} \quad (4.23)$$

Equation (4.23) can be extended to different size distribution by considering macro, meso and micro pores, which for simplicity can be related to the ratios of sand, silt and clay:

$$K = \frac{\theta}{2\pi} \sum_1^{n=3} D_n = \frac{\theta}{2\pi} (D_{\text{sand}} + D_{\text{silt}} + D_{\text{clay}}) \quad (4.24)$$

Considering the pores diameters in equation (4.24) to be as follows for a top soil layer macropores (20 – 2000 μm), mesopores (2 – 20 μm) and micropores (0.2 – 20 μm):

$$K = \frac{\theta}{2\pi} \sum_1^{n=3} D_n = 0.25\theta((d_2^2 - d_1^2)r_{\text{sand}} + (d_3^2 - d_2^2)r_{\text{silt}} + (d_4^2 - d_3^2)r_{\text{clay}}) \quad (4.25)$$

In conclusion the final form takes the form shown in equation (4.26):

$$K = \frac{\theta}{2\pi} \sum_1^{n=3} D_n = 0.25\theta(a_1r_{\text{sand}} + a_2r_{\text{silt}} + a_3r_{\text{clay}}) \quad (4.26)$$

Where $a_1 = 10^{-6}$, $a_2 = 10^{-10}$, $a_3 = 10^{-12}$. The power of this equation is that it allows the researcher to get reasonable permeability values to be used for the simulation input based on firstly classifying the site soil type.

This is followed by extracting the ratios of sand, silt and clay from the soil texture triangle shown on Figure 58.

4.7. Soil Porosity

The volume of soil is referred to as the bulk volume of soil. Soils differ strongly in porosity. An adequate supply to plant roots of soil mineral solution and soil air especially oxygen is essential for the plant growth and the crops production.

Fluid flows only through the interconnected pores. The volume fraction of the interconnected pores is called the effective porosity. The soil solution and the soil air are stored and transported within the soil pores.

Plant roots also exist in the soil pores. The rocks will be neglected in this study of the soil porosity. The porosity of the surface soil typically decreases as the particle size increases. This is due to soil aggregate formation in finer textured surface soils when subjected to soil biological processes.

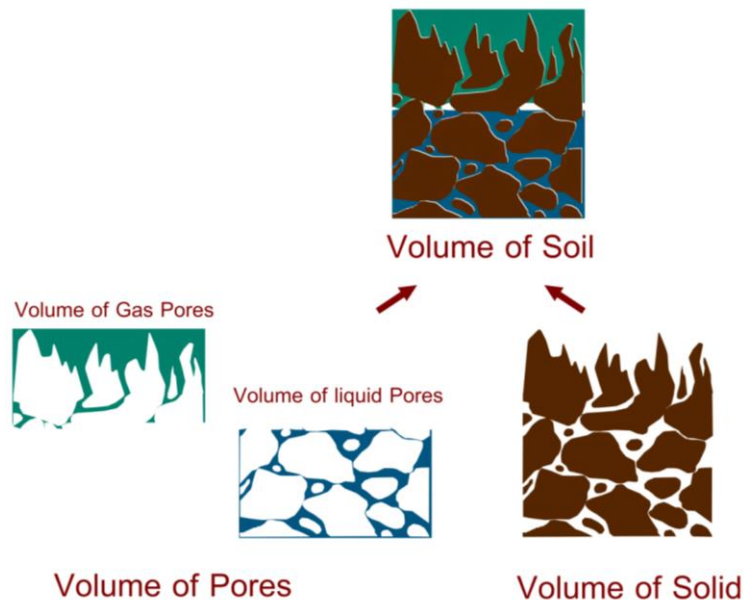


Figure 59: Porosity is the ratio of the total volume of pores in a soil sample over the total volume of the soil sample.

Thus, looking at Figure 59 the volume fraction of soil pores is ϵ furthermore it is referred to as porosity.

It is an important property for the study of porous media whereby it is the ratio of void volumes over the volume of voids plus the volume of the soil matrix. Consequently, the porosity formula can be written in following form:

$$\epsilon = \frac{V_V}{V_T} = \frac{\text{total volume of pores}}{\text{volume of soil}} \quad (4.27)$$

Whereby it is the fraction of void space in the soil sample in particular the void volume is V_V notably V_V can be decomposed into a gas volume V_g and a liquid volume V_l as shown in equation (4.28):

$$V_V = V_g + V_l \quad (4.28)$$

Similarly, the total or bulk volume of the soil represents the void volume of pores plus the volume of the solids mass V_B as given in the following equation:

$$V_T = V_B + V_V \quad (4.29)$$

Hence by using equations (4.27), (4.28) and (4.29) result in a formula for porosity represented by volumes:

$$\epsilon = \frac{V_g + V_l}{V_B + V_g + V_l} \quad (4.30)$$

Porosity is the volume fraction ratio that varies in value between 0 and 1. As an example case for a studied grassland site whereby identifying the soil texture in it as a loamy soil sample. It can be concluded as seen in Table 4 that the porosity

ranges from 0.30 to 0.60. Hence a grassland site can be considered to have an averaged porosity value of $\epsilon = 0.45$.

Porosity has an effect on atmospheric gases getting dissolved into the soil liquid volume pores and the solid volume soil pores. This results in getting carbonic constituents leading to acid production which will affect the pH of the soil [164]. Figure 60 shows the volume cavities in 3D by using a three-dimensional scanning electron microscopy on a soil cube sample.

Table 4: Soil porosities depending on type of texture [34].

Soil Texture	Porosity range
Sandy Soils	0.35-0.60
Clay Soils	0.35-0.70
Silty Soils	0.30-0.60
Peat Soils	0.80-0.85
Loamy Soils	0.30-0.60

The Comparison between different 3D voxel representations of a Fontainebleau sandstone generated using different reconstruction techniques. Pores can either be very large or very small it all depends on location furthermore they some of them are connected and others are not.

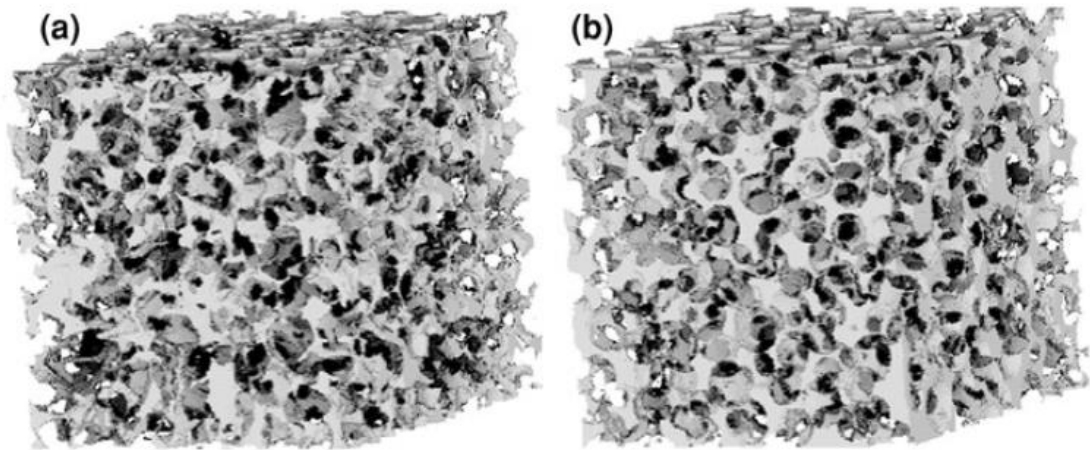


Figure 60: The side length of each sample is 2.25 mm. (a) is taken using X-ray microtomography. (b) is taken using the Object-based modelling [218].

There are three main categories for pore sizes given in Table 5. Macropores refer to pores greater than 100 [μm] in diameter. These pores are too large to have a significant capillary force. Once the pores reach field capacity, the pores are filled with air, thus facilitating air diffusion. Mesopores refers to pores which are greater than 30 [μm] and less than 100 [μm] in diameter which occur mostly in clay. These are the water storage pores after the excess water has been drained away.

The stored water is useful to plants. The capillary forces are not too great; therefore, plants do not find the adsorption of water limited in mesopores. Micropores refer to pores smaller than 30 μm in diameter.

The movement in micropores takes place through an activated diffusion which occurs mostly in clay through the adsorption onto the surfaces of the clay molecules, thus facilitating the diffusion of the soil substrates. The flow through the mesopores is described by Knudsen diffusion [32] especially the pores at the nanoscales. The water held in the micropores is essential for the activity of the microbes creating moist

anaerobic conditions. The moisture in the micropores is difficult for the plant roots to use.

Table 5 : The diameter of the pores classification [34].

Type of Pore	Pore Dimension
Macropores	> 100 μm
Mesopores	30 – 100 μm
Micropores	< 30 μm

Water is a unique molecule in both its physical and chemical characteristics. It has higher than expected boiling and melting points and can dissolve a great variety of compounds. In the soil it is even more unique in that it occurs in the liquid, gaseous, and solid (frozen) states. The water content of soil is highly variable, ranging from dry air, with as little as 1% water to saturated, where all void spaces are filled with water.

4.8. Summary

The presented laminar numerical model here is to be used simulate the static case operational mode for the respiration chamber simulation. Furthermore, the K-Epsilon model is covered here for that it is applied for the dynamic operational mode case for the respiration chamber simulation.

Likewise, the K-Epsilon model is applied to the rotating mesh domain case. Additionally, the Darcy model is covered here because it is applied for the porous soil domain simulation for all the discussed three cases.

A soil permeability equation is derived here for that it can be applied on the grassland case study furthermore for different locations of interest for future studies. In particular this is done by locating the site on the soil texture triangle. Consequently a grassland location is characterized as medium loamy sand [219] consequently leading to a porosity value of 0.45 and permeability value of 10^{-10} [m²]. This leads us to the next chapter that deals with the experimental and numerical results.

Chapter 5

CFD simulations and Experimental Results and Discussion

5.1. Introduction

The chapter will initially present collected experimental data for the static chamber case. The experimental data then is corrected and curve fitted to be ready for comparison with the CFD built model. The same approach is applied to the experimental data for the dynamic chamber case. The data is first filtered from all the un-necessary disturbance using MATLAB. This is firstly by cutting off the saw teeth peaks. Then sample filtering is applied to the measured concentrations. The next step is capturing the concentration slop. Absolute and relative concentration values are found during the process. Consequently, once done the efflux function can be calculated hence the locations biological activity is determined. Based on the previous stage that found species concentrations within the chamber internal partial pressure for air and carbon dioxide become easy to find. The chambers dry point and dew point temperature are compared with species measured concentrations. The process is also applied for the measured moisture content within the chamber volume. Radiative sunlight effects on species. Concentrations are also investigated using the light intensity sensor. Based on the measured values through the experiment the simulation input parameters are identified. A static mode chamber CFD simulation case is modelled and setup with all the necessary input values and the required boundary conditions whereby its later run and validated. This is by selecting the laminar flow model. It is followed by a dynamic chamber CFD case simulation with no fan rotating mesh. It is also run and validated this is achieved using the RANS turbulence model.

Finally, the rotating mesh CFD simulation is run and validated using the same mentioned model. The chapter is concluded with how feasible is CFD when applied to the two operational cases of dynamic and static.

5.2. Static Case Experimental Data Analysis

A MATLAB software was written during the process of data analysis which matured into a powerful tool assisting in the data Analysis process as covered in (section 3.7). This was achieved by going through the five main steps covered in [8] whereby this is firstly and secondly done by making the observation and formulating the hypothesis: This is achieved by monitoring the concentration of carbon dioxide in relation to time inside the chamber gas volume. Readings were taken using the gas sensor connected to the sampling tube this was done specifically for a grass land location. Thirdly follows the stage of drawing the graph. The fourth stage is the design and the steps to perform the experiment. Finally, the fifth stage is to evaluate data with the appropriate statistical design as shown in the Figure 61. After verifying in several initially tests that repeatability of experiment was achieved a static run case was conducted on the 8 May. The big peaks leading to 5000 [ppm] had to be omitted out to correct the readings, these jumps have been attributed to external blowing winds or to individuals passing by near the location of study. The sampling period was 5000 [s] the reason for long duration of sampling which was over 360 [s] for the purpose to formulate and test the research hypothesis. Commenting on Figure 61 it is noticeable that big concentration jumps occur every now and then. These jumps need to be omitted out based on previous knowledge that grassland locations are not characterized to have these kinds of concentrations jumps that reach values of 5000 [ppm]. The wrong

readings are identified in a red colour furthermore the concentration jumps all had a similar pattern with a rectangular shape. Hence any reading that has a wrong measurement is assigned a concentration of 470 [ppm] through the written code as visible in the second bottom plot of Figure 61. This is shown in equation (5.1) where read in data matrix is $A(t)$ and the corrected concentration matrix is $C(t)$:

$$C(t) = \begin{cases} 470 & 470 \leq A(t) \leq 5000 \\ A(t) & A(t) < 470 \end{cases} \quad (5.1)$$

Consequently, the required data plot comes to be visible hence the next step is to curve fit the data this is achieved by applying a linear regression function. The evident extrapolated function is a linear one with a positive slope. This means that an increase of species concentration within the gas volume of the chamber is occurring with the progression of time of the experiment.

The measured concentrations at the start of the data sampling process start at a reasonable value of 370 [ppm] making close to what recorded measured atmospheric values of concentration 401[ppm] [212]. To correct the concentration measurements another basic filtering process is conducted as shown in Figure 62. This is applied to concentration values of 470 [ppm] whereby the values are replaced by a value of 420 [ppm]. Figure 63 shows absolute measured concentration values, these values are obtained by subtracting the atmospheric concentration value of carbon dioxide from the measurement. This makes concentration measurements start at a zero value this allows the researcher to identify the soil efflux jump much clearly. Consequently, capturing the soil total biological activity efflux in the chamber.

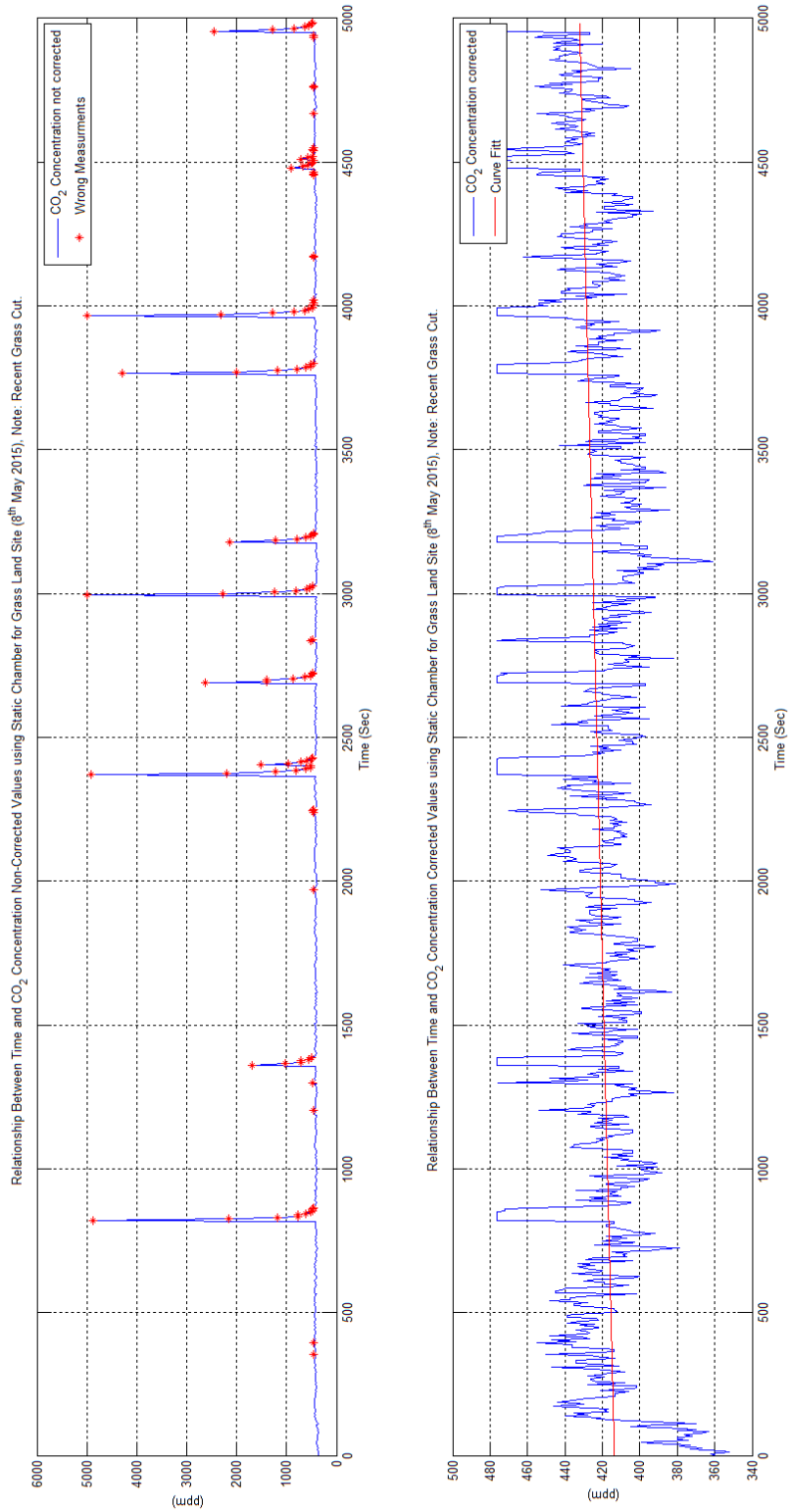


Figure 61: A comparison between non-corrected concentration measurements and correct ones.

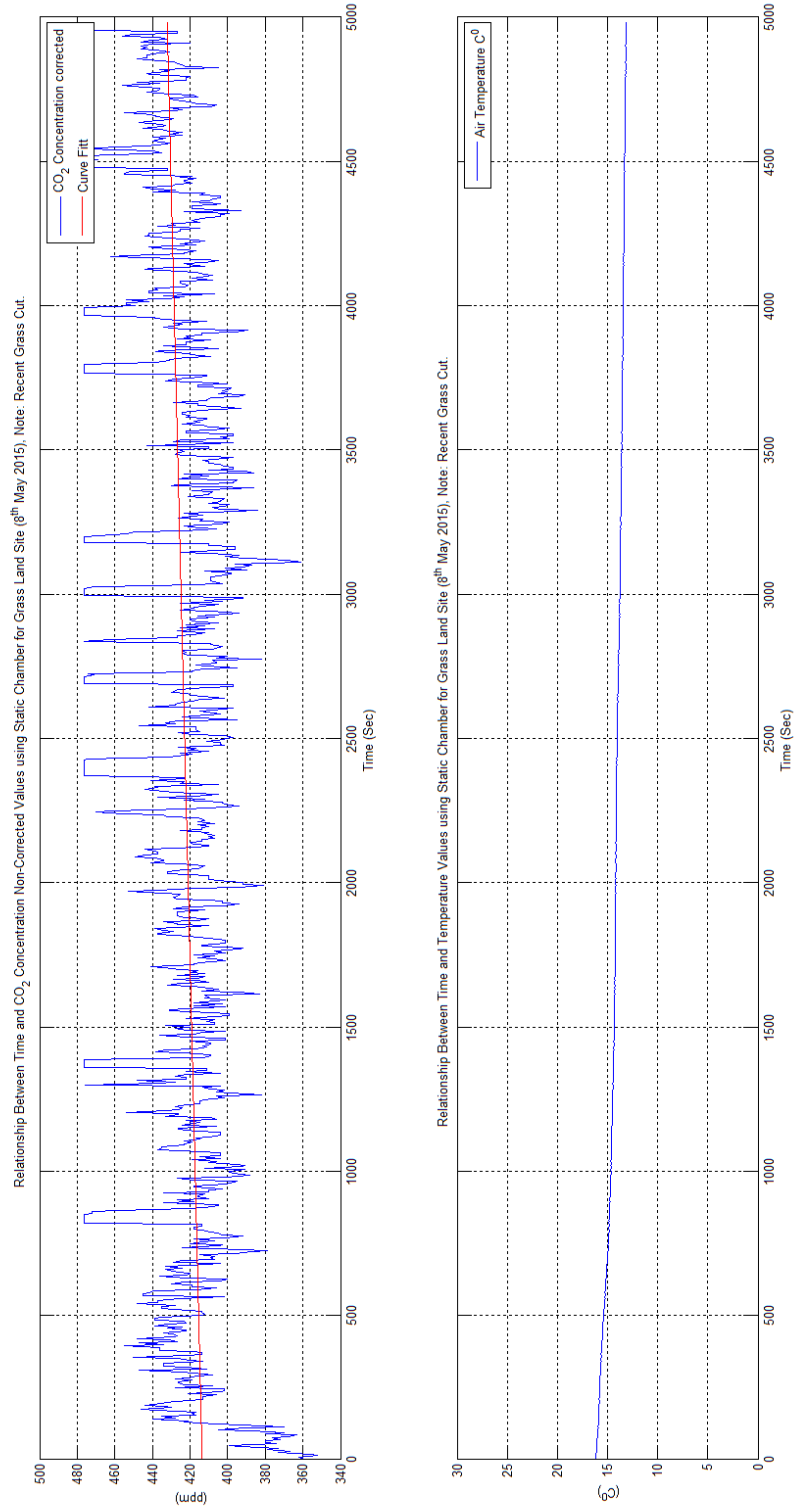


Figure 62: This plot shows a comparison between chamber temperature and species concentration levels, it shows the linear relationship through curve fitting MATLAB provides also exponential curve fitting.

It is common knowledge that the atmosphere is composed of many gases at different volume fractions. The measured atmospheric value of carbon dioxide concentration is 402.80 [ppm] according to the [206]. Hence to find absolute species concentration values inside the chamber atmospheric values of carbon dioxide were subtracted from the measurements. Consequently, the absolute measured values were considered which start from zero to about 120 [ppm] as shown in the. It is evident when looking at Figure 63 in the top figure there is lots of disturbance to the measurements; therefore, a MATLAB data filter is used at the bottom plot. The absolute concentration values are shown in the top figure while the bottom one shows the absolute concentration after applying a filtering function on it noting that the filtered function is coloured blue furthermore the unfiltered one is in red. Basically exponential functions with one term can be used to curve fit the distributed set of data this is shown in the obtained equation (5.2) :

$$C(t) = 414 e^{(4e^{-6})t} \quad (5.2)$$

The power of using the filtering function is that it provides the initial slope to measure the biological soil activity. Consequently by multiplying the function in equation (5.2) by a filter $H(z)$ the general formula can be found (5.3)

$$\tilde{C}(t) = C(t)H(z) \quad (5.3)$$

A MATLAB built in function is applied on the gathered dataset from the experiment this is a 1-D digital filter [220]. This kind filter is used in signal analysis furthermore it can also be applied to the collected data. A moving average filter is used and is represented by equation (5.4):

$$y(n) = \frac{1}{\text{windowSize}} (x(n) + x(n - 1) + \dots + x(n - (\text{windowSize} - 1))) \quad (5.4)$$

Hence the numerator coefficients of the rational transfer function are defined. For the studied case it is taken as to have a value of $\text{windowSize} = 30$. Moreover, the denominator coefficients of the rational transfer function are taken to have the value of 1. Filtering the rows or columns of the efflux matrix with the following rational transfer function (5.5):

$$H(z) = \frac{1}{1 - 0.0333 Z^{-1}} \quad (5.5)$$

From Figure 63 by curve fitting the filtered function of concentration using an exponential function with one term in relation to time equation (5.6) is obtained:

$$\widetilde{C}(t) = 391.8 e^{(2.4e^{-5})t} \quad (5.6)$$

What is evident when comparing equations (5.2) with (5.6) that both the filtered and unfiltered function with a one term exponential function didn't capture the exact curve hence the single term function was not considered. Furthermore, an exponential function with two terms was adopted for curve fitting resulting in equation (5.7):

$$\widetilde{C}(t) = 420 e^{(3.5e^{-6})t} - 504 e^{-0.0129t} \quad (5.7)$$

The extracted experimental equation is later used for the numerical simulation part of the project whereby this obtained equation is read in into the ANSYS-CFX code. Consequently, its assigned as a source term inside the biologically active soil. Without equation (5.7) it is very difficult to obtain correct results using CFD simulations.

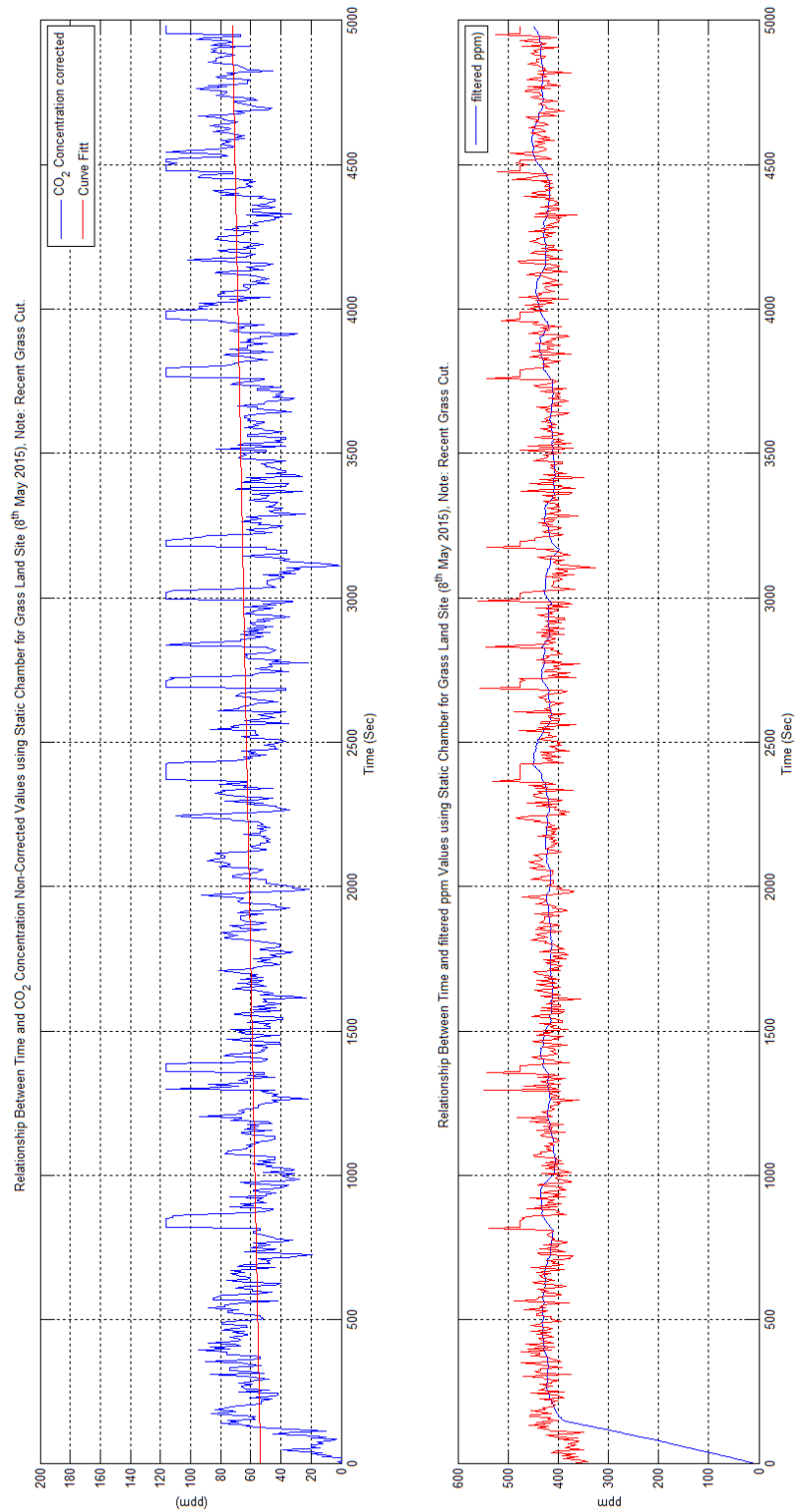


Figure 63: Absolute values of measured carbon dioxide measurements, filtered measurements of carbon dioxide.

Firstly, from the measured species concentration data the derivative of concentration dc/dt is calculated in relation to time. Looking at Figure 64 by curve fitting the collected data the following function can be obtained in equation (5.8). This is based on each instance of time

$$ef_t = 2 + 0.00055 \left(\frac{\partial c}{\partial t} \right)_t \quad (5.8)$$

From equation (5.8) the ratio $V/A = 0.55$ can be calculated by hand whereby both chamber gas volume and covered soil surface are known. The general formula for the efflux equation can be derived shown in equation (5.9) which is as follow hence giving the following form whereby $a = 10^4$ is a conversion factor.

$$ef_t = ef_0 + 0.55 a \left(\frac{\partial c}{\partial t} \right)_t \quad (5.9)$$

The curve fit proves the locations efflux for the grass land which is $ef_0 = 2$ [g/m²h] as stated in literature Zhou et al. [221]. It is evident from the comparison in Figure 64 between the two plots that the efflux plot shows how the rise of efflux in relation to time. This is attributed to the rise of inner chamber concentration in a smooth manner. Furthermore, the absolute carbon dioxide concentration plot captures the diffusive gas behaviour in the chamber with which doesn't make the rise in species concentration obvious. Figure 65 shows a comparison between relative humidity values with species concentration values in relation to time. There is no evident relationship between both the only issue is that the relative humidity is to some extent steady throughout the measurement process. The value seems to have a slight rise with decrease in chamber temperature this will be evident in Figure 66 .

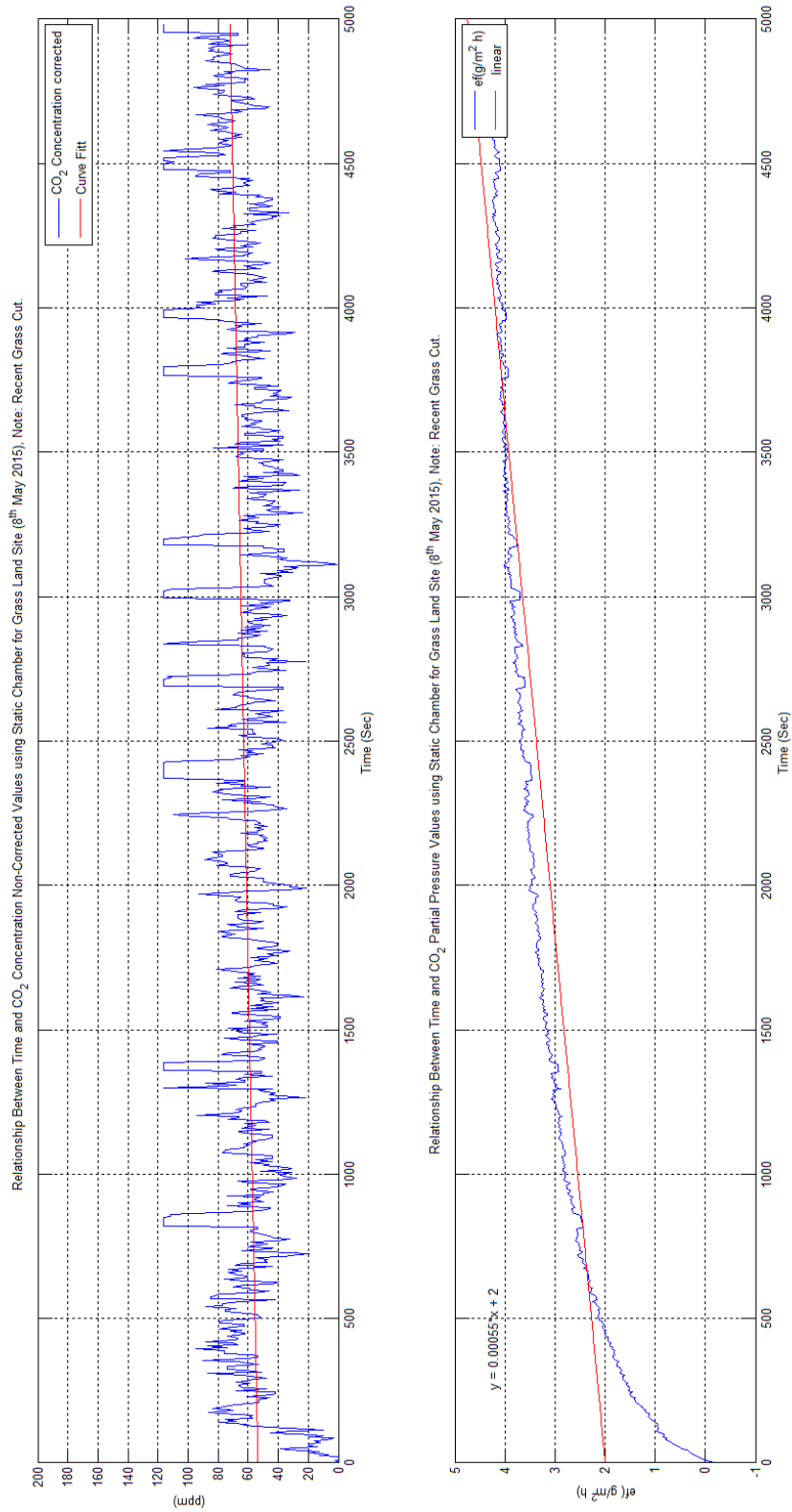


Figure 64: Absolute conctracation measurmnts compared with eflux measurmnts in time for a two our experiment.

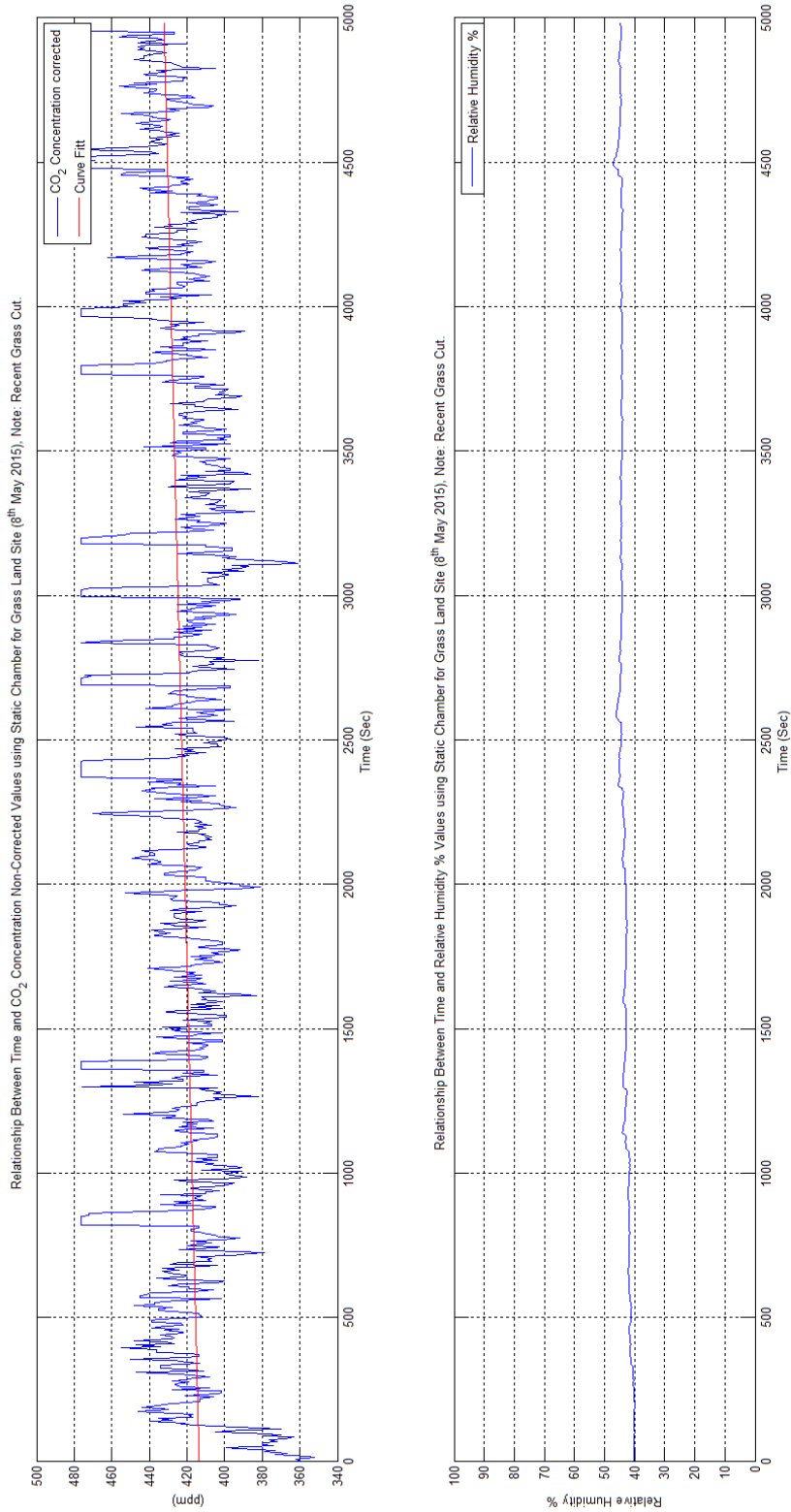


Figure 65: measured relative carbon dioxide concentrations with relative humidity affects.

Commenting on Figure 66 using equation during the measurement time of 2.5 [h] the location temperature was decreasing. The chamber is provided with a temperature sensor measuring temperature T_t at each instance of time. The dew point temperature $(T_d)_t$ at each instance of time is not measured directly by a sensor it is calculated based on previously knowing what the atmospheric moisture content RH_t in the chamber in parallel with temperature T_t is using equation (5.10):

$$(T_d)_t = \frac{243.12 \left(\ln \left(\frac{RH_t}{100} \right) + \frac{17.62 T_t}{243.12 + T_t} \right)}{17.62 - \left(\ln \left(\frac{RH_t}{100} \right) + \frac{17.62 T_t}{243.12 + T_t} \right)} \quad (5.10)$$

Comparing both plots in Figure 66 didn't show any visible relationship between the dew point temperature and location temperature with species concentration. Both mentioned temperatures are nearly constant in value throughout the measurement period. Likewise, the same applies to the air relative humidity. This shows that the measurement was taken at a steady state and no big temperature variations did occur during the measurement process hence the chamber gas volume preserved to some extent the ecological and biological state inside the chamber gas volume. From the measurements concentrations showed a more unsteady turbulent pattern. Figure 67 shows no visible relationship between the measured light intensity inside the chamber gas volume and measured carbon dioxide species concentration. What is evident is that light intensity disturbance at the start of the measurement can be attributed to the nonhomogeneous state of the gas mixture inside the chambers. This is at the initial first 150 seconds then after it takes steady value. Comparing Figure 66 with Figure 67

shows that there is some time lag between the chamber inner light intensity and inner chamber temperature this is mostly due to the inner heat capacity of air.

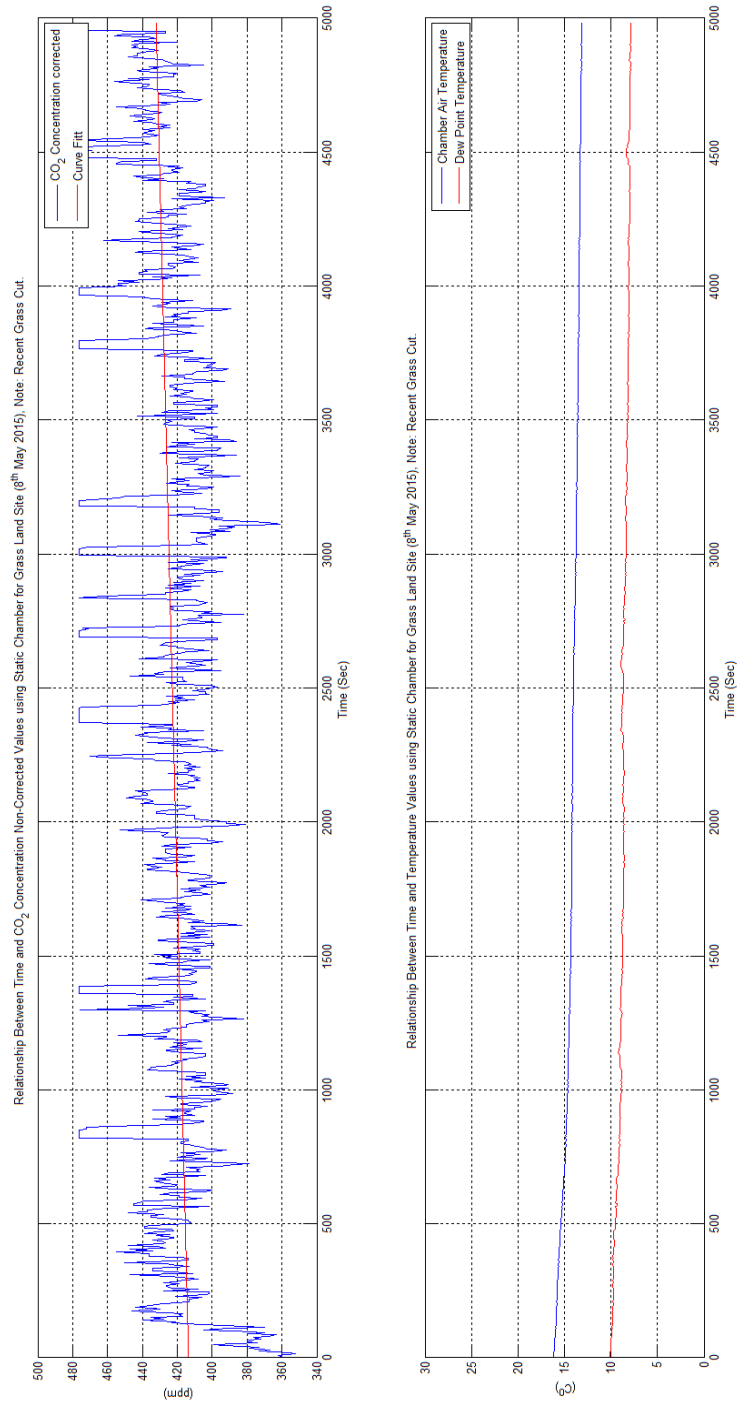


Figure 66: Dew point temperature and temperature plots in comparison with concentration.

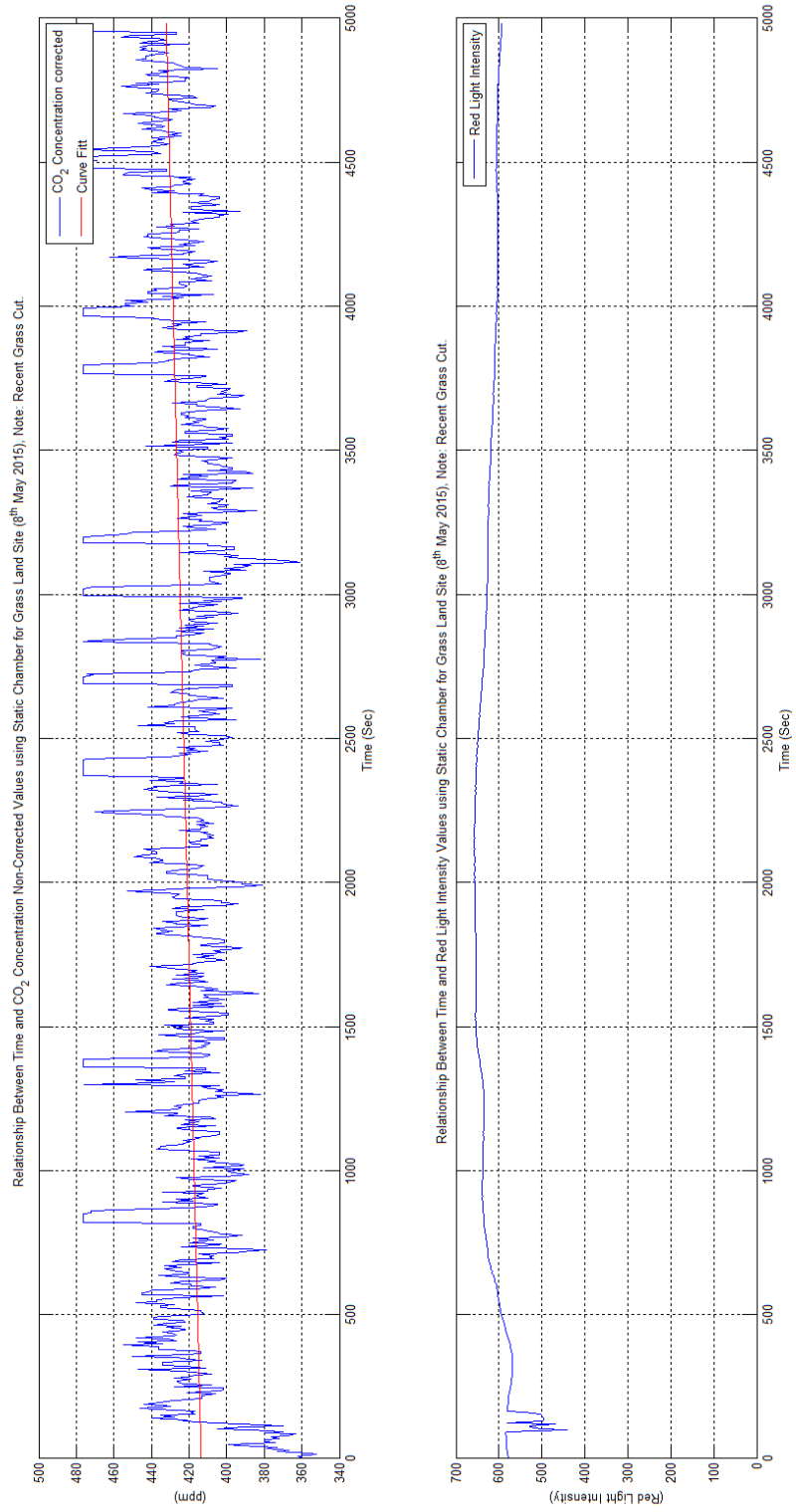


Figure 67: The relationship between species concentration and light intensity inside the chamber.

No chamber pressure sensor was used therefore chamber internal pressure difference was calculated using equation (5.11) derived in (section 2.7.2). Whereby the case for constant internal chamber volume (Isochoric process) is considered starting with the initial atmospheric pressure at location:

$$(\Delta P_{in\ 1})_t = P_{t+1} \frac{T_{t+1}}{T_t} - P_t \quad (5.11)$$

When plotting the calculated pressure data in Figure 68 the very small fluctuating changes take the form of a step function.

This small temperature drop becomes clear when curve fitting the data whereby there is a small curve slope drop this is due to the fall of temperature with time this is attributed to time of day where by the data was collected before the sunset.

This fluctuating behaviour is due to the summation of the many small air heat parcels contribution to mass diffusion. Looking at Figure 68 it is evident that the absolute pressure change is in the range of ∓ 600 [Pa] inside the chamber hence:

$$(\Delta P_{in\ 1})_t = \mp 600 \text{ Pa} \quad (5.12)$$

By comparing both plots in Figure 68 no direct relationship between the pressure difference values and species concentration fluctuations were evident hence both parameters are independent from each other.

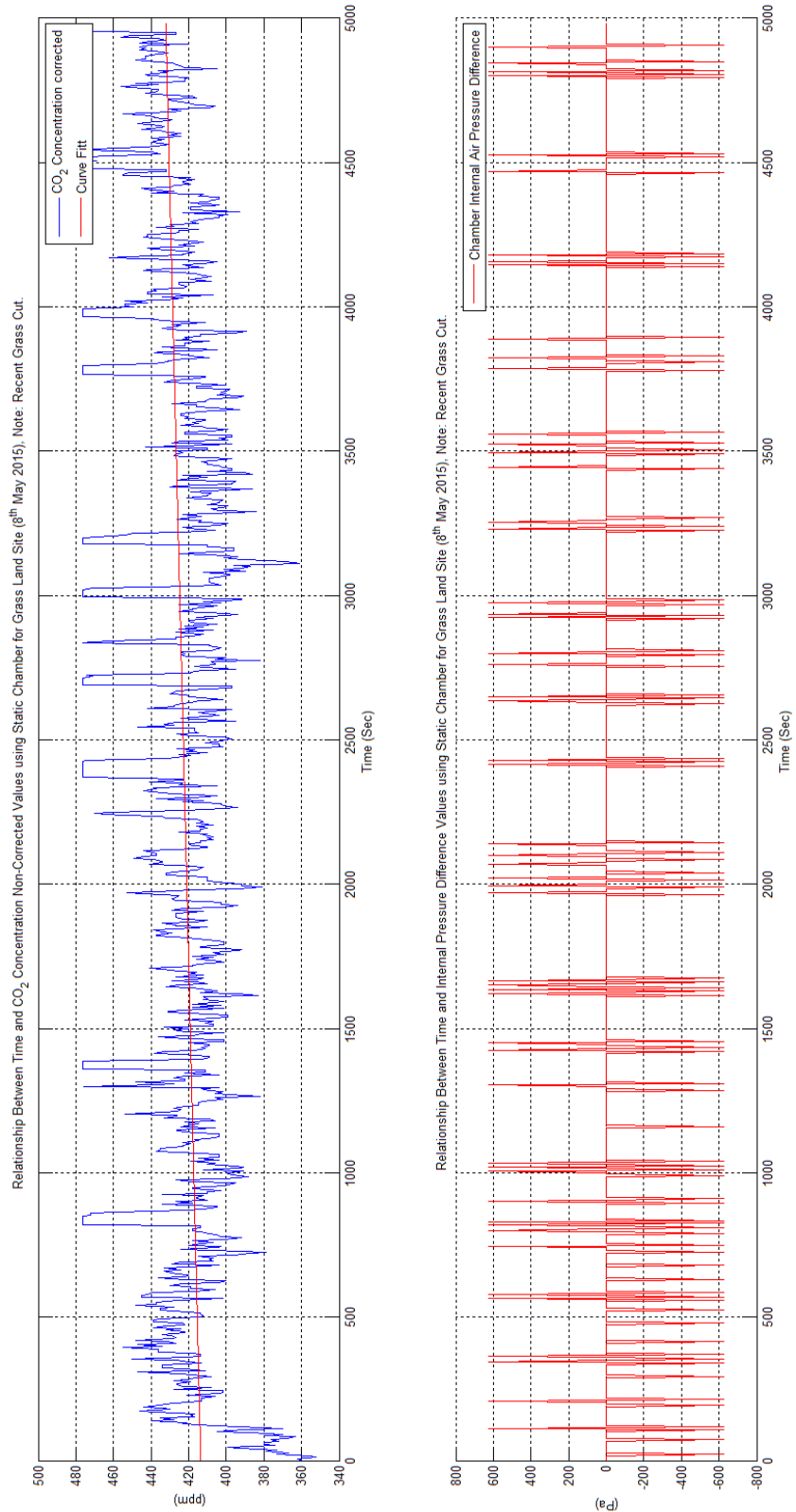


Figure 68: Change of internal pressure as a function of temperature.

To calculate the partial for carbon dioxide $P_{(\text{CO}_2)_t}$ at every instance of time equation (5.13) is applied in the data analysis code.

Furthermore, carbon dioxide concentration in the chamber at each instance of time is $x_{(\text{CO}_2)_t}$ its value is measured using the gas sensor. Likewise chamber internal pressure at each instance of time is $P_{(\text{total})_t}$ has been previously calculated in equation (5.7).

$$P_{(\text{CO}_2)_t} = x_{(\text{CO}_2)_t} P_{(\text{total})_t} \quad (5.13)$$

Air partial pressure $P_{(\text{air})_t}$ at each instance of time is calculated using equation (5.14) based on the measured absolute carbon dioxide pressure:

$$P_{(\text{air})_t} = (1 - x_{(\text{CO}_2)_t}) P_{(\text{total})_t} \quad (5.14)$$

By using both equation (5.13) and (5.14) the partial pressure data is produced.

Looking at Figure 69 the fall of air partial pressure is due to the rise of carbon dioxide concentration inside the chamber. From the calculated total pressure, the partial pressures can be calculated.

Furthermore, by comparing the light intensity plot in Figure 67 with the carbon dioxide partial pressure in Figure 69 shows that carbon dioxide partial pressure is sensitive to light intensity changes as covered previously in the literature section 2.6.4.

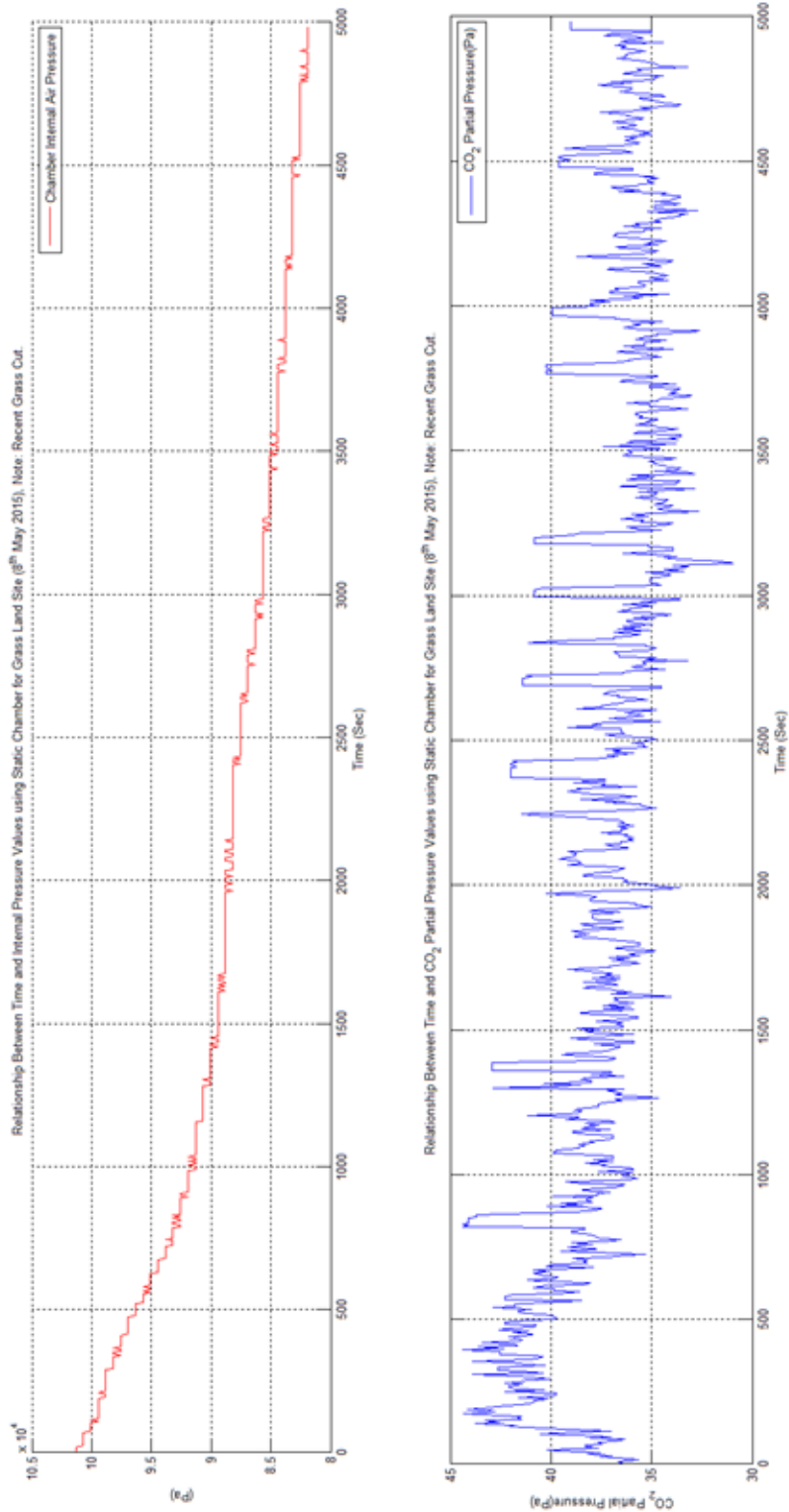


Figure 69: Internal chamber partial air Pressure shown in red and internal partial carbon dioxide pressure shown in blue.

5.3. Conclusions from Experimental Data

In conclusion the experimental data helps out in identifying the steady and unsteady parameters to build the CFD numerical model. It points out the relationships of the measured parameters with carbon dioxide measured concentrations. Initially the criteria to select the simulation time duration is based on the requirement to firstly just capture the initial concentration slop. Secondly comes the step of extracting the specific efflux of the location. Hence for the 5000 [s] data collections period 360 [s] are enough for the setup CFD simulation. It was seen that minor changes in temperature inside the chamber gas volume produce inner pressure changes. According to turbulence models pressure changes can be modelled using

$$P = \bar{P} + \dot{P} \quad (5.15)$$

The experimental studied case is a static one hence $\bar{P} \approx 0$ is considered this due its very small value when curve fitting the experimental data:

$$P = \mp \dot{P} \quad (5.16)$$

These contribute to the diffusive mass transport within the chamber as seen in the turbulence behaviour of carbon dioxide measured concentrations. Hence species concentration can be modelled using:

$$C = \bar{C} \mp \dot{C} \quad (5.17)$$

Where by the extrapolated unfiltered function can be the following

$$C(t) = 414 e^{(4e^{-6})t} \mp 20 \quad (5.18)$$

Hence it is recommended from the experimental data to use the laminar model for the static case simulation more over the RANS turbulence model can be used for low inner chamber speeds while for higher inner fan blowing speeds than the LES Turbulence model is recommended. As shown in Figure 70 it is recommended to use a histogram function plots for concentration values using the number of time bins equal to the square root of the number of elements in data and then to fit it to a normal density function. This is for the first 6 [min] of measurements to get good efflux measurements of nearly 100 [ppm].

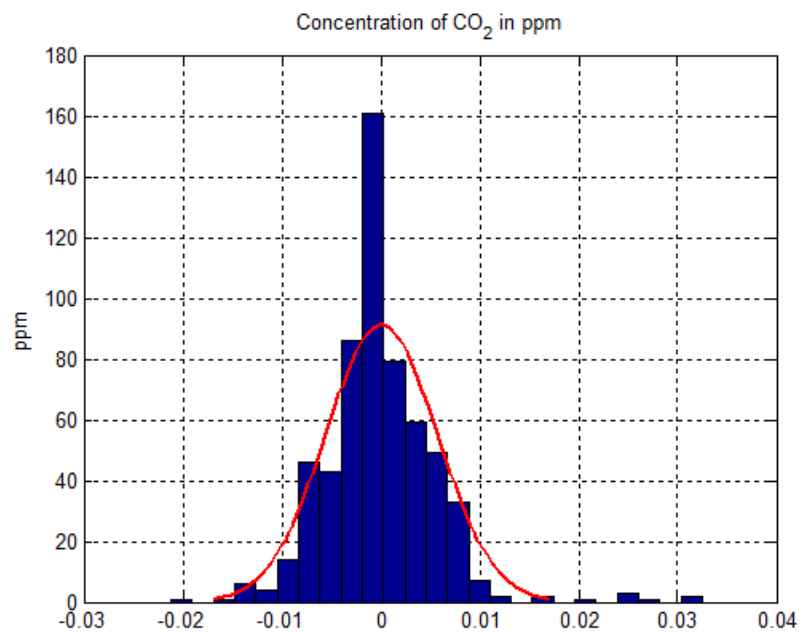


Figure 70: Using histogram for concentration and fitting the data to a normal density function to get good measurements for the efflux.

A fixed simulation temperature can be considered throughout the simulation time calculation (as found in Figure 66). Furthermore, there is no necessity to include the dew point temperature (as found in Figure 66) into the CFD simulation calculations likewise the same applies for the relative humidity parameter (as found in Figure 65)

where it was noted to be fixed in value. This is for the reason that our study is not concerned with water vapour condensation issues that occur when big temperature changes do occur. Carbon dioxide and air partial pressures for the study only come of necessity when soil water samples are sampled to identify carbon dioxide concentrations. Sunshine light intensity measurements are nearly constant (as found in Figure 67) hence it proves that no need for considering the occurring radiative heat transfer inside the chamber gas volume.

5.4. The Static Chamber Case Numerical Simulation

Based on the conclusions in the previous paragraph for the static case Laminar flow model is considered. The laminar model option is available for use in ANSYS-CFX. Laminar flow is governed by the unsteady Navier-Stokes equations whereby the laminar model does not apply a turbulence to the simulation. For the static chamber case the reliance is on the energy transfer in the fluid which accomplished by molecular interaction (diffusion). The simulations are run on an hp Z620 Workstation with a 32 gigabyte RAM machine with 12 quad core Intel i7 processors with an available option to use a multithreading option which doubles the number of calculation cores to 24.

5.4.1. Simulation Setup

The simulation setup process is summarized in conducting the numerical simulation in relation to time and space is a requirement to achieve the required data output. This process is composed of selecting the numerical model to resolve the flow field whereby all the soil physical parameters are applied as input parameters. Furthermore, applying the appropriate simulation boundary conditions and the right time stepping

method is also a necessity moreover selecting the simulation initial conditions to achieve solution convergence. Lastly is the convergence plot for several resolved simulation parameters which is followed by the validation plot to check that the simulation is generating the correct results in relation to experimental data.

5.4.1.1. Setting up the Simulation in Relation to Space

In this section two necessary steps have to be accomplished to set up the simulation in the space wise perspective whereby the first is the making the geometrical model the second is the simulation mesh. Setting up the simulation in relation to space is for the reason to solve the Navier-Stokes derivatives in relation to space.

5.4.1.1.1. Geometric Model

Two cylindrical geometries are created using ANSYS design modeller package whereby one represents the inner chamber gas volume and the second represents the soil porous volume. Furthermore, the designed respiration chamber with all the solid parts that make it up are imported into the two created cylindrical geometries. The chamber as a whole is imported into a predefined location within the two geometries hence ensuring that all physical parameters are captured when the flow calculation is run. The next step is to subtract all the chamber solid parts from both cylindrical domains which result in two new domains shown in Figure 71. The reason for that is to create the gas and porous volume necessary to mesh to later solve the flow equations in. Consequently, the created porous domain volume is 0.06219 m^3 moreover the chamber gas volume is $0.057596 \text{ [m}^3\text{]}$. The volume values for each domain are helpful, the chamber gas volume helps in knowing the circulation rate of the inner gas

volume. Furthermore, the porous domain volume helps in estimating the amount of air and solid in the considered domain.

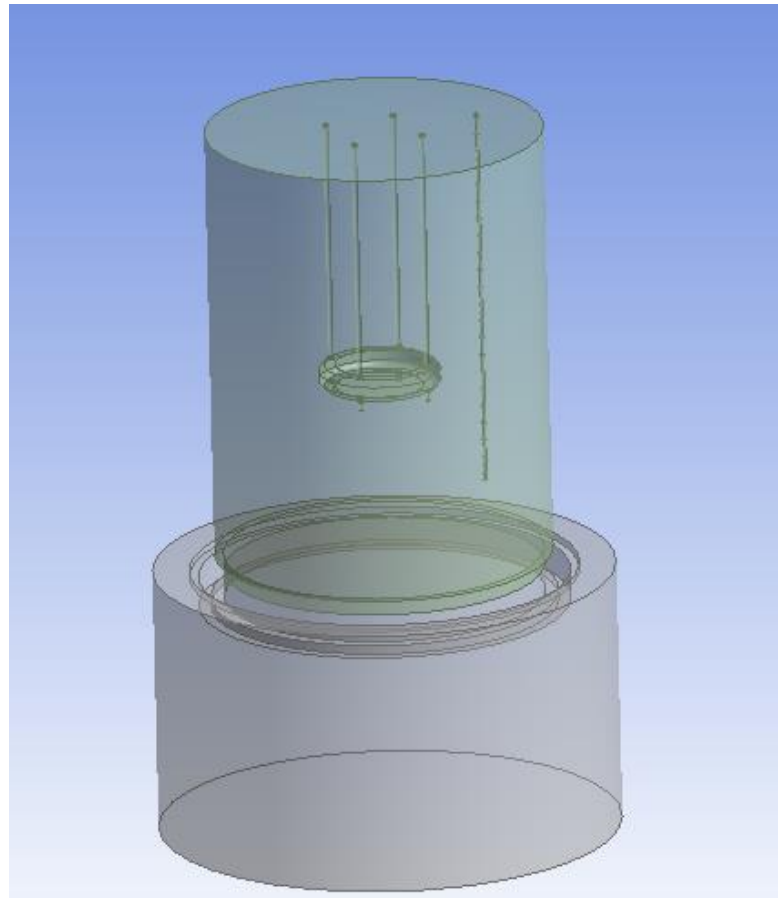


Figure 71: The modelled gas and porous domain.

5.4.1.1.2. Simulation Mesh

The two modelled geometries data is transferred to ANSYS mesh generation package an initial meshing process is conducted using the coarse mesh option as presented in Figure 72. This action is to check no deficiencies exist in the generated mesh. The finite element model is composed of two domains; a porous domain (brown in colour) representing the soil, and a gas domain (Blue in colour) representing the air. The green

coloured surface represents the grass area covered by the chamber its importance is that it will be considered as an interface boundary condition to model the mass transport occurring between both domains.

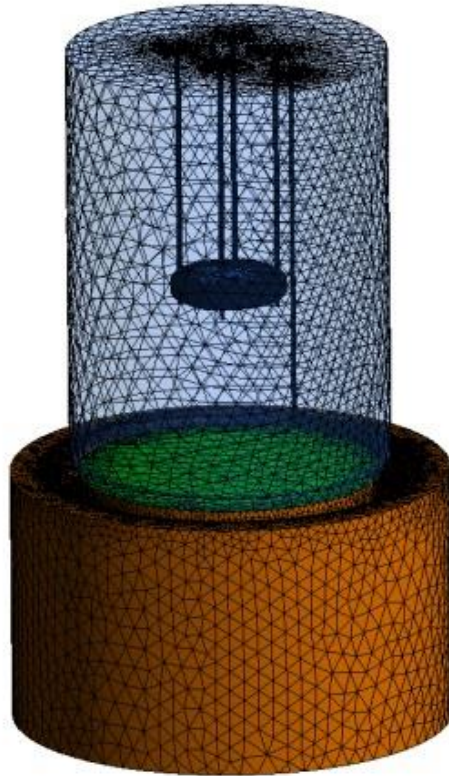


Figure 72: The created geometrical domain used to generate the calculation mesh.

To apply the differential equations mentioned in Chapter 4 the two domains have to be broken up into discrete elements as shown on Figure 73. The tetrahedral mesh type is selected with medium size relevance centre this mesh generation algorithm generates a homogenous size of elements in both domains as evident in right hand side image of Figure 73. Consequently, this helps in providing volume elements that transport gas species at an instance of time uniformly from the bottom of the soil domain to the tip of the gas sensor tip located in the gas volume domain. Hence these cell volumes have a Peclet number [222] surely less than 0.9 for the gas domain. On

the contrary for the soil domain the volume elements should have a Peclet number smaller than 0.9 considering a coarse sand case. As you travel down in depth in the porous media domain a decrease of the occurring Reynolds number is evident whereby the Peclet Number would reach a value of 0.01 [223]. Table 6 shows all the statistical data of the meshed domains for the number of nodes and number of elements.

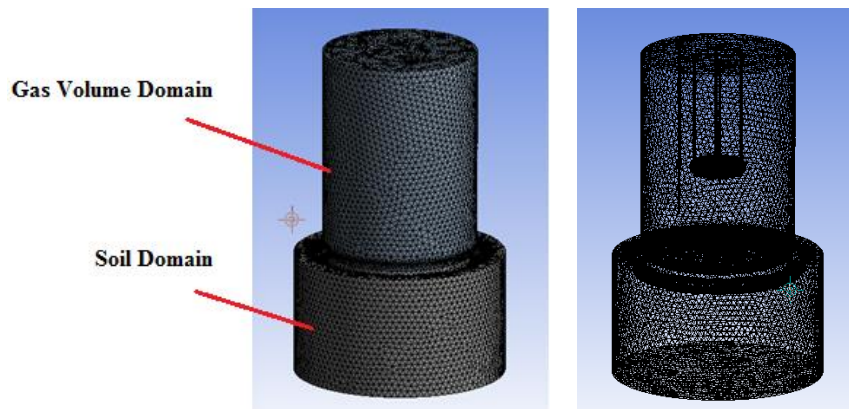


Figure 73: on the left the image shows the gas and porous soil domain moreover the right handside image shows the generated mesh quality for both the soil and gas volume domain..

This statistical data referring to the total number of nodes or elements helps in estimating the required computational time in relation to time and number of calculation cores more over checking the Courant–Friedrichs–Lewy condition.

Table 6: Mesh information for the static chamber case.

Domain Name	Number of Elements	Number of Nodes
Chamber	1240210	1917854
Soil	133990	202867
Total	1374200	2120721

5.4.1.1.3. Applied Solid/Flow Models

Due to those two types of domains are to be studied therefore two separate models are applied for each to simulate the gas flow. Firstly, considering the porous medium according to soil porosity value each mesh cell volume is split into a gas volume and a solid volume. The heat equation is applied to the porous solid media furthermore the Darcy equation (see section 4.5. Darcy Model) and heat equations are applied to the gas volume. Secondly the laminar flow model (see section 4.4. The None-Linear Eddy Viscosity Model) is applied to the chamber air gas volume.

5.4.1.1.3.1. Porous Media Solid Model

A solid model is available in ANSYS-CFX once a porous media option is selected consequently once it is added to the simulation it calculates the occurring heat transfer. Fluid solid heat transfer coefficient is taken to have the value $12 \text{ [W/m}^2 \cdot \text{K]}$ [224]. The following geotechnical values for the grass land soil are used assuming that its composed totally of sand (SiO_2) therefore it has a density value of $2650 \text{ [kg/m}^3]$ and a molar mass of 60 [kg/kmole] with a heat capacity of $700 \text{ [J/kg} \cdot \text{K]}$ This assumption is based considering that the sand sample is a loamy sand one with 80% sand. The porous domain is assigned a value of 0.45 porosity based on [34] from this value the model will calculate the solid part ratio of the mesh element.

5.4.1.1.3.2. Porous Media Flow Model

The simulation permeability value is $10^{-10} \text{ [m}^2]$ the value is calculated from equation (1.6) mentioned on page 156 after analysing the soil sample experimentally. The Darcy equation (1.17) is solved in the porous domain to resolve the occurring flow in it. Both domains model multiple species using the mixture model whereby air and

carbon dioxide are studied. Consequently the interface length scale for interphase transfer is 1 mm moreover the interfacial area value was taken to be $10^3 \text{ [cm}^{-1}\text{]}$ [225]. More details about the selection criteria of this value in relation to Porosity and interfacial surface area for wet sand samples [226] .

5.4.1.1.3.3. Respiration Chamber Gas Volume Flow Model

Both atmospheric temperature and pressure are considered to be constant with time this is according to the experimental data mentioned on page 180 is for temperature and page 180 for pressure. Consequently, the atmospheric pressure is taken to be 1 [atm] and ambient temperature to be 16 [°C] . The Navier-Stokes equations are solved to resolve the occurring flow field inside the chamber gas volume this by using the Laminar flow model. For the reason that momentum transport is due to diffusion the convective flow part of the Navier-Stokes equation is very small and will have no role in mass transport.

5.4.2. Setting up the Simulation in Relation to Time

For a transient simulation setup two main issues have to be resolved the simulation time step and initial conditions.

5.4.2.1. Simulation Time Stepping

Time stepping is conducted using first order Euler method. A time step of 1 [s] is considered. The total simulation time is 360 [s] this time period is enough to capture the gas species concentration jump which usually the first 120 [s] for a grass land location as experiments showed in section (5.2). The total simulation time is equivalent to the 6 [min] measurement time taken on site of deployment. The selected

advection scheme is a high resolution one with a transient scheme of second order backward Euler method. Time step initialization is based on the previous step option. Unsteady time simulations are a must to obtain results that can be validated in accordance with the available experimental research data. The time stepping method used for the run simulations is a low order turbulence scheme with an upwind backward facing method.

5.4.2.2. Simulation Fluid Media Initialization

To sustain a stable converging solution for the trainset simulation domain initialization comes of importance and is dealt with separately.

5.4.2.2.1. Fluid Media Simulation Initialization

In order to achieve numerical stability for the static case flow, velocity components are all assigned a zero value as an initial condition for both considered gases. Air volume fractions are taken to be one at the start of the simulation in all domains.

The reason for this is to show how carbon dioxide diffuses during the processes in pure domains having only air in them. Ambient temperature is taken to be constant that has a value of 289 [K]. The assigned initial condition for Air volume fraction is one, so that the simulation calculation starts with a pure air case for both the soil and the gas domain. As the simulation progresses with time carbon dioxide species disperses gradually through the two domains.

5.4.2.2.2. Porous Media Simulation Initialization

In order to achieve numerical stability at an early stage of the simulation iteration process turbulence fluctuations were taken to be 1% for inflow boundary conditions.

The Darcy equation is solved for the soil porous domain. The absolute pressure value is taken zero for the porous domain. The Velocity components are all taken to be zero for both carbon dioxide and air. Air volume fractions are taken to be one at the start of the simulation in the porous domain, that gives time for carbon dioxide to diffuse in the soil and then mix in the chamber. Temperature is taken to be constant and has the value of 15 [°C].

5.4.3. Boundary Conditions

The main reason why boundary conditions are covered after the space and time setup issues is that the interface boundary condition is dependent on space and time. The fan inflow and out flow boundary condition for the static is considered as a smooth wall boundary condition.

There are two soil surfaces for the porous media which are direct contact with atmosphere as shown in Figure 74. One is located inside the chamber numbered as 1 and the other is outside the chamber numbered 2.

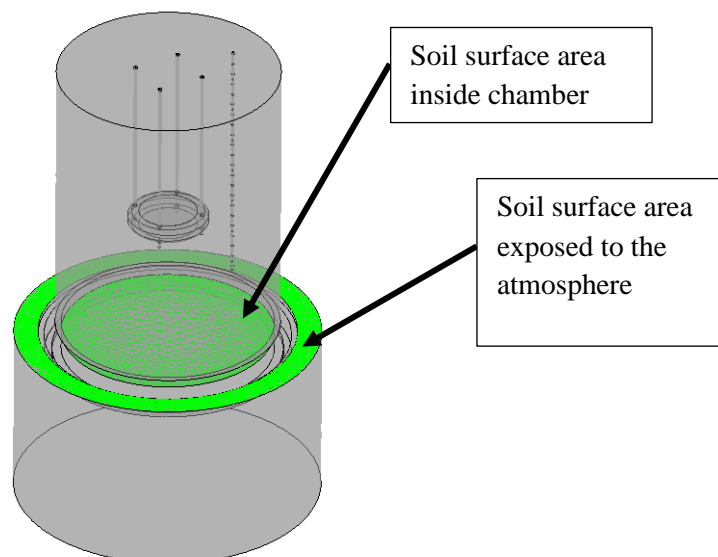


Figure 74: The highlighted boundary condition represents the interface boundary condition between the gas volume and soil porous domain furthermore represents the boundary of the porous domain with the atmosphere.

The top soil surface outside the chamber is assigned an atmospheric pressure boundary condition with an opening temperature of 295 [K]. The surface inside the chamber is assigned the interface boundary condition while all the inner walls inside the chamber gas volume are applied smooth wall boundary condition. For simplicity the carbon dioxide efflux is a result of biological activity in the soil and plants at the location. To represent this occurring biological activity without over complicating the project by considering detailed chemical kinetics a source term is considered. In conclusion the interface surface of the soil numbered 1 of the porous domain is assigned a carbon dioxide source term. The soil surface is applied the carbon dioxide source term equation (5.19) while air is considered as the sink term equation (5.20).

Several statistical models can be applied to model the carbon dioxide source term. The reason for using the exponential function is enforced by the way the problem is solved.

Two gases are studied air and carbon dioxide it is commonly known that air is also a gas mixture that has a fixed amount of carbon dioxide. This makes the data analysis stage of the project to consider carbon dioxide concentrations in the absolute form. Modelling respiration chambers accumulation of carbon dioxide gas in their gas volume in perspective is very much similar to the charging and discharging of electrical capacitors modelling method.

The value of the chamber volume fraction carbon dioxide which the measurement should be asymptotic to is $Y_{CO_2}^0 = 10^{-4}$ (100 ppm) this is while the constant $a = 10$

whereby its value is obtained through simulation calibration. The carbon dioxide volume fraction is a function of time t while $T_d = 360$ [s] is the end time of the experiment hence the concentration equation materializes into this form:

$$Y_{CO_2}(t) = Y_{CO_2}^0 (1 - e^{-\frac{at}{T_d}}) \quad (5.19)$$

The air volume fraction function related to time is as follows

$$Y_{Air}(t) = 1 - Y_{CO_2}(t) \quad (5.20)$$

This would form a standard equation to be used on other sites depending on the location of interest, where $Y_{CO_2}^0$ would change from a location to another including the constant a . As a result, from this discussion both equations (5.19) and (5.20) are assigned to the soil surface boundary condition.

Furthermore, the chamber efflux is represented by equation shown on page 22 this equation is programmed into ANSYS-CFX using the CFL programming language. By finding the derivate of equation (5.19) this results in the following equation (5.21):

$$\frac{\partial c}{\partial t} = \frac{a \cdot Y_{CO_2}^0}{T_d} e^{-\frac{at}{T_d}} \quad (5.21)$$

Consequently, the applied carbon dioxide species source term for the interface boundary condition is through applying the following equation (5.22):

$$\dot{m}_{CO_2} = MW_{CO_2} \frac{a \cdot Y_{CO_2}^0}{T_d} e^{-\frac{at}{T_d}} \quad (5.22)$$

The carbon dioxide species source term represented by mass flow equation (5.22) furthermore the flow is split in half whereby one is assigned to interface boundary condition in the perpendicular direction consequently one in the upper direction into the chamber and the other in the direction of the soil. Finally comes the efflux velocity is calculated from equation (5.23) this is also an input requirement for the boundary condition interface

$$v_{\text{CO}_2} = \frac{\dot{m}_{\text{CO}_2}}{\rho_{\text{CO}_2} A} \quad (5.23)$$

Open boundary conditions are applied to the sides of the porous domain as seen in Figure 75 highlighted in green to mimic the real-life condition. The reason for applying the open boundary condition is to avoid species build up in the porous domain.

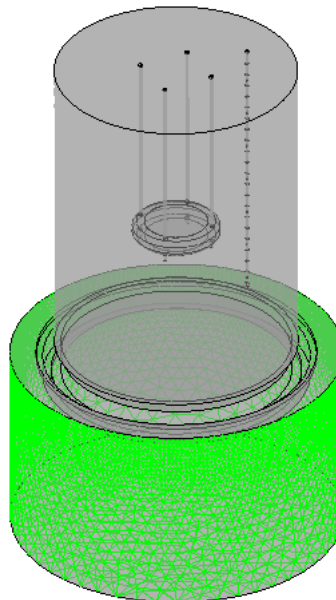


Figure 75: The side boundary surfaces that have been assigned an opening boundary condition are laminated in light green.

The temperature boundary conditions are later applied in the form of the ambient temperature for the porous domain side openings the same is applied to the bottom surface of the porous domain. The heat equation is solved in the simulation for the reason to resolve the heat field inside the porous domain. The soil thermo-physical properties are inputted into the solvers database.

5.4.4. Simulation Validation

The objective of the simulation is to conduct a flow simulation that can be applied to either a steady state or transient one.

A Steady state simulation is initially used as the foundation case to verify that the numerically built model works this is achieved after the simulation solver solution converges after 100 iterations. Steady conditions are assumed to have been reached after a relatively long-time interval this is convenient in testing a species diffusion case.

Consequently, the steady state simulation showed that a species concentration in the range of 10 to 100 [ppm] which is acceptable as a value. In conclusion this helps in selecting the number of outer loop iterations for the solver to achieve convergence for an unsteady simulation.

From Figure 76 is evident that solution convergence was obtained after 25 accumulated time steps. It was not necessary to increase the number of outer loops because that would increase the calculation time. Relying on an implicit scheme helped to achieve numerical solution stability.

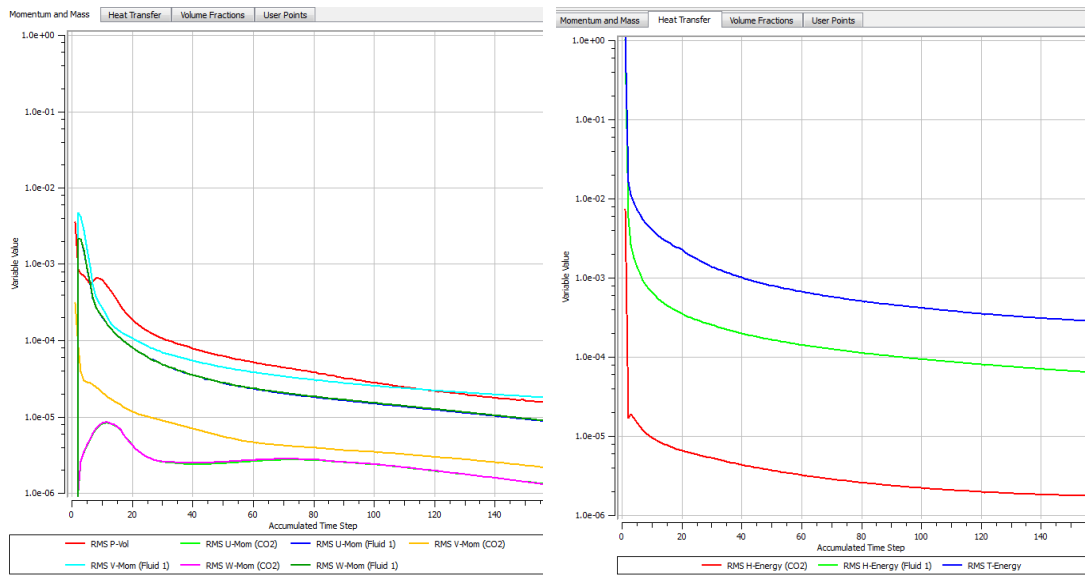


Figure 76: Convergence of the solution check in relation to accumulated time step, momentum and mass solution convergence on the left and the mass transfer on the right.

A test was applied to use a 0.5 [s] accumulation time step was conducted whereby it led to a total number of steps of 720 calculated time steps. In conclusion it only resulted in additional produced data with no evident improvement to the results quality hence 1 [s] time step was selected. The purpose of Figure 77 is validation to show that the right measurement is conducted whereby the red dots represent the experimental points.

In conclusion the concentration curve in relation to time after the point of saturation becomes asymptotic. Usually, the first 150 [min] is required to capture the soil produced flux as proven experimentally on page 174. What happens after the saturation point is that any addition of gas species doesn't contribute to any addition of concentration jumps.

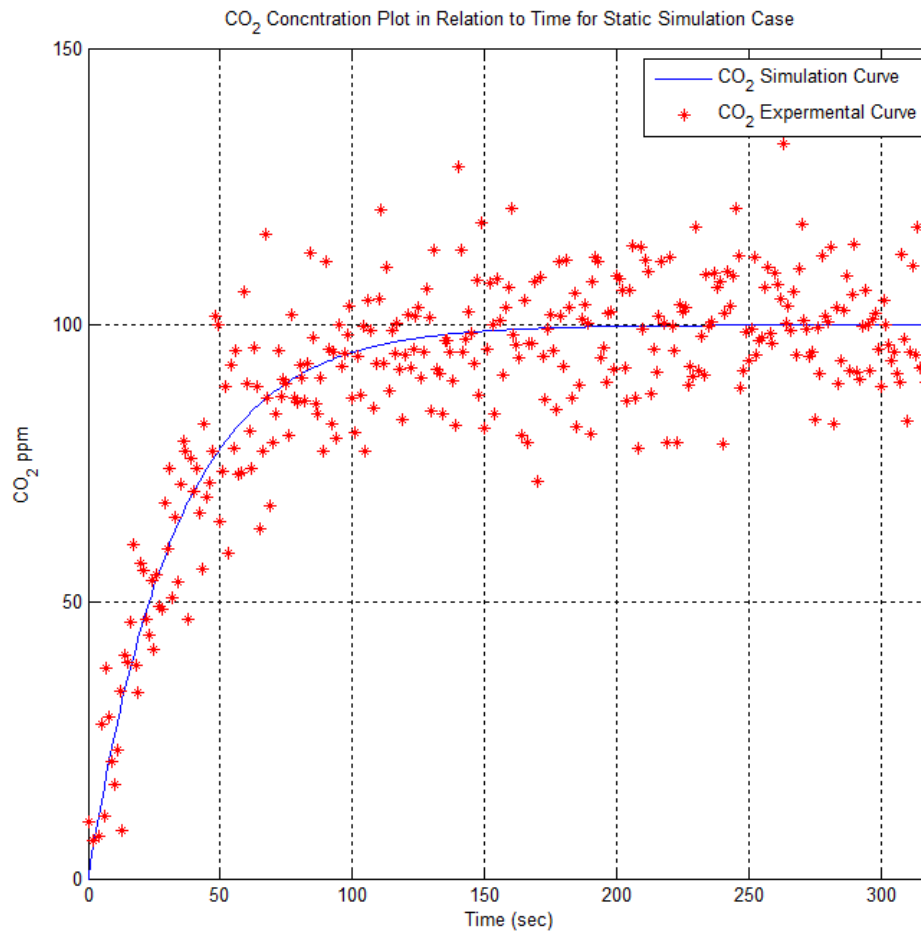


Figure 77: validation plot showing a comparison case of concentration measurements between an experimental and numerical case.

5.4.5. Simulation Results from the Static Chamber Case

Three essential parameters that will be studied for the static chamber case these are temperature, Courant number and carbon dioxide species concentration.

5.4.7. The Static Chamber Temperature Diffusion

Mass transport in the static operational mode case occurs due to changes in occurring temperature within the chamber as evident within Figure 78. The sampling plane was taken exactly in the central mid-section of the chamber. Considering that the chamber outer plastic shell has a heat capacitance and is about two degrees more than the inner

gas temperature which is colder. This is evident at the chamber walls whereby it is emitting heat the same applies for the soil top surface.

The air parcels are visible these represent the buoyancy affects due to temperature changes whereby a circulation occurs inside the top and bottom of the chamber till a thermal equilibrium happens. This is when the cold blue blob gains heat and rises around going the blowing fan assembly. Three air parcels or sometimes called air blobs are visible at the top and one colder at the bottom near the soil surface.

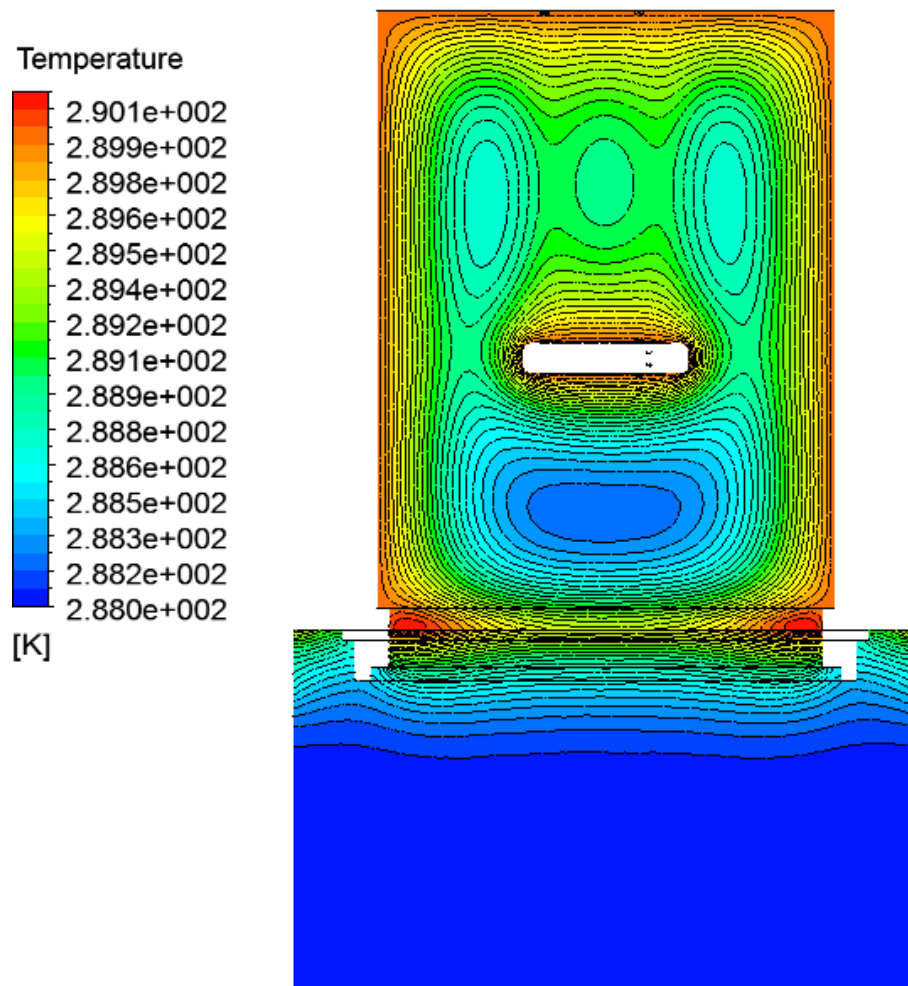


Figure 78: The distribution of temperature contours in the static operational mode of a chamber at time instance 80 [s].

Commenting on Figure 79 the cold region shows the direction of heat transport is occurring.

Temperature difference is what links the measured changes in measured concentration values at two instances of time shown in Figure 77. The selected time difference is 10 [s] to show how heat is transferred to show regions of heat gain and heat loss.

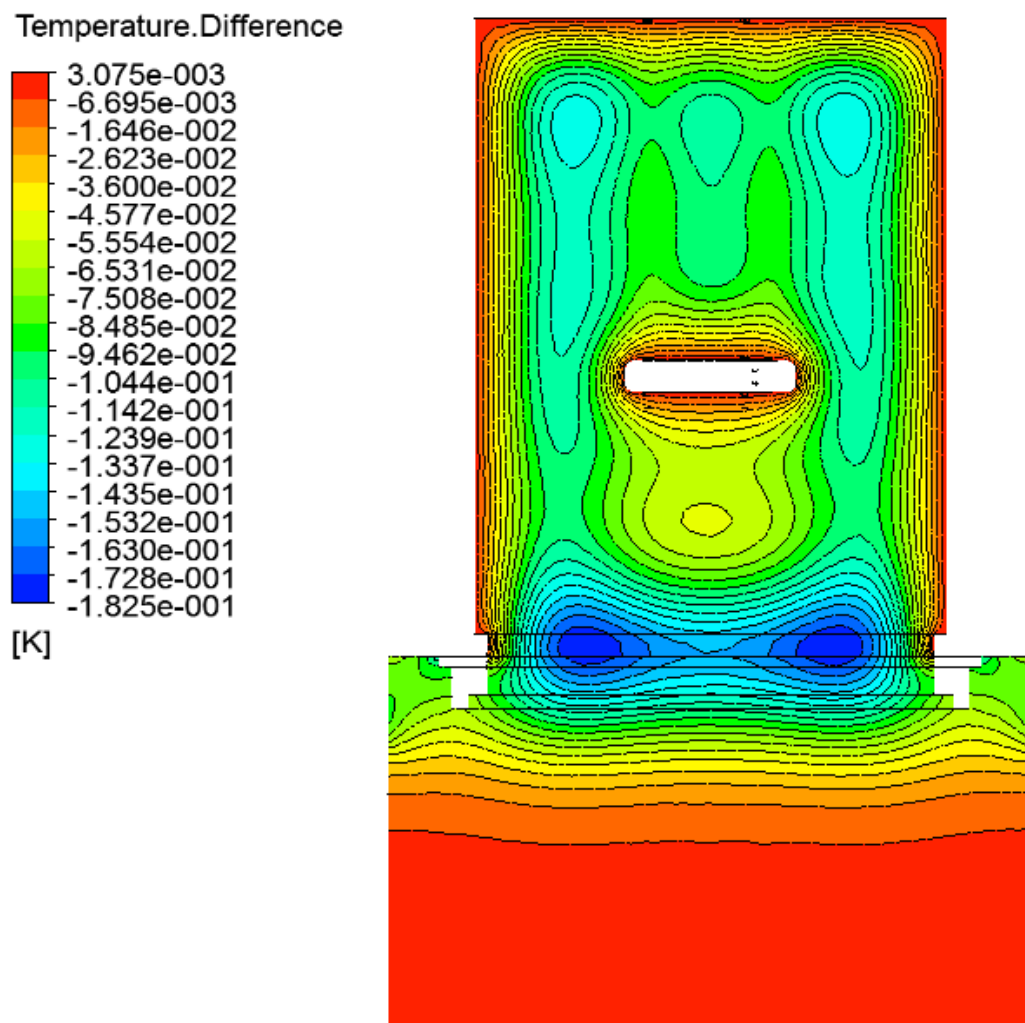


Figure 79: Temperature difference contours for a 10 [s] time difference inside the chamber gas volume and porous soil domain.

5.4.8. The Static Chamber Concentration Diffusion

The Courant number shown in Figure 80 is to see the amount of mass being transferred in every single finite element cell in the chamber gas domain and the gas volume in the porous domain. The reason for a nearly constant fixed colour contour that is blue is due to the dominance of the diffusive physical behaviour for a static chamber case. Furthermore, the light blue regions show that higher diffusive transport is occurring due to the cylindrical chamber base installed in the soil likewise it is also because the active top soil part is the source of carbon dioxide assigned in the simulation.

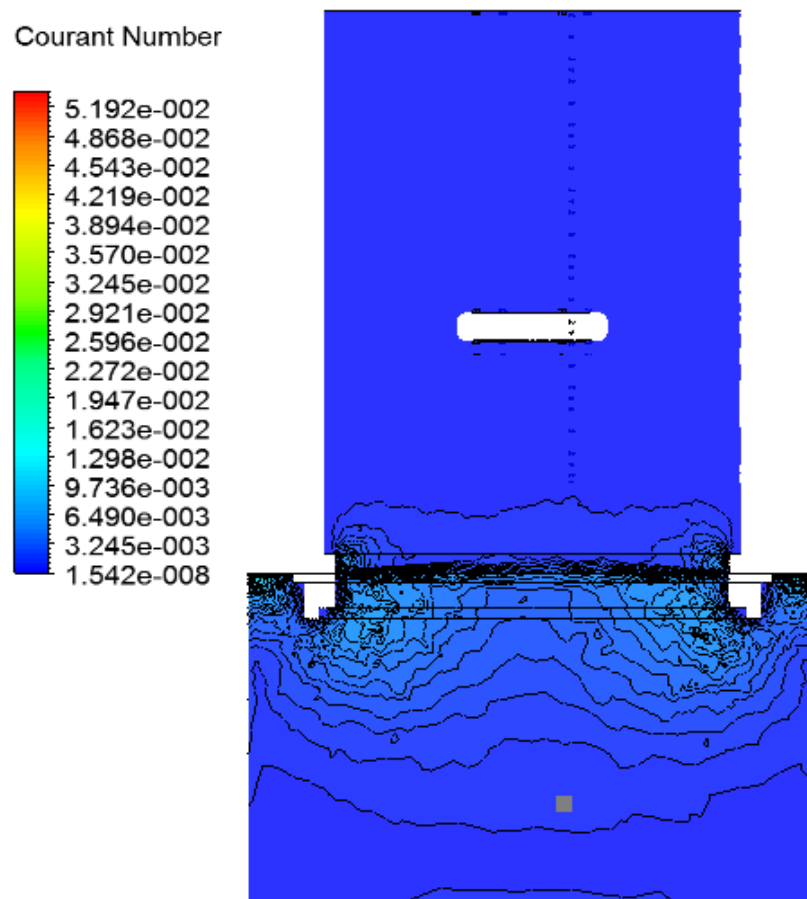


Figure 80: The contour plot of the courant number at an instance of time 80 [s] from 360 [s].

Commenting on Figure 81 which represents an unsteady simulation whereby the positive difference in Courant number means accumulation of mass in finite element while negative difference means that diffusion is occurring. As evident in Figure 81 due to the atmospheric opening the yellow colour represents the section whereby there is an easy way to diffuse. Furthermore, the red colour represents regions of mass accumulation due to the chambers fixture base. Consequently, the direction of species gas diffusion is shown to be going upwards into the chamber.

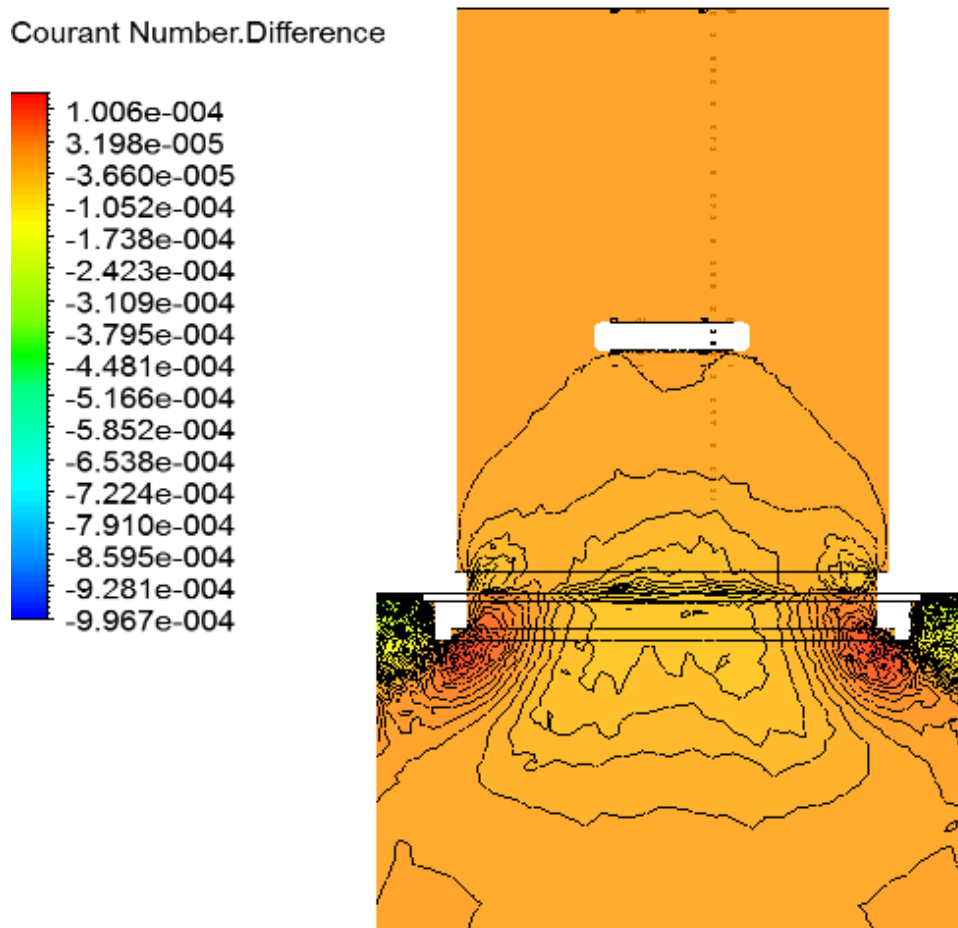


Figure 81: A Courant number contour plot according to time difference of frames of 5 [s] between 75 [s] and 80 [s].

Species concentration in a volume fraction form is shown in Figure 82 whereby it is applied on the chambers mid plane section at an instance of time 20 [s]. The light-coloured contours illustrate the diffusion of the gas species from the soil surface at the most active part of the soil layer. In conclusion Figure 82 supports the correctness of assigning the interface surface with a source term that produces carbon dioxide in the vertical direction in the positive and negative direction.

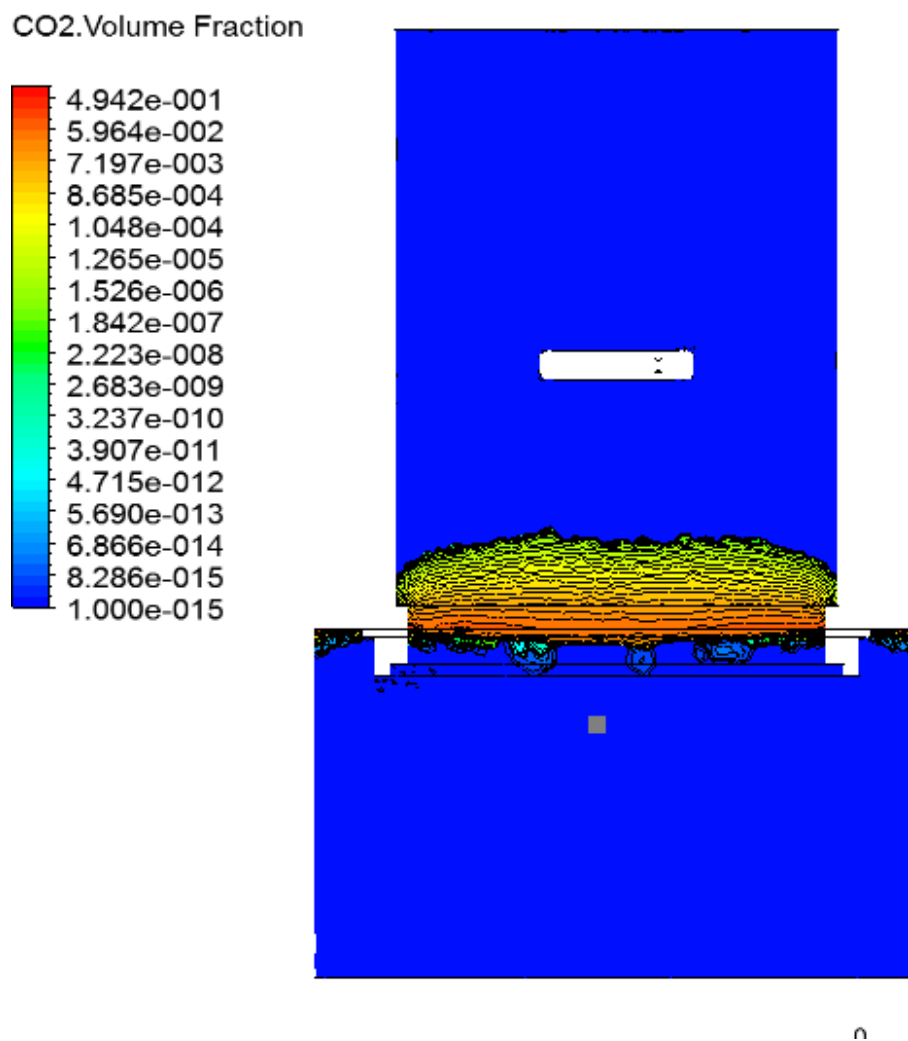


Figure 82: The numerical simulation at the first 20 [s] showing how mass gradually diffuses within time.

Moreover, species would travel easier in the chamber gas volume than in the porous domain. Furthermore, what is evident that heat inner affect creates the buoyancy affects that draws up the species from the soil interface into the chamber gas volume.

5.4.6. Conclusion about the Laminar Model

What is evident from the study is that laminar model can be applied to the static chamber case gives good results as shown in the results validation. Temperature gradients contribute to the mass diffusion process likewise concentration changes also contribute to the process.

Pressure contours weren't considered in the study for the reason no evident pattern was. The Courant number can be used to capture the species diffusive behaviour furthermore the difference of the Courant number helps in validating the chambers base design in the soil.

5.5. The Dynamic Chamber Case Numerical Simulation

This simulation considers the blowing fans working. There is a big similarity in the setup procedure between the static and dynamic respiration chamber case hence in order to avoid repetition only the modified paragraphs will be covered here. For the reason that the dynamic chamber case uses a blowing fan the K-Epsilon Turbulence model which requires some changes in the boundary conditions. The same model is used for the porous domain which uses the Darcy equation. The used mesh stays and geometry stay the same. Minor changes are applied to the simulation time stepping method. Minor changes are applied to the initial condition.

5.5.1. Simulation Setup

Only the unique paragraphs are discussed here to avoid repetitions due to similarity of some steps of simulation setup procedures.

5.5.5.1. Setting up the Simulation in Relation to Space

In this section two necessary steps have to be done to set up the simulation space wise whereby the first is the making the geometrical model the second is the simulation mesh.

5.5.2.1. Geometric Model

The used simulation geometric model is covered in (section 5.4.1.1.1).

5.5.2.2. Simulation Mesh

The simulation mesh is discussed in (section 5.4.1.1.2).

5.5.3.3. Applied Solid/Flow Models

The same fluid model is used for the porous media hence only the.

5.5.3.3.1. Porous Media Solid Model

The used porous media solid model is described in (section 5.4.1.1.3.1).

5.5.3.3.2. Porous Media Flow Model

The porous media model is discussed in (section 5.4.1.1.3.2).

5.5.3.3.3. Respiration Chamber Gas Volume Flow Model

Both atmospheric temperature and pressure are considered to be constant with time this is according to the experimental data covered in section (5.2). Consequently, the atmospheric pressure is taken to be 1 [atm] and ambient temperature to be 16 [°C] .

The Navier-Stokes equations are solved to resolve the occurring flow field inside the chamber gas volume this by using the K-Epsilon model. For the reason that momentum transport is due to diffusion the convective flow part of the Navier-Stokes equation is very small and will have no role in mass transport. Homogenous turbulence was considered for the simulation setup up that uses the k-Epsilon model.

5.5.4. Setting up the Simulation in Relation to Time

For transient simulation two main issues have to be resolved the simulation time step and initial conditions

5.5.4.1. Simulation Time Stepping

Time stepping is conducted using first order Euler method. A time step of 1 [s] is considered. The total simulation time is 360 [s], this time period is generally enough to capture the gas species concentration jump which usually occurs the first 120 [s], the total time is equivalent to the 6 [min] measurement time taken on site of deployment.

The advection scheme selected was a high resolution one with a transient scheme of second order backward Euler, time step initialization is based on the previous step option. The time stepping method used for the run simulations was a first order turbulence with an upwind backward facing method.

5.5.4.2. Simulation Fluid Media Initialization

To sustain a stabile converging solution for the trainset simulation domain initialization comes of importance and is dealt with separately.

5.5.4.2.1. Simulation Fluid Media Initialization

In order to achieve numerical stability for the dynamic case all flow velocity components are assigned a zero value as an initial condition for both considered gases in the simulation. Moreover, air volume fractions are taken to be one at the start of the simulation in all domains. The reason for this is to show how carbon dioxide diffuses during the processes in pure domains having only air in them. Ambient temperature is taken to be constant that has a value of 288 K. The assigned initial condition is zero velocity with a volume fraction of one for Air. So that the simulation calculation starts with a pure air case for both the soil and gas domain. As the simulation progresses with time carbon dioxide species disperses gradually through the two domains.

5.5.4.2.2. Simulation Porous Media Initialization

In order to achieve numerical stability at an early stage of the simulation iteration process turbulence fluctuations were taken to be 1% for inflow boundary conditions. The Darcy equation is solved for the soil porous domain. The absolute pressure value is taken zero for the porous domain. The Velocity components are all taken to be zero for both carbon dioxide and air. Air volume fractions are taken to be one at the start of the simulation in the porous domain this gives time for carbon dioxide to diffuse in the soil and then mix in the chamber gas volume. Temperature is taken to be constant and has the value of 289 [K].

5.5.5. Boundary Conditions

Apart from the following discussed boundary conditions all wall surfaces are assigned a smooth wall boundary condition. The two most essential boundary conditions to setup the simulation are the blowing fan inflow and outflow boundaries. Both interface

surfaces between the gas volume and porous domain are mentioned in the following two sections.

5.5.5.1. Blowing Fan Simulation inflow and outflow boundary conditions

Figure 83 shows the fan inflow and outflow boundary condition for the chamber gas volume whereby the fan outputs boundary and input are highlighted in light green each assigned the values of 2.7 [m/s].

To ensure periodic boundary conditions to occur this is achieved by conservation of mass for the species inflowing and outflowing from the fan's inlet and outlet.

Consequently, what is required is to model the rise of concentration with time this done by applying an exponential volume fraction function for the inflow and outflow boundary condition numbered as 1 and 2 in Figure 83. The value of the chamber volume fraction carbon dioxide $Y_{CO_2}^0 = 1e - 4$ while $a = 10$ is a constant obtained experimentally. The carbon dioxide volume fraction is a function of time t while $T_d = 360$ [s] is the end time of the experiment:

$$Y_{CO_2}(t) = Y_{CO_2}^0 (1 - e^{-\frac{at}{T_d}}) \quad (5.24)$$

The air volume fraction function related to time is as follows

$$Y_{Air}(t) = 1 - Y_{CO_2}(t) \quad (5.25)$$

This would form a standard equation to be used on other sites depending on the location of interest. The value of $Y_{CO_2}^0$ and the constant would change from one location to another.

Open boundary conditions are applied to the sides of the porous domain as shown previously in Figure 75 highlighted in green to mimic the real-life condition.

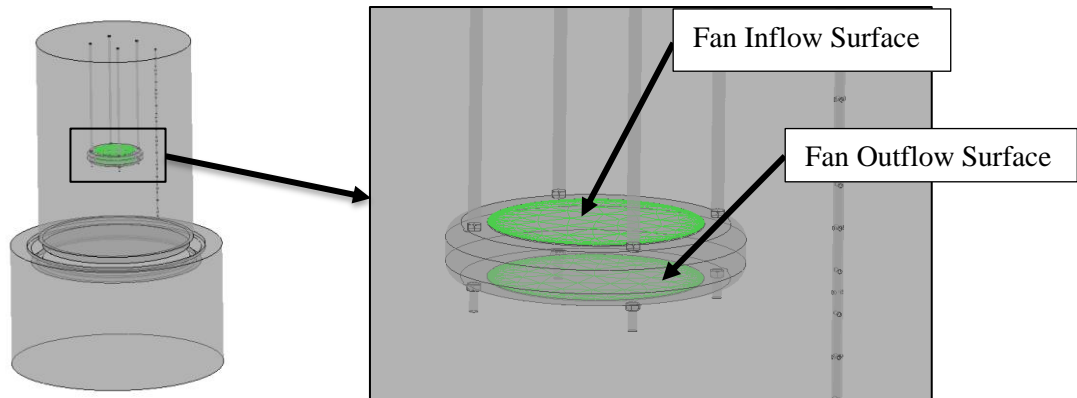


Figure 83: The inflow and out flow boundary surface for the fan location is highlighted in green.

5.5.5.2. Simulation Interface Boundary Conditions

The simulation interface boundary condition assigned is for the two interface surfaces between the two studied surfaces. The porous media soil side interface area is assigned the carbon dioxide source term as covered previously on page 193.

5.5.6. Simulation Validation

Looking at Figure 84 shows plots that are necessary to conduct a convergence check for the conducted numerical simulation this is done for a 100-time iteration. Moreover, the left plot shows the convergence of the solution for the rms (root mean square) for the velocity components in the x y and z axis.

Likewise, the same is conducted for the rms pressure term. The three velocity components iterate at the same extent is due to the homogenous vector field created in the gas volume. The reason for the fluctuations with the accumulated times steps is

due to the changes of flow energy inside the chamber gas volume. This is more evident on the right-hand side for the convergence plot for the K-Epsilon turbulence model terms. Consequently, the rms term for the kinetic energy term fluctuates and the same applies for the epsilon term which is responsible for dissipating the flow kinetic energy.

Furthermore, commenting on Figure 85 shows a more constant iteration pattern for the rms temperature term this is attributed to a steady heat transfer rate is occurring inside the chamber. The evident noise in both rms enthalpy energy gas components is attributed to the dominance of flow convective behaviour in the gas volume.

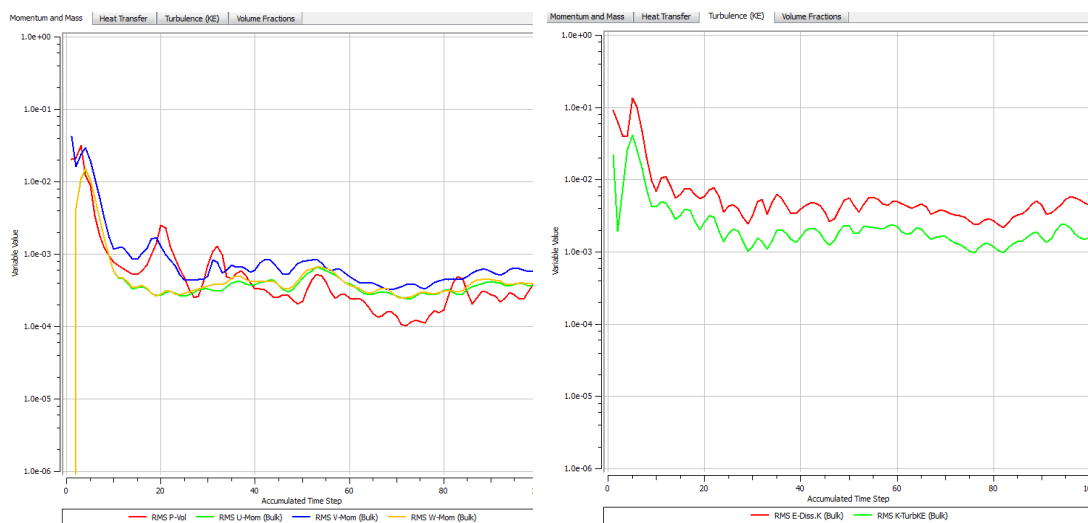


Figure 84: Convergence of the solution check in relation to accumulated time step, momentum and mass solution convergence on the left and the K-Epsilon components used in the turbulence model on the right.

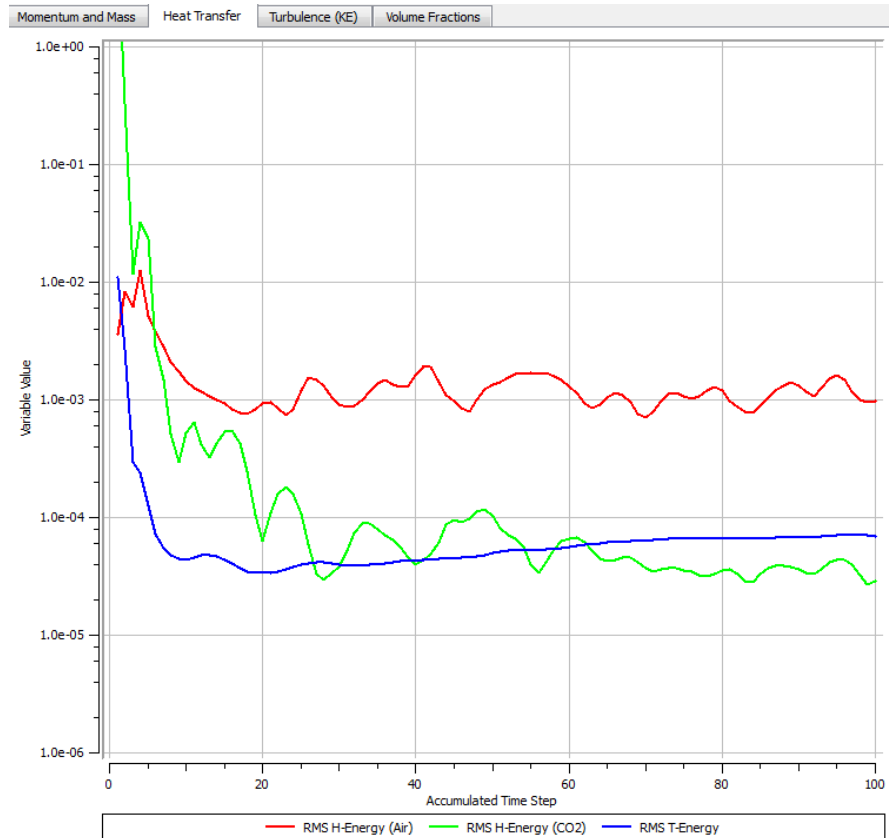


Figure 85: A convergence check of the solution for temperature in the energy equation moreover the same check for both gases enthalpy convergence.

The purpose of Figure 86 is results validation; it is to show that the right measurements are conducted. Lots attention was given to detail due to small concentration changes occur in relation time. Usually, the first 150 [min] are required to capture the soil produced flux slope. What happens after the saturation point is that only small quantities of gas species are applied but they do not contribute substantially to large concentration jumps. In conclusion the concentration curve in relation to time after the point of saturation becomes asymptotic. The numerical models did achieve some accuracy with a discrepancy of 35% with the use of the K-Epsilon model. That is attributed to the requirement of much refined mesh for both domains.

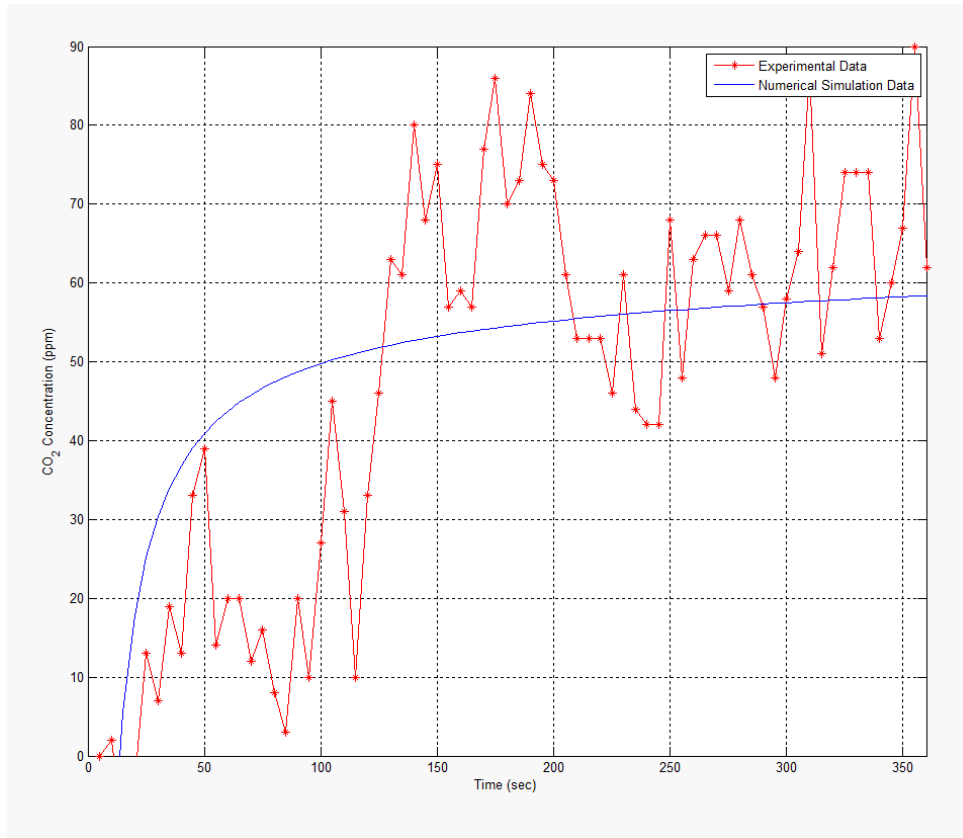


Figure 86: Validation plot showing a comparison case between experiential results and the numerical model concentration.

5.5.8. Simulation Results from the Dynamic Chamber Case

All the necessary parameters for analysis are covered in this section for the dynamic chamber case air velocity become essential further more temperature inner chamber pressure the Courant number inside the gas domain and the porous domain separately.

5.5.8.1. The Dynamic Chamber Velocity Study

The used inner circulation fan creates a nearly axisymmetric velocity field as evident in Figure 87 . The reason for the minor deviation from an axisymmetric flow is due to the use of the sampling tube inserted within the chamber gas volume hence flow deviation is occurring on the left-hand side where the sampling tube is located. The

pressure field is shown both inside the chamber and in the porous media. The parabolic velocity profile is an indicator that the solution is correct furthermore the light green colour represents the maximum velocity value from the fan's outlet. Only the large turbulence structures are resolved in the calculation for the chamber gas volume as seen in Figure 87. The reason for this is due to the use of the K-Epsilon turbulence model whereby the average velocity component value is the dominant.

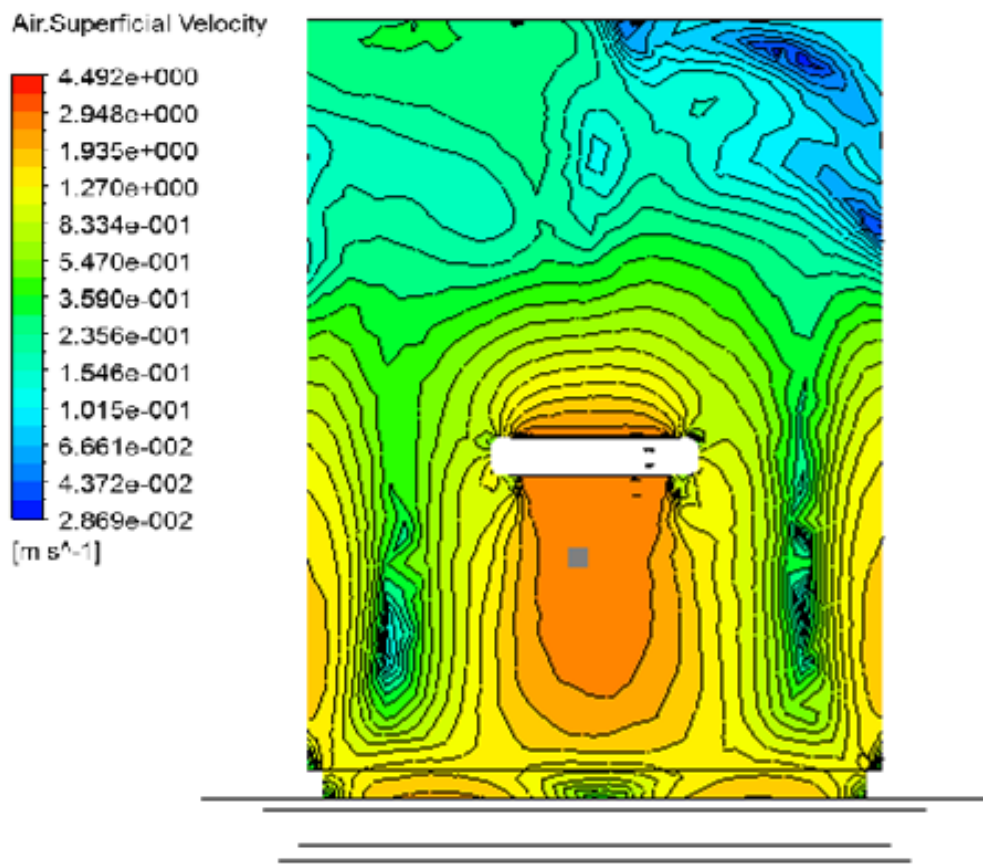


Figure 87: Vertical velocity values of the velocity field inside the chamber gas volume.

5.5.8.2. The Dynamic Chamber Pressure Study

The used inner circulation fan creates a uniform pressure field Figure 88. The pressure field forms a symmetrical pressure field and that is due to the chambers shape and the

fan fixture inside it. The pressure field is show both inside the chamber and in the porous media.

Previously on page 107 the predicted pressure value at the soil surface was -0.7 [Pa] this was calculated using the mass flux equation applied at a fixed distance of 22 [cm]. Form Figure 88 the pressure value is -1 [Pa] which proves how near the obtained numerical simulation calculation is near to the calculated value using the flux equation.

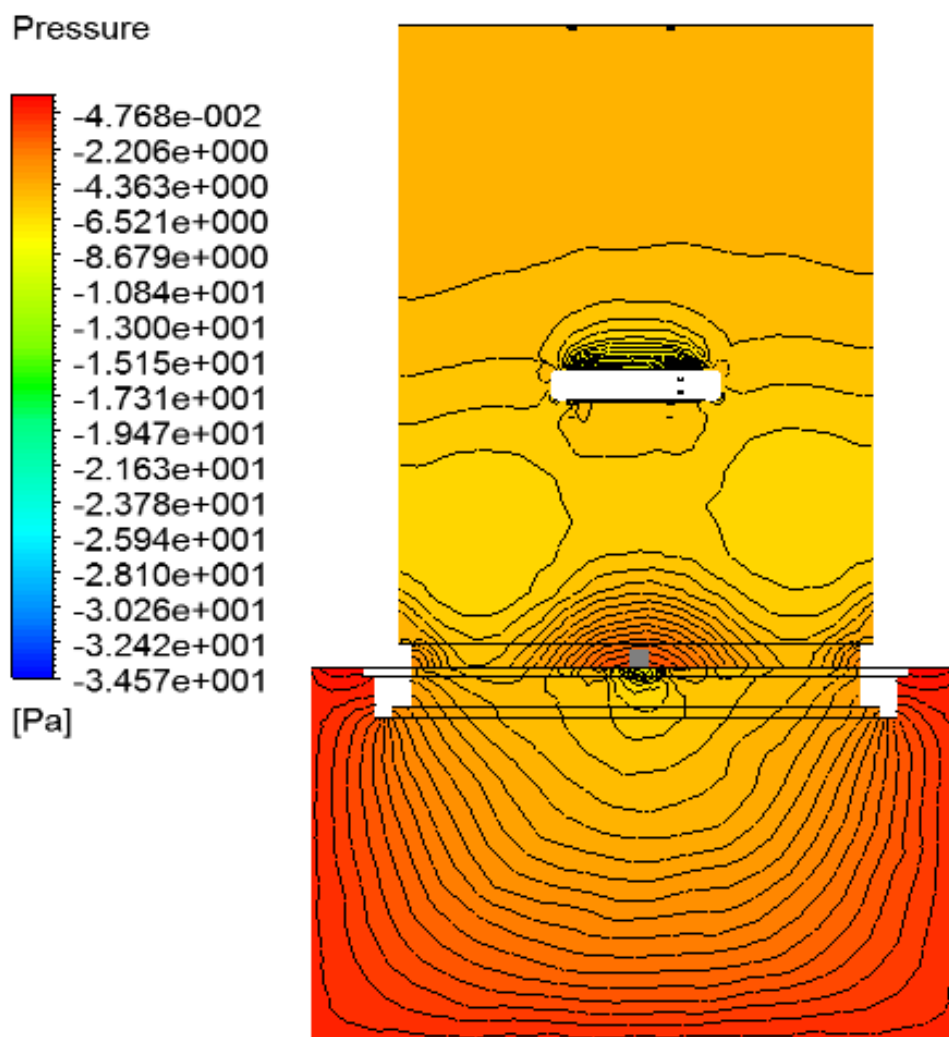


Figure 88: Inner pressure distribution inside a dynamic respiration chamber and within the porous domain.

5.5.8.3. The Dynamic Chamber Temperature Convection

The used inner circulation fan enhances the distribution of the heat to create a homogenous temperature field as visible Figure 87 mass transport in the dynamic operational mode case occurs due to forced convection created by the blowing fan within the chamber Figure 89. The sampling plane was taken exactly in the central mid-section of the chamber. One of the reasons that there is no symmetry in Figure 89 for the temperature field is due to the installed internal sampling tube within the gas volume.

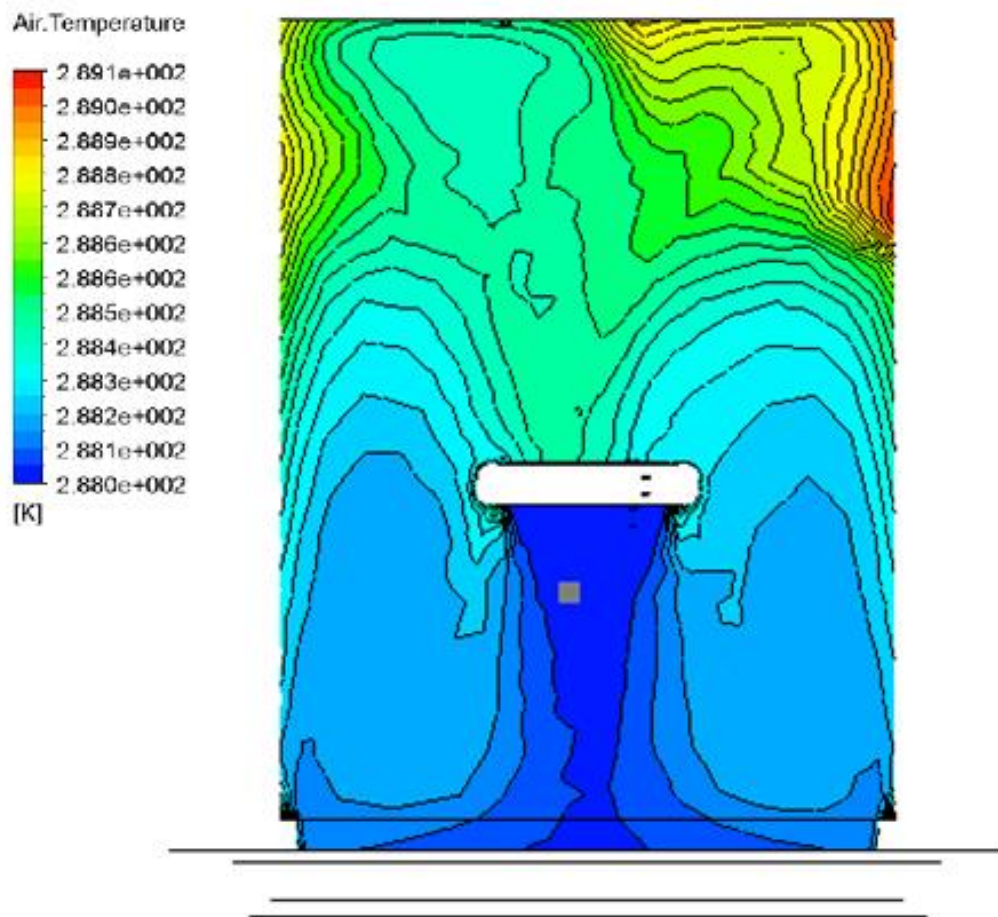


Figure 89: The distribution of temperature contours in the static operational mode of a chamber at time instance 30 [s].

The used inner circulation fan enhances the distribution of the heat to create a homogenous temperature field as visible. Temperature variations are very small to an order of ∓ 0.1 [K] hence the temperature field inside the chamber can be considered as homogenous. Commenting on Figure 89 the cold region shows the direction of heat transport is occurring. Where by the cold air at the bottom of the chamber is pushed upwards by forced fan convection.

5.5.8.4. The Dynamic Chamber Concentration Convection

Commenting on Figure 90 firstly the gas volume domain is studied separately followed by the porous domain.

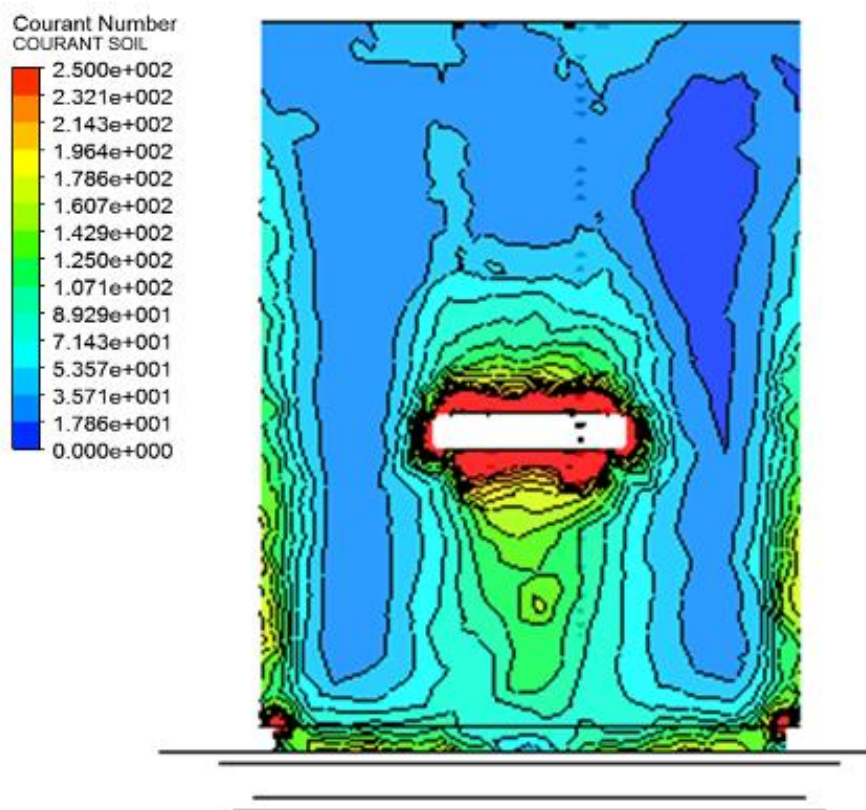


Figure 90: The contour plot of the courant number at an instance of time 80 sec from 360 [s].

The use of the Courant number is to see the amount of mass being transferred in every single finite element cell of the gas and porous domain. Consequently, the red and yellow regions show higher convective transport at both fan inlet and outlet regions. This is attributed to forced convection by the installed blowing fan likewise another region is near the soil surface part whereby a speedup of flow occurs.

Commenting on the courant number difference contour plot presented in Figure 91 shows not too many colour gradients exist.

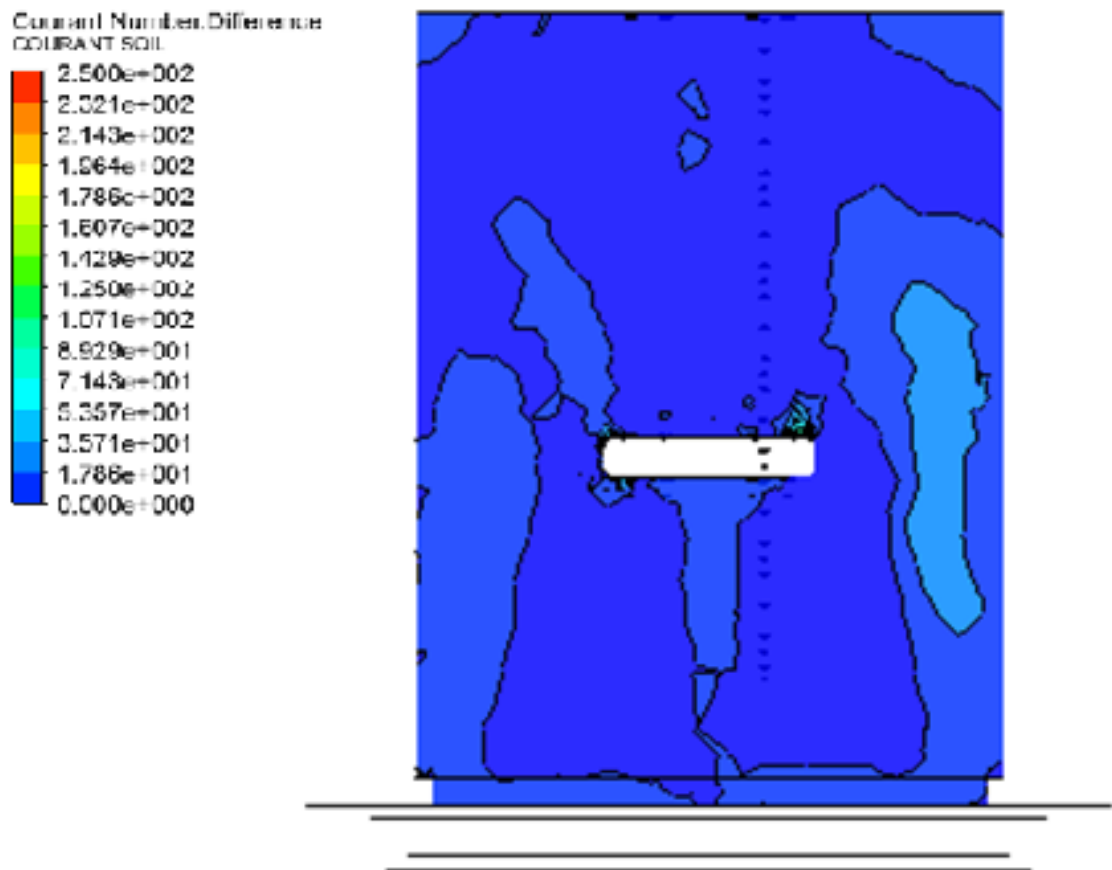


Figure 91: A time difference of frames of 5 [s] between 75 [s] and 80 [s].

Hence it proves that mass transport within the finite element volumes is nearly the same when operating the chamber in dynamic mode consequently creating a homogenous gas mixture.

The courant number in the porous domain is shown in Figure 92 as evident the regions whereby mass diffusion is dominant its represented in dark blue. Converging colour contours become more evident as we move towards the soil top surface. The Figure 91 indicates that mass transport is strong at the top soil surface in the direction to the inside of the chamber which is projected to the fan blowing flux.

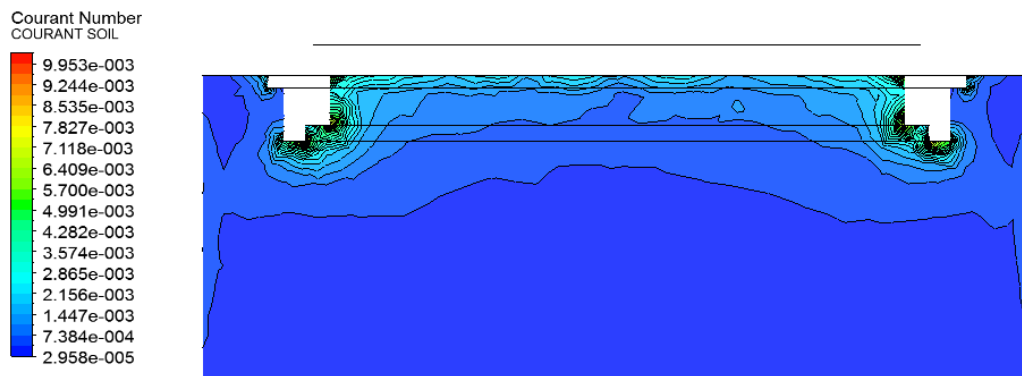


Figure 92: The static case Courant number contour plot in the porous domain.

The courant number difference in the porous domain is shown in Figure 93. As evident from the image those regions of high pressure in red are due to air stagnation regions taking a circular shape as seen near the soil surface. Moreover, regions of species suction are shown in a blue colour.

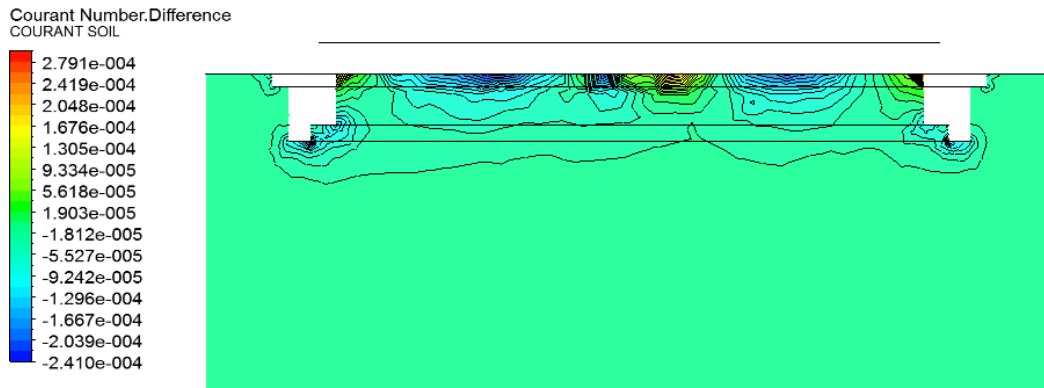


Figure 93: The courant number difference contour plot in the porous media.

Figure 94 shows the aeration process of the top soil surface layer this is achieved by circulated flow pattern created by the blowing fan. The advantage of using a streamline function is that it illustrates how that the most active layer of the soil is aerated. The analysis process is achieved by assigning a stream line function to the soil surface interface between the gas volume and the soil porous domain.

This creates an array of particle tracking path lines starting from the surface moreover in order to capture the stream lines inside the porous media and inside the chamber gas volume a forward and backward facing step is selected.

By applying a vector field function to the stream line's function generates a vector field as evident in Figure 94. Consequently, the velocity vector field mimics a similar case to a magnetic field.

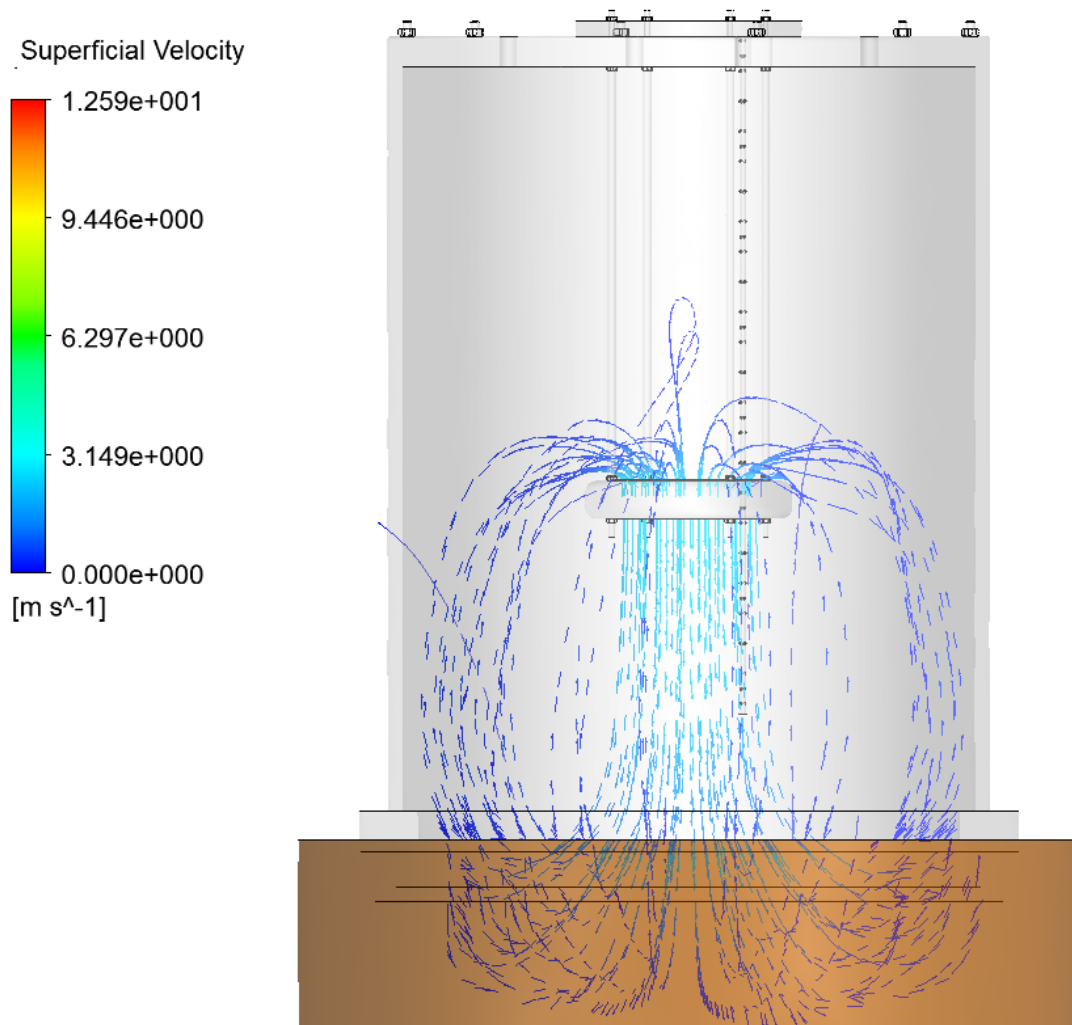


Figure 94: The captured vector field for the applied streamline function showing the aeration process for the top soil layer.

Furthermore Figure 95 applies the streamline function to the blowing fans surface outlet for the purpose to capture the circulatory behaviour of the flow inside the gas volume only. According to the assigned inlet and outlet conditions for the fan what is evident that the uniformity of the flow in the fan's outlet section is due to no obstacles are in front of the flow to obstruct it. This kind of case can be regarded as an ideal case considering a flat surface case for the soil interface whereby for a real studied case surface roughness adds simulation calculation complexities and solution instability.

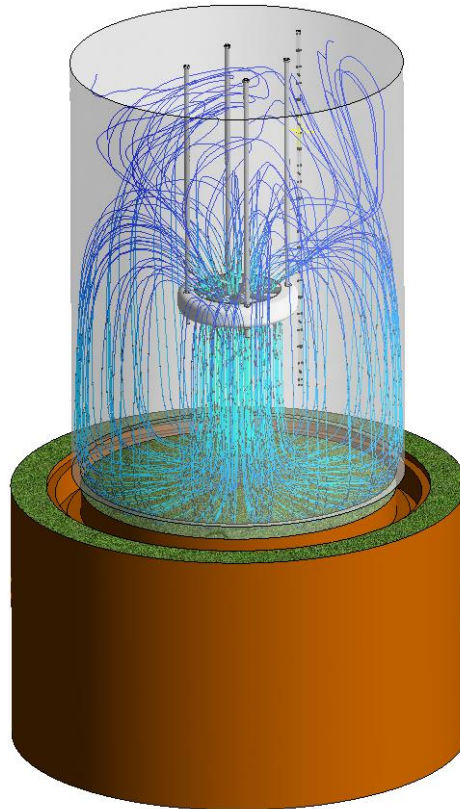


Figure 95: Stream lines show the circulated flow pattern within the chamber gas volume.

This conclusion was achieved through the many simulation trials by adding mesh refinement at the surface of interface and testing different soil surface roughness values ranging from 0.1 to 20 [cm] in height. That always resulted in the need to access additional computational resources which would over stretch the required data storage capacity required for produced data sets. Species concentration at the instance of time 20 [s] is presented in Figure 96. The convection of the carbon dioxide gas species from the soil surface occurs closest to the most active part of the soil layer. Hence it has an absolute concentration of 58 [ppm] moreover a concentration 53 [ppm] located at the chambers head. The described values are reasonable to what is usually found by experiments as shown previously in Figure 86.

CO2 Conservative Volume Fraction
Chamber Volume

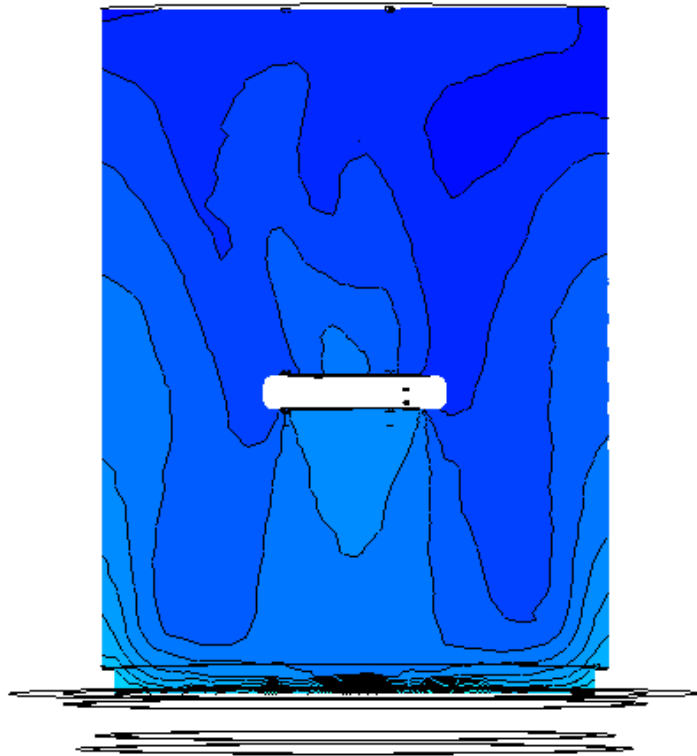
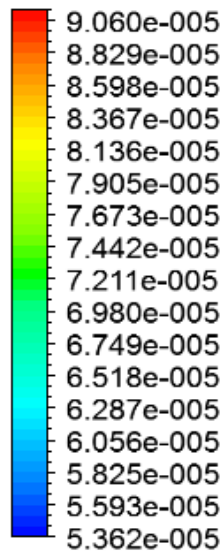


Figure 96: The numerical simulation at the first 35 [s] capturing how mass gradually diffuses within time.

Figure 97 shows a concentration difference contour plot at time step of 34 and 35 [s] whereby two carbon dioxide gas species concentration contour plots are applied independently to the gas and porous domain. These contours are applied on a mid-section slice plane additionally the two contour keys are applied whereby the left-hand side one is for the gas volume domain and the right-hand side one is for the porous domain. In the porous domain a change of 150 [ppm] occurs all over the porous domain at 1 [s] time step difference. Moreover 2 [ppm] concentration difference

occurs in the gas volume domain. Noting that a negative concentration difference means that a gas species movement is occurs in both domains.

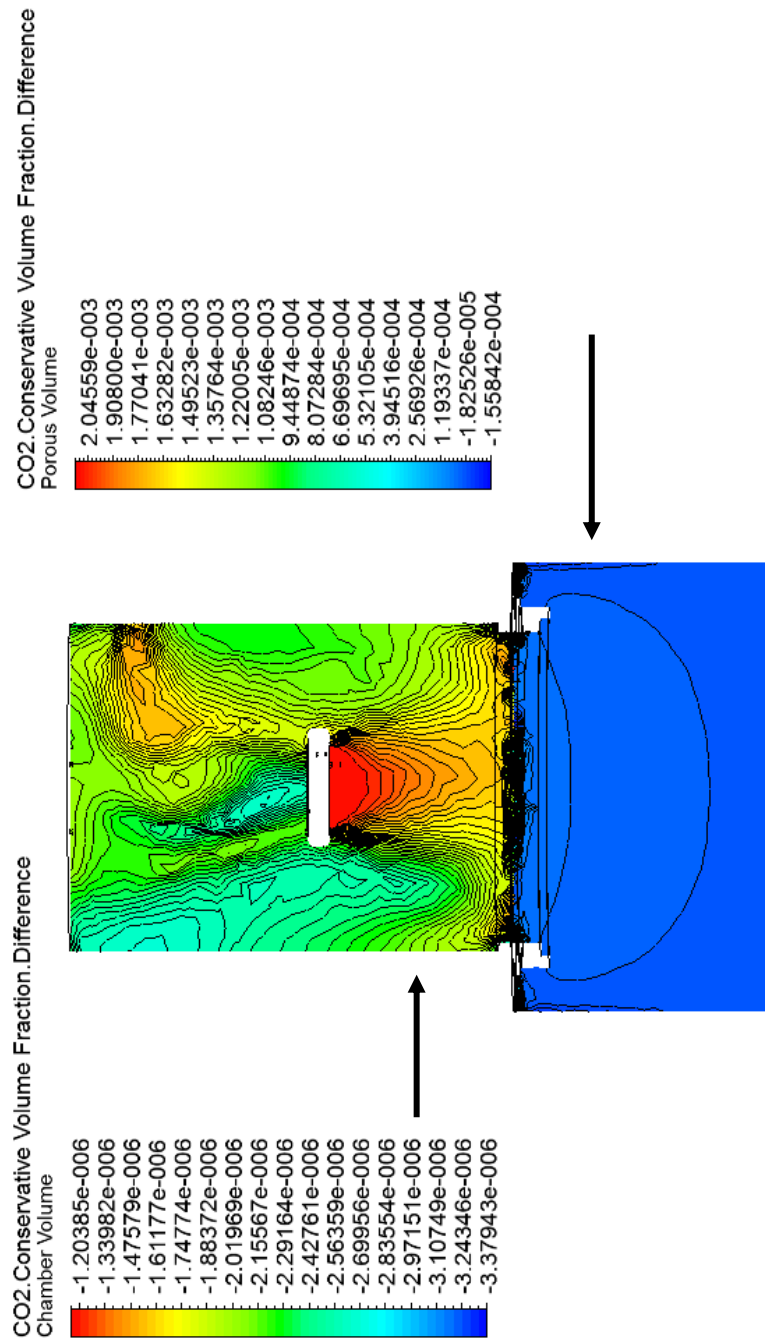


Figure 97: Concentration difference between two seconds time step at instance 33 and 34.

5.5.9. Conclusion about the Dynamic Case Study

The K-Epsilon model can be applied for the study of respiration chambers based on the applied validation process. The temperature field within the chamber can be regarded as a homogenous field. Mass transport occurs in a homogenous manner within the chamber as proven by the Courant number. Concentration changes are higher in the porous volume in comparison with the chamber gas volume as the discussion showed for Figure 97.

Minor deviations of the velocity and temperature field within the chamber are attributed to having the sampling tube. Chamber fixture base cases slowdown of diffusion at the top soil surface. The top soil surface is aerated as shown by the applied streamlines function. Furthermore, the blowing fan creates a velocity vector field similar to a magnetic one whereby the magnetic poles are situated at the two sides of the blowing fan hence a nearly symmetrical velocity field is created by the fan. The power of using the Courant number is that it showed total mass transport for both species occurring in the finite volume cells. A pressure field with a high stagnation point is created at the first point of impact on the soil surface after the fan.

Hence a finer mesh is required for future run simulations similarly it is advisable to apply the LES turbulence model to resolve the flow eddies that contribute to the rise and drop of the concentration values with time.

5.6. The Dynamic Chamber Case with a Rotating Fan Mesh

The main difference of the new simulation setup is the addition of an additional rotating mesh for the fan. This simulation is advantageous because it adds blowing fan interactional dynamics within the chambers gas volume due to applying a rotating fan. As a consequence, this would add an additional challenge to the work whereby additional computational resources are acquired for the new rotating mesh furthermore additional turbulence parameters can be analysed relating to gas mixture mixing.

5.6.1. Simulation Setup

The same simulation setup structure heading will be mentioned. Only the important parts are discussed here to avoid repetitions from the previous two simulation setups.

5.6.1.1. Setting up the Simulation in Relation to Space

In this section two necessary steps that have to be done the first is to set up the simulation space wise perspective whereby the first step is by modelling the geometrical fluid volumes secondly comes meshing the gas volumes.

5.6.1.1.1. Geometric Model

Three cylindrical geometries are created using ANSYS design modeller package whereby one represents the inner chamber gas volume and the second represents the soil porous volume and the third represents the fans gas volume. Furthermore, the designed respiration chamber with all the solid parts make are imported into the two created cylindrical geometries. The chamber is imported into a predefined location within the three geometries hence ensuring that all physical parameters captured when the flow calculation is run. The next step is to subtract all the chamber solid parts from

the two main cylindrical domains. Moreover, by subtracting the fan geometry from the third small cylindrical geometry results in total three new domains shown in Figure 98. The reason for that is to create the gas and porous volume necessary to mesh to later solve the flow equations. Likewise, the third cylindrical fan geometry represents the rotating fan volume. Consequently, the created porous domain volume is $0.06219 \text{ [m}^3\text{]}$ moreover the chamber gas volume is $0.0574492 \text{ [m}^3\text{]}$ in addition to the new gas volume for the blowing fan $8.28197e^{-5} \text{ [m}^3\text{]}$. The mentioned volume values are necessary to know the volume of air within the chamber. While the volume value of the porous media assists to link data interpretation stage with Figure 55 and Figure 56.

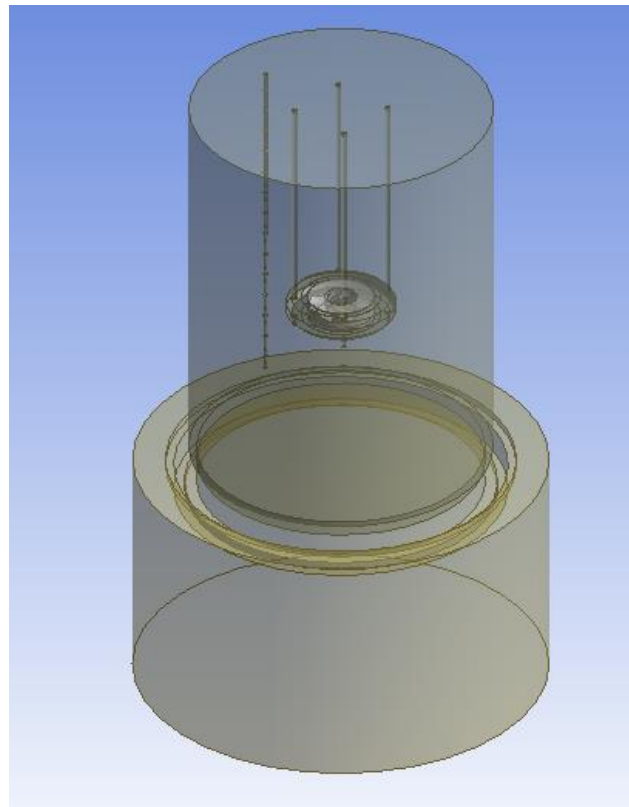


Figure 98: The modelled gas volume with the fan cylindrical geometry in addition to the porous domain shown at the bottom.

5.6.1.1.2. Simulation Mesh

The rotating fan mesh was a challenging task to model generate and couple with the chamber gas volume due to its confined location it is located in. Figure 99 shows a close-up image for the rotating fan mesh shown in a green colour furthermore the blue coloured mesh is the chamber gas volume one. The automatic mesh generation algorithm is used where by Tetrahedral mesh elements are generated for the fan mesh. The chamber gas volume also used a tetrahedral mesh which was also generated using the automatic meshing algorithm. Table 7 shows all the statistical data of the meshed domains for the number of nodes and number of elements.

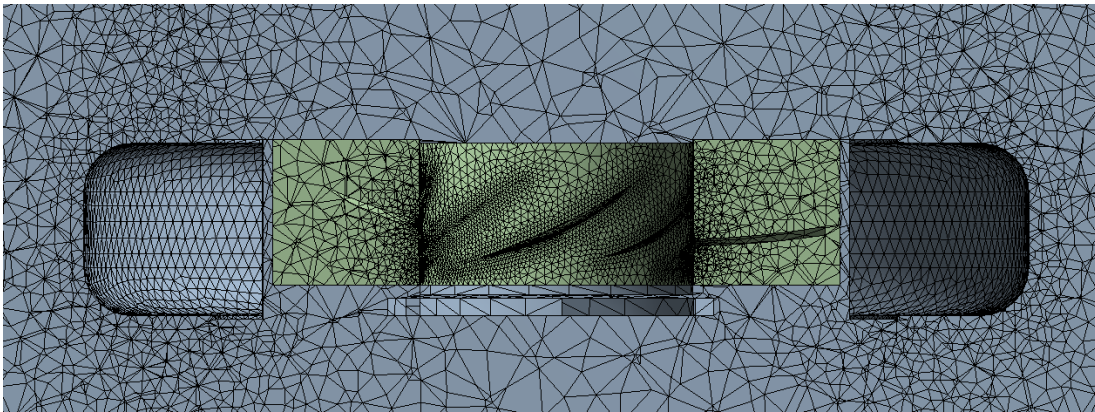


Figure 99: a close up image of the rotating fan mesh coupled with the chamber gas volume mesh.

This statistical data referring to the total number of nodes or elements helps in estimating the required computational time in relation to time and number of calculation cores more over checking the Courant–Friedrichs–Lewy condition. Consequently, this will be later evident in Figure 108.

Table 7: Mesh information representing the dynamic rotating mesh case.

Domain Name	Number of Elements	Number of Nodes
Chamber	1240210	1917854
Soil	133990	202867
Fan Mesh	181678	35901
Total	1555878	2156622

5.6.1.1.3. Applied Solid/Flow Models

The same fluid model is used for the porous media domain.

5.6.1.1.3.1. Porous Media Solid Model

The same model is used here as for the one applied for the static and dynamic chamber covered on page 190.

5.6.1.1.3.2. Porous Media Flow Model

The same model is used here as for the one applied for the static and dynamic chamber previously the reader is referred to page 190.

5.6.1.1.3.3. Respiration Chamber Gas Volume Flow Model

Both atmospheric temperature and pressure are considered to be constant with time this is according to the experimental data covered in (section 5.2). Consequently, the atmospheric pressure is taken to be 1 [atm] and ambient temperature to be 16 [°C] . The Navier-Stokes equations are solved to resolve the occurring flow field inside the chamber gas volume this by using the K-Epsilon turbulence model. Two coordinate

systems are used for the simulation whereby one is for the two fixed domains which are the chambers gas volume and soil porous media. The second coordinate system will be discussed in (section 5.6.1.1.3.4.)

5.6.1.1.3.4. Gas volume Fan media Model

The k-Epsilon turbulence model is also applied for the fan mesh volume. A rotating mesh is applied to the simulation that incorporates the rotating fan wall surfaces. The mesh volume is assigned an independent coordinate system so that the rotational axis can be defined as shown in Figure 100. This coordinate system is assigned to be in the centre of the fans inflow surface. Furthermore the alternating model option [227] is selected. The rotational fan velocity is set to a value of 3000 [rpm]. The rotating mesh creates the suction pressure and pressure build up after its blades consequently this helps in

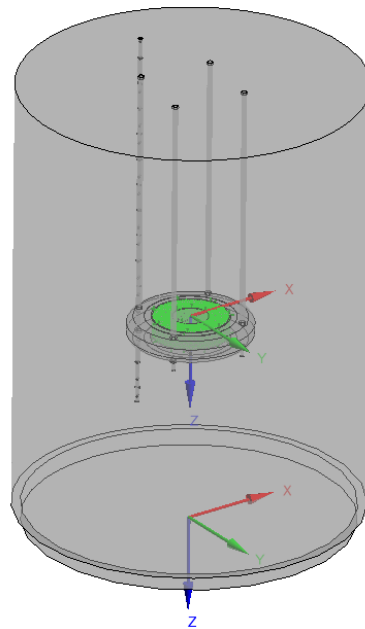


Figure 100: The two separate coordinate systems setups for the simulation whereby one is setup as a fixed one for the chamber gas volume furthermore the second is assigned for the rotating fan volume as shown highlighted in green.

5.6.1.2. Setting up the Simulation in Relation to Time

For transient simulation two main issues have to be resolved the simulation time step up and simulation initial conditions.

5.6.1.2.1. Simulation Time Stepping

The time stepping method for the simulation is the first order backward Euler furthermore the upwind method is applied for the advection scheme moreover regarding turbulence numerics a first order method is selected. For convergence control 1 loop is selected for the solver for the reason to reduce calculation time for the simulation. The one loop selection is based on that the species distribution time requires the first 20 [s] of time steps for the simulation this allows for convergence of solution to take place whereby the species are in distribution phase in the gas volume. Consequently, there was no evident need to increase the number of convergence loops for every time step after several calculation tests. The number of total time steps for the simulation is taken to be 360 [s] whereby the timesteps for the run is selected to be 1 sec taking the initial time as 0 [s].

5.6.1.2.2. Simulation Initialization

Initialization for the simulation is made up of 3 domains whereby they are split into two types the first is a porous type domain and the latter two are fluid domains.

5.6.5.1. Simulation Porous Media Initialization

The porous domain initialization is assigned a zero-value volume fraction hence this would leave the gas species of carbon dioxide to diffuse in the porous domain as the

simulation progresses in time. An initial velocity of zero is assigned in the porous media.

5.6.5.2. Simulation Fan Gas Media Initialization

An initial velocity of 2.7 [m/s] is assigned for the z axis component whereby this value is assigned to all the volume elements in the fan gas media moreover the x and y axis velocity component is assigned a zero value. Furthermore, a low turbulence intensity of 1% is applied to the domain with the selection of a rotating frame type option from the start of the calculation. Moreover, considering for simulation initialization the rotating domain is considered to be rotating from the start of the 360 sec simulation.

5.6.5.3. Simulation Chamber Gas Media Initialization

For the gas volume media each cell in the gas volume is assigned a zero-value velocity component as an initial condition with a zero-value static pressure. This would help in replicating the real case whereby the fan is firstly switched on then the chamber is turned over and setup on the location site.

5.6.2. Boundary Conditions

There is a minor difference between the previous two simulation setup cases mentioned on section 5.4 and section 5.5 whereby an additional cylindrical mesh is added. The cylindrical mesh incorporates the fan blades surfaces that rotate in time. Apart from those all-other boundary conditions are the same.

5.6.2.1. Interface Boundary Conditions between the Porous and Gas Domain

The same equations (5.23) and (5.24) are used to apply the source term boundary condition.

5.6.2.2. Simulation Gas Volume Interface Boundary Conditions

As shown previously in Figure 99 from the perspective side of the gas volume the subtracted volume cavity of the fan location creates a cylindrical cavity the surfaces of the created cavity form the interface boundary condition with the rotating fan.

5.6.2.3. Simulation Fan Interface Boundary Conditions

All of the outer surfaces for the rotating fan domain are assigned an interface boundary condition with the chamber gas volume cavity surfaces which incorporate the fan domain. Furthermore, the conservation of interface flux mass and momentum option is selected.

5.6.2.4. Simulation Fan Wall Boundary Conditions

A no slip boundary condition is selected with a smooth wall roughness option furthermore the wall contact model is a volume fraction one.

5.6.3. Simulation Validation

An initial run is conducted to check that the rotating mesh is performing its intended task. Rotational velocity applied to the fan's rotor generates a pressure difference between the fan's inflow and outflow hence a circulation flux is generated. By checking the resulting vector field from Figure 101 this verifies that the used rotational model on the fan mesh is creating the necessary pressure difference to create the fan

flux correctly. Consequently, the generated outlet vectors had a value of 2.7 [m/s]. This is will be more evident later in the chamber velocity study in Figure 105.

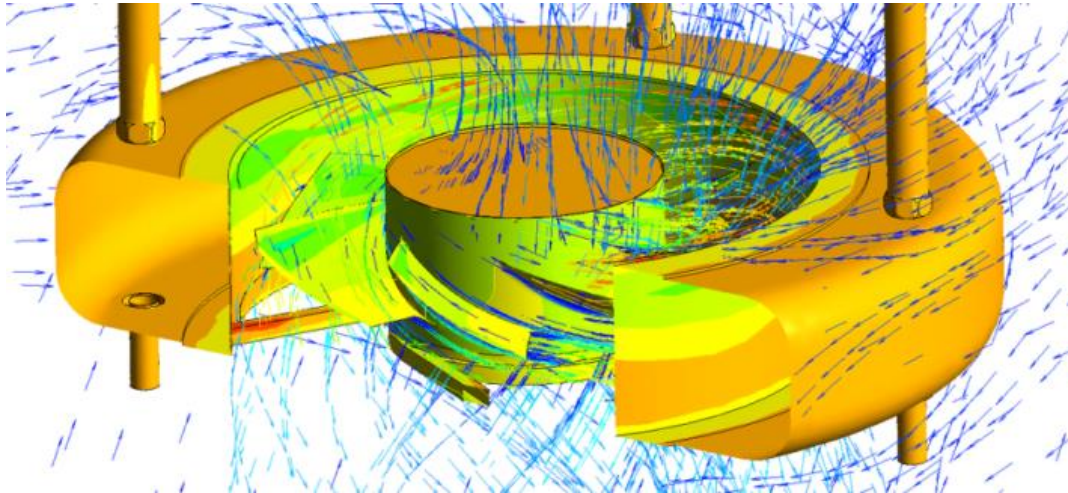


Figure 101: A close up view of the blowing fan, through using a cross sectional plane that goes through the blowing fan setup. This shows the velocity vector field while the coloured contours represent the pressure gradient.

The purpose of Figure 102 is validation to show that the right measurement is conducted this is by plotting both numerical and experimental results. As evident from the concentration plot in relation to time that concentration fluctuations are captured.

This proves that by using the rotating mesh the K-Epsilon model becomes capable of also modelling the fluctuations that had diminished because of the turbulence model averaging method of the velocity components. Moreover, the initial slop jump is obtained mimicking the real-life case as shown previously in Figure 63.

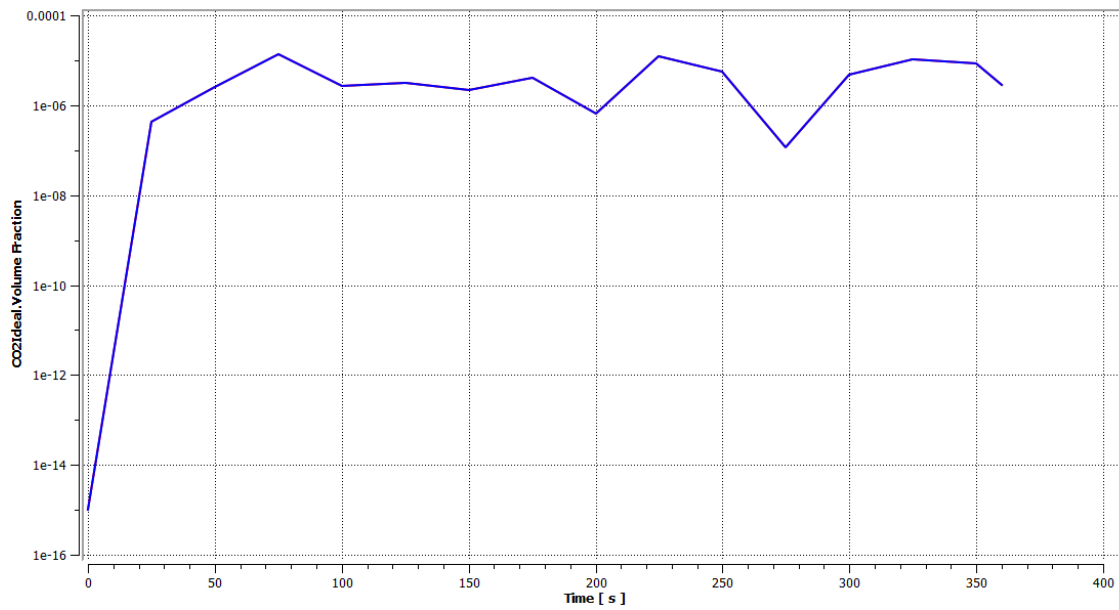


Figure 102: Validation plot showing a 100 [ppm] asymptotic behaviour concentration for a rotating mesh case.

The conversions of solution plots are necessary for solution validation purposes as shown on Figure 103. Commenting on the top plot whereby the carbon dioxide species is shown in red moreover air is shown in green. Consequently, this means that the assigned source term for carbon dioxide gas is applying species into the gas volume and porous domain.

A constant convergence pattern for both gas species is obtained with the progression in time of the solution. The interpretation for the convergence is that because both species are modelled using an exponential function with asymptotic characteristics this is consequently reflected onto the solution.

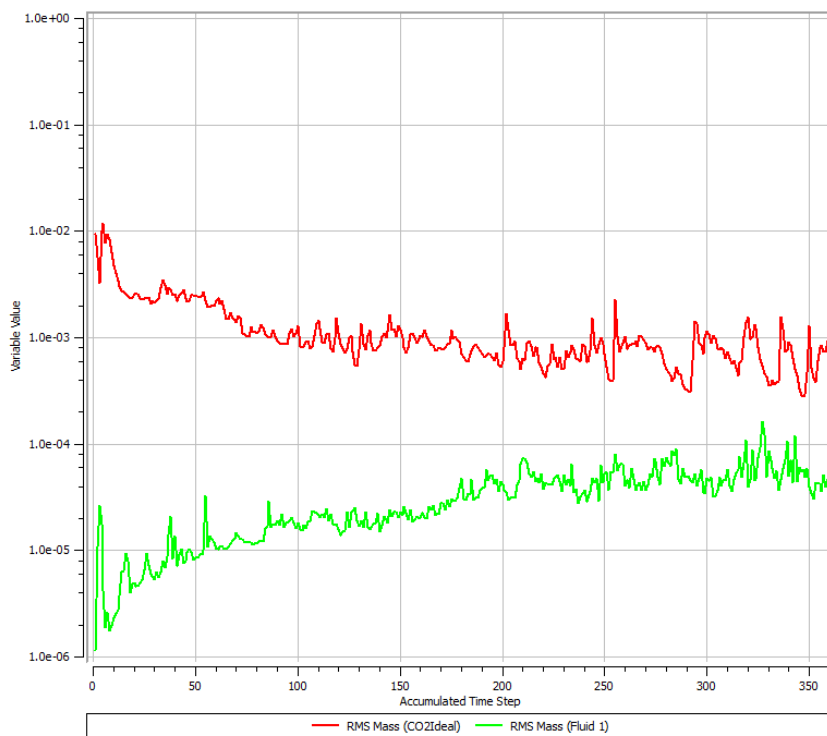
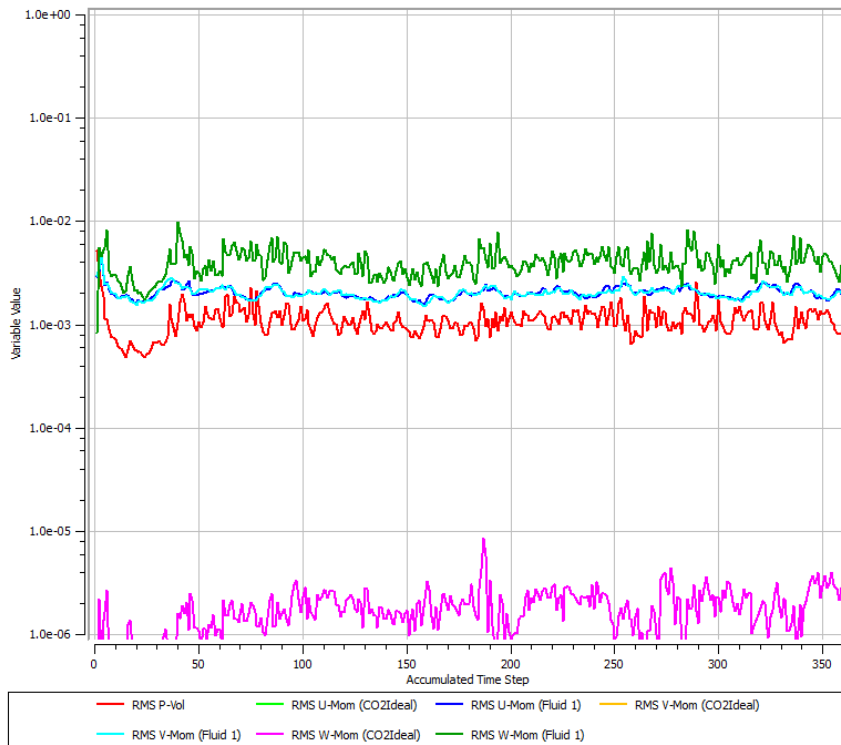


Figure 103: Convergence of the solution check for 360 time step accumulation, this is for mas momentum and volume fractions.

The bottom plot shows the solution plots for momentum, pressure and for both gas species. All the velocity components converge together at the same level apart from the z axis velocity component (shown in a purple colour) which is separately converging at a different level because the species source term velocity component is in the z-axis direction.

5.6.4. Simulation Results from the Dynamic Chamber Case

All the necessary parameters which are of importance are analysed in this section. The advantage of using the rotating mesh case is that it excludes out from the simulation the periodic inflow and outflow boundary conditions which add complications to the setup simulation. The rotating mesh considers more design detail to the simulation hence the effects of the blowing fan blade tips, blade profile, number of blades and fan rotational speed are added to the simulation.

5.6.4.1. The Dynamic Chamber Velocity Study

Figure 104 Show the velocity vector field inside the chamber's gas domain. The velocity vectors are shown in blue meaning the air velocity is from 2.7 to 0 [m/s]. These velocities are reasonable for the aeration process for the top soil layer in addition to that it ensures the homogenous mixing of the gas mixture through a swirling motion. The applied energy to the gas volume domain is visible in image Figure 101. What differentiates this case from the previous dynamic state simulation shown in Figure 95 is that the previous was without a rotating domain. Discussing the velocity distribution contours shown in Figure 106 starting firstly with the porous domain. The values of velocity vectors in the porous media domain average an air velocity of 2.6×10^{-4} [m/s]. Furthermore, commenting on the direction of velocity vectors they

are into the porous domain near the inner diameter for the chamber shell as shown in Figure 104. Likewise, the blue spot represents a region where the flow direction is from the porous domain into the chamber gas volume. The fan velocity profile expands sideways is for the reason that it is near to the soil surface. The total velocity profile is not symmetrical because of the helical behaviour that happens as shown later in the stream lines presentation shown in Figure 106 in addition to the effect of the sampling tube. The dominant velocity profile is the axial component one which mimics the velocity profile presented in the study of [228].

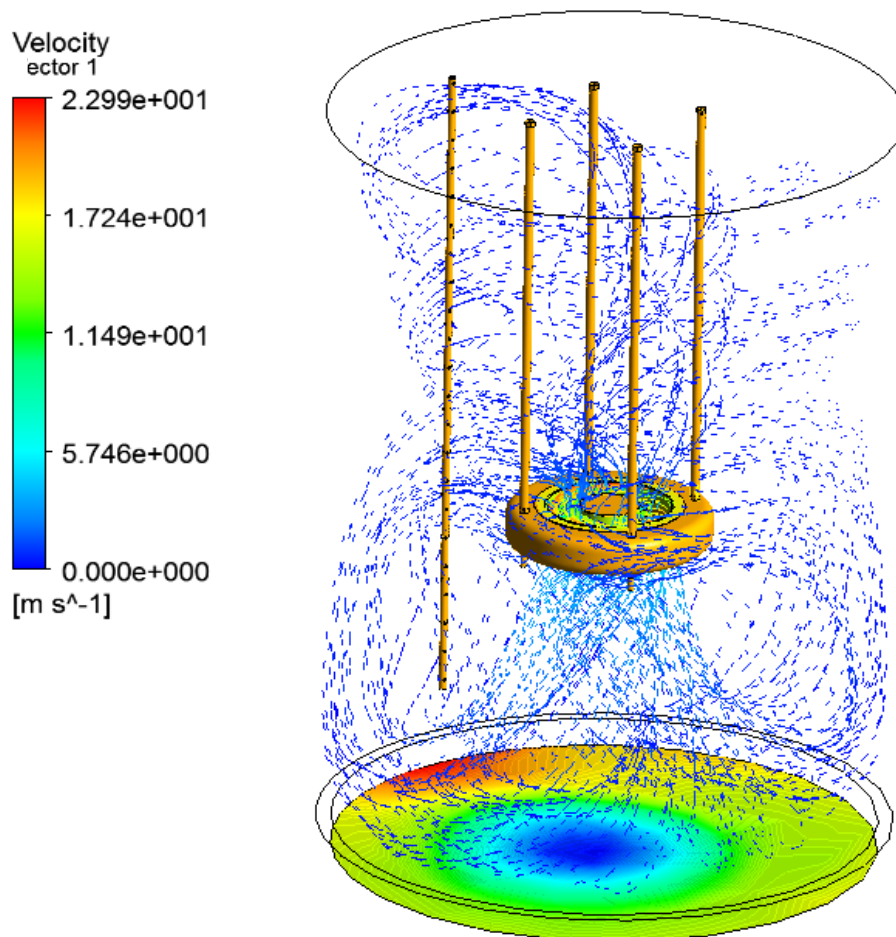


Figure 104: The pressure distribution on the soil surface is shown furthermore the velocity vector field is also illustrated with the provided colour key for it.

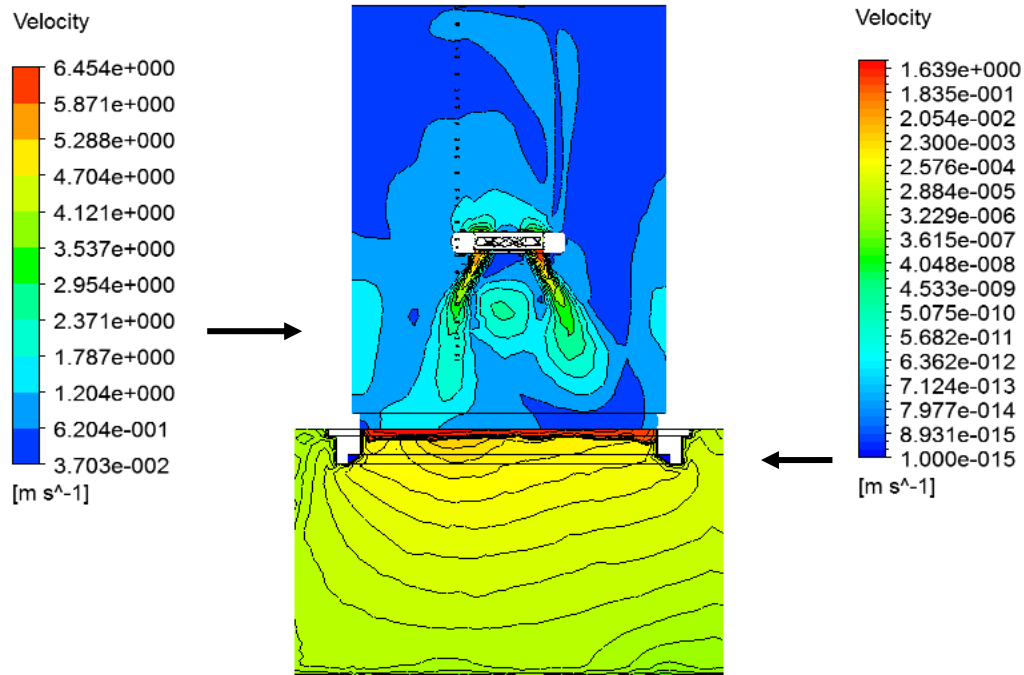


Figure 105: Air Velocity distribution in both the gas volume domain and the porous domain at instance of time 350 [s], the left-hand key is for the gas volume likewise the right-hand side key is for the porous domain.

What is evident in Figure 106 with the introduction of a rotating fan mesh is that a Taylor flow pattern becomes evident inside the chamber. This is something that wasn't visible in the previous dynamic chamber simulation. The spiral pattern created by the fan is helpful in pulling a charge of gas mixture from the soil surface to the top head section of the chamber hence this helps the mixing and transport process towards the gas sensor. Consequently, the fan contributes to speeding up the process of creating a homogenous gas mixture inside the gas volume during the concentration measurements. Looking at Figure 106 the soil surface pressure gradient is of importance because it shows the regions of high and low pressure on the soil surface.

Pressure

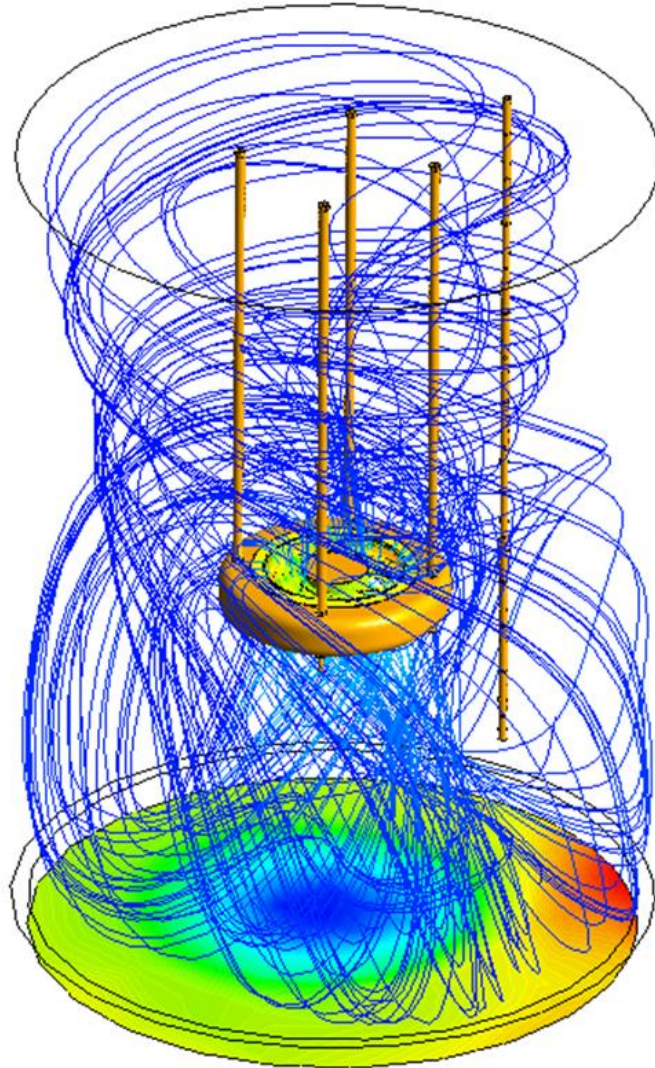
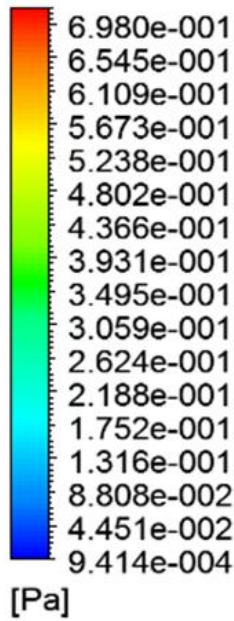


Figure 106: The stream line distribution in the chamber. The colour key is for pressure distribution contour on the soil surface.

The fans cyclic tip generated vortex creates a cyclic ventilation process to the soils top layer surface covered by the chamber. The high pressure resulting from pressure stagnation causes carbon dioxide to be pushed out of the surrounding regions of the red region area.

5.6.4.2. The Dynamic Chamber Inner Pressure Distribution

From the pressure contours shown on Figure 107 it is evident that a regular aeration of the soil surface is enforced hence sucking out and pumping air into the soil. The suction affect in the porous domain is evident from the negative values of pressure.

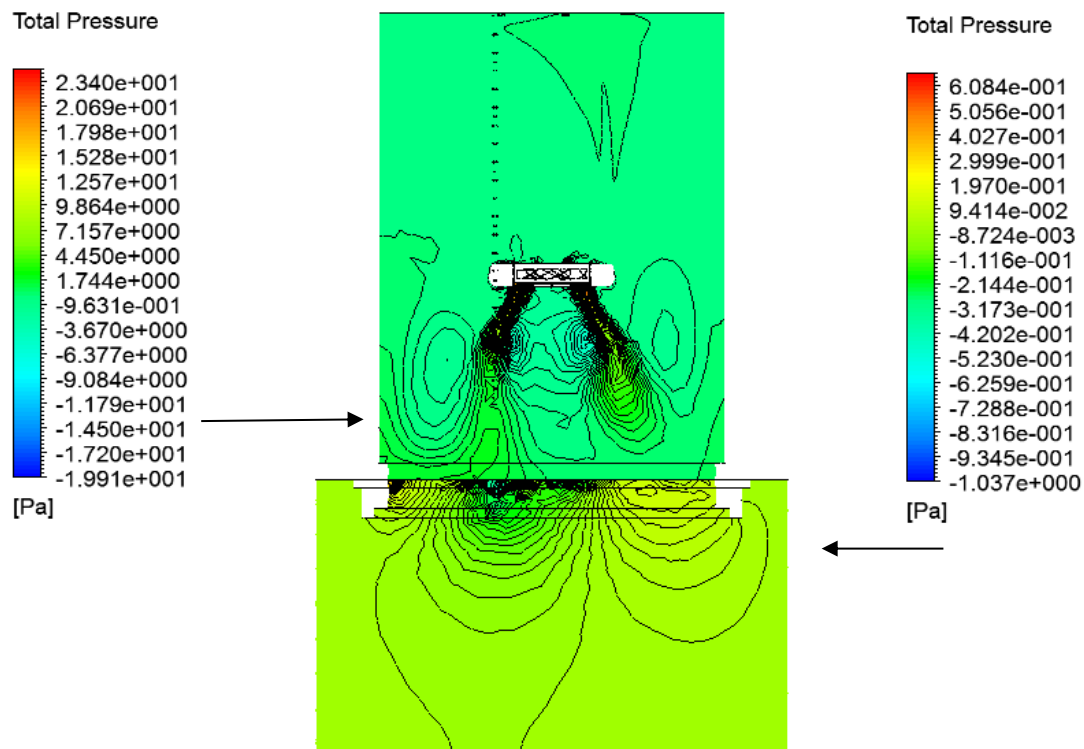


Figure 107: The study of pressure distribution in both the porous and gas volume domains at an instance of time 350 [s].

As you move away from the soil surface in-depth into the porous domain the value of pressure is very small of the magnitude of 9×10^{-2} [Pa]. Air pumping happens at a value of 3×10^{-1} [Pa] at the outer regions near to the chambers inner shell. While suction happens at a value of 1.1×10^{-1} [Pa].

5.6.4.3. The Dynamic Chamber Inner Courant Number Distribution

The Courant number shown on Figure 108 as evident the regions of increase of velocity showed a brighter blue colour this resulting from the fan fixture with the chambers body. The average value for Courant number in the chamber is 3.94. Furthermore, talking about the courant number in the porous media mainly the mass transfer occurs on the soil surface near at the interface region with chamber gas volume entrainment. Apart from that the rest of the porous domain has the same Courant number of 8×10^{-5} .

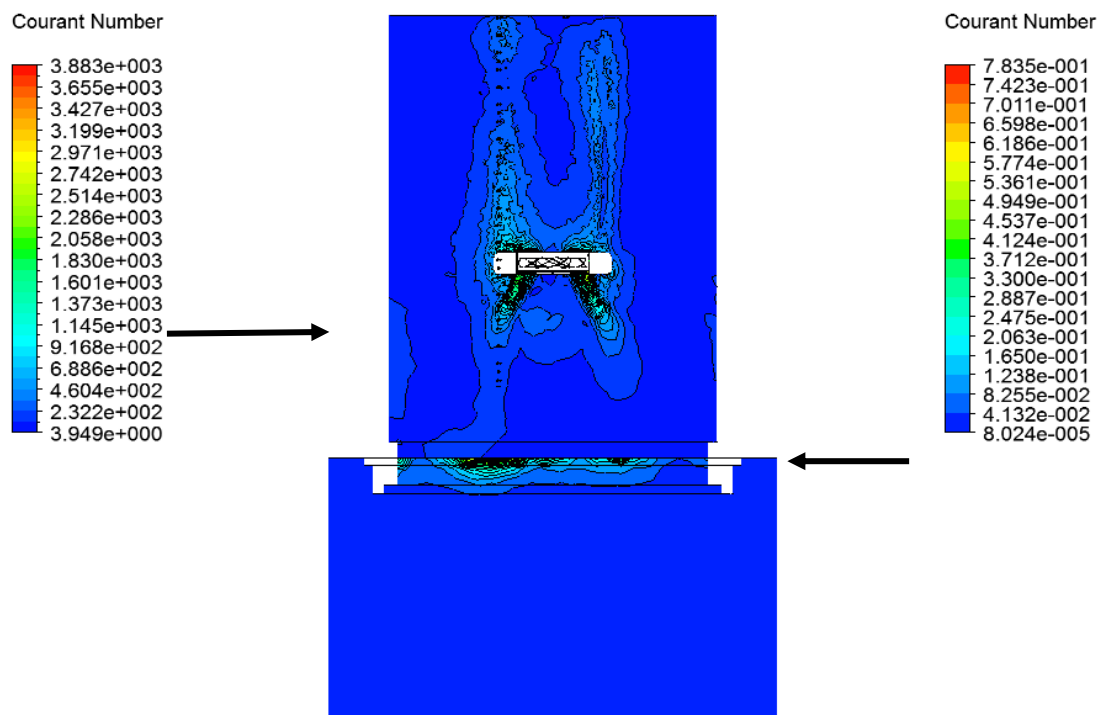


Figure 108: The Courant number contours both in the gas volume and porous domain at an instance of time 350 [s].

5.6.4.4. The Dynamic Chamber Inner Species Concentration Distribution

The gas species concentration plot shown on Figure 109 at a time instance of 350 [s] whereby it shows how the gas species in the gas volume are distributed in a uniform

manner due to the blowing fan circulation. Furthermore, as evident the biologically active layer near the soil surface has the most concentration of carbon dioxide this for the location near to the chamber base foundation meanwhile species concentration at the top layer in the regions covered by the chamber is the same as the one in the chamber giving a concentration of 81 [ppm].

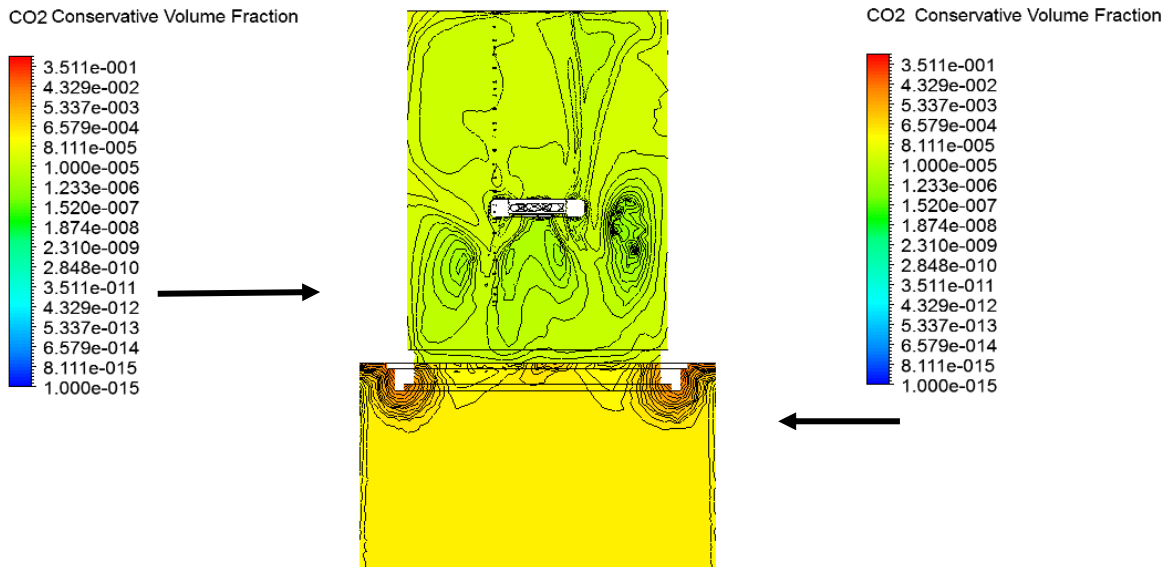


Figure 109: The concentration distribution in both the gas chamber volume and porous domain at time instance 350 [s].

5.6.5. Conclusion about the Dynamic Case Study

By introducing the rotating mesh this introduces more detail to the simulation from one aspect it bypasses the setup process to ensure periodic boundary conditions at the fan inlet and outlet. The fan blades tips produce the helical flow pattern which can either be visualized using the Q-Criterion or through the use of the available streamline function shown on Figure 106. This introduces additional kinetic energy to the simulation that is usually taken out due to that the fluctuating velocity component is

assigned a zero value. The Courant number and species concentration contour plots prove that homogenous mixing within the gas volume is achieved. It is evident when comparing the courant number contour plots between the porous domain and the gas domain is the high rate of mixing within the gas volume. Periodic pressure suction and pumping at the soil top surface acting on the most active layer to the soil surface are shown on Figure 106. Commenting on the discussed figure the blue contour region at the soil surface stays fixed. While when viewing the simulation in relation to time the red region moves around the blue region in a circular path.

5.7. Summary

The static experimental case formed the foundation to build the numerical model for all the cases. It was followed by a static case model simulation moreover a dynamic chamber case simulation and finally a rotating mesh simulation studying the dynamic case. From the generated data with the comparison of the validation plots between the numerical and experimental data for the three studied cases what is evident proof that CFD can be used as a reliable tool for future chamber development.

Chapter 6

Conclusion and Future Research

6.1. Conclusion

An innovative portable device was designed, made and tested. This is the first thesis that studies in detail Dynamic and static chambers using numerical models provided in commercial CFD codes. It proved that it can be used to measure accurately carbon dioxide concentration resulting from biological activity at specific locations of interest. The project objectives were achieved by running numerical tests and then through comparing them with the onsite measurements using the designed chamber on the grass land location. Validation of the produced data from the run simulations and apparatus showed the applicability of using such an apparatus for carbon dioxide efflux measurements. The major points of this study can be summarized as follows:

- Several forms of efflux equations were derived to link soil physical mechanisms, parameters and soil biological and types of soil textures that affect soil biological efflux respiration.
- A new chamber design was made, tested and validated. Its novelty comes in using a new sampling tube configuration that collects gas samples along the height of the chamber. Furthermore, the blowing fan setup and location was selected in the manner to provide the necessary suction pressure to draw out carbon dioxide from the most active soil layer without disturbing the biological statuses of the location.

-
- The results of this project significantly contribute towards the growing research in this area. This is for the reason that the innovations of the respiration chamber design in its operational mode either static or dynamic that it delivered accurate concentration measurements to a level of ± 20 [ppm] for a frequency sampling period of 5 seconds by the used gas sensor.
 - A software code using MATLAB was developed to incorporate interface windows that can assist in the data analysis stage of the project for the grassland location. Consequently, testing and calibrating new sensor technologies compatibility with any developed chamber designs.
 - The K-Epsilon turbulence model proved that it can be used to model flows in closed dynamic respiration chambers for the chamber gas volume. For both cases of rotating fan mesh and without one. Moreover, the Laminar flow model can be applied to model the static flow case where mass diffusion is dominant. Furthermore, the Darcy equation proved to be applicable to be used in porous media for a grassland location.

In summary, this thesis advances the state of knowledge in respiration chamber design and technology, contributing to related areas such carbon dioxide flow modelling in relation to greenhouse gas exchange and introducing CFD as a new tool for respiration chamber design.

6.2. Future Work

The considered parameters for the soil study are enough to build a soil biological efflux model. This research contributes towards allowing the opportunity for different soil

sites that can be studied with the developed chamber. These investigations point towards further directions of work flowing from this research in the area of field of soil biology and CFD that would help expand and strengthen the results, involving the modification of the respiration chamber design, and the following research is therefore recommended for future study.

- The written MATLAB software can be developed to take into account more parameters. This chamber with its software can be developed and commercialized at low cost to offer a better look into specific parameters relating to soil biological activity. Hence incorporating soil chemistry is required to model electro static charge transport occurring in the soil, the ions and catons depending on the mineral distribution in the soil.

References

1. Pope, S.B., Turbulent flows 2000: Cambridge university press.
2. Widén, B. and A. Lindroth, A calibration system for soil carbon dioxide-efflux measurement chambers. *Soil Science Society of America Journal*, 2003. 67(1): p. 327-334.
3. Roelle, P., et al., Measurement of nitrogen oxide emissions from an agricultural soil with a dynamic chamber system. *Journal of Geophysical Research: Atmospheres* (1984–2012), 1999. 104(D1): p. 1609-1619.
4. Website, L.C. Automated Soil CO₂ Flux System and soil chambers. 2015 09/16/2015]; Available from: <http://www.licor.com/corp/history.html>.
5. Pihlatie, M.K., et al., Comparison of static chambers to measure CH₄ emissions from soils. *Agricultural and Forest Meteorology*, 2013. 171: p. 124-136.
6. Levine, J.S., Measurement of nitrogen oxide emissions from an agricultural soil with a dynamic chamber system. *Journal of geophysical research*, 1999. 104(D1): p. 1609-1619.
7. Cambardella, C., et al., Field-scale variability of soil properties in central Iowa soils. *Soil Science Society of America Journal*, 1994. 58(5): p. 1501-1511.
8. Kutsch, W.L., M. Bahn, and A. Heinemeyer, Soil carbon dynamics: an integrated methodology 2009: Cambridge University Press.
9. Raich, J.W. and C.S. Potter, Global patterns of carbon dioxide emissions from soils. *Global Biogeochemical Cycles*, 1995. 9(1): p. 23-36.

-
10. Bazzaz, F.A., The response of natural ecosystems to the rising global CO₂ levels. *Annual review of ecology and systematics*, 1990: p. 167-196.
 11. Joos, F., G. Müller-Fürstenberger, and G. Stephan, Correcting the carbon cycle representation: How important is it for the economics of climate change? *Environmental Modeling & Assessment*, 1999. 4(2-3): p. 133-140.
 12. Cramer, W., et al., Global response of terrestrial ecosystem structure and function to CO₂ and climate change: results from six dynamic global vegetation models. *Global Change Biology*, 2001. 7(4): p. 357-373.
 13. Parkinson, K., An improved method for measuring soil respiration in the field. *Journal of Applied Ecology*, 1981: p. 221-228.
 14. Schlesinger, W.H. and J.A. Andrews, Soil respiration and the global carbon cycle. *Biogeochemistry*, 2000. 48(1): p. 7-20.
 15. Omer, A.M., Energy, environment and sustainable development. *Renewable and sustainable energy reviews*, 2008. 12(9): p. 2265-2300.
 16. Omer, A.M., Power, people and pollutions. *Renewable and sustainable energy reviews*, 2008. 12(7): p. 1864-1889.
 17. Bugaje, I., Renewable energy for sustainable development in Africa: a review. *Renewable and sustainable energy reviews*, 2006. 10(6): p. 603-612.
 18. Omer, A.M., Green energies and the environment. *Renewable and sustainable energy reviews*, 2008. 12(7): p. 1789-1821.
 19. Sumathi, S., S. Chai, and A. Mohamed, Utilization of oil palm as a source of renewable energy in Malaysia. *Renewable and sustainable energy reviews*, 2008. 12(9): p. 2404-2421.
-

-
20. Niven, R.K., Ethanol in gasoline: environmental impacts and sustainability review article. *Renewable and sustainable energy reviews*, 2005. 9(6): p. 535-555.
 21. Evans, A., V. Strezov, and T.J. Evans, Assessment of sustainability indicators for renewable energy technologies. *Renewable and sustainable energy reviews*, 2009. 13(5): p. 1082-1088.
 22. Mata, T.M., A.A. Martins, and N.S. Caetano, Microalgae for biodiesel production and other applications: a review. *Renewable and sustainable energy reviews*, 2010. 14(1): p. 217-232.
 23. Banos, R., et al., Optimization methods applied to renewable and sustainable energy: A review. *Renewable and sustainable energy reviews*, 2011. 15(4): p. 1753-1766.
 24. Hepbasli, A., A key review on exergetic analysis and assessment of renewable energy resources for a sustainable future. *Renewable and sustainable energy reviews*, 2008. 12(3): p. 593-661.
 25. Bhat, I. and R. Prakash, LCA of renewable energy for electricity generation systems—a review. *Renewable and sustainable energy reviews*, 2009. 13(5): p. 1067-1073.
 26. Alanne, K. and A. Saari, Distributed energy generation and sustainable development. *Renewable and sustainable energy reviews*, 2006. 10(6): p. 539-558.

-
27. Keith, H. and S. Wong, Measurement of soil CO₂ efflux using soda lime absorption: both quantitative and reliable. *Soil Biology and Biochemistry*, 2006. 38(5): p. 1121-1131.
 28. Maier, M. and H. Schack-Kirchner, Using the gradient method to determine soil gas flux: A review. *Agricultural and Forest Meteorology*, 2014. 192: p. 78-95.
 29. Aubinet, M., T. Vesala, and D. Papale, *Eddy covariance: a practical guide to measurement and data analysis* 2012: Springer Science & Business Media.
 30. Lai, D., et al., The effect of atmospheric turbulence and chamber deployment period on autochamber CO₂ and CH₄ flux measurements in an ombrotrophic peatland. *Biogeosciences*, 2012. 9(8): p. 3305-3322.
 31. Jassal, R., et al., Relationship between soil CO₂ concentrations and forest-floor CO₂ effluxes. *Agricultural and Forest Meteorology*, 2005. 130(3): p. 176-192.
 32. Cussler, E.L., *Diffusion: mass transfer in fluid systems* 2009: Cambridge university press.
 33. Nay, S.M., K.G. Mattson, and B.T. Bormann, Biases of chamber methods for measuring soil CO₂ efflux demonstrated with a laboratory apparatus. *Ecology*, 1994: p. 2460-2463.
 34. Koorevaar, P., G. Menelik, and C. Dirksen, *Elements of soil physics*. Vol. 13. 1983: Elsevier.
 35. YONEMURA, S., et al., Soil CO₂ concentrations and their implications in conventional and no-tillage agricultural fields. *農業気象*, 2009. 65(2): p. 141-149.
-

-
36. Hanson, P., et al., Separating root and soil microbial contributions to soil respiration: a review of methods and observations. *Biogeochemistry*, 2000. 48(1): p. 115-146.
 37. Rochette, P., et al., Description of a dynamic closed chamber for measuring soil respiration and its comparison with other techniques. *Canadian journal of soil science*, 1997. 77(2): p. 195-203.
 38. Ng, B., et al., Carbon fluxes from an urban tropical grassland. *Environmental Pollution*, 2014.
 39. Scurlock, J. and D. Hall, The global carbon sink: a grassland perspective. *Global Change Biology*, 1998. 4(2): p. 229-233.
 40. Najafpour, G., *Biochemical engineering and biotechnology* 2006: Elsevier.
 41. Dilly, O., Microbial respiratory quotient during basal metabolism and after glucose amendment in soils and litter. *Soil Biology and Biochemistry*, 2001. 33(1): p. 117-127.
 42. Smith, K., et al., Exchange of greenhouse gases between soil and atmosphere: interactions of soil physical factors and biological processes. *European Journal of Soil Science*, 2003. 54(4): p. 779-791.
 43. Smith, K., Exchange of greenhouse gases between soil and atmosphere: interactions of soil physical factors and biological processes. *Advances in Animal Biosciences*, 2010. 1(01): p. 360-360.
 44. Pengthamkeerati, P., et al., Soil carbon dioxide efflux from a claypan soil affected by surface compaction and applications of poultry litter. *Agriculture, ecosystems & environment*, 2005. 109(1): p. 75-86.
-

-
45. Conklin, A.R., Introduction to soil chemistry: Analysis and instrumentation 2013: John Wiley & Sons.
 46. Sancı, R., H.O. Panarello, and H.A. Osters, Assessment of soil moisture influence on CO₂ flux: a laboratory experiment. *Environmental geology*, 2009. 58(3): p. 491-497.
 47. Butnor, J.R., K.H. Johnsen, and C.A. Maier, Soil properties differently influence estimates of soil CO₂ efflux from three chamber-based measurement systems. *Biogeochemistry*, 2005. 73(1): p. 283-301.
 48. Marshall, T., A relation between permeability and size distribution of pores. *Journal of Soil Science*, 1958. 9(1): p. 1-8.
 49. McNeill, A. and P. Kolesik, X-ray CT investigations of intact soil cores with and without living crop roots. *Super Soil*, 2004.
 50. Barnes, G.E., Soil mechanics: principles and practice 2010: Palgrave macmillan.
 51. Kaviany, M., Principles of heat transfer in porous media 1995: Springer.
 52. Kaviany, M., Principles of heat transfer in porous media 2012: Springer Science & Business Media.
 53. Lin, C.-J., et al., Novel dynamic flux chamber for measuring air-surface exchange of H₂O from soils. *Environmental science & technology*, 2012. 46(16): p. 8910-8920.
 54. Butnor, J.R. and K.H. Johnsen, Calibrating soil respiration measures with a dynamic flux apparatus using artificial soil media of varying porosity. *European Journal of Soil Science*, 2004. 55(4): p. 639-647.
-

-
55. Venterea, R.T., Simplified method for quantifying theoretical underestimation of chamber-based trace gas fluxes. *Journal of environmental quality*, 2010. 39(1): p. 126-135.
 56. Valentini, C.M.A., et al., Soil respiration and aboveground litter dynamics of a tropical transitional forest in northwest Mato Grosso, Brazil. *Journal of Geophysical Research: Biogeosciences (2005–2012)*, 2008. 113(G1).
 57. Jassal, R., et al., Relationship between soil CO₂ concentrations and forest-floor CO₂ effluxes. *Agricultural and Forest Meteorology*, 2005. 130(3): p. 176-192.
 58. Liang, N., et al., In situ comparison of four approaches to estimating soil CO₂ efflux in a northern larch (*Larix kaempferi* Sarg.) forest. *Agricultural and Forest Meteorology*, 2004. 123(1): p. 97-117.
 59. Smith, D.L. and L. Johnson, Vegetation-mediated changes in microclimate reduce soil respiration as woodlands expand into grasslands. *Ecology*, 2004. 85(12): p. 3348-3361.
 60. Xu, L. and D.D. Baldocchi, Seasonal variation in carbon dioxide exchange over a Mediterranean annual grassland in California. *Agricultural and Forest Meteorology*, 2004. 123(1): p. 79-96.
 61. Subke, J.A., M. Reichstein, and J.D. Tenhunen, Explaining temporal variation in soil CO₂ efflux in a mature spruce forest in Southern Germany. *Soil Biology and Biochemistry*, 2003. 35(11): p. 1467-1483.
 62. LI-6400XT Portable Photosynthesis System. [27/08/2015]; Available from: <http://www.licor.com/env/products/photosynthesis/>.
-

-
63. LI-8100A Automated Soil Gas Flux System. 21/08/2015]; Available from: http://www.licor.com/env/products/soil_flux/.
 64. Hobby Greenhouse Construction. 21/08/2015]; Available from: <http://www.aces.edu/pubs/docs/A/ANR-1105/index2.tmpl>.
 65. Heinemeyer, A. and N.P. McNamara, Comparing the closed static versus the closed dynamic chamber flux methodology: Implications for soil respiration studies. *Plant and soil*, 2011. 346(1-2): p. 145-151.
 66. Pihlatie, M.K., et al., Comparison of static chambers to measure CH₄ emissions from soils. *Agricultural and Forest Meteorology*, 2013. 171: p. 124-136.
 67. Bekku, Y., et al., Examination of four methods for measuring soil respiration. *Applied Soil Ecology*, 1997. 5(3): p. 247-254.
 68. Delle Vedove, G., et al., Automated monitoring of soil respiration: an improved automatic chamber system. *Italian Journal of Agronomy*, 2010. 2(4): p. 377-382.
 69. Gao, F., et al., Design, fabrication, and application of a dynamic chamber for measuring gas emissions from soil. *Environmental science & technology*, 1996. 31(1): p. 148-153.
 70. Angell, R. and T. Svejcar, A chamber design for measuring net CO₂ exchange on rangeland. *Journal of Range Management*, 1999: p. 27-31.
 71. Luo, Y. and X. Zhou, *Soil respiration and the environment* 2006: Academic press.
-

-
72. Imhof, R., et al., Closed-chamber transepidermal water loss measurement: microclimate, calibration and performance. *International journal of cosmetic science*, 2009. 31(2): p. 97-118.
 73. Davidson, E., et al., Minimizing artifacts and biases in chamber-based measurements of soil respiration. *Agricultural and Forest Meteorology*, 2002. 113(1): p. 21-37.
 74. Gao, F. and S.R. Yates, Simulation of enclosure-based methods for measuring gas emissions from soil to the atmosphere. *Journal of Geophysical Research: Atmospheres* (1984–2012), 1998. 103(D20): p. 26127-26136.
 75. Palau-Salvador, G., et al., Large eddy simulations and experiments of flow around finite-height cylinders. *Flow, turbulence and combustion*, 2010. 84(2): p. 239-275.
 76. Matthias, A.D., D.N. Yarger, and R.S. Weinbeck, A numerical evaluation of chamber methods for determining gas fluxes. *Geophysical Research Letters*, 1978. 5(9): p. 765-768.
 77. Schlichting, H. and K. Gersten, *Boundary-layer theory*2000: Springer Science & Business Media.
 78. Schlichting, H. and K. Gersten, *Boundary-layer theory*2003: Springer Science & Business Media.
 79. Fröhlich, J. and W. Rodi, LES of the flow around a circular cylinder of finite height. *International journal of heat and fluid flow*, 2004. 25(3): p. 537-548.
 80. Simpson, R.L., Turbulent boundary-layer separation. *Annual Review of Fluid Mechanics*, 1989. 21(1): p. 205-232.
-

-
81. Blevins, R.D., Flow-induced vibration. 1990.
 82. Sparks, P. and Z. Huang, Gust factors and surface-to-gradient wind-speed ratios in tropical cyclones. *Journal of Wind Engineering and Industrial Aerodynamics*, 2001. 89(11): p. 1047-1058.
 83. Williamson, C. and G. Brown, A series in $1/\sqrt{\text{Re}}$ to represent the Strouhal–Reynolds number relationship of the cylinder wake. *Journal of Fluids and Structures*, 1998. 12(8): p. 1073-1085.
 84. Fyrrippis, I., P.J. Axaopoulos, and G. Panayiotou, Wind energy potential assessment in Naxos Island, Greece. *Applied Energy*, 2010. 87(2): p. 577-586.
 85. McClean, J. and D. Sumner, An experimental investigation of aspect ratio and incidence angle effects for the flow around surface-mounted finite-height square prisms. *Journal of Fluids Engineering*, 2014. 136(8): p. 081206.
 86. Kolari, P., et al., Evaluation of accuracy in measurements of VOC emissions with dynamic chamber system. *Atmospheric Environment*, 2012. 62: p. 344-351.
 87. Systems, P. SRC-1 Soil efflux Respiration Chamber 2015; Available from: <http://ppsystems.com/soil-and-canopy-flux/>.
 88. Lin, C.-J., et al., Empirical models for estimating mercury flux from soils. *Environmental science & technology*, 2010. 44(22): p. 8522-8528.
 89. Acarlar, M. and C. Smith, A study of hairpin vortices in a laminar boundary layer. Part 1. Hairpin vortices generated by a hemisphere protuberance. *Journal of Fluid Mechanics*, 1987. 175: p. 1-41.
 90. White, F., Fluid mechanics 2015: McGraw-Hill Higher Education.
-

-
91. Pape, L., et al., An automated dynamic chamber system for surface exchange measurement of non-reactive and reactive trace gases of grassland ecosystems. *Biogeosciences*, 2009. 6(3): p. 405-429.
 92. Szepessy, S. and P. Bearman, Aspect ratio and end plate effects on vortex shedding from a circular cylinder. *Journal of Fluid Mechanics*, 1992. 234: p. 191-217.
 93. Xu, L., et al., On maintaining pressure equilibrium between a soil CO₂ flux chamber and the ambient air. *Journal of Geophysical Research: Atmospheres* (1984–2012), 2006. 111(D8).
 94. Davidson, P., *Turbulence: an introduction for scientists and engineers* 2015: Oxford University Press, USA.
 95. Pumpanen, J., et al., Comparison of different chamber techniques for measuring soil CO₂ efflux. *Agricultural and Forest Meteorology*, 2004. 123(3): p. 159-176.
 96. Eckley, C., et al., The influence of dynamic chamber design and operating parameters on calculated surface-to-air mercury fluxes. *Atmospheric Environment*, 2010. 44(2): p. 194-203.
 97. Christiansen, J.R., et al., Assessing the effects of chamber placement, manual sampling and headspace mixing on CH₄ fluxes in a laboratory experiment. *Plant and soil*, 2011. 343(1): p. 171-185.
 98. Martin, J.G., P.V. Bolstad, and J.M. Norman, A carbon dioxide flux generator for testing infrared gas analyzer-based soil respiration systems. *Soil Science Society of America Journal*, 2004. 68(2): p. 514-518.
-

-
99. Pumpanen, J., et al., Comparison of different chamber techniques for measuring soil CO₂ efflux. *Agricultural and Forest Meteorology*, 2004. 123(3): p. 159-176.
 100. Fan, Z., J.C. Neff, and N.P. Hanan, Modeling pulsed soil respiration in an African savanna ecosystem. *Agricultural and Forest Meteorology*, 2015. 200: p. 282-292.
 101. Liang, N., G. Inoue, and Y. Fujinuma, A multichannel automated chamber system for continuous measurement of forest soil CO₂ efflux. *Tree physiology*, 2003. 23(12): p. 825-832.
 102. Wohlfahrt, G., et al., Quantifying nighttime ecosystem respiration of a meadow using eddy covariance, chambers and modelling. *Agricultural and Forest Meteorology*, 2005. 128(3): p. 141-162.
 103. Atkins, P. and J. De Paula, *Elements of physical chemistry* 2013: Oxford University Press, USA.
 104. Drewitt, G., et al., Measuring forest floor CO₂ fluxes in a Douglas-fir forest. *Agricultural and Forest Meteorology*, 2002. 110(4): p. 299-317.
 105. Rayment, M. and P. Jarvis, An improved open chamber system for measuring soil CO₂ effluxes in the field. *Journal of geophysical research*, 1997. 102(D24): p. 28779-28,784.
 106. Pongracic, S., M. Kirschbaum, and R. Raison, Comparison of soda lime and infrared gas analysis techniques for in situ measurement of forest soil respiration. *Canadian Journal of Forest Research*, 1997. 27(11): p. 1890-1895.
-

-
107. Wharton, S. and R. Pyles Pressure Pumping Effects on Soil Efflux Measurements of CO₂. 2008.
 108. Moncrieff, J.B., et al., A system to measure surface fluxes of momentum, sensible heat, water vapour and carbon dioxide. *Journal of Hydrology*, 1997. 188: p. 589-611.
 109. Drewitt, G., et al., Measuring forest floor CO₂ fluxes in a Douglas-fir forest. *Agricultural and Forest Meteorology*, 2002. 110(4): p. 299-317.
 110. Goulden, M.L., et al., Measurements of carbon sequestration by long-term eddy covariance: Methods and a critical evaluation of accuracy. *Global Change Biology*, 1996. 2(3): p. 169-182.
 111. Conen, F. and K. Smith, An explanation of linear increases in gas concentration under closed chambers used to measure gas exchange between soil and the atmosphere. *European Journal of Soil Science*, 2008. 51(1): p. 111-117.
 112. Schulze, E.-D., A new type of climatized gas exchange chamber for net photosynthesis and transpiration measurements in the field. *Oecologia*, 1972. 10(3): p. 243-251.
 113. Systems, P. CPY-4 Model Chamber. 2015; Available from: <http://ppsystems.com/wp-content/uploads/EDSCPY41.pdf>.
 114. Bergman, T.L., F.P. Incropera, and A.S. Lavine, *Fundamentals of heat and mass transfer* 2011: John Wiley & Sons.
 115. Ham, J.M. and G. Kluitenberg, Modeling the effect of mulch optical properties and mulch-soil contact resistance on soil heating under plastic mulch culture. *Agricultural and Forest Meteorology*, 1994. 71(3): p. 403-424.
-

-
116. Marshall, T.J., J.W. Holmes, and C.W. Rose, Soil physics 1996: Cambridge University Press.
 117. Ozgener, O., L. Ozgener, and J.W. Tester, A practical approach to predict soil temperature variations for geothermal (ground) heat exchangers applications. *International Journal of Heat and Mass Transfer*, 2013. 62: p. 473-480.
 118. Graf, A., et al., Measurement depth effects on the apparent temperature sensitivity of soil respiration in field studies. *Biogeosciences Discussions*, 2008. 5(3): p. 1867-1898.
 119. Parkin, T.B. and T.C. Kaspar, Temperature controls on diurnal carbon dioxide flux. *Soil Science Society of America Journal*, 2003. 67(6): p. 1763-1772.
 120. Ozgener, O., L. Ozgener, and D.Y. Goswami, Experimental prediction of total thermal resistance of a closed loop EAHE for greenhouse cooling system. *International Communications in Heat and Mass Transfer*, 2011. 38(6): p. 711-716.
 121. Fang, C. and J. Moncrieff, The dependence of soil CO₂ efflux on temperature. *Soil Biology and Biochemistry*, 2001. 33(2): p. 155-165.
 122. Monson, R.K., et al., Winter forest soil respiration controlled by climate and microbial community composition. *Nature*, 2006. 439(7077): p. 711-714.
 123. Camarda, M., S. Gurrieri, and M. Valenza, Effects of soil gas permeability and recirculation flux on soil CO₂ flux measurements performed using a closed dynamic accumulation chamber. *Chemical Geology*, 2009. 265(3): p. 387-393.

-
124. Reth, S., M. Reichstein, and E. Falge, The effect of soil water content, soil temperature, soil pH-value and the root mass on soil CO₂ efflux—A modified model. *Plant and soil*, 2005. 268(1): p. 21-33.
 125. White, F.M. and I. Corfield, *Viscous fluid flow*. Vol. 3. 2006: McGraw-Hill New York.
 126. Powers, H.H., et al., A dynamic soil chamber system coupled with a tunable diode laser for online measurements of $\delta^{13}\text{C}$, $\delta^{18}\text{O}$, and efflux rate of soil-respired CO₂. *Rapid Communications in Mass Spectrometry*, 2010. 24(3): p. 243-253.
 127. Tagesson, T., Seasonal variation and controlling factors of soil carbon effluxes in six vegetation types in southeast of Sweden 2006: SKB.
 128. Yuste, J.C., et al., Soil respiration in a mixed temperate forest and its contribution to total ecosystem respiration. *Tree physiology*, 2005. 25(5): p. 609-619.
 129. Falge, E., et al., Gap filling strategies for defensible annual sums of net ecosystem exchange. *Agricultural and Forest Meteorology*, 2001. 107(1): p. 43-69.
 130. Pilegaard, K., et al., Two years of continuous CO₂ eddy-flux measurements over a Danish beech forest. *Agricultural and Forest Meteorology*, 2001. 107(1): p. 29-41.
 131. Nay, S.M., K.G. Mattson, and B.T. Bormann, Biases of chamber methods for measuring soil CO₂ efflux demonstrated with a laboratory apparatus. *Ecology*, 1994. 75(8): p. 2460-2463.
-

-
132. Fahey, T.J., et al., Soil respiration and soil carbon balance in a northern hardwood forest ecosystem. *Canadian Journal of Forest Research*, 2005. 35(2): p. 244-253.
 133. Ross, F.C., *Concepts in biology*2003: McGraw-Hill College.
 134. Feng, X., et al., Distribution, accumulation, and fluxes of soil carbon in four monoculture lysimeters at San Dimas Experimental Forest, California. *Geochimica et cosmochimica acta*, 1999. 63(9): p. 1319-1333.
 135. Takle, E.S., et al., Influence of high-frequency ambient pressure pumping on carbon dioxide efflux from soil. *Agricultural and Forest Meteorology*, 2004. 124(3): p. 193-206.
 136. Flechard, C., et al., Temporal changes in soil pore space CO₂ concentration and storage under permanent grassland. *Agricultural and Forest Meteorology*, 2007. 142(1): p. 66-84.
 137. Gu, L., et al., Objective threshold determination for nighttime eddy flux filtering. *Agricultural and Forest Meteorology*, 2005. 128(3): p. 179-197.
 138. Yiqi, L. and X. Zhou, *Soil respiration and the environment*2010: Academic press.
 139. Townend, J., Effects of elevated carbon dioxide and drought on the growth and physiology of clonal Sitka spruce plants (*Picea sitchensis* (Bong.) Carr.). *Tree physiology*, 1993. 13(4): p. 389-399.
 140. Tagesson, T., Calibration and analysis of soil carbon efflux estimates with closed chambers at Forsmark and Laxemar2006: SKB.
-

-
141. Baldocchi, D.D. and T.P. Meyers, Trace gas exchange above the floor of a deciduous forest. 1. Evaporation and CO₂ efflux. *J. Geophys. Res.*, 1991. 96(D4): p. 7271-7285.
 142. Lund, C., et al., The effects of chamber pressurization on soil-surface CO₂ flux and the implications for NEE measurements under elevated CO₂. *Global Change Biology*, 1999. 5(3): p. 269-281.
 143. Kimball, B. and E. Lemon, Spectra of air pressure fluctuations at the soil surface. *Journal of geophysical research*, 1970. 75(33): p. 6771-6777.
 144. Takle, E.S., et al., High-frequency pressure variations in the vicinity of a surface CO₂ flux chamber. *Agricultural and Forest Meteorology*, 2003. 114(3): p. 245-250.
 145. Kimball, B. and E. Lemon, Theory of soil air movement due to pressure fluctuations. *Agricultural meteorology*, 1972. 9: p. 163-181.
 146. Massman, W. and X. Lee, Eddy covariance flux corrections and uncertainties in long-term studies of carbon and energy exchanges. *Agricultural and Forest Meteorology*, 2002. 113(1-4): p. 121-144.
 147. Mahrer, Y., A numerical model for calculating the soil temperature regime under transparent polyethylene mulches. *Agricultural Meteorology*, 1980. 22(3): p. 227-234.
 148. Sui, H.-j., D.-c. Zeng, and F.-z. Chen, A numerical model for simulating the temperature and moisture regimes of soil under various mulches. *Agricultural and Forest Meteorology*, 1992. 61(3): p. 281-299.
-

-
149. Bahn, M., et al., Soil respiration in European grasslands in relation to climate and assimilate supply. *Ecosystems*, 2008. 11(8): p. 1352-1367.
 150. Adolfo Campos, C., Response of soil surface CO₂-C flux to land use changes in a tropical cloud forest (Mexico). *Forest ecology and management*, 2006. 234(1): p. 305-312.
 151. Bain, W.G., et al., Wind-induced error in the measurement of soil respiration using closed dynamic chambers. *Agricultural and Forest Meteorology*, 2005. 131(3): p. 225-232.
 152. Xu, L., et al. Critical Considerations for Accurate Soil CO₂ Flux Measurement. 2005.
 153. McDermitt, D.K., et al., Equalizing Pressures Between A Soil CO₂ Flux Chamber and the Ambient Air Under Windy Conditions. *LI-COR® Biosciences*, 2005. 4421.
 154. Suleau, M., et al., Wind velocity perturbation of soil respiration measurements using closed dynamic chambers. *European Journal of Soil Science*, 2009. 60(4): p. 515-524.
 155. Hongxing, Z., et al., Multichannel automated chamber system for continuous monitoring of CO₂ exchange between the agro-ecosystem or soil and the atmosphere. *Acta Ecologica Sinica*, 2007. 27(4): p. 1273-1281.
 156. Sachs, T., et al., Methane emission from Siberian wet polygonal tundra on multiple spatial scales: vertical flux measurements by closed chambers and eddy covariance, Samoylov Island, Lena River Delta. 2008.
-

-
157. Stull, R.B., *Meteorology for scientists and engineers: a technical companion book with Ahrens' Meteorology Today*2000: Brooks/Cole.
 158. PAVELKA, M., et al., Chamber techniques versus eddy covariance method during nighttime measurements.
 159. Najafpour, G., *Biochemical engineering and biotechnology*2015: Elsevier.
 160. Couwenberg, J., R. Dommain, and H. Joosten, Greenhouse gas fluxes from tropical peatlands in south-east Asia. *Global Change Biology*, 2010. 16(6): p. 1715-1732.
 161. Hillel, D., *Soil and water: physical principles and processes*1971: Academic Press.
 162. Kindler, R., et al., Dissolved carbon leaching from soil is a crucial component of the net ecosystem carbon balance. *Global Change Biology*, 2011. 17(2): p. 1167-1185.
 163. Sposito, G., *The chemistry of soils*2008: Oxford University Press, USA.
 164. Conklin, A.R., *Introduction to soil chemistry: Analysis and instrumentation*. Vol. 167. 2005: John Wiley and Sons.
 165. Suh, S.U., et al., A chamber system with automatic opening and closing for continuously measuring soil respiration based on an open-flow dynamic method. *Ecological Research*, 2006. 21(3): p. 405-414.
 166. Risk, D., et al., Forced Diffusion soil flux: A new technique for continuous monitoring of soil gas efflux. *Agricultural and Forest Meteorology*, 2011.
 167. Liu, X., et al., A survey on gas sensing technology. *Sensors*, 2012. 12(7): p. 9635-9665.
-

-
168. Silva, J., P. Feijóo, and R. Santos, Underwater measurements of carbon dioxide evolution in marine plant communities: A new method. *Estuarine, Coastal and Shelf Science*, 2008. 78(4): p. 827-830.
169. Ngao, J., et al., Cross-calibration functions for soil CO efflux measurement systems. *Annals of forest science*, 2006. 63(5): p. 477-484.
170. Heinemeyer, A., et al., Soil respiration: implications of the plant-soil continuum and respiration chamber collar-insertion depth on measurement and modelling of soil CO₂ efflux rates in three ecosystems. *European journal of soil science*, 2011. 62(1): p. 82-94.
171. Sah, R.L.Y., et al., Biosynthetic response of cartilage explants to dynamic compression. *Journal of Orthopaedic Research*, 1989. 7(5): p. 619-636.
172. Healy, R.W., et al., Numerical Evaluation of Static-Chamber Measurements of Soil—Atmosphere Gas Exchange: Identification of Physical Processes. *Soil Science Society of America Journal*, 1996. 60(3): p. 740-747.
173. Nobuhiro, T., et al., Development of the IRGA enclosed-chamber system for soil CO₂ efflux measurement and its application to a spatial variation measurement. *Journal of Forest Research*, 2003. 8(4): p. 297-301.
174. Aneja, V., et al., Dynamic Chamber System to Measure Gaseous Compounds Emissions and Atmospheric-Biospheric Interactions. *Environmental simulation chambers: application to atmospheric chemical processes*, 2006: p. 97-109.
-

-
175. Parkin, T.B. and R.T. Venterea, USDA-ARS GRACEnet Project Protocols Chapter 3. Chamber-Based Trace Gas Flux Measurements 4. Book Chapter, 2010: p. 1-39.
176. Buchmann, N., Biotic and abiotic factors controlling soil respiration rates in *Picea abies* stands. *Soil Biology and Biochemistry*, 2000. 32(11): p. 1625-1635.
177. Ngao, J., et al., Cross-calibration functions for soil CO₂ efflux measurement systems. *Annals of forest science*, 2006. 63(5): p. 477-484.
178. Reth, S., M. Reichstein, and E. Falge, The effect of soil water content, soil temperature, soil pH-value and the root mass on soil CO₂ efflux—a modified model. *Plant and Soil*, 2005. 268(1): p. 21-33.
179. Program, U.o.N.L.T.S. Soil Testing for Turf Areas. 2012 [30/10/2012]; Available from: <http://turf.unl.edu/pdfcaextpub/SoilTesting2012g.pdf>.
180. Xu, M. and Y. Qi, Soil-surface CO₂ efflux and its spatial and temporal variations in a young ponderosa pine plantation in northern California. *Global Change Biology*, 2001. 7(6): p. 667-677.
181. Hoorman, J.J., *The Role of Soil Bacteria*. 2011.
182. Jobbágy, E.G. and R.B. Jackson, The distribution of soil nutrients with depth: global patterns and the imprint of plants. *Biogeochemistry*, 2001. 53(1): p. 51-77.
183. Gagliardi, J.V. and J.S. Karns, Leaching of *Escherichia coli* O157: H7 in diverse soils under various agricultural management practices. *Applied and environmental microbiology*, 2000. 66(3): p. 877-883.
-

-
184. Singh, O., et al., Phytoremediation: an overview of metallic ion decontamination from soil. *Applied Microbiology and Biotechnology*, 2003. 61(5-6): p. 405-412.
 185. Silver, S. and L.T. Phung, A bacterial view of the periodic table: genes and proteins for toxic inorganic ions. *Journal of Industrial Microbiology and Biotechnology*, 2005. 32(11-12): p. 587-605.
 186. Duval, B.D., et al., Plant– Soil Distribution of Potentially Toxic Elements in Response to Elevated Atmospheric CO₂. *Environmental science & technology*, 2011. 45(7): p. 2570-2574.
 187. Wong, M. and A. Bradshaw, A comparison of the toxicity of heavy metals, using root elongation of rye grass, *Lolium perenne*. *New Phytologist*, 1982. 91(2): p. 255-261.
 188. Uchida, M., et al., Contribution of micro-organisms to the carbon dynamics in black spruce (*Picea mariana*) forest soil in Canada. *Ecological Research*, 1998. 13(1): p. 17-26.
 189. Wood, C., et al., Free-air CO₂ enrichment effects on soil carbon and nitrogen. *Agricultural and Forest Meteorology*, 1994. 70(1-4): p. 103-116.
 190. Monod, J., The growth of bacterial cultures. *Selected Papers in Molecular Biology* by Jacques Monod, 2012: p. 139.
 191. Ferenci, T., Growth of bacterial cultures' 50 years on: towards an uncertainty principle instead of constants in bacterial growth kinetics. *Research in microbiology*, 1999. 150(7): p. 431-438.
-

-
192. Shuler, M.L. and F. Kargi, *Bioprocess engineering* 2002: Prentice Hall New York.
 193. Valarini, P.J., et al., Integrated evaluation of soil quality after the incorporation of organic matter and microorganisms. *Brazilian Journal of microbiology*, 2002. 33(1): p. 35-40.
 194. Ratkowsky, D., et al., Relationship between temperature and growth rate of bacterial cultures. *Journal of Bacteriology*, 1982. 149(1): p. 1-5.
 195. Ratkowsky, D., et al., Model for bacterial culture growth rate throughout the entire biokinetic temperature range. *Journal of Bacteriology*, 1983. 154(3): p. 1222-1226.
 196. Madenjian, C.P., Nighttime pond respiration rate: oxygen or temperature dependent? *Canadian Journal of Fisheries and Aquatic Sciences*, 1990. 47(1): p. 180-183.
 197. Ann McCauley, S.S., Clain Jones, Extension Soil Fertility Specialist and Jeff Jacobsen, Soil Scientist. BASIC SOIL PROPERTIES. Soil and water management module 1 2005 [13/08/2012]; Available from: http://landresources.montana.edu/SWM/PDF/Final_proof_SW1.pdf.
 198. Papendick, R. and G. Campbell, Theory and measurement of water potential. *Water potential relations in soil microbiology*, 1981. 3: p. 1-22.
 199. Abbott, L.K. and D.V. Murphy, *Soil Biological Fertility: A Key to Sustainable Land Use in Agriculture* 2003: Kluwer Academic Publishers.
 200. Füllner, K., The influence of spatially heterogeneous soil temperatures on plant structure and function. Vol. 76. 2007: Forschungszentrum Jülich.
-

-
201. Nepstad, D., et al., The effects of partial throughfall exclusion on canopy processes, aboveground production, and biogeochemistry of an Amazon forest. *Journal of Geophysical Research: Atmospheres* (1984–2012), 2002. 107(D20): p. LBA 53-1-LBA 53-18.
 202. Gaumont-Guay, D., et al., Interpreting the dependence of soil respiration on soil temperature and water content in a boreal aspen stand. *Agricultural and Forest Meteorology*, 2006. 140(1): p. 220-235.
 203. Havlin, J., et al., *Soil fertility and fertilizers: An introduction to nutrient management*. Vol. 515. 2005: Pearson Prentice Hall Upper Saddle River, NJ.
 204. Troeh, F.R. and L.M. Thompson, *Soils and soil fertility* 2005: Blackwell Iowa.
 205. Drager. Drager X-am 7000. 2015; Available from: <http://pdf.directindustry.com/pdf/drager-safety/drager-x-am-7000/20351-105897.html>.
 206. CO2Now. 2016 6/1/2016]; Available from: <http://co2now.org/>.
 207. Means, R.E. and J.V. Parcher, *Physical properties of soils*. 1963.
 208. University of West of Scotland Weather Station. Available from: <http://weather.uws.ac.uk/>.
 209. Gao, F. and S. Yates, Laboratory study of closed and dynamic flux chambers: experimental results and implications for field application. *Journal of geophysical research*, 1998. 103(D20): p. 26115-26,125.
 210. Heinemeyer, A. and N.P. McNamara, Comparing the closed static versus the closed dynamic chamber flux methodology: Implications for soil respiration studies. *Plant and soil*, 2011: p. 1-7.
-

-
211. Topographic Map Website. 2015 [09/22/2015]; Available from: <http://en-gb.topographic-map.com/>.
 212. CO2 Monthly. 2015; Available from: <http://co2now.org/>.
 213. Hillel, D., Introduction to soil physics 2013: Academic press.
 214. <http://www.metoffice.gov.uk/climate/uk/datasets/>, Met Office Download regional values, 2012, Met Office.
 215. Lee, M., et al., Effects of rainfall events on soil CO₂ flux in a cool temperate deciduous broad-leaved forest. *Ecological Research*, 2002. 17(3): p. 401-409.
 216. Ismail, B.I. and W.H. Ahmed, Thermoelectric power generation using waste-heat energy as an alternative green technology. *Recent Patents on Electrical & Electronic Engineering (Formerly Recent Patents on Electrical Engineering)*, 2009. 2(1): p. 27-39.
 217. ANSYS, ANSYS CFX-Solver Modelling Guide, 2009.
 218. Coutelieiris, F.A. and J. Delgado, *Transport Processes in Porous Media*. Vol. 20. 2012: Springer.
 219. De Gryze, S., et al., Water repellence and soil aggregate dynamics in a loamy grassland soil as affected by texture. *European journal of soil science*, 2006. 57(2): p. 235-246.
 220. mathworks. 1-D digital filter. Available from: <http://uk.mathworks.com/help/matlab/ref/filter.html>.
 221. Zhou, X., S. Wan, and Y. Luo, Source components and interannual variability of soil CO₂ efflux under experimental warming and clipping in a grassland ecosystem. *Global Change Biology*, 2007. 13(4): p. 761-775.
-

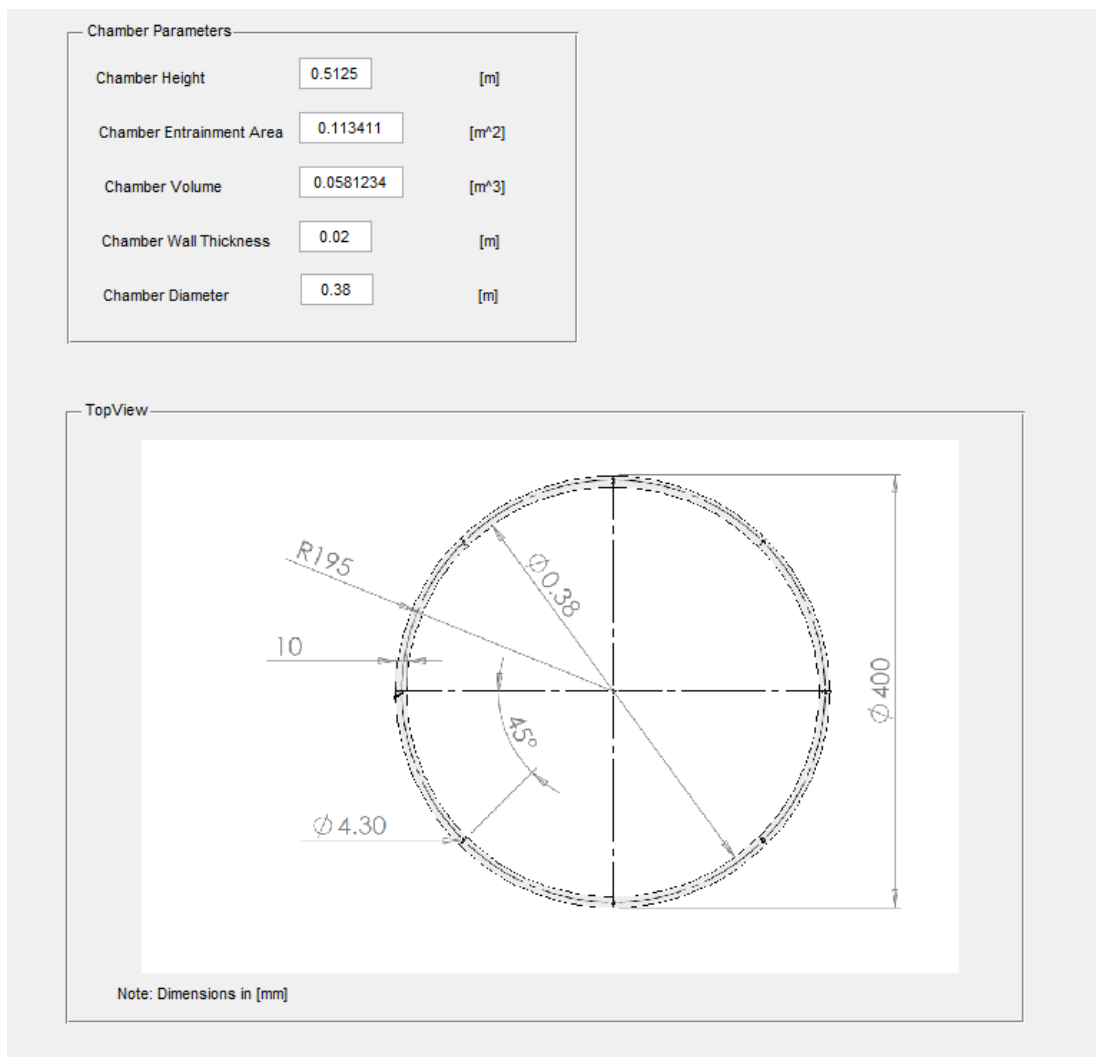
-
222. Date, A.W., Introduction to computational fluid dynamics 2005: Cambridge University Press.
223. Apostolos Kantzas, P.P.E.J.B., PhD P. Eng. Saeed Taheri, PhD, FUNDAMENTALS OF FLUID FLOW IN POROUS MEDIA.
224. Incropera, F.P., et al., Principles of heat and mass transfer 2013: Wiley.
225. Peng, S. and M.L. Brusseau, Impact of soil texture on air-water interfacial areas in unsaturated sandy porous media. Water resources research, 2005. 41(3).
226. Gregg, S. and K.S. Sing, Adsorption, Surface Area, and Porosity. 1983.
227. SAS IP, I. Rotating Frames of Reference. 2016 [cited 29/1/2016; Available from: https://www.sharcnet.ca/Software/Ansys/16.0/en-us/help/cfx_mod/i1299175.html].
228. Akturk, A. and C. Camci, Experimental and computational assessment of a ducted-fan rotor flow model. Journal of Aircraft, 2012. 49(3): p. 885-897.

This page is intentionally left blank

Appendices

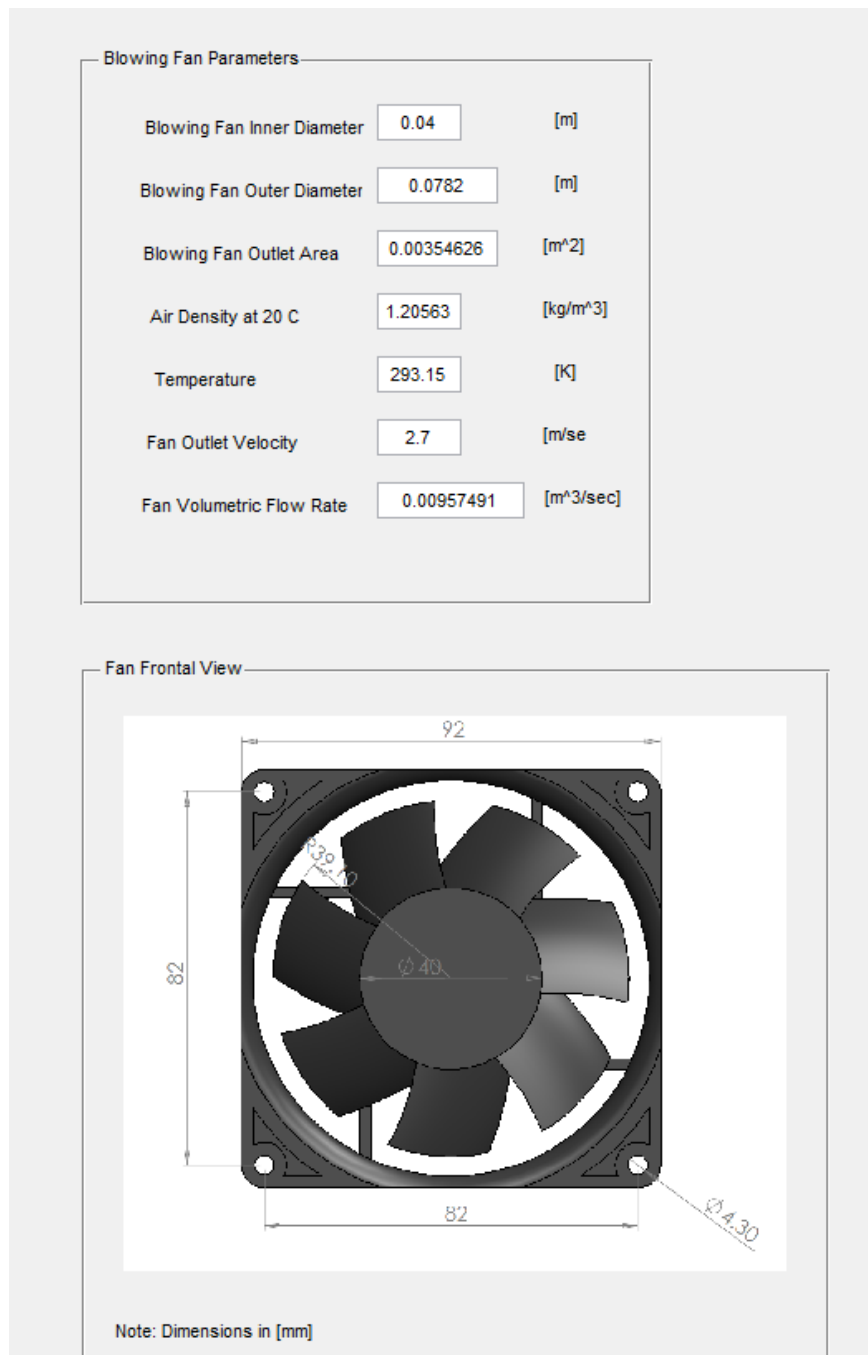
A-I Chamber dimensions

A screen shoot taken from the chamber developed MATLAB software showing the used chamber dimension values.



A-II Blowing Fan Parameters

A screen shoot taken from the chamber developed MATLAB software showing the used blowing fan parameters values likewise the dimensional ones.



A-III Lead Battery Parameters

A screen shoot taken from the chamber developed MATLAB software showing the used lead battery and other important values.

The screenshot displays a MATLAB interface with several calculation panels for lead battery parameters and fan power details.

Battery Calculations for Lead Battery

Battery Capacity Calculator for a Specified Number of Hours Run

Required Output Current I:	<input type="text" value="0.185"/>	(amp)
Required Battery Working Time T:	<input type="text" value="24"/>	(hour)
Required Battery Capacity C:	<input type="text" value="4.44"/>	(amp hour)

Used Fan Power Details

Voltage	<input type="text" value="12"/>	DC
Electrical Current	<input type="text" value="185"/>	mA
Fan Power	<input type="text" value="2.2"/>	watt
Fan Voltage Range	<input type="text" value="8-15"/>	DC

Life Cycle Consideration for a Lead Acid Battery

Life Cycle Efficiency	<input type="text" value="0.8"/>	[1]
Battery Capacity with Life Cycle Consideration	<input type="text" value="5.55"/>	(amp hour)

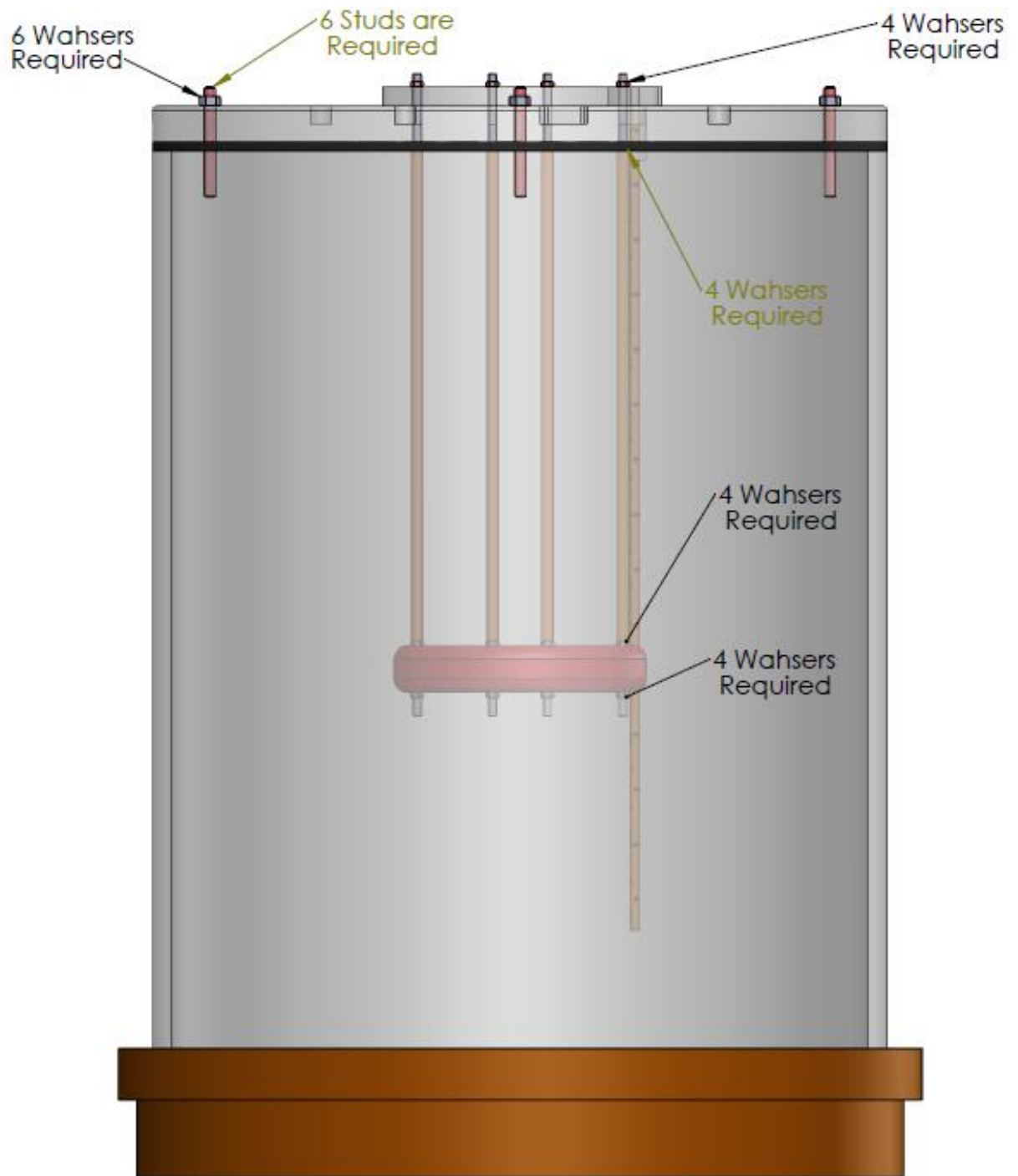
Electrical Fan Power

Inverter Efficiency	<input type="text" value="0.85"/>	[1]
Blowing Fan Power	<input type="text" value="2.2"/>	watt
Required Fan Blowing Time	<input type="text" value="5"/>	hour
Required Battery Capacity for the Blowing Time	<input type="text" value="11"/>	watt-hour
Required Battery Capacity for the Blowing Time	<input type="text" value="12.9412"/>	watt-hour

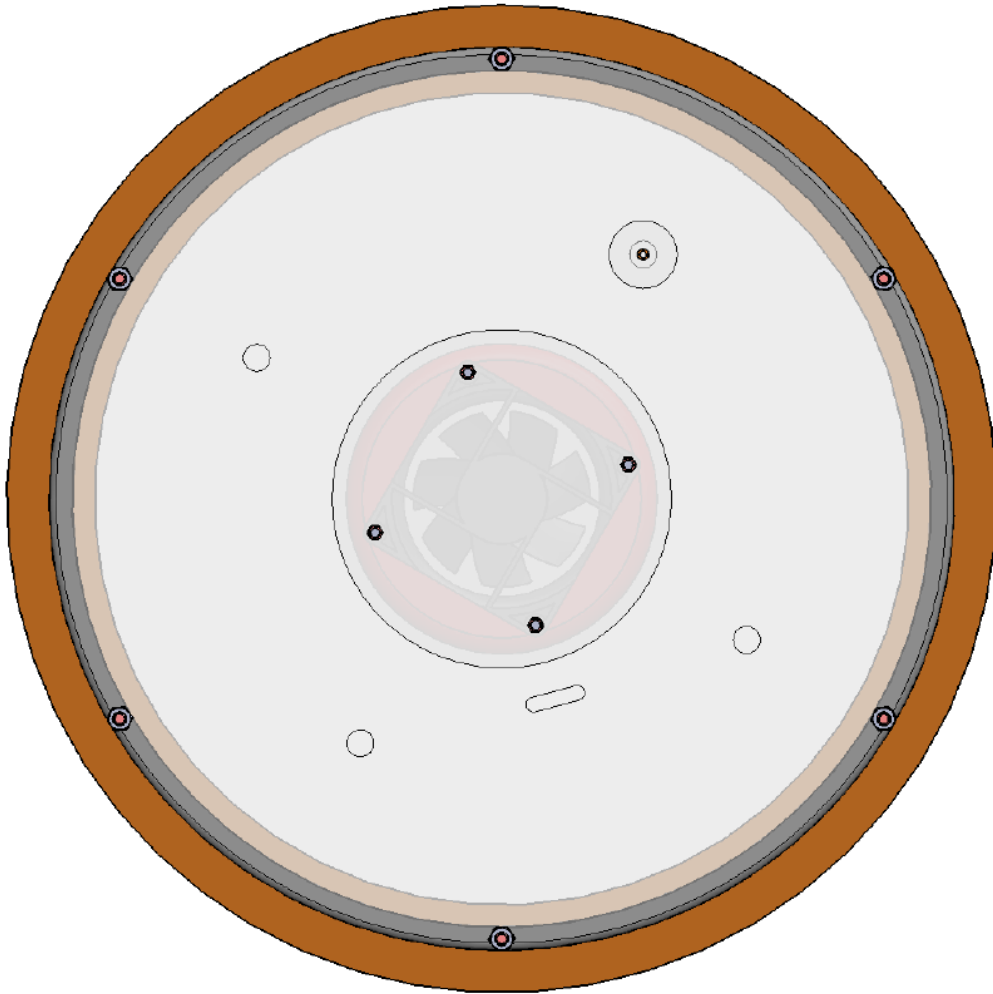
A-IV The Respiration Chamber Perspective View



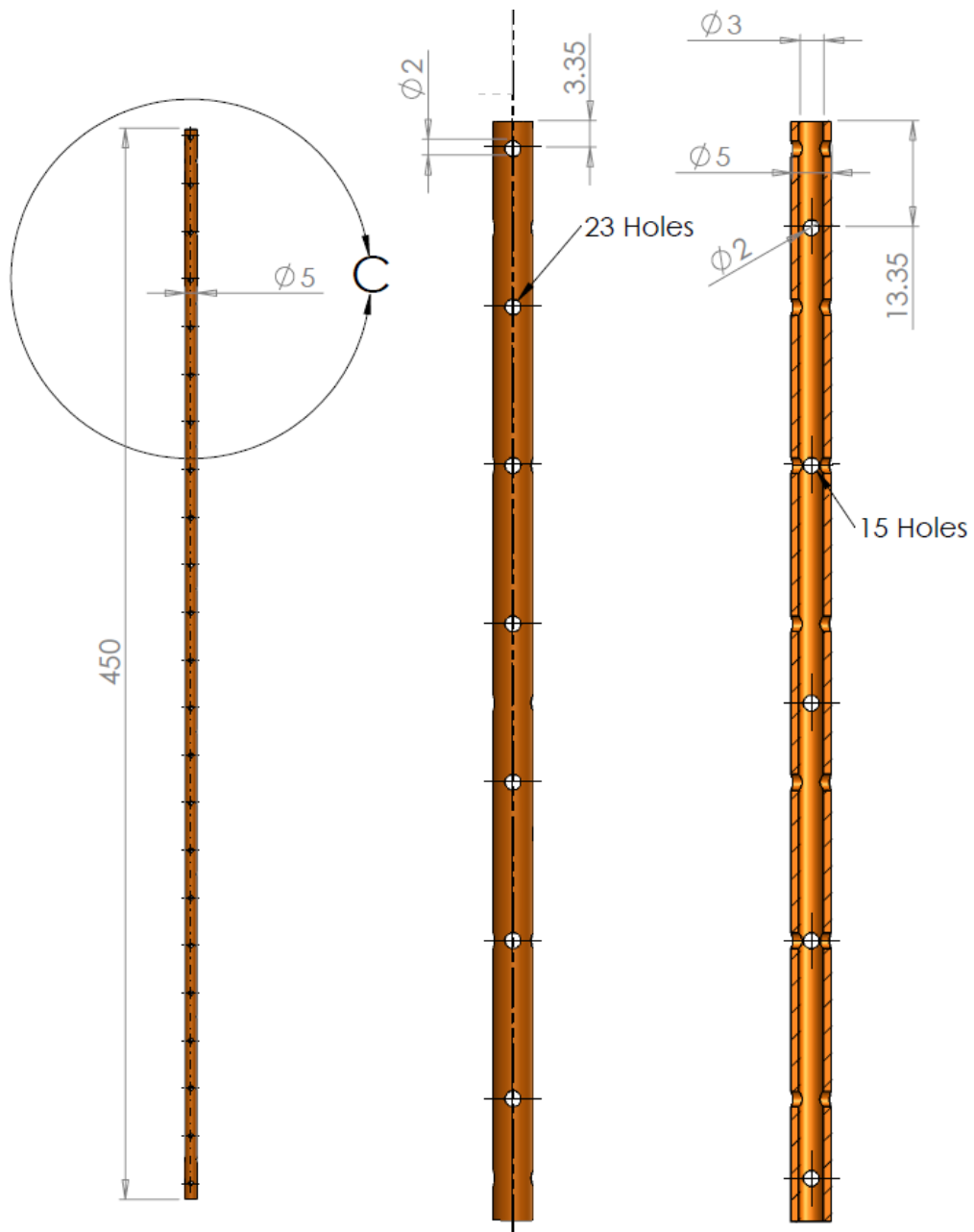
A-V The Side View of the Respiration Chamber



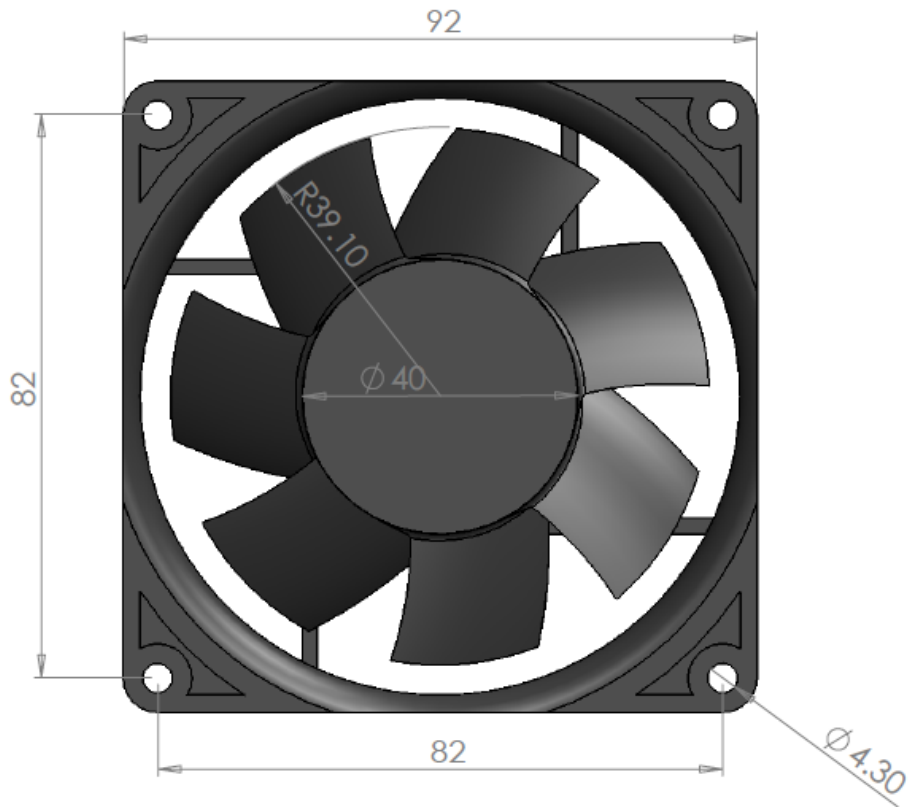
A-VI The Top View of the Respiration Chamber



A-VII The Respiration Sampling Tube



A-VIII The Circulation Fan Model



SCALE 1 : 1



SCALE 1 : 1

This page is intentionally left blank

This page is intentionally left blank

About the Author:

Ahmed Al Makky is currently honoured to hold a teaching position of Assistant Professor at Sharjah University (UOS). This is at the department of Sustainable and Renewable Energy Engineering (SREE). The modules he teaches at UOS are in the area of Wind Energy theory and lab, Energy Storage lab, Hydraulics, Fluid Mechanics and Lab, Fuel Cells, and Engineering Management. He obtained his doctorate degree (PhD) in the year 2016. Specialized in the area of Computational Fluid Dynamics (CFD), modelling carbon dioxide exchange between the surface of the earth and the atmosphere from the University of the West of Scotland. Beginning of the year 2008 he was awarded a Master's degree (MSc) in the area of Sustainable Energy and Environment from Cardiff University. The master's program got him involved extensively with combustion flame characterization and methods of fuel atomization. His bachelor's degree (BSc) is in Mechanical Engineering specialized in General Engineering (Thermal) from Damascus University 2005.



Picture taken on the grassland lawn outside the Mclean Building, Paisley, Glasgow, 2016.